UNIVERSIDADE FEDERAL DO RIO GRANDE DO SUL
INSTITUTO DE GEOCIÊNCIAS
PROGRAMA DE PÓS-GRADUAÇÃO EM GEOCIÊNCIAS

ESTRATIGRAFIA DE ALTA RESOLUÇÃO DE SISTEMAS EÓLICOS DURANTE PERÍODOS DE ICEHOUSE, FORMAÇÃO PIAUÍ, BACIA DO PARNAÍBA

CARREL KIFUMBI

ORIENTADOR – Prof. Dr. Claiton Marlon dos Santos Scherer

Porto Alegre, 2021

UNIVERSIDADE FEDERAL DO RIO GRANDE DO SUL
INSTITUTO DE GEOCIÊNCIAS
PROGRAMA DE PÓS-GRADUAÇÃO EM GEOCIÊNCIAS

ESTRATIGRAFIA DE ALTA RESOLUÇÃO DE SISTEMAS EÓLICOS DURANTE PERÍODOS DE ICEHOUSE, FORMAÇÃO PIAUÍ, BACIA DO PARNAÍBA

CARREL KIFUMBI

ORIENTADOR – Prof. Dr. Claiton Marlon dos Santos Scherer

BANCA EXAMINADORA

Profa. Dra. Ana Maria Góes– Universidade de São Paulo

Prof. Dr. Juliano Kuchle – Universidade Federal do Rio Grande do Sul

Prof. Dr. Roberto Iannuzzi – Universidade Federal do Rio Grande do Sul

Tese de Doutorado apresentada como requisito parcial para a obtenção do Título de Doutor em Ciências.

Porto Alegre, 2021

CIP - Catalogação na Publicação

Kifumbi, Carrel
ESTRATIGRAFIA DE ALTA RESOLUÇÃO DE SISTEMAS EÓLICOS DURANTE PERÍODOS DE ICEHOUSE, FORMAÇÃO PIAUÍ, BACIA DO PARNAÍBA / Carrel Kifumbi. -- 2021.
213 f.
Orientador: Claiton Marlon dos Santos Scherer.

Tese (Doutorado) -- Universidade Federal do Rio Grande do Sul, , Porto Alegre, BR-RS, 2021.

1. Sistemas eólicos. 2. Glaciação do Pensilvaniano. 3. Carbonífero. 4. Formação Piauí. 5. Bacia do Parnaíba. I. Marlon dos Santos Scherer, Claiton, orient. II. Título.

Elaborada pelo Sistema de Geração Automática de Ficha Catalográfica da UFRGS com os dados fornecidos pelo(a) autor(a).

AGRADECIMENTOS

Faz 12 anos que eu deixei a minha família, saí do meu país em busca da realização de um sonho e nunca sonhei ir tão longe. O que era pra ser apenas uma graduação se transformou na jornada mais importante da minha vida. As linhas a seguir não poderão expressar toda a gratidão que eu sinto por todos que acompanharam minha trajetória, me apoiaram e foram testemunhas das minhas realizações. Tantos nomes passam neste momento pela minha cabeça. Eu não tenho como citar todos vocês e eu me sentiria ingrato de esquecer algum.

Agradeço a Deus pelo dom da vida. Mais eu avanço e mais percebo Sua grandeza, Seu amor e Sua presença na minha vida. Tudo que eu sou e tudo que eu conquistei é dEle, por Ele, para Ele.

Agradeço ao meu querido orientador Claiton Scherer, meu mentor, meu segundo pai e um amigo de verdade. Por confiar em mim, ter me oferecido essa oportunidade incrível de aprender ao seu lado. Serei eternamente grato.

Aos meus colegas e amigos da Estrati. Eu entrei nesse prédio muito tímido e vocês foram os com quem eu passei a maior parte da minha vida na UFRGS. Aprendi muito com esse grupo, mas o que eu levo de mais valioso foi a amizade sincera que construímos. Vocês são a minha família. Agradeço também a todos meus colegas de graduação, vocês fazem parte da minha vida.

À minha querida mãe. Nunca esqueci o sorriso que eu conseguia te dar todas as vezes que eu tirava boas notas no colégio. Meus diplomas são a minha forma de sempre tentar te deixar mais feliz. Tu es tudo para mim.

Aos meus irmãos: Fabrice, Yannick, Clive e Bénédicte, vocês me apioaram incondicionalmente, me ajudaram e acreditaram em mim. Bénédicte, obrigado por tudo. Os anos passados contigo foram lindos. Tu não imagina como foi valioso ter minha irmã por perto.

A ti Carol que entrou na minha vida num período em que eu estava tão ocupado, mas tu soube me entender, esperar e achar as palavras certas para me erguer. Nossa história só começa! Por fim, agradeço à minha pequena Eva. Tu entrou na minha vida como um furacão, bagunçando meus planos, meus sonhos e minha casa. Mas incrivelmente tu conseguiu me deixar mais focado, mais maduro e tu me ensinou o verdadeiro sentido das prioridades.

Obrigado a todos.

À toi Papa! Je sais que tu aurais été très fier de ce chemin que j'ai accompli.
Tu m'as appris à ne jamais baisser les bras et qu'a force de courage on atteint toujours notre but. Ce diplôme te revient.
Je t'aime.

“... há um só Deus, e um só Mediador entre Deus e os homens, Jesus Cristo homem.” 1 Timóteo 2:5

“Disse-lhe Jesus: Eu sou o caminho, e a verdade e a vida; ninguém vem ao Pai, senão por mim.” João 14:6

RESUMO

Os campos de dunas são sistemas deposicionais complexos cuja construção, acumulação e preservação resultam da combinação entre fatores autogênicos oriundos da dinâmica de processos eólicos e da interação com os sistemas deposicionais adjacentes, e fatores alogênicos como o clima. Períodos glaciais ou *icehouse* são comumente considerados ideais para o desenvolvimento dos campos de dunas. Através da análise estratigráfica de alta resolução da sucessão superior da Formação Piauí, esta tese buscou entender a influência da glaciação do Pensilvaniano na sedimentação eólica. A sucessão superior da Formação Piauí é caracterizada por três intervalos estratigráficos: (i) O primeiro intervalo estratigráfico (IS-1) é dominantemente constituído por depósitos fluviais recobertos por estratos eólicos no topo; (i) O IS-2 é composto por depósitos lacustres silicificados, em contato abrupto com os depósitos sotopostos e sobrepostos; e por fim (iii) o IS-3 é essencialmente caracterizado por estratos eólicos nos quais a identificação de supersuperfícies permitiu identificar três ciclos sedimentares relacionados às fases de expansão e contração do campo de duna. A mudança de depósitos fluviais na base para essencialmente eólicos no topo indica uma progressiva aridificação na Bacia do Parnaíba durante o Pensilvaniano. No entanto, o registro sedimentar das bacias posicionadas em paleolatitudes mais elevadas indica que o Pensilvaniano foi um período caracterizado por uma das glaciações mais significativas do Carbonífero. Com base na revisão dos modelos de circulação atmosféricos durante o Pensilvaniano, o presente estudo comprovou a simultaneidade entre a presença de cobertura de gelo nas altas latitudes e a intensificação da aridez nas médias latitudes. Além do mais, foi possível demonstrar que as mudanças climáticas associadas à alternância entre períodos glaciais e interglaciais controlaram a dinâmica do campo de duna, ocasionando as fases de expansão e contração.

PALAVRAS-CHAVE: Sistemas eólicos, Glaciação do Pensilvaniano, Carbonífero, Formação Piauí, Bacia do Parnaíba.

ABSTRACT

Dune fields are complex depositional systems in which the construction, accumulation and preservation result from a combination of autogenic factors, which arise from the dynamics of aeolian processes and its interaction with adjacent depositional systems, and allogeneic factors such as the climate. Icehouse periods are usually considered ideal for the development of dune fields. Through high-resolution stratigraphic analysis of the upper succession of the Piauí Formation, this thesis aimed to understand the influence of Pennsylvania glaciation on aeolian sedimentation. The upper Piauí Formation is characterized by three stratigraphic intervals: (i) the first stratigraphic interval (SI-1) is predominantly constituted by fluvial deposits overlain by eolian strata at the top; (i) the SI-2 is composed of silicified lacustrine deposits, in sharp contact with underlying and overlapping deposits; and finally (iii) the SI-3 is essentially characterized by eolian strata. Within this later stratigraphic unit, the identification of supersurfaces allowed for the interpretation of three sedimentary cycles related to phases of expansion and contraction in the dune field. The shift from fluvial deposits at the base to essentially eolian strata at the top indicates a progressive aridification in the Parnaíba Basin during the Pennsylvanian period. Although, the sedimentary record of basins located in higher paleolatitudes indicates that the Pennsylvanian was a period characterized by one of the main glaciations of the Carboniferous. Detailed analysis of atmospheric circulation during the Pennsylvanian suggests simultaneity between the presence of ice cover in high latitudes and the intensification of aridification in mid-latitudes. Furthermore, we demonstrate that climate change associated with the alternation between glacial and interglacial periods controlled the dynamics of the dune field, triggering expansion and contraction fases.

KEYWORDS: Aeolian systems, Pennsylvanian glaciation, Carboniferous, Piauí Formation, Parnaíba Basin.

LISTA DE FIGURAS

SUMÁRIO

ESTRUTURA DA TESE

Essa tese de doutorado está estruturada em um texto integrador e três artigos científicos. O artigo 1, "*Missing and preserved strata: keys for spatio-temporal variability in aeolian dune-field, Pennsylvanian Upper Piauí Formation (Parnaíba Basin), Brazil*", foi submetido no periódico Sedimentology Journal (Qualis-CAPES A1). O artigo 2, intitulado *"A Pennsylvanian saline-alkaline lake in Gondwana mid-latitude: Evidence from the Piauí Formation, Parnaíba Basin, NE Brazil"*, foi submetido para o periódico Palaeogeography, Palaeoclimatology, Palaeoecology. (Qualis-CAPES A1). O artigo 3, intitulado "Late Pennsylvanian aridification in Gondwana mid-latitudes contemporaneous to high-latitudes ice cap expansion. Upper Piauí Formation. Brazil", foi submetido no periódico Journal of South American Earth Sciences (Qualis-CAPES A3). O texto integrador compreende os seguintes capítulos: (1) introdução; (2) objetivos; (3) estado da arte; (4) dados e métodos; (5) contexto geológico; (6) resultados e discussões; (7) conclusões; (8) referências bibliográficas.

TESE

ESTRATIGRAFIA DE ALTA RESOLUÇÃO DE SISTEMAS EÓLICOS DURANTE PERÍODOS DE ICEHOUSE, FORMAÇÃO PIAUÍ, BACIA DO PARNAÍBA

1 INTRODUÇÃO

Os campos de dunas são sistemas complexos que se desenvolvem quando três principais requisitos são preenchidos, a saber: 1) alto suprimento sedimentar; 2) disponibilidade de areia seca e; 3) energia de vento suficiente para transportar a areia ou retrabalhá-la in-situ (Kocurek & Lancaster, 1999). Alterações nesses parâmetros afetam a dinâmica do campo de duna ocasionando a sua expansão ou contração. Essas alterações são principalmente causadas por fatores externos, como tectônica, clima e eustasia (Kocurek, 1999). Embora esses fatores compartilhem uma relação estreita e interdependente, vários estudos têm tentado isolar e quantificar o efeito dos mesmos (Kocurek, 1999; Cosgrove et al., 2021).

No que diz respeito às condições climáticas, depósitos eólicos se desenvolvem tanto durante períodos de *greenhouse* (Crabaugh & Kocurek, 1993; Kocurek et al., 1992; Kocurek & Day, 2018) quanto *icehouse* (Mountney & Jagger, 2004; Mountney, 2006; Jordan & Mountney, 2010). No entanto, diferentemente dos períodos de *greenhouse*, os períodos de *icehouse* são comumente associados com: (i) rebaixamento do nível do mar, (ii) alto contraste térmico marinho entre regiões polares e equatoriais; e (iii) aumento das velocidades do vento em latitudes baixas (<30º) (Frakes et al., 1992; Forster et al., 2007). Além do mais, os períodos de *icehouse* são caracterizados por oscilações cíclicas entre fases glaciais áridas e interglaciais úmidas, relacionadas com os ciclos de Milankovitch (Wanless & Shepard, 1936; Dickinson et al., 1994). Logo, a transição entre fases interglaciais para glaciais permite a combinação de vários fatores favoráveis

para a construção de campos de dunas (Kocurek, 1999; Kocurek & Lancaster, 1999).

A Formação Piauí (Small, 1914) da Bacia do Parnaíba constitui um estudo de caso ideal para analisar a influência de períodos glaciais na sedimentação eólica. Por décadas, a Formação Piauí de idade Pensilvaniana foi interpretada como depositada em contexto costeiro, devido à alternância entre depósitos eólicos, marinhos e fluviais (Lima & Leite, 1978; Lima Filho, 1998; Vaz et al., 2007, Vieira & Scherer, 2017). Contudo, no que diz respeito à sucessão superior dessa formação (Lima & Leite, 1978), foco deste estudo, a análise estratigráfica de alta resolução revelou uma ausência de depósitos marinhos e uma mudança de depósitos fluviais na base para essencialmente eólicos no topo, sugerindo condições cada vez mais áridas. O presente estudo investigou a hipótese de que a glaciação do Pensilvaniano (Carbonífero superior) foi responsável pela aridificação em médias paleolatitudes, registrada na sucessão superior da Formação Piauí. O estudo permitiu a identificação de ciclos de alta resolução na sucessão eólica da Formação Piauí, os quais indicam alternância entre períodos glaciais e interglaciais.

2 OBJETIVOS

O principal objetivo desta tese é a entender a influência da glaciação na sedimentação eólica. Para esse fim, foi escolhida como estudo de caso a sucessão superior da Formação Piauí de idade Pensilvaniana. Destacam-se como objetivos específicos os seguintes:

- Investigar a sincronicidade entre a glaciação do Pensilvaniano e a sedimentação eólica da Formação Piauí;
- Definir a arquitetura de fácies das unidades estudadas;
- Propor um arcabouço da estratigrafia de sequência de alta resolução dos depósitos eólicos;
- Entender os mecanismos controladores da sedimentação eólica e;
- Construir modelos deposicionais da evolução estratigráfica e paleogeográfica da Bacia do Parnaíba durante o Pensilvaniano.

3 ESTADO DA ARTE

O reconhecimento dos estratos eólicos é de extrema relevância, pois neles são registrados informações sobre condições climáticas e eustáticas do passado (Chan & Kocurek, 1988; Christie Blick *et al*., 1990; Kocurek, 1999). Neste ponto de vista, o estudo de Hunter (1977) é considerado um marco histórico, por ter facilitado a identificação de estratos eólicos e sua diferenciação dos depósitos subaquosos.

O propósito deste capítulo é sintetizar o estado atual de conhecimento sobre os sistemas eólicos examinando os elementos fundamentais da análise estratigráfica de depósitos eólicos. Dessa forma, o capítulo está organizado nos seguintes itens: (1) *Construção de campos de dunas:* subcapítulo onde são examinados os fatores controladores da deposição e migração de dunas eólicas, os critérios de reconhecimentos de estruturas eólicas, e as feições que resultam das interações entre os campos de dunas e os sistemas deposicionais adjacentes; (2) *Acumulação:* subcapítulo onde são apresentados os mecanismos de geração das superfícies de acumulação; e (3) *Preservação:* subcapítulo onde se trata das condições necessárias para preservação dos depósitos acumulados.

3.1 Construção de campos de dunas

3.1.1 Fatores controladores da distribuição dos campos de dunas

Os maiores campos de dunas são localizados em regiões submetidas à ação do vento e que possuem grande reserva de areia (Pye, 1983). Assim sendo, os campos de dunas podem se formar em regiões costeiras ou intracontinentais desde que sejam atendidos os principais requisitos para a construção de um campo de dunas, a saber: 1) Alto suprimento sedimentar; 2) disponibilidade de areia seca e; 3) energia de vento suficiente para transportar a areia ou retrabalhá-la *in-situ*. Esses fatores foram apontados por Kocurek & Lancaster (1999) como componentes do regime sedimentar (*sediment state*) de um sistema eólico (Figura 1). Por outro lado os fatores alocíclicos, como tectônica, clima e eustasia, podem afetar de maneira direta ou indireta o regime sedimentar (Mckee, 1983; Kocurek, 1999).

3.1.1.1 Suprimento Sedimentar

O suprimento sedimentar é o volume de sedimentos que serve como fonte de material para um sistema eólico contemporâneo ou futuro (Kocurek & Lancaster, 1999). A magnitude do suprimento sedimentar depende do tipo de litologias aflorantes, do grau de alteração/erosão, da extensão da cobertura vegetal e da eficiência dos processos de transporte (Pye & Tsoar, 2009).

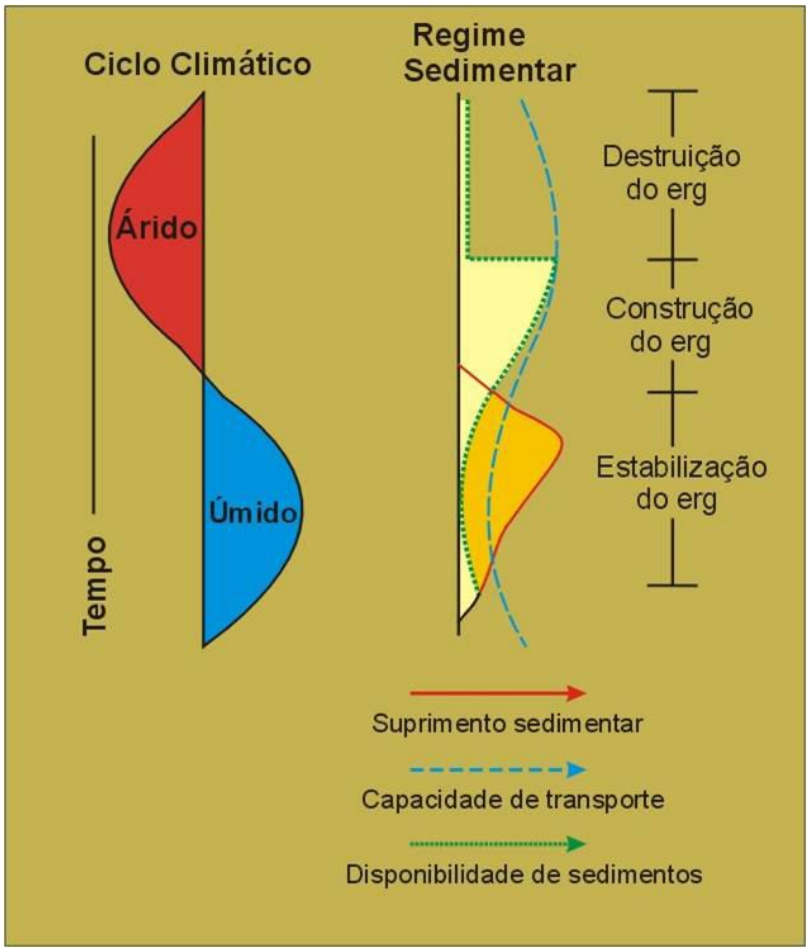

Figura 1: Diagrama idealizado do regime sedimentar. Condições climáticas úmidas ocasionam o aumento do suprimento sedimentar, mas a umidade reduz a disponibilidade de sedimentos. Em períodos áridos a redução da umidade permite aumento da disponibilidade, mas se a capacidade de transporte for superior à disponibilidade de areia ocorre destruição do campo de duna (Modificado de Kocurek, 1999).

A deflação constitui o processo primário de erosão pelo vento. Todavia, a quase totalidade dos grãos necessários para formar um campo de dunas é apenas raramente derivada da deflação, mas sim oriunda do retrabalhamento de sedimentos fluviais/aluviais, costeiros ou lacustres.

Kocurek (2003) sugere que a produção de sedimentos pode ser melhorada de três maneiras: com o aumento das taxas de alteração/erosão na área fonte, com o aumento da energia das correntes alimentadoras e em períodos áridos, pela redução ou eliminação da cobertura vegetal. Langbein & Schumm (1958) reconheceram pela primeira vez que o cenário que produz máxima erosão e transporte de sedimentos ocorre na transição de condições sub-úmidas para semi-áridas (Figura 1). Durante essa transição, a cobertura vegetal é reduzida e as rochas previamente intemperizadas, no período úmido, ficam sujeitas a erosão eólica (Clemmensen *et al*., 1989).

3.1.1.2 Disponibilidade de Sedimentos

A disponibilidade de sedimentos corresponde à suscetibilidade dos grãos a serem transportados pelo vento (Kocurek & Lancaster, 1999). A disponibilidade é otimizada com o aumento da aridez, porém se a aridez perdurar ocorre exaustão do suprimento e se inicia a deflação do campo de duna (Figura 1) (Wilson, 1971). Portanto, o volume de sedimentos disponíveis está intimamente ligado aos parâmetros atmosféricos e às condições do substrato de tal forma que a disponibilidade é diretamente proporcional à energia do vento, mas inversamente proporcional à umidade do solo e à extensão da cobertura vegetal (Ash & Wasson, 1983; Lancaster, 1997).

3.1.1.3 Energia de Vento

A energia do vento refere-se à capacidade que o vento tem para transportar sedimentos (Kocurek & Lancaster, 1999). Bandold (1941) conduziu vários experimentos teóricos e empíricos para determinar a velocidade mínima necessária para iniciar o transporte de sedimentos (Figura 2A). Os principais fatores que afetam a velocidade mínima de transporte pelo vento são o tamanho do grão, a coesão entre as partículas, o grau de seleção, a vegetação, a rugosidade e a umidade do terreno (Pye e Tsoar, 2009). Uma vez a velocidade mínima alcançada os grãos entram em movimento por rolamento e em seguida por saltação (Figura 2B). Os grãos conseguem se manter em movimento com uma velocidade inferior à velocidade limiar pois o impacto da saltação fornece energia suplementar para o transporte (Figura 2C e D) (Bagnold, 1937).

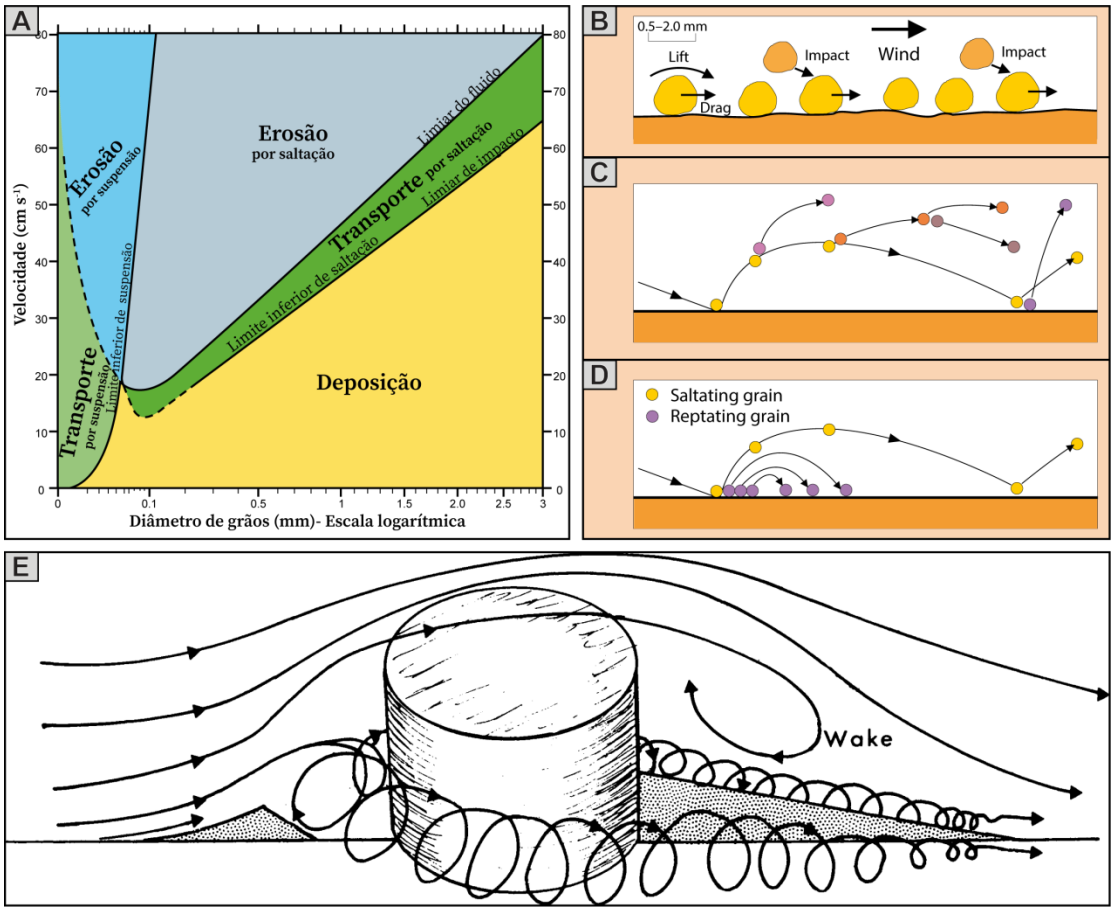

Figura 2: Características do vento no transporte de sedimentos. A) Diagrama de velocidade de fluido em relação ao tamanho de grão. A velocidade mínima necessária para iniciar a movimentação do grão (limiar do fluido) é superior à velocidade mínima necessária para que este grão continue em movimento (limiar de impacto). B) O impacto dos grãos em saltação com os grãos mais grossos gera energia para estes últimos iniciarem o movimento por rolamento. C) O choque entre os grãos em saltação fornece energia para que os mesmos se mantenham em movimento. D) Tipos e trajetórias de saltação. E) Diagrama esquemático da influência de uma barreira: Formação de *vortex* à barlavento e expansão do vento a sotavento (Figura A modificada de Bagnold, 1941; B, C e D extraídas de Mountney, 2006; E extraída de Pye & Tsoar, 2009).

A areia pode ser transportada por centenas a milhares de quilômetros até a desaceleração dos ventos (Wilson 1971, 1973), que pode ser causada por influencia dos padrões de ventos regionais, gradientes de pressão ou devido à interferência de alguma barreira topográfica (Pye, 1983b; Fryberger *et al*., 1979; Kocurek, 1988). Os altos topográficos, como, por exemplo, as cadeias de montanhas, atuam como obstáculos ao vento e promovem deposição de areia tanto à barlavento quanto à sotavento (Figura 2E). À barlavento a desaceleração rápida e a coalescência de ventos gera um *vortex* reverso que causa a deposição instantânea dos sedimentos e à

sotavento a expansão vertical do vento ocasiona a redução da energia (Ash & Wasson, 1983).

3.1.1.4 Clima, Tectônica e Eustasia

O suprimento sedimentar, a disponibilidade de sedimentos e a capacidade de transporte são governados diretamente ou indiretamente pelo clima, a tectônica e as flutuações do nível relativo do mar (Figura 3) (Kocurek, 1999).

A tectônica afeta diretamente o suprimento sedimentar (Figura 3) pelo soerguimento de área fonte que aumenta as taxas de erosão mecânica e a velocidade de escoamento das drenagens (Blakey, 1988; Kocurek, 1988), e indiretamente a disponibilidade de sedimentos (Figura 3) pelas flutuações do nível freático e pela fração granulométrica gerada (Kocurek, 1999). A fração granulométrica, por sua vez, controla a coesão intergranular e a energia mínima necessária para iniciar a movimentação dos grãos.

O clima afeta o suprimento pela intensidade do escoamento de sistemas aluviais/fluviais de maneira que, durante fases úmidas, o escoamento e a descarga são intensificados (Wilson, 1971; Kocurek, 1988). Períodos de precipitação elevada aumentam o suprimento sedimentar pelo aumento da erosão e da energia do escoamento superficial, no entanto, a disponibilidade de areia à jusante é reduzida por causa do aumento da cobertura vegetal e da subida do nível freático que aumenta a coesão entre os grãos (Kocurek, 2003). Inversamente, durante períodos áridos ocorre redução da cobertura vegetal e rebaixamento do nível freático gerando o aumento da disponibilidade de areia (Kocurek, 2003). Já a energia do vento por sua vez é fortemente condicionada pelo clima e a pressão atmosférica. De forma geral, a força de arraste é proporcional à densidade do vento e esta última é inversamente proporcional à temperatura. Logo, os ventos em altas latitudes carregam os sedimentos de forma mais eficiente (Pye e Tsoar. 2009). Tem sido amplamente comprovado que em períodos glaciais (*icehouse*) a energia do vento é maior (Glennie, 1987). Este fato se deve ao alto contraste nos gradientes de temperatura e de pressão (Parrish & Peterson, 1988; Kocurek, 1988; Kocurek, 2003; Pye & Tsoar, 2009). Segundo

Parrish & Peterson (1988), as células de circulação de vento se formam em decorrência do contraste de temperatura entre o mar e o continente. Quanto maior for esse contraste, mais fortes serão os ventos. O padrão de circulação resultante pode ser: (i) zonal, em que o contraste de temperatura entre o equador e os pólos, ea rotação da terra controlam as rotas de circulação do vento; ou (ii) monsonal, no qual a diferença de pressão entre as massas de terra e o oceano controla a direção do vento (Parrish, 1993; Compagnucci, 2011; Parrish & Peterson, 1988). Consequentemente o aumento do contraste térmico e barométrico, que ocorrem respectivamente durante períodos quentes e durante a aglutinação de massas de terras (como aconteceu no Pangeia), promove circulações atmosféricas mais intensas e ventos mais fortes.

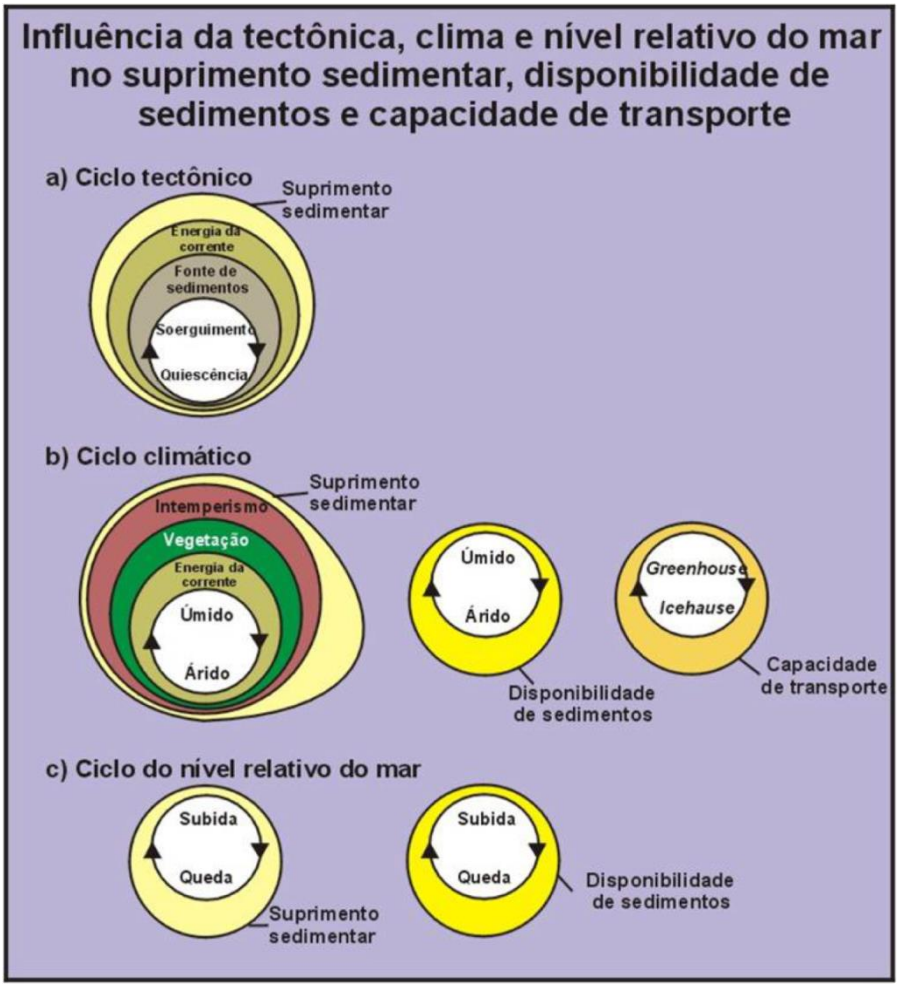

Figura 3: Influência da tectônica, clima e nível relativo do mar no suprimento sedimentar, disponibilidade de sedimentos e capacidade de transporte (Kocurek, 1999).

As flutuações do nível do mar afetam diretamente o suprimento e a disponibilidade de sedimentos e indiretamente a energia de vento (Figura 3). As oscilações do nível do mar controlam a extensão da plataforma (Chan & Kocurek, 1988; Kocurek, 1988), o perfil de equilíbrio do rio (Blum & Törnqvist, 2000; Holbrook *et al*., 2006) e o nível do freático (Crabaugh & Kocurek, 1993; 1998). Durante as regressões marinhas ocorre aumento da disponibilidade de areia, pois uma grande porção da plataforma fica submetida à ação do vento (Chan & Kocurek, 1988). Adicionalmente, o rebaixamento do nível do mar causa a queda do nível freático e a redução gradual do efeito da franja capilar sobre os grãos. Consequentemente, a coesão entre os grãos é reduzida e a disponibilidade de sedimentos aumenta (Kocurek *et al*., 1991). Inversamente, transgressões marinhas tendem a diminuir o volume de sedimentos disponíveis. Períodos glaciais (*icehouse*) são geralmente associados a rebaixamentos significativos do nível do mar.

3.1.2 Características diagnósticas de dunas eólicas

Para diferenciar os depósitos eólicos dos demais, o sedimentólogo precisa reconhecer os principais atributos de uma duna: composição, textura, estruturas e morfologias de dunas.

3.1.2.1 Composição

A predominância de um mineral na composição de um campo de duna depende geralmente da sua abundância na rocha fonte e a taxa com a qual esse mineral é destruído por processos de intemperismo mecânico e químico (Edgett & Lancaster, 1993). O quartzo constitui o principal grão encontrado nas dunas em virtude da sua abundância na crosta continental e a sua alta resistência ao intemperismo.

As dunas podem ser formadas também por minerais evaporíticos, carbonatos, agregados de argila ou materiais vulcanoclásticos (Mckee, 1983; Pye & Tsoar, 2009). Os cristais de gipsita são formados por precipitação química em lagos e playas e, quando o nível da água desce o suficiente, os evaporitos cristalizam e o substrato lamoso seca e se fragmenta. O vento consegue então remover os fragmentos e os cristais (Pye & Tsoar, 2009). A areia carbonática é formada por acreção de camadas concêntricas de

carbonatos em volta de fragmentos de conchas, de carbonatos ou de grãos siliciclásticos. As areias vulcanoclásticas originam-se do retrabalhamento de sedimentos epiclásticos ou piroclásticos nas proximidades de províncias vulcânicas (Edgett & Lancaster, 1993; Mountney & Russel, 2004).

3.1.2.2 Textura

Os sedimentos eólicos frequentemente exibem características peculiares de tamanho de grãos, arredondamento e seleção dos grãos que são úteis para o reconhecimento de estratos eólicos (Lancaster, 1986). O vento é um agente altamente seletivo em termos de fração granulométrica que pode transportar. O grau de seleção é controlado pelo tamanho de grão disponível e pelas variações da energia do vento. As dunas podem apresentar grãos grossos se a área fonte encontra-se próxima. A bimodalidade de tamanho de grão é frequente observada em sedimentos eólicos.

Durante o transporte de areia pelo vento ocorre colisão entre as partículas e abrasão de minerais menos resistentes, enquanto os grãos mais resistentes se tornam arredondados e ocasionalmente esféricos (Mountney, 2006b). Os grãos mais grossos (areia grossa e grânulos) se movimentam por arraste quando a energia do vento é mais intensa e são preferencialmente encontrados em lençóis de areia. Nesses depósitos ocorrem eventualmente ventifactos: seixos e blocos apresentando as superfícies voltadas contra o vento abradadas e aplainadas pelo impacto constante de partículas tamanho areia. Embora a textura possa ajudar no reconhecimento dos depósitos eólicos, a mesma só pode ser usada como critério convincente quando associada às estruturas sedimentares caraterísticas (Kocurek & Dott, 1981).

3.1.2.3 Estruturas

Nos depósitos eólicos, as partículas são organizadas em estratos ou lâminas. Um estrato *sensu* Mckee & Weir (1953) é uma camada única de litologia homogênea ou gradacional separada das camadas (estratos) adjacentes por uma superfície de erosão ou não deposição, ou uma superfície caracterizada pela mudança abrupta de um dos parâmetros da camada. Considerando que o termo “estrato” não tem conotação de

espessura, o mesmo será usado aqui indiferentemente para lâminas (menos de 1 cm) ou camadas (mais de 1 cm) .

A identificação do tipo de estratificações constitui uma ferramenta confiável para reconhecer os estratos eólicos do passado (Hunter, 1977; Kocurek & Dott, 1981). Cinco tipos principais de estratificações podem ser reconhecidos nos estratos eólicos, são eles: estratos horizontais, estratos cruzados de fluxos de grãos, estratos de queda de grãos, estratos cruzados transladantes cavalgantes e estratos de adesão (Hunter, 1977). As estruturas mais comumente atribuídas ao contexto eólico são as estratificações cruzadas de grande porte. Tais estruturas são, na realidade, compostas internamente por uma combinação entre as principais estratificações acima listadas.

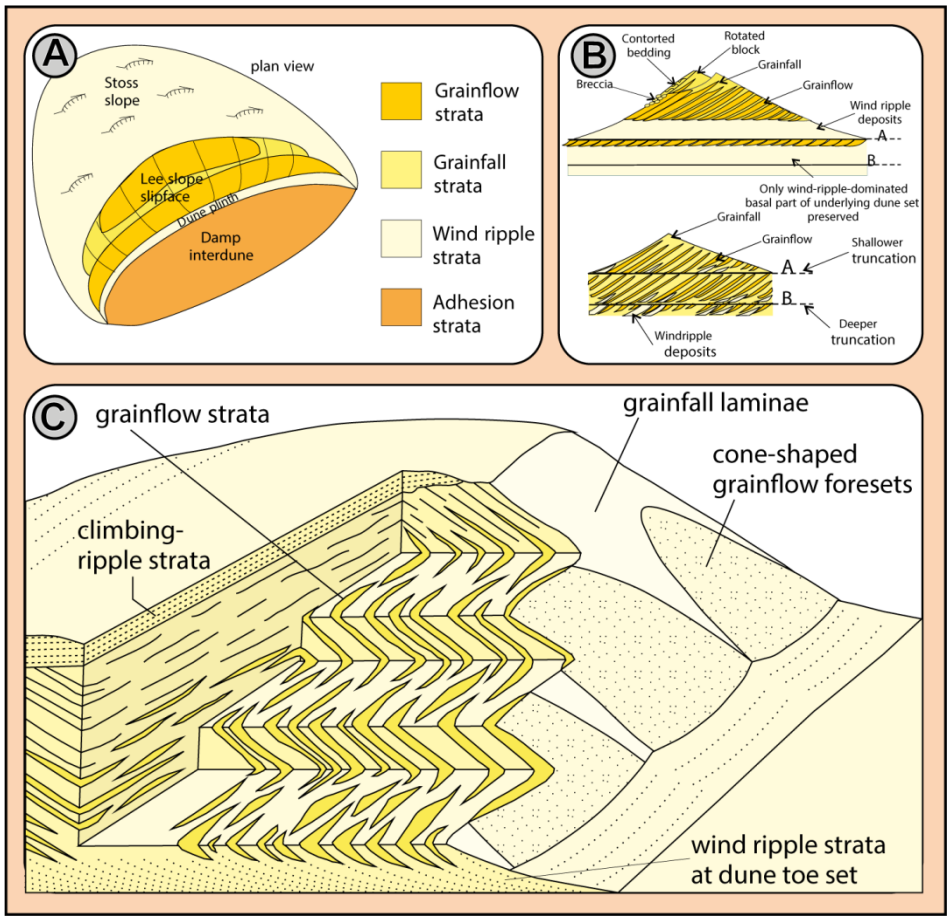

Figura 4: As principais estruturas eólicas e sua distribuição em uma duna. A) No dorso da duna predominam estratos cruzados cavalgantes (*wind ripples*). Na face frontal da duna se encontram estratos cruzados cavalgantes e estruturas de fluxo e queda de grão. Na interduna úmida ocorrem estruturas de adesão. B) Modelo esquemático de dunas com morfologia dos estratos em corte vertical paralelo ao fluxo (Modificado de Kocurek & Dott, 1981). C) Detalhe da parte interna da duna em diferentes cortes. Observa-se a forma em cunha dos estratos de fluxo de grão enquanto os de queda

livre são retos e contínuos e se interdigitam na base com estratos cavalgantes (Modificado de Hunter, 1977).

3.1.2.3.1 Estratos horizontais

Os estratos horizontais são gerados por tração intensa, impossibilitando a formação de estratos cruzados (Hunter, 1977; Kocurek & Dott, 1981). A energia elevada do transporte causa erosão progressiva e aplainamento das marcas onduladas (*ripples*) preexistentes. No entanto, a velocidade do vento não se mantém constante. As oscilações na energia do vento possibilitam a deposição de grãos mais grossos (Hunter, 1977).

3.1.2.3.2 Estratos cruzados de fluxo de grãos

Os estratos cruzados de fluxo de grãos se formam por avalanche na face frontal da duna (Figura 4A). Tal situação ocorre sempre que a acumulação de areia seca excede o ângulo crítico de repouso (cerca de 32-34°) na crista da duna (Hunter, 1977; Allen,1970). Os estratos cruzados de fluxo de grãos geram corpos com geometria lenticular, quando observados em cortes horizontais e verticais transversais à direção do vento (Figura 4B e C). Quando o corte for vertical paralelo à direção do vento, esses aparecem como cunhas afunilando levemente em direção ao pé da duna (Figura 4C) (Hunter, 1977). Internamente os estratos cruzados de fluxo de grãos apresentam espessuras variáveis, arcabouço frouxo e comumente homogêneo, e são separados por estratos cruzados de queda livre de grãos. (Bagnold, 1941).

Quando a areia apresenta umidade e, portanto, coesão interna, a avalanche ocorre na forma de fluxos de massas (*slides* e *slumps)*. Blocos arenosos escorregam ao longo da face de deslizamento e geram feições deformativas (Figura 4B) (Mckee & Bigarella, 1972; Mckee *et al*., 1971).

3.1.2.3.3 Estratos cruzados de queda livre de grãos

A queda livre de grãos é caracterizada pelo assentamento gravitacional dos grãos no momento em que os mesmos atingem a face frontal da duna (Figura 4A). A face frontal da duna é uma zona de sombra, abrigada do vento, onde ocorre separação do fluxo de ar. Nesta região os grãos transportados em suspensão perdem seu *momentum* e são depositados (Hunter, 1977; Kocurek & Dott, 1981). Os estratos cruzados de

queda livre de grãos se depositam paralelamente ao relevo da face de deslizamento da duna (Kocurek & Dott, 1981). Em cortes verticais e horizontais os depósitos de queda livre de grãos são caracterizados por lâminas retas e contínuas (Figura 4C). Os estratos de queda livre de grãos apresentam espessura milimétrica e granulometria homogênea decorrente da boa seleção de grãos capazes de serem transportados em suspensão.

3.1.2.3.4 Estratos cruzados transladantes cavalgantes

Estes estratos são ditos “cavalgantes” porque concomitantemente à migração ocorre deposição de sedimentos (Hunter, 1977). Os estratos cavalgantes, ou *ripples* eólicas (*wind ripples*), são encontrados no dorso da duna, na face frontal da duna e nas interdunas secas. O ângulo de cavalgamento dos estratos é diretamente proporcional à taxa de deposição e inversamente proporcional à taxa de migração das marcas onduladas. De acordo com o ângulo de cavalgamento, os estratos cruzados transladantes podem ser subdivididos em subcríticos, críticos e supercríticos (Figura 5) (Hunter, 1977). Os estratos cruzados cavalgantes subcríticos são os mais comuns e constituem a estrutura mais útil para reconhecer estratos eólicos.

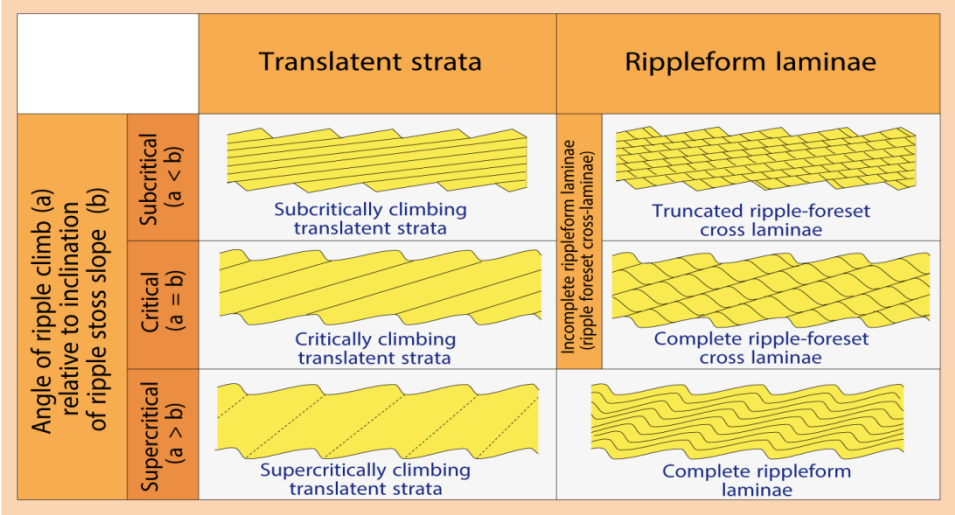

Figura 5: Classificação dos estratos cruzados transladantes em função do ângulo de cavalgamento (Modificado de Hunter, 1977).

Os estratos cavalgantes comumente apresentam gradação inversa (Figura 6). Tal feição deve-se à segregação de grãos durante a migração porque os grãos mais finos tendem a se acumular nas calhas das ripples enquanto os grãos mais grossos se concentram na crista (Sharp, 1963;

Fryberger & Schenk, 1988). Assim como a gradação inversa, a laminação finamente espaçada *pinstripe* (Figura 6) constitui uma feição diagnóstica de estratos eólicos. Esta feição é amplamente distribuída dos estratos eólicos e pode ocorrer em marcas onduladas, estratos de queda livre e estratos transladantes cavalgantes (Fryberger & Schenk, 1988).

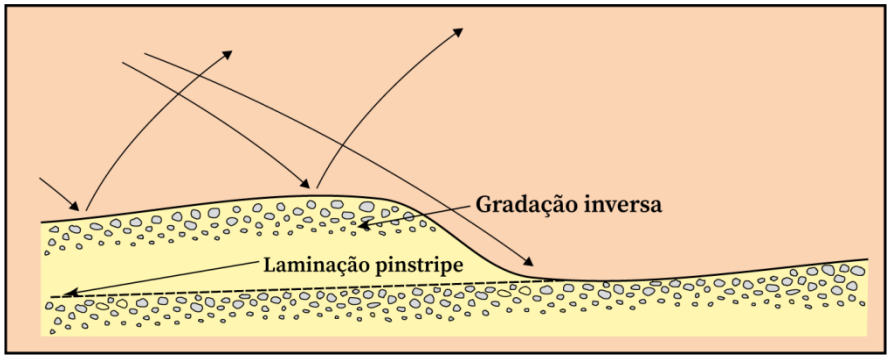

Figura 6: Modelo esquemático de geração de laminação *pinstripe* e gradação inversa. Os grãos grossos se concentram na crista enquanto os mais finos se localizam na base e formam a laminação *pinstripe* (Modificado de Fryberger & Schenk, 1988).

3.1.2.3.5 Estruturas de adesão

As estruturas de adesão são geralmente observadas em superfícies úmidas (Hummel & Kocurek, 1984; Kocurek & Fielder, 1982). A morfologia das estruturas de adesão varia amplamente (Figura 7). Os tipos mais documentados são: (i) *micro-cristas eólicas* (Hunter, 1969) renomeadas de marcas onduladas de adesão (Kocurek & Fielder, 1982) e; (ii) *domos de adesão* simétricos e assimétricos (Olsen *et al*., 1989). Segundo Hunter (1969), a adesão ocorre quando a areia seca, transportada por saltação, é aprisionada numa superfície úmida onde a franja capilar está alta. Os grãos se acumulam até que a franja capilar não consiga mais exercer efeito sobre os grãos. Se a deposição continuar, a superfície é progressivamente modificada e formam-se marcas onduladas de adesão (Figura 7). Olsen *et al*. (1989) destacam que a morfologia das marcas onduladas de adesão é herdada da topografia inicial. Enquanto, no experimento de Kocurek & Fielder (1982) as marcas onduladas se originaram a partir de uma superfície já ondulada por correntes subaquosas (Figura 7A), nas observações de Olsen *et al*. (1989) a superfície original era marcada por impressões de chuva (Figura 7B). Quanto aos domos de adesão (Figura 7D), Kocurek & Fielder

(1982) sugeriram que essas estruturas têm distribuição aleatória decorrente de fortes ventos com constante variação de sentido. Porém, os autores foram incapazes de reproduzir essas estruturas em laboratório. Segundo Olsen *et al*., (1989) os domos de adesão podem apresentar uma direção preferencial e são gerados com a diminuição progressiva da umidade, que ocorre devido ao rebaixamento do freático ou ao contínuo acúmulo de sedimentos. Conforme os autores, a heterogeneidade de umidade do terreno faz com que as cristas das marcas onduladas de adesão não avancem de forma uniforme, mas gere feições alongadas.

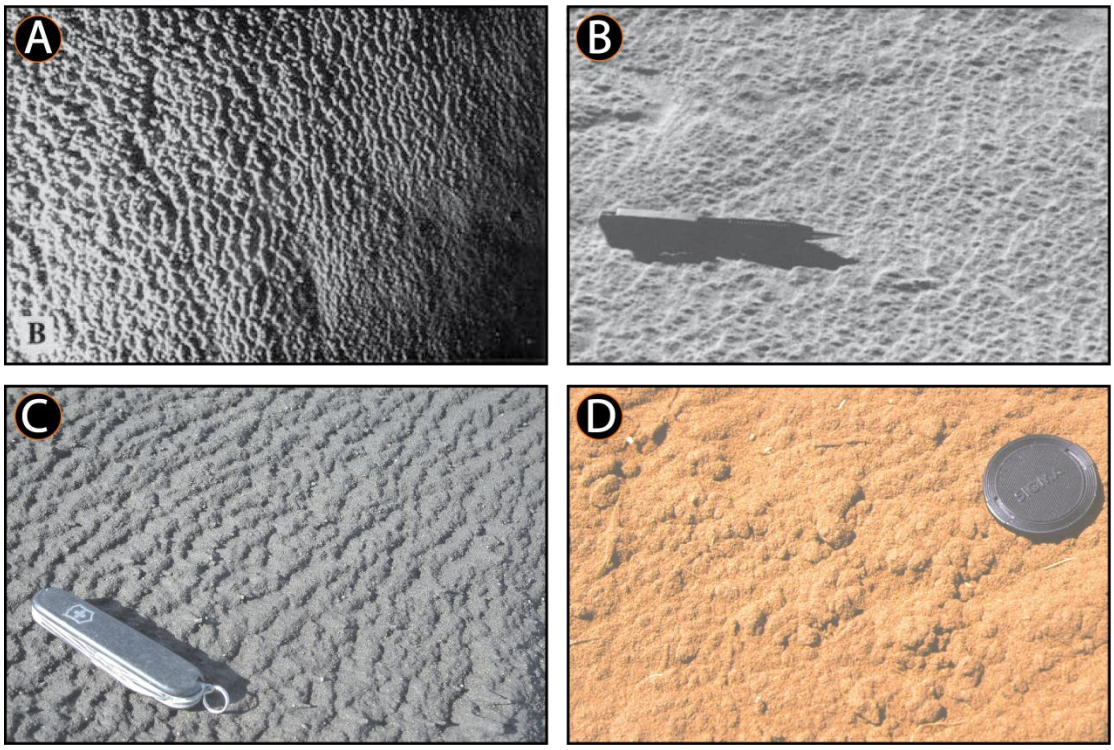

Figura 7: Estruturas de adesão. A) *Ripples* de adesão geradas experimentalmente sobre uma superfície saturada em água. A área de observação tem cerca de 20 cm (Kocurek & Fielder, 1982). B) *Ripples* de adesão com relevos na face frontal. Caneta com 13 cm e indicando a direção do vento. C) Migração de *ripples* de adesão. D) Domos de adesão (Mountney, 2006).

Morfologicamente as marcas onduladas de adesão possuem cristas retas ou sinuosas e faces de deslizamento íngremes ou verticais enquanto os domos de adesão formam protuberâncias com orientação caótica (Kocurek & Fielder, 1982) ou paralela à direção do vento (Olsen *et al*., 1989). No registro, as marcas onduladas de adesão normalmente formam lâminas planas, mas a microtopografia pode ser preservada (Kocurek & Nielson, 1986). Os domos

de adesão, por sua vez, costumam ser bem preservados e podem ser observados em planta.

3.1.2.3.6 Estruturas deformacionais

O estudo de estruturas deformacionais em estratos eólicos é de enorme valia na geologia do petróleo devido ao efeito da deformação na modificação da porosidade e permeabilidade do reservatório. A deformação da estrutura primária de uma duna ocorre em sedimentos inconsolidados e é causada por tensão de cisalhamento ou aumento da pressão de poros na areia (McKee *et al*., 1971; Loope *et al*., 2001). A deformação pode ser induzida por processos sin-deposicionais (Mckee *et al*., 1971; Bigarella *et al,* 1969; Bigarella, 1975;) ou por processos pós-deposicionais como transgressões marinhas (Glennie & Buller, 1983; Kamola & Chan, 1988) ou atividade sísmica (Horowitz, 1982; Plaziat & Poisson, 1992; Moretti, 2000).

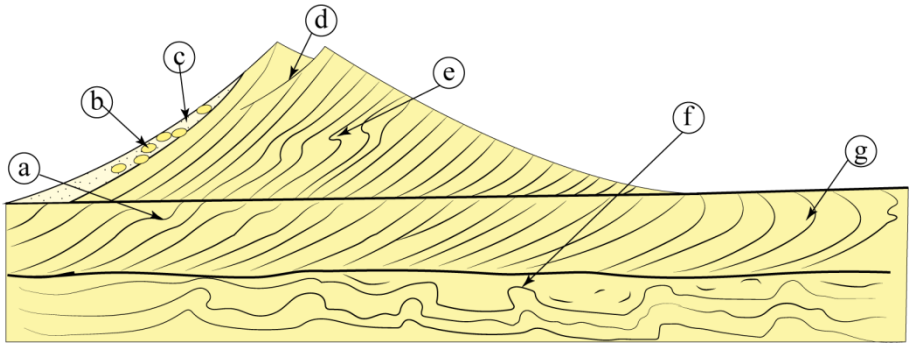

Figura 8: Diagrama esquemático indicando a posição e os tipos de deformação: a) Contorção na base da duna devido à carga da duna sobre o substrato; b) Escorregamento e dobramento de estratos não coesos; c) Brecha e *slumping* de estratos coesos; d) Fraturamento devido a comportamento dúctil de sedimentos coesos; e) Dobras recumbentes nos estratos dentro da duna; f) Contorção de sedimentos pré-depositados devido à sobrecarga (fluidização) e; g) Dobramento de sedimentos saturados devido ao avanço da duna.

Estruturas deformacionais sin-deposicionais ocorrem na face frontal da duna pela avalanche de grãos (Figura 8) (Mckee *et al*., 1971). A deformação por avalanche se caracteriza por contorção, obliteração da estrutura primária ou dos planos de cisalhamentos. As estruturas de contorção são geradas por tensão e compressão durante o movimento dos sedimentos (Doe & Dott, 1980). Os planos de cisalhamentos podem se desenvolver na parte inferior ou superior da face frontal da duna dependendo da distância percorrida durante o deslizamento dos grãos. O grau de obliteração da estrutura original é proporcional ao grau de coesão entre os grãos. Cabe ressaltar que os

sedimentos secos e saturados em água são caracterizados por ausência de coesão (Mckee *et al*., 1971). Nos sedimentos secos a falta de coesão se deve ao ar presente nos espaços intergranulares enquanto nos sedimentos saturados em água os espaços intergranulares são preenchidos por água. Nos dois casos o atrito entre os grãos é baixo e os grãos se movimentam individualmente. Como resultado desse fluxo de grãos, a estrutura original pode ser totalmente modificada (Mckee *et al*., 1971). Porém, quando os sedimentos são umedecidos (e.g. por causa da chuva; Loope *et al*., 2001) a água causa aumento da coesão entre os grãos. Durante a deformação os grãos se movimentam como uma massa e a estrutura primária tende a ser preservada. Esse tipo de deformação é denominado de *slumping* (Mckee *et al*., 1971).

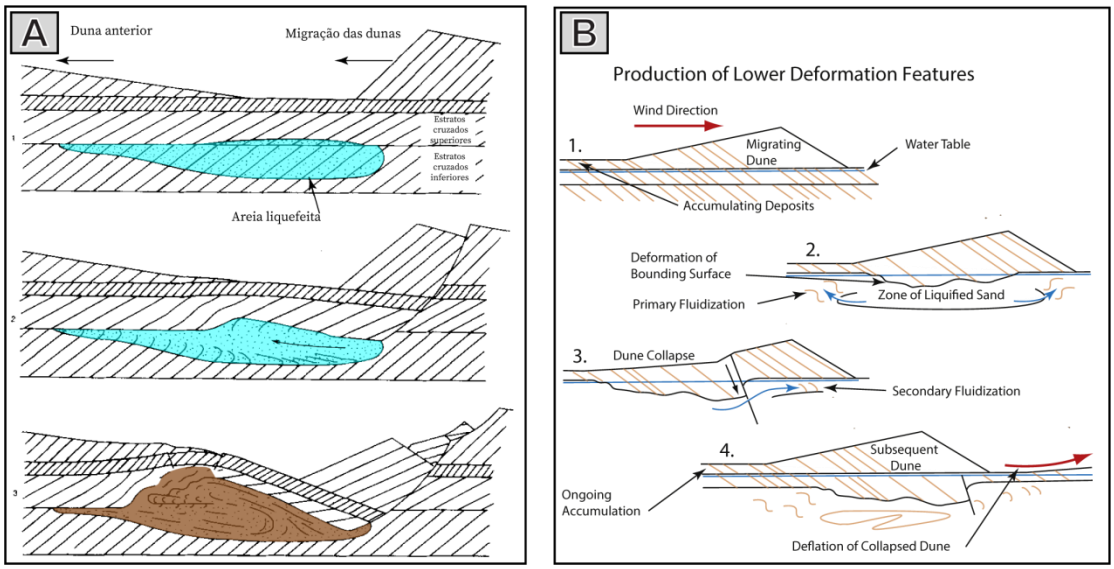

Figura 9: Reconstrução de eventos causando falhamentos e dobramentos de grande escala. A) Sedimentos saturados são liquefeitos por um terremoto e a parte frontal da duna desmorona comprimindo a areia saturada (Modificado de Horowitz, 1982). B) Deformação causada por freático alto. Uma parte da duna afunda num substrato fluidizado e é subsequentemente erodido por uma duna em migração (Extraído de Bryant & Miall, 2010).

Os processos deformacionais pós-deposicionais podem ser observadas em várias posições da duna (Figura 8). A migração de uma duna sobre uma interduna encharcada pode gerar instabilidades e ocasionar a fluidização dos estratos acumulados. Durante transgressões marinhas os estratos eólicos podem ser deformados devido ao retrabalhamento pelas ondas de tempos normais ou de tempestades (Glennie & Buller, 1983). A

atividade tectônica é outro agente potente de deformação da estrutura, porém difícil de identificar uma vez que, para determinar com confiança a deformação foi causada por atividade sísmica é preciso descartar todos os mecanismos sedimentares e identificar o epicentro e a distância alcançada pelas ondas sísmicas. (Moretti, 2000). Falhamentos e dobramentos de grande escala podem ocorrer nos estratos eólicos, principalmente quando o nível do freático é alto. Devido ao peso da duna em migração, a pressão hidrostática aumenta e, como consequência, uma parte da duna ativa afunda (Figura 9).

3.1.2.3.7 Outras estruturas sedimentares

Fraturas poligonais, impressões de chuva, marcas onduladas simétricas ou assimétricas subaquosas, assim como estratificações cruzadas subaquosas e laminações onduladas truncadas constituem estruturas originadas por processos não eólicos, mas que podem ser encontrados em sistemas eólicos, especialmente nos sistemas eólicos costeiros onde as interações com ambientes marinhos são comuns (Kocurek & Hunter, 1986; Ahlbrandt *et al*., 1978; Langford, 1989). Estruturas de origem química, derivadas de precipitação e evaporação, bem como estruturas biogênicas (pegadas, bioturbações) e paleossolos também podem ser observados (Ahlbrandt *et al*., 1978; Loope, 1988; Kocurek *et al*., 1991; Kamola & Chan, 1988). A obliteração da estrutura primária em dunas pode ainda ser causada pela penetração de raízes de plantas que crescem na duna. Casos similares foram relatados em dunas costeiras do Brasil (Mckee & Bigarella, 1972; Bigarella, 1975).

3.1.3 Elementos Arquiteturais

O campo de duna pode ser dividido em função dos seus elementos morfológicos. Os elementos morfológicos ou arquiteturais resultam da migração das formas de leito e do arranjo interno das estruturas. Este subcapítulo apresenta e discute o desenvolvimento dos principais elementos arquiteturais encontrados em um sistema eólico (Figura 10). Os elementos arquiteturais dos sistemas eólicos são: Dunas, Interdunas, Lençóis de areias e Sabkhas, quando existem.

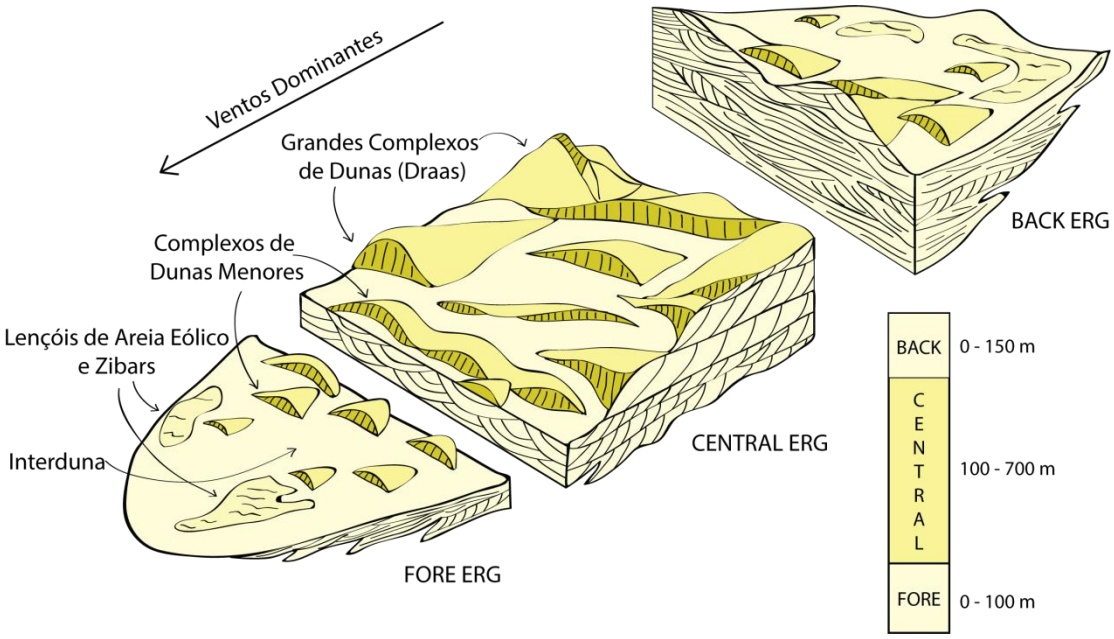

Figura 10: Modelo de migração de *erg*/campo de dunas. A divisão é baseada na escala das formas de leito eólicas. O modelo ilustra os elementos arquiteturais presentes num campo de dunas e a variação morfológica das formas de leito (Modificado de Porter, 1986).

3.1.3.1 Dunas

A duna é um elemento arquitetural característico do sistema eólico. A duna é constituída no seu dorso por *ripples* eólicas e internamente por estratos cruzados depositados na face frontal durante a migração da forma de leito.

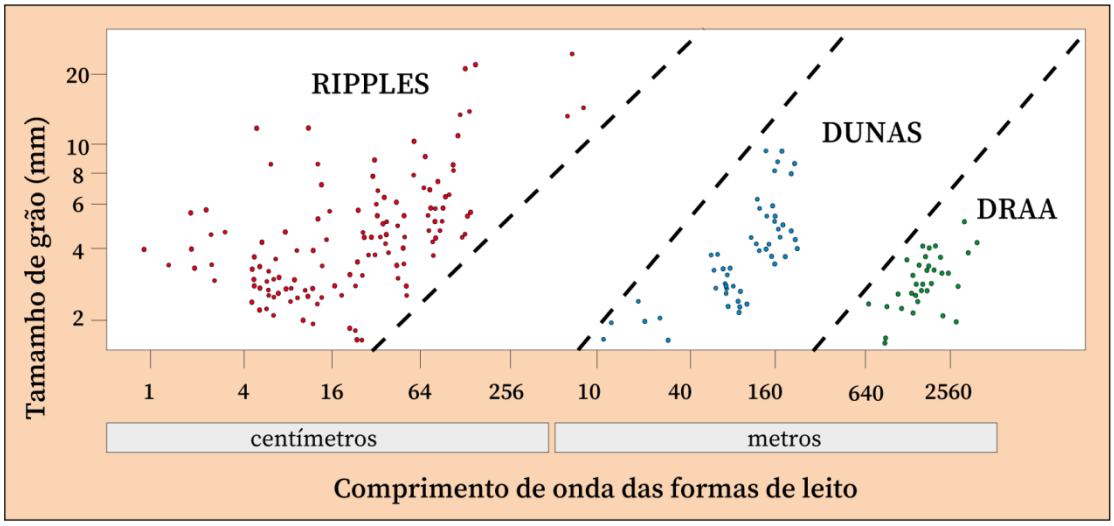

Figura 11: Gráfico de tamanho de grão e comprimento de ondas. Nota-se que não existem formas de leito intermediárias entre os três grandes grupos: ripples, dunas e draa (Modificado de Wilson, 1972).

Usando como critério de classificação o comprimento de onda, Wilson (1971) sugere que existem três hierarquias de formas de leitos eólicos: as

marcas onduladas eólicas (0,01 a 10m), as dunas (10 a 500m) e os *draas* (500 a 5000m) (Figura 11). O *draa* é caracterizado por dunas migrando no dorso ou na face frontal e constitui a forma de leito de maior escala (Kocurek, 1981).

As dunas podem ser classificadas em função da morfologia (Mckee, 1966; Mckee & Bigarella, 1979) ou da morfodinâmica (Hunter *et al*., 1983). A classificação morfológica leva em consideração características geométricas como sinuosidade da linha de crista, número de faces de deslizamento e presença ou ausência de dunas superpostas (Figura 12A). Segundo esses critérios existem: (i) dunas crescentes, quando existe apenas uma face frontal com relevo acentuado e o dorso tem um mergulho suave; (ii) dunas lineares, que são simétricas e apresentam cristas retas ou onduladas e; (iii) dunas estrelas, que têm três ou mais faces frontais e cujas cristas partem de um ou dois picos centrais. As dunas crescentes são formadas em condições de ventos unidirecionais enquanto dunas lineares resultam de ventos bidirecionais e dunas estrelas indicam regime de ventos multidirecionais (Hunter *et al*., 1983).

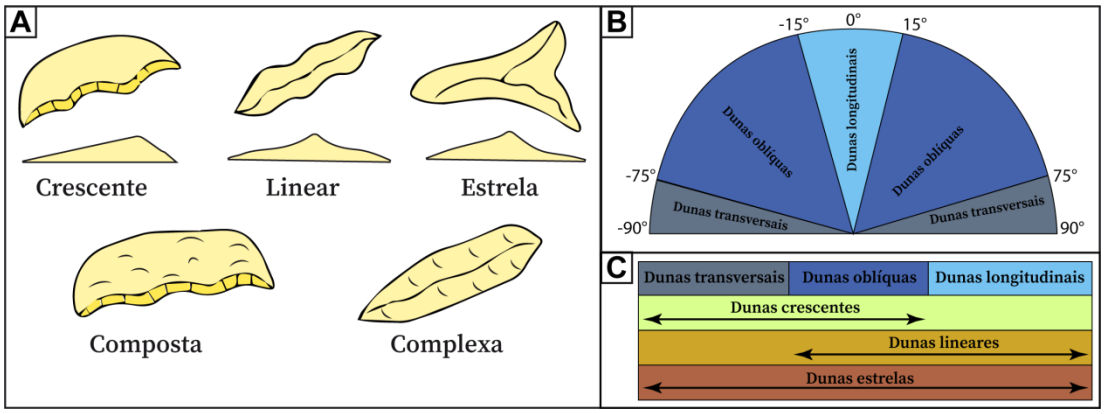

Figura 12: Classificação de dunas. (A) Tipos morfológicos de dunas. Cortes transversais e vistas em planta de dunas simples, compostas e complexas. (B) Tipos morfodinâmicos de dunas eólicas baseados na orientação da linha de crista em relação ao vetor médio dos ventos. (C) Comparação entre os tipos morfodinâmicos e morfológicos (Modificado de Kocurek, 1991).

Cabe ressaltar que existem nomes mais específicos para dunas com morfologias peculiares como: (i) dunas barcanas, para dunas concêntricas com pontas orientadas a favor do vento (Bagnold, 1941); (ii) dunas *Seif*, quando uma das pontas da duna é mais comprida (Lancaster, 1980; Tsoar, 1984); (iii) dunas barcanóides, quando dunas barcanas coalescem e formam

cristas sinuosas; (iv) dunas parabólicas, com forma em U e pontas voltadas contra o vento (Anthonsen *et al*., 1996; Tsoar & Blumberg 2002); (v) dunas *Hummock*, com formato irregular e parcialmente imobilizadas (Hesp, 1981; Pye & Tsoar, 2009); (vi) dunas dômica, de baixo relevo e relativamente aplainadas (Mckee and Bigarella, 1979) e; (vii) dunas zibar, associados a sedimentos grossos e caracterizadas por pela ausência de face de deslizamento (Wilson, 1973; Nielson & Kocurek, 1986; Kocurek & Nielson, 1986).

A classificação morfodinâmica considera a orientação da crista da duna em relação à direção de vento predominante (Figura 12B). As dunas podem ser longitudinais, quando a linha de crista é orientada paralelamente ao vento; oblíquas, quando a crista apresenta ângulo de 15 a 75° em relação ao vento e transversais, quando a linha de crista tem orientação praticamente ortogonal ao vento (Hunter *et al*., 1983; Kocurek, 1991).

As dunas parabólicas constituem o tipo de duna mais comumente encontrado em ambientes úmidos e vegetado (Bigarella, 1975). Dunas parabólicas têm formas em U ou V em vista em planta, são formadas por ventos unidirecionais e são caracterizadas por extremidades alongadas e parcialmente estabilizadas pela vegetação (Price, 1950; Pye, 1982). Se houver redução da cobertura vegetal, as dunas parabólicas podem evoluir para dunas transversas ou barcanóides (Hack, 1941), e inversamente quando houver aumento da vegetação (Tsoar & Blumberg, 2002; Anthonsen *et al*., 1996). A transformação de uma duna transversa em parabólica pode ser realizada através de 3 mecanismos : 1) quando o pé ou os braços da duna encontram uma área úmida ou vegetada que bloqueia seu avanço (Figura 13A) (Pye, 1982), 2) por "*blowout*", quando a deflação eólica cava depressões circulares ou alongadas no dorso da duna (Figura 13B) (Pye, 1982; Hesp & Hyde, 1996; Hesp, 2002) ou; 3) quando a vegetação coloniza a crista da duna (Tsoar & Blumberg, 2002). Nesses mecanismos a vegetação age como uma âncora, imobilizando a frente da duna enquanto a erosão do dorso da duna muda progressivamente a geometria da duna, de convexa para côncava (Hesp, 2002; Tsoar & Blumberg, 2002).

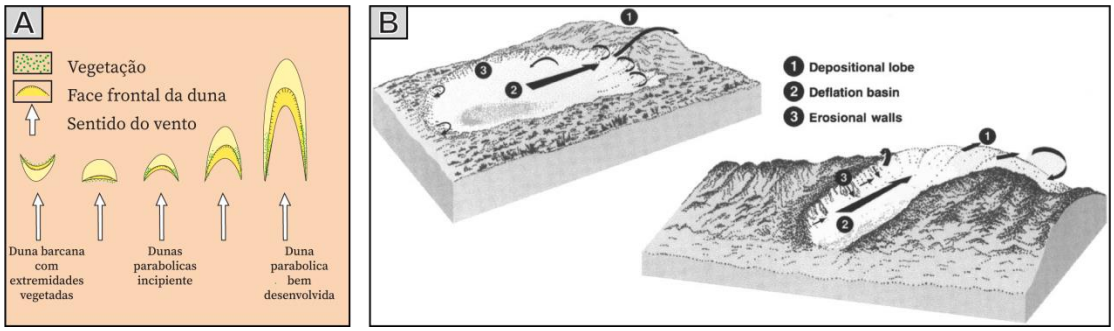

Figura 13: Formação de dunas parabólicas. A) Uma duna barcana pode evoluir para parabólica se os braços forem vegetados (Modificado de Pye, 1982). B) Por causa de ventos muito fortes, se forma um *blowout* no dorso da duna deixando apenas os braços ancorados (Extraído de Hesp 2002).

3.1.3.2 Interduna

As interdunas são depressões ou planícies localizadas entre duas dunas. A geometria da interduna é controlada pela morfologia e o espaçamento entre as dunas adjacentes (Mckee & Moiola, 1975; Ahlbrandt & Fryberger, 1981). O espaçamento depende da saturação em areia do sistema. Segundo Wilson (1971), existem três tipos de sistemas eólicos dependendo do grau de saturação em areia do sistema (Figura 14). Nos sistemas subsaturados não há deposição de areia nem geração de formas de leito, em sistemas metassaturados a cobertura de areia é incompleta e em sistemas saturados a cobertura de areia é total, ocorrendo, neste caso, cavalgamento de dunas/draas e interdunas secas. Nos sistemas metassaturados as interdunas são extensas enquanto nas regiões saturadas as interdunas são pequenas e restritas entre a face frontal de uma duna e o dorso da duna subsequente. As interdunas secas são típicas de regiões de ventos saturados, enquanto as interdunas encharcadas e úmidas costumam ser encontradas em regiões de ventos metassaturados.

Segundo Ahlbrandt & Fryberger (1981) as interdunas podem ser classificadas em deflacionárias ou deposicionais dependendo do processo predominante. Em interdunas deflacionárias ocorre remoção de sedimentos e formação de *lag* residual, com grânulos e clastos facetados. Quando a erosão atinge o freático, formam-se *ripples* de adesão. As interdunas deposicionais podem ser secas, encharcadas ou úmidas.

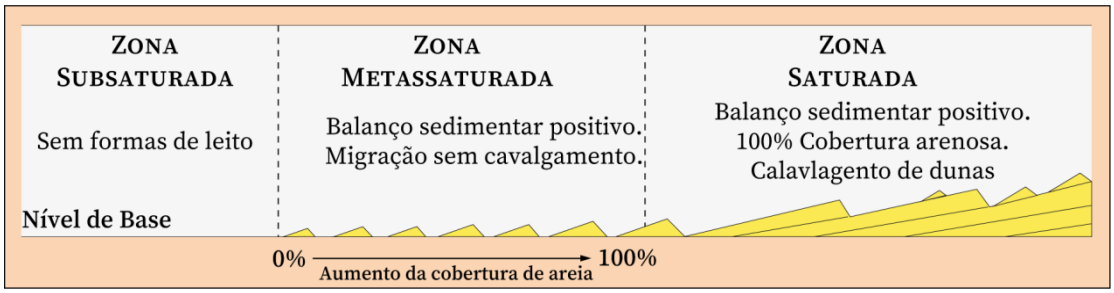

Figura 14: Seção esquemática de um campo de duna com interdunas secas. As dunas se expandem até eliminar as interdunas (Baseado em Wilson, 1971).

A interduna é dita seca quando a deposição de areia não é influenciada pela umidade (Figura 14). As interdunas secas são dominadas por marcas onduladas eólicas (transladantes cavalgantes e de grânulos), estratos horizontais e por vezes *lags* de deflação (Ahlbrandt & Fryberger, 1981). Como a umidade é baixa nessas regiões a cobertura vegetal e o grau de bioturbação são mínimos (Mountney, 2006).

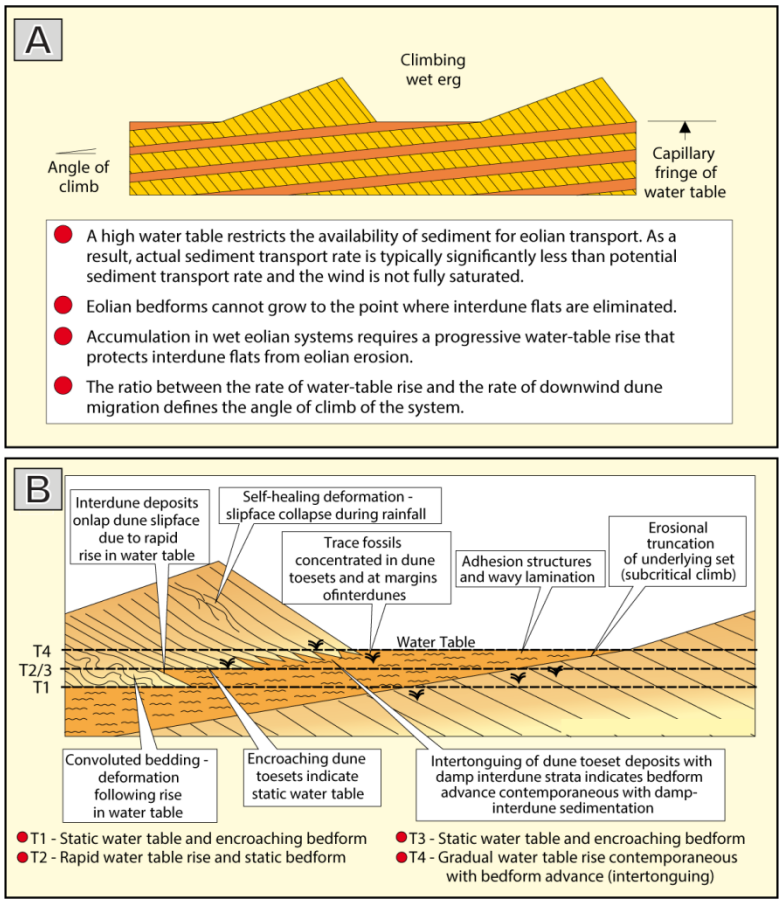

Figura 15: Interdunas úmidas. A) O nível do freático controla a sedimentação (Modificado de Mountney & Jagger, 2004). B) interação entre duna e interduna (Extraído de Mountney, 2006).

A interduna é considerada encharcada quando a superfície de deposição se encontra em contato com o nível do freático ou sua franja capilar, de tal forma que a sedimentação é influenciada pela umidade da superfície (Figura 15A) (Mountney, 2006). As interdunas encharcadas são caracterizadas por estruturas de adesão (Kocurek & Fielder, 1982), precipitação de evaporitos (Ahlbrandt & Fryberger, 1981; Kocurek, 1981) e/ou fraturas poligonais (Kocurek & Hunter, 1986). Nessas interdunas, podem ocorrer também bioturbações e marcas de raízes dado que a umidade do terreno favorece o crescimento de plantas e a proliferação de organismos (Ahlbrandt *et al*., 1978, Hummel & Kocurek, 1984; Loope, 1988)

Nas interdunas úmidas o nível do freático sobe até ou acima da superfície de deposição, de tal maneira que a interduna é periodicamente ou constantemente inundada (Figura 15B) (Crabaugh & Kocurek, 1993; Mountney, 2006). Por vezes ocorrem carbonatos e sais evaporíticos na interduna úmida (Kocurek, 1981).

3.1.3.3 Lençóis de areia

Os lençóis de areia são áreas cobertas por areia eólica, onde não se encontram formas de leitos de alto relevo e faces de deslizamento bem desenvolvidas (Fryberger *et al*., 1979). Segundo Kocurek & Nielson (1986) o desenvolvimento dos lençóis de areia é controlado por uma série de fatores que reduzem a disponibilidade de areia para a construção de dunas. Esses fatores incluem a altura do freático e da franja capilar, a cimentação ou coesão dos grãos, a frequência de inundações, o tamanho de grão predominante e a extensão da cobertura vegetal. As estruturas mais comumente encontradas nos lençóis de areia modernos são as marcas onduladas eólicas arenosas e de grânulos (Fryberger & Schenk, 1981; Fryberger *et al*., 1992).

3.1.3.4 Sabkha

O termo *Sabkha* representa áreas relativamente planas, episodicamente inundadas, e caracterizadas por extensa precipitação de evaporitos (Kinsman, 1969). A precipitação de sal requer inundação e subsequente ressecamento da área. A inundação pode ser causada por

elevação do nível freático (Crabaugh & Kocurek, 1993), transgressões marinhas (Fryberger *et al*., 1983) ou inundações fluviais (Langford, 1989).

Os *sabkhas* costeiros se formam no horizonte de máxima invasão marinha que corresponde geralmente à superfície de maré alta. Por esta razão, os sabkhas costeiros são por vezes chamados de evaporitos de supra-maré (Kinsman,1969). Existem várias regiões do globo onde predomina o clima árido, mas nem todos esses locais são favoráveis à precipitação de evaporitos. Esta limitação na distribuição geográfica dos evaporitos se deve ao fato que além do critério climático, há um requisito fisiográfico para possibilitar a precipitação (Kinsman,1969). O *sabkha* deve ser desconectado da água do mar por uma barreira topográfica para permitir o aumento da concentração dos sais na salmoura e evitar a diluição.

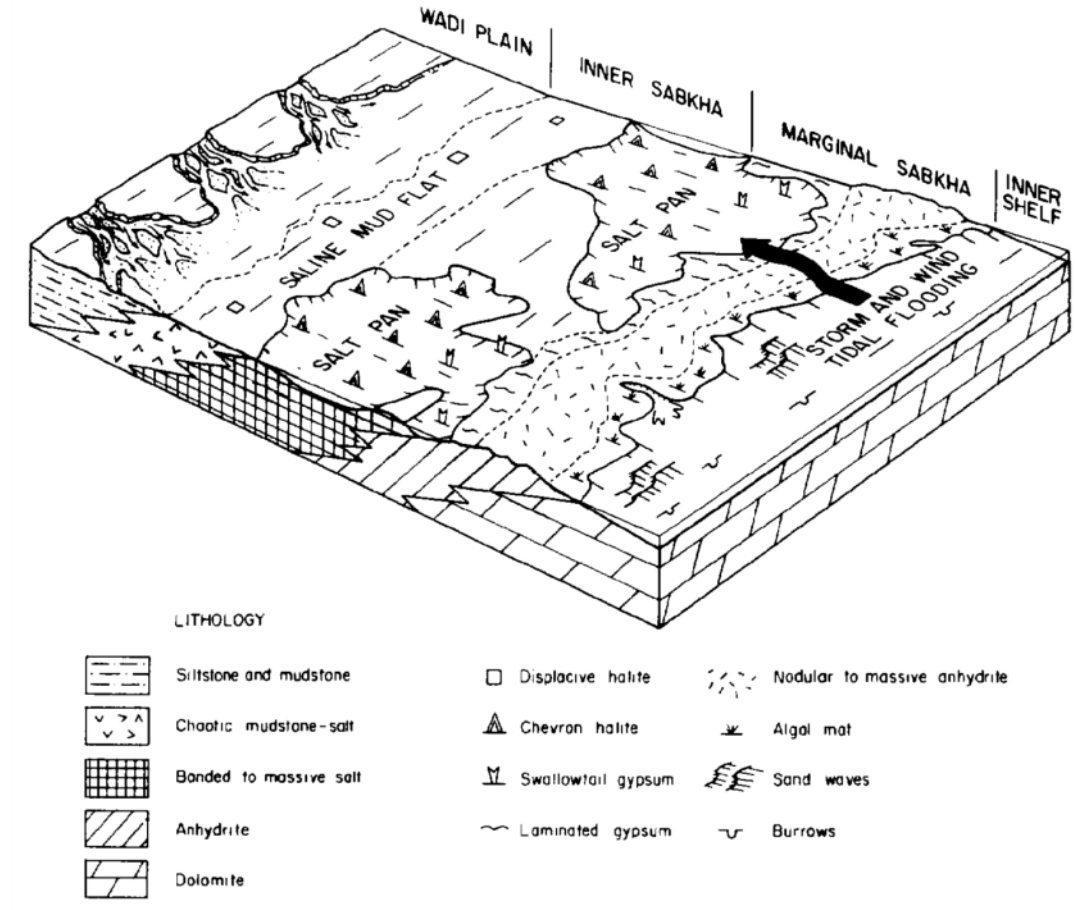

Figura 16: Modelo esquemático de *sabkha* com planície aluvial (Extraído de Handford, 1981).

A formação da salmoura depende diretamente da taxa de evaporação, que se caracteriza pela razão entre a perda de água por evaporação e a diluição do fluido. Com o aumento da taxa de evaporação inicia a

precipitação dos primeiros minerais evaporíticos que serão, subsequentemente, substituídos por nova associação mineralógica mais estável com as novas condições climáticas e químicas do fluido. Os primeiros minerais a precipitar são cristais de aragonita e/ou dolomita seguidos de gipsita e/ou anidrita na margem do sabkha. Na porção interna do sabkha, precipita halita, enquanto na porção continental do sabkha podem ocorrer sistemas fluviais efêmeros e planícies de inundação (Figura 16) (Handford, 1981).

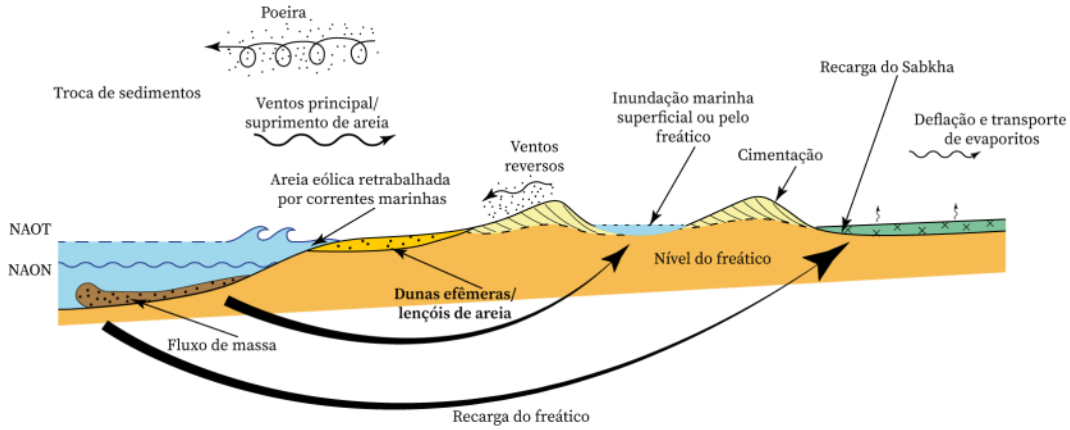

Figura 17: Modelo de interação marinha-eólica (Modificado de Chan & Kocurek, 1988).

3.1.4 Interações entre o campo de duna e os sistemas deposicionais adjacentes

As margens dos campos de dunas são geralmente caracterizadas por interações com sistemas fluviais ou com o mar (Figura 17). Essas interações podem favorecer a construção dos campos de dunas através do suprimento de sedimento, da cimentação precoce e/ou preservação da paleomorfologia. No entanto, essas interações podem também ocasionar a erosão do campo de duna ou a redução da disponibilidade de sedimentos pela subida do freático (Chan & Kocurek, 1988).

Do ponto de vista econômico, a interação entre o campo de duna e os sistemas deposicionais adjacentes resulta em sucessões estratigráficas marcadas por heterogeneidades litológicas e petrofísicas (Figura 18), onde os depósitos fluviais, lacustres ou marinhos de baixa permeabilidade atuam como selos do reservatório (Fryberger *et al .,* 1983*;* Fryberger *et al.,* 1990).

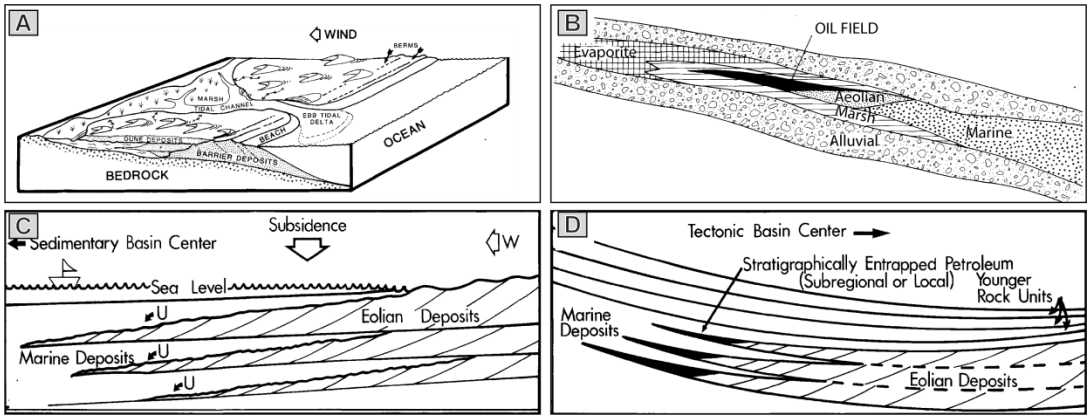

Figura 18: Exemplo de sistema petrolífero associado a sistema eólico costeiro. A) Avanço das dunas costeiras sobre canais e planícies de maré. B) Modelo hipotético de *trap* e selo em sistema eólico costeiro (Fryberger *et al.,* 1990). C) Progradação de dunas eólicas sobre sedimentos marinhos. Observam o contato erosivo durante transgressões marinhas. D) A seção estratigráfica é basculada pela tectônica e favorece acumulação de petróleo (Fryberger *et al.,* 1983).

3.1.4.1 Interações com o ambiente marinho

O registro geológico está repleto de exemplos de depósitos eólicos costeiros interdigitados com depósitos marinhos. Dos inúmeros exemplos documentados podemos citar as formações Morgan (Driese & Dott, 1984), Rico e Cedar Mesa (Loope, 1984, 1985; Jordan & Mountney, 2010), Minnelusa (Fryberger, 1984) e Page (Eschner & Kocurek, 1986) nos Estados Unidos; Rotliegend-Weissliegend (Glennie & Buller, 1983), Escucha e Utrillas (Rodríguez-López *et al.*, 2008; Rodríguez-López *et al.,* 2012) na Europa; e Agrio (Veiga *et al*., 2002) na América latina. Existem inúmeros exemplos modernos de interação entre sistemas eólicos e os ambientes marinhos adjacentes. A maioria desses ocorre em ambientes plataformais dominados por ondas, mas existem poucos exemplos de interação eólica com marés. Os principais exemplos deste tipo são documentados no deserto do Qatar e o estuário *Ojo de Liebre* na Península da Baixa Califórnia (Figura 19).

O contato entre depósitos eólicos e depósitos marinhos sobrepostos pode representar um hiato indicando destruição do campo de duna. Esta superfície é geralmente caracterizada por uma base erosiva ou fraturas poligonais (Chan & Kocurek, 1988), e é gerada pela deflação do campo de duna. Com a subida do nível do mar, ocorre simultaneamente a subida do freático e, como consequência, a migração da duna é freada e as dunas

podem ser aprisionadas no meio da água (Figura 19D) e progressivamente deflacionadas (Stokes, 1968).

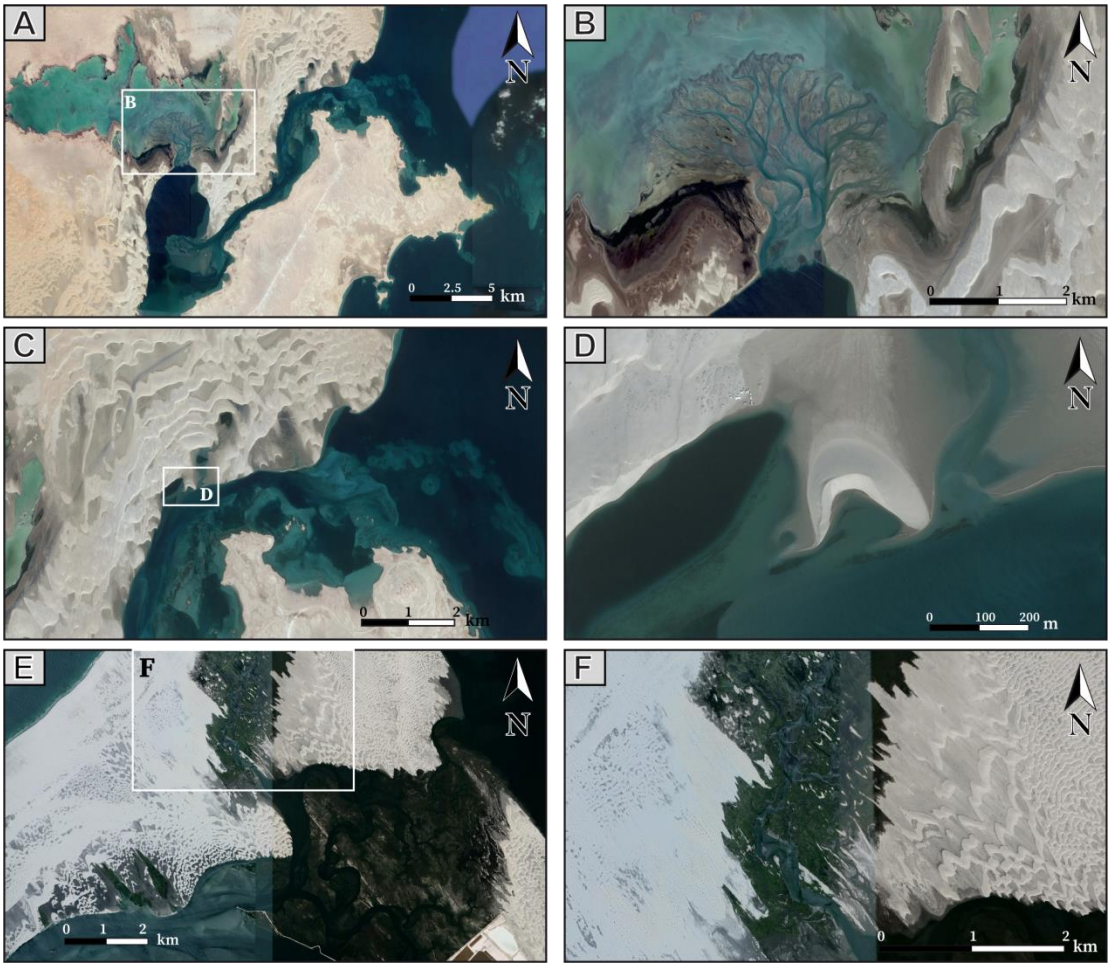

Figura 19: Interação do campo de duna eólico com marés. A) Região sudeste do deserto do Qatar mostrando interação do deserto com o Golfo Pérsico. B) Zoom de imagem A) mostrando um delta de maré enchente. C) Campo de duna interagindo com o Golfo Pérsico. D) Zoom da imagem C) mostrando uma duna ilhada no meio da água. E) Campo de duna interagindo com marés na Baixa Califórnia. F) Zoom da imagem E) mostrando canais de marés e planície de maré entre as dunas.

A interação entre o campo de duna e o mar é materializada por feições de retrabalhamento marinho nos estratos eólicos (e.g. estruturas de fluidização e de escape de fluido, estruturas de cargas) e/ou a ocorrência de estruturas geradas por processos marinhos interdigitadas com depósitos eólicos (Chan & Kocurek, 1988). Quando as ondas constituem o processo predominante, depositam-se estratos característicos de fluxo oscilatório como *wave* ripples ou laminações onduladas truncadas *hommocky* ou *swaley* (Glennie & Buller, 1983; Blakey *et al.,* 1996; Chakraborty & Sesarma, 2008; Jordan & Mountney, 2010). Por outro lado, quando a maré for o principal

processo, observam-se drapes de lama no pé da duna, concentração de matéria orgânica nos *forsets* ou marcas onduladas assimétricas em sentidos opostos sugerindo marés enchente e vazante (Fryberger *et al.,* 1990; Rodrígues-López *et al.,* 2012). Já na margem do campo de duna podem se desenvolver planícies de maré, *sabkha* ou canais de marés.

3.1.4.2 Interações Fluvio-eólicas

Nas últimas décadas, as interações flúvio-eólicas têm sido amplamente estudadas através da observação de análogos modernos (e.g. Langford, 1989; Al-Masrahy & Mountney, 2015, Langford & Chan, 1989; Chakraborti & Chaudhuri, 1993; Veiga *et al*., 2002).

Os sistemas fluviais localizados na margem dos campos de dunas podem ser permanentes, intermitentes ou efêmeros (Figura 20). O impacto das drenagens fluviais no campo de duna depende principalmente do quão as drenagens conseguem penetrar o campo de duna. A distância percorrida pelas drenagens é controlada: (1) pelo tipo morfológico de dunas; (2) pela orientação das dunas em relação às drenagens; (3) pela morfologia das interdunas, isso é: o comprimento, a largura e a continuidade lateral das interdunas; (4) pela taxa de migração das dunas eólicas; e (5) pela frequência e a intensidade das inundações fluviais (Langford, 1989; Al-Masrahy & Mountney, 2015). Os sistemas fluviais alcançam uma maior distância dentro do campo de duna quando a direção das drenagens for paralela à linha de crista das dunas e as dunas forem de cristas retas, regularmente espaçadas e com interdunas amplas e planas.

As dunas com alta sinuosidade atuam como barreiras e podem ocasionar a bifurcação das drenagens. Quando a drenagem incide perpendicularmente à linha de cristas, ela é reorientada, forma corpos de água (Figura 20A) ou infiltra e seca durante o percurso (Figura 20B). O tipo e o espaçamento das interdunas dependem do grau de saturação do sistema. Em sistemas saturados a distância alcançada pelas drenagens é relativamente baixa porque as interdunas são pouco espaçadas e a taxa de infiltração é elevada.

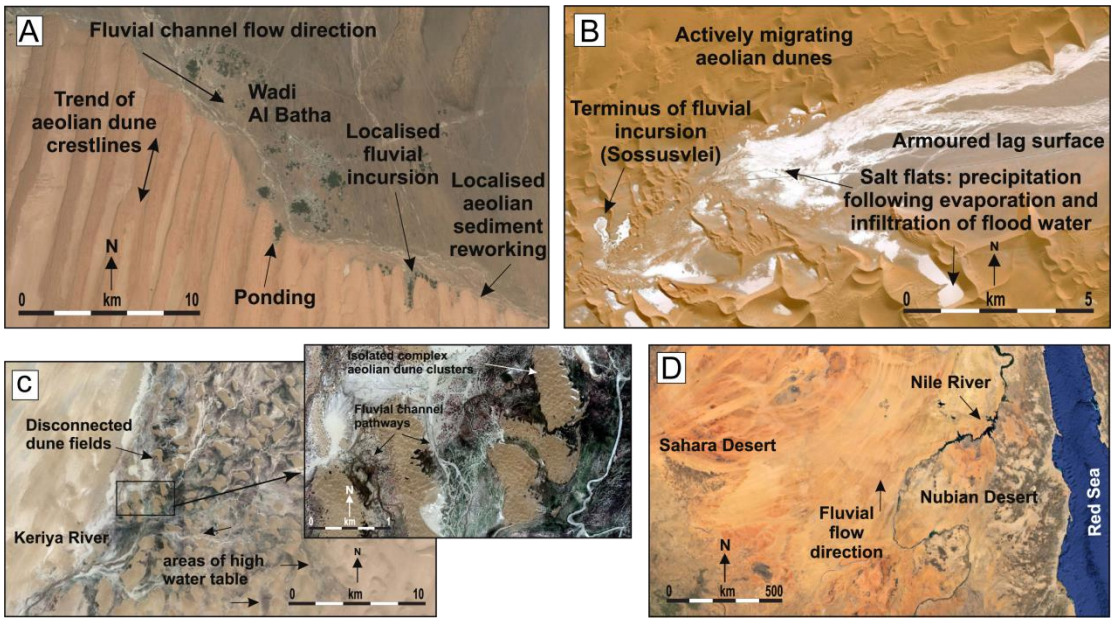

Figura 20: Interações fúlvio-eólicas. A) Sistema fluvial orientado perpendicularmente à linha de crista das dunas. Observam a formação de corpos de água e as invasões localizadas. Campo de dunas Wahiba, Oman. B) Contração de parte do erg por causa da invasão fluvial. A evaporação da água gera Playas. Deserto do Namibe, Namíbia. C) Inundação fluvial e desconexão de parte do campo de dunas. Deserto Taklamakan, China. D) Exemplo de sistema fluvial atravessando o campo de duna inteiro. Leste do Deserto do Saara. As imagens A), C) e D) são de campos de dunas continentais e servem de ilustração para casos que podem ocorrer em sistemas eólicos costeiros (Al-Masrahy & Mountney, 2015).

A taxa de migração das dunas e a frequência das inundações fluviais são fatores antagonistas que controlam a expansão ou contração do campo de duna. Com o aumento da frequência e intensidade das inundações ocorre a subida do nível do freático e as interdunas evoluem de secas para encharcadas e até úmidas. Consequentemente, as dunas se desconectam e, ficam isoladas no meio das drenagens (Figura 20C) reduzindo o potencial de migração das dunas. Inversamente, durante períodos secos o freático é rebaixado e, as dunas migram sobre os depósitos fluviais (Mountney, 2006b). Em alguns casos no entanto, o rio consegue atravessar o campo de duna inteiro. Como exemplos, destaca-se o Rio Nilo que separa o deserto do Saara do deserto da Núbia (Figura 20D).

As feições características da invasão do campo de duna por correntes fluviais são as erosões localizadas do pé das dunas, a deposição de estratos com estruturas subaquosas, a deposição de pelitos de planícies de inundação, a interdigitação dos estratos fluviais com o pé de duna e as

deformações de sedimentos inconsolidados (Langford & Chan, 1989; Clemmensen *et al*., 1989; Chakraborti & Chaudhuri, 1993; Tisgaard & Oxnevad,1998; Veiga *et al*., 2002).

3.2 ACUMULAÇÃO

Na análise do registro sedimentar o sistema eólico é visto como um volume dinâmico em que o balanço sedimentar é determinado pelo fluxo de sedimentos (Mainguet & Chemin, 1983). A entrada de sedimentos é uma função do suprimento sedimentar e da capacidade de transporte do fluxo, e a saída de sedimentos depende das mudanças espaciais e temporais desse volume (Kocurek & Havholm, 1993). Segundo Mainguet & Chemin (1983), quando a entrada de sedimentos supera a saída, o balanço sedimentar é positivo, e quando a entrada é inferior à saída o balanço é negativo. Um balanço positivo acarreta na migração e cavalgamento das dunas, possibilitando a acumulação do campo de dunas. A acumulação eólica é o resultado da deposição total de sedimentos com o passar do tempo, gerando um corpo tridimensional de estratos que pode ser incorporado no registro geológico (Kocurek & Havholm, 1993). A superfície de acumulação é uma superfície plana que liga as calhas das dunas, de modo que, os sedimentos acima são considerados em transporte e os abaixo estão fora da ação do vento (Figura 21A). Para que ocorra acumulação é necessário que o ângulo de cavalgamento das dunas seja positivo em relação à superfície de acumulação (Rubin & Hunter, 1982) possibilitando a incorporação dos estratos eólicos no registro (Rubin & Hunter, 1983). O ângulo de cavalgamento é definido pela razão entre a taxa de migração das formas de leito e a taxa de subida relativa da superfície de acumulação, de tal forma que, o ângulo de cavalgamento pode ser subcrítico, crítico ou supercrítico (Figura 21B) (Hunter, 1977). Em sistemas secos a taxa de subida relativa da superfície de acumulação depende da taxa de deposição de sedimentos, enquanto nos sistemas úmidos a taxa de subida do freático controla a superfície de acumulação.

As alternativas à acumulação são o *by-pass*, quando o balanço sedimentar é neutro, logo, a superfície de acumulação permanece sem

mudança; e a erosão ou deflação, quando o balanço é negativo, logo a superfície de acumulação é rebaixada e forma-se uma supersuperfície (Figura 22A) (Kocurek, 1988). Os sistemas eólicos podem ser classificados em secos, úmidos e estabilizados, de acordo com os processos eólicos que controlam a acumulação (Kocurek & Havholm, 1993).

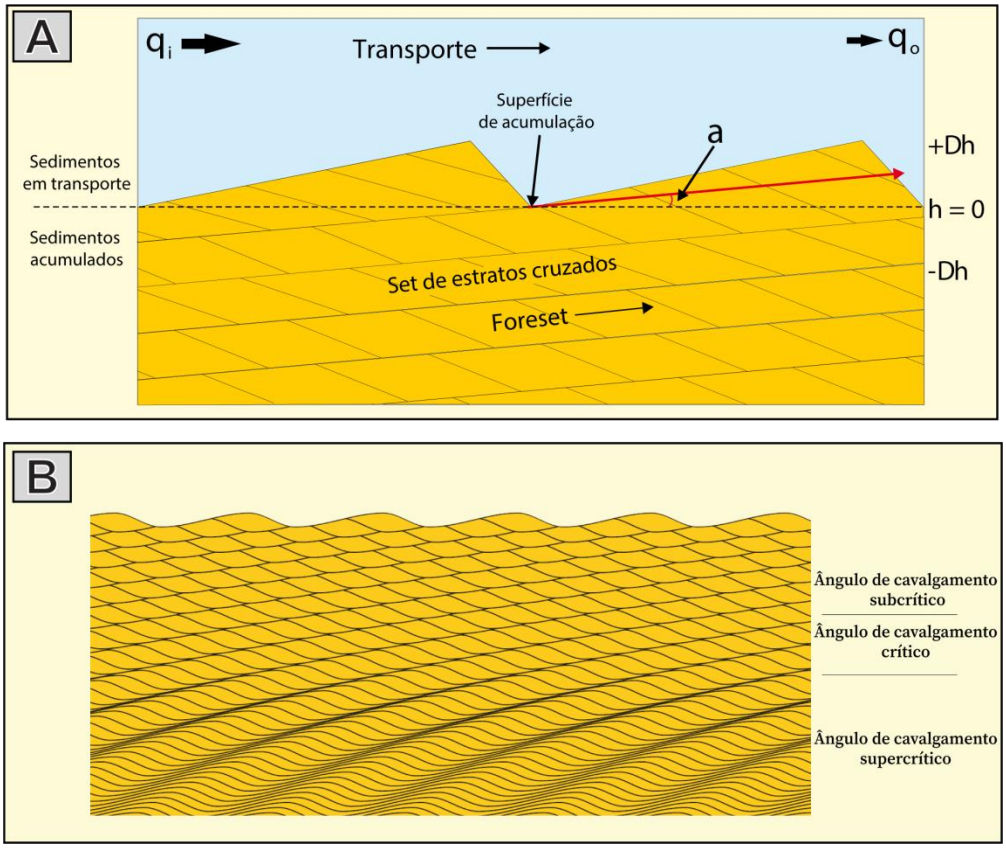

Figura 21: A) O ângulo de cavalgamento **a** é determinado pela razão entre a taxa de subida da superfície de acumulação **Dh** e a taxa de migração. **h** representa o nível da superfície de acumulação, **qi** é a taxa de entrada de sedimento e **qo** a taxa de saída (Modificado de Kocurek & Havholm, 1993). B) Illustração dos tipos de cavalgamento em função do ângulo (Mountney, 2006a).

Em sistemas eólicos secos as interdunas são secas, ou seja, o lençol freático e a franja capilar não têm efeitos na retenção de sedimentos. Desse modo, todo o sedimento no substrato é potencialmente disponível para o transporte eólico. Para que ocorra acumulação em um sistema eólico seco é preciso que o suprimento sedimentar seja alto (sistema saturado, Wilson, 1971). Desta forma, as dunas aumentam em tamanho até que as interdunas sejam eliminadas, e então as dunas começam a cavalgar umas sobre as outras. Por conseguinte, o registro sedimentar de sistemas eólicos secos é

essencialmente constituído por estratos cruzados de dunas eólicos enquanto os depósitos de interdunas são raros ou delgados.

Em sistemas eólicos úmidos, o nível do freático ou sua franja capilar se encontram próximos ou em contato com a superfície de acumulação. Nesses sistemas, a deposição, o *by-pass* e a deflação são controlados pela umidade do solo e a configuração aerodinâmica (Kocurek & Havholm, 1993). Como a areia úmida tem um grau de coesão elevada, os sedimentos de interduna são menos passíveis de deflação e apresentam um alto potencial de preservação. Neste contexto, para ocorrer acumulação é necessária a subida do nível freático. A subida pode ser absoluta, quando é causada pela subida do nível do mar (Mountney & Jagger, 2004), ou relativa, quando a subsidência coloca os estratos eólicos abaixo do freático (Mountney & Howel, 2000). O ângulo de cavalgamento é determinado pela razão entre a taxa de subida relativa do freático e a taxa de migração das dunas eólicas.

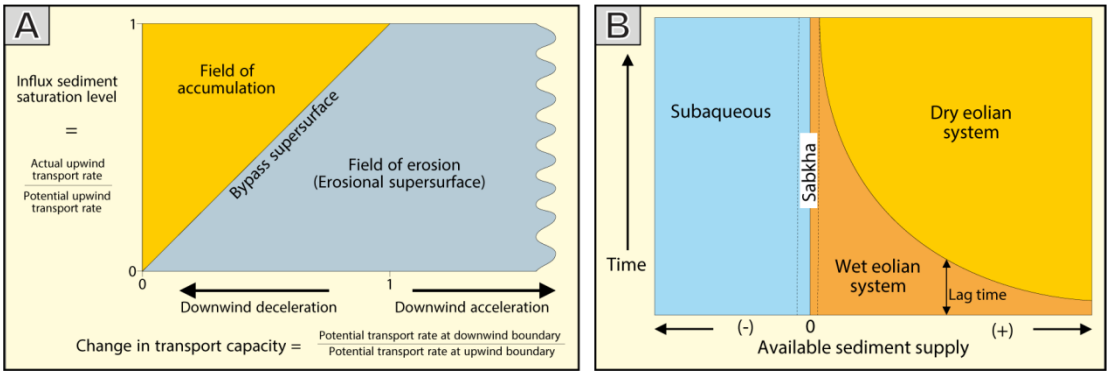

Figura 22: A) campos de acumulação, erosão e *by-pass* em função da entrada de sedimentos e da capacidade de transporte. B) Campos de ambientes eólicos secos, úmidos, sabkhas e subaquosos em função da disponibilidade de sedimentos ao longo do tempo. Assume-se que a superfície original está em contato com o freático ou a franja capilar (Kocurek & Havholm, 1993).

Em sistemas eólicos estabilizados algum fator superficial estabiliza periodicamente ou constantemente o substrato (Kocurek & Havholm, 1993). Esses fatores podem ser: (i) a vegetação (Bigarella *et al*., 1969; Bigarella, 1975; Ash & Wasson, 1983), (ii) a cimentação precoce e/ou (iii) alguma superfície residual ou drapes de lama (Langford & Chan, 1989, Rodrígues López *et al.,* 2012). Os sistemas úmidos podem ser considerados estabilizados se o nível freático for considerado como fator de estabilização.

3.2.1 Superfícies limítrofes e Sequências deposicionais

Uma sequência é uma sucessão de estratos depositados durante um ciclo inteiro de mudança na acomodação ou no suprimento sedimentar. A sequênciaé limitada no topo e na base por discordâncias ou concordância correlata (Catuneanu *et al*., 2009). No caso de sistemas eólicos, a discordância corresponde à interrupção da acumulação eólica que ocorre quando o balanço sedimentar passa de positivo para negativo. Essa mudança é caracterizada pelo rebaixamento da superfície de acumulação, a erosão dos sedimentos acumulados e o desenvolvimento de uma superfície de deflação, a supersuperfície (Kocurek, 1988).

As demais superfícies se formam por processos autocíclicos. Durante a migração de uma duna eólica, parte da duna anterior é erodida e desenvolvem-se superfícies erosivas que truncam os estratos cruzados da duna anterior (Figura 23A). As superfícies originadas pela migração e/ou cavalgamento de dunas são classificadas em 3 (três) tipos, de acordo com sua hierarquia (Brookfield, 1977). Elas são denominadas de superfície de interduna, superfície de superimposição e superfície de reativação.

A análise das superfícies limítrofes é fundamental na exploração de hidrocarbonetos uma vez que os principais *traps* estratigráficos de reservatórios eólicos se desenvolvem ao longo dessas superfícies que agem como barreiras de permeabilidade (Fryberger, 1986; 1990). De fato, dependendo do tipo de superfície, a mesma pode constituir um local preferencial para cimentação e/ou diagênese ou ainda colocar em contato litologias com contrastes de permeabilidade.

3.2.1.1 Superfície de Interduna

A superfície de interduna representa a erosão gerada pela migração e cavalgamento de *draas* (Brookfield, 1977) ou duna simples (Kocurek, 1988) (Figura 23A, D). Esta superfície marca a base da interduna. O tipo de interduna determina os depósitos acima da superfície de migração. As superfícies de interduna são geralmente erosivas, planas ou com mergulho suave em sentido oposto à migração das dunas eólicas.

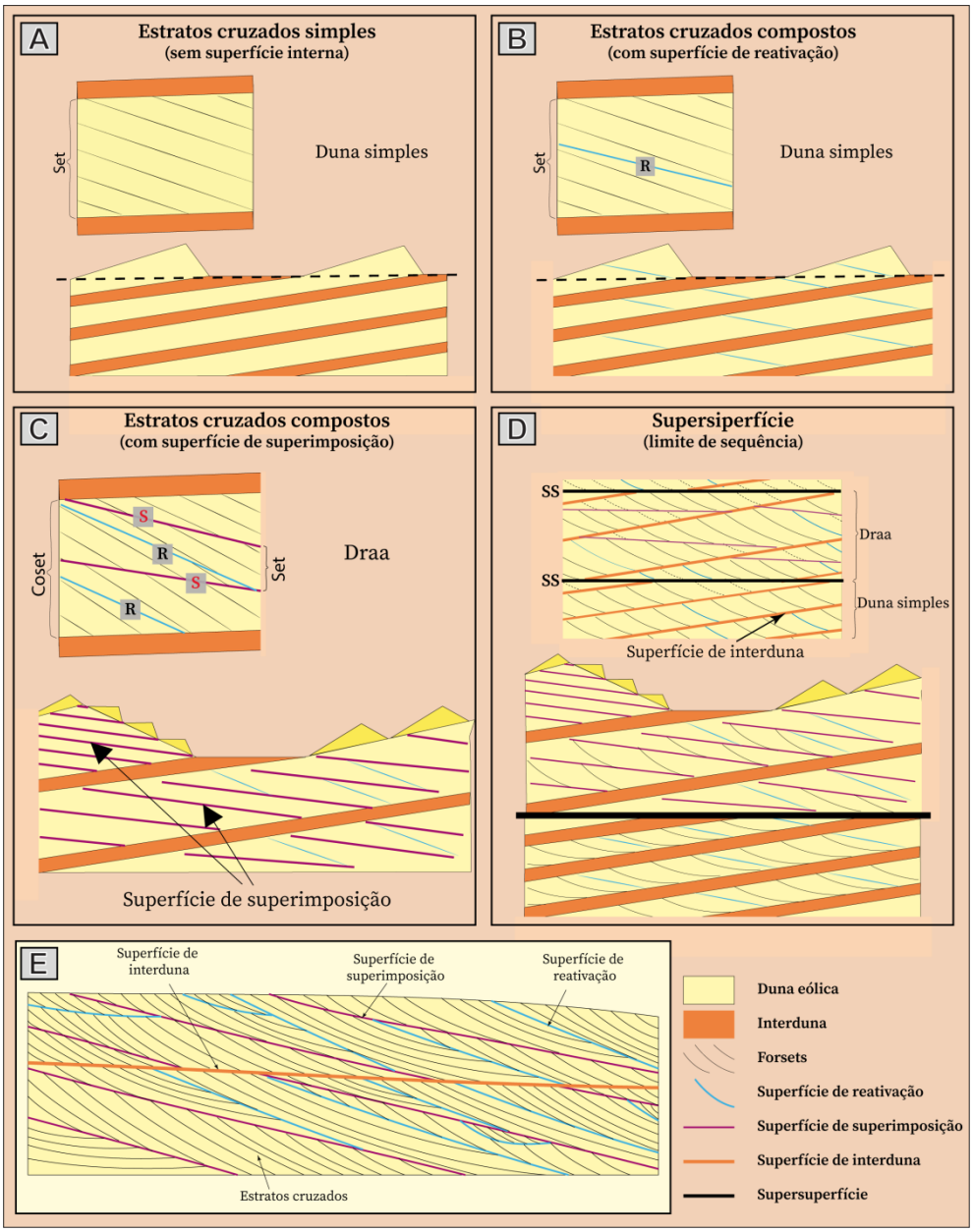

Figura 23: Modelo de geração das superfícies limítrofes de sistemas eólicos.

3.2.1.2 Superfícies de Superimposição

As superfícies de superimposição são originadas pela migração de dunas na face frontal de um *draa* (Figura 23C) (Brookfield, 1977). As superfícies de superimposição ocorrem dentro de *cosets* eólicos e são planas ou erosivas. Essas superfícies mergulham em uma grande variedade de direções apresentando uma relação de downlap com a superfície de migração da base e sendo truncada pela superfície de migração de topo. Quando ambas as superfícies de reativação e de superimposição forem presentes, a de superimposição trunca a de reativação (Figura 23C, D).

3.2.1.3 Superfície de Reativação

A Superfície de reativação resulta da erosão parcial da face de deslizamento e da subsequente retomada da sedimentação em uma duna (Figura 23B). Esta superfície é associada à mudança na direção ou na energia de vento (Bagnold, 1941; Fryberger, 1990). Quando as superfícies de reativação se repetem de forma cíclica, elas indicam mudanças sazonais no sentido de vento (Hunter & Richmond, 1988; Loope *et al*., 2001).

As superfícies de reativação ocorrem internamente aos *sets* eólicos e truncam os *forsets*. Elas podem ser planas ou levemente irregulares e mergulham no sentido do vento com inclinações de 10 a 20°(Mountney, 2006).

3.2.1.4 Supersuperfície

A supersuperfície representa o término da deposição e o início de um período de não deposição ou deflação em uma porção do erg ou no campo de duna inteiro (Figura 23D) (Kocurek, 1988). A destruição do campo de duna resulta geralmente de fatores externos. O clima, a tectônica e as mudanças eustáticas controlam a interrupção da acumulação e/ou deflação do erg (Kocurek, 1981). A supersuperfície pode representar um evento isócrono, como é o caso quando o nível regional do freático sobe, reduz a disponibilidade de areia e promove deflação do campo de duna inteiro; ou diácrono, quando a margem do campo de duna (*Back-erg*) desenvolve progressivamente uma supersuperfície devido ao avanço do erg (Porter, 1986). A supersuperfície é uma ferramenta poderosa para correlação de estratos e subdivisão do registro (Blakey *et al*., 1996).

As feições características da supersuperfícies são: base plana, extensão regional, fraturas poligonais, *lags* de deflação e bioturbação (Kocurek & Hunter, 1986; Loope, 1985).

3.3 PRESERVAÇÃO DO CAMPO DE DUNA

A acumulação de estratos eólicos não garante automaticamente sua preservação. Isso porque, durante períodos de balanço sedimentar negativo, os sedimentos acumulados podem ser erodidos e colocados novamente à

disponibilidade no sistema (Kocurek, 1999). Logo, a preservação de estratos exige que os mesmos sejam colocados abaixo do nível de base da erosão. O espaço abaixo do nível de base é designado de espaço de acomodação (Jervey, 1988). Os principais fatores que favorecem a preservação são a subsidência e o soterramento, e/ou a subida do freático (Porter, 1986; Kocurek, 1999). Em campos de dunas costeiros, o nível de base é definido pelo nível do freático que, por sua vez, é controlado pelas flutuações do nível do mar (Figura 24). A preservação do erg é geralmente associada a períodos de transgressões marinhas, quando o erg é progressivamente inundado.

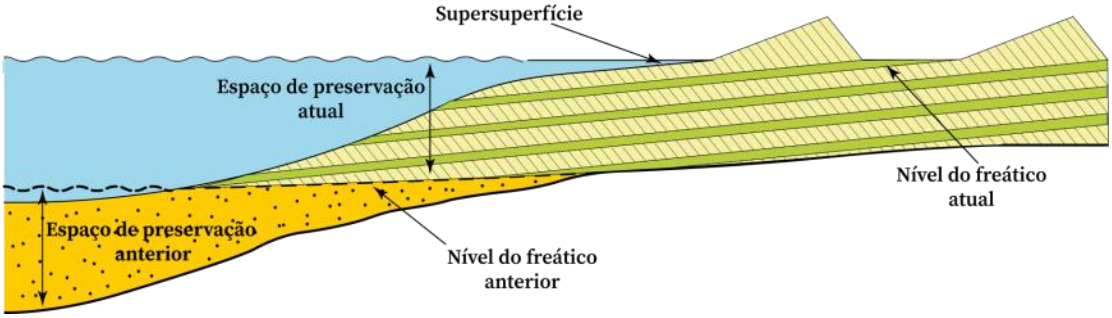

Figura 24: Modelo básico de preservação no contexto de sistemas eólicos costeiros (Modificado de Kocurek, 1999).

4 DADOS E MÉTODOS

A área de estudo desta tese abrange a região entre os municípios de Amarante / PI e Palmeirais / PI (Figura 25). Esta área de cerca de 60 km por 40 km (2400 km²), foi escolhida por apresentar extensos chapadões e morros testemunhos íngreme que permitiram o levantamento estratigráfico de detalhe, a identificação dos elementos arquiteturais e a correlação das principais superfícies estratigráficas. Dois níveis topográficos foram usados como datum para correlacionar as seções estratigráficas. O primeiro consiste em uma camada delgada de brecha silicificada que pode ser rastreada ao longo de toda a área de estudo. A silicificação pervasiva confere a essa camada uma resistência elevada ao intemperismo, o que resulta na sua preservação formando um nível topográfico vegetado quase horizontal que ocorre na base dos morros. O segundo datum é o limite superior da sucessão estratigráfica estudada e representa um contato abrupto com a Formação de Pedra do Fogo sobrejacente. Esta superfície forma um nível topográfico horizontal com vegetação abundante e ocorre no topo das serras e dos morros.

Treze (13) seções estratigráficas foram levantadas em campo utilizando planilhas padronizadas (Figura 26) onde estão reservados campos para o preenchimento de informações básicas do afloramento (Nome do ponto e coordenada, código de fácies, medida de paleocorrente, número da foto e da amostra quando houver e descrição detalhada da rocha). A descrição das fácies foi realizada seguindo o método clássico proposto por Walker (1992), em que as fácies são reconhecidas com base na sua textura, estrutura sedimentar, geometria e continuidade lateral. Em seguida as fácies foram agrupadas em associações de fácies, caracterizando subambientes deposicionais dentro de sistemas deposicionais definidos (Miall, 1984; Dalrymple, 2010). O código de fácies utilizado neste trabalho foi modificado do código proposto por Miall (1996).

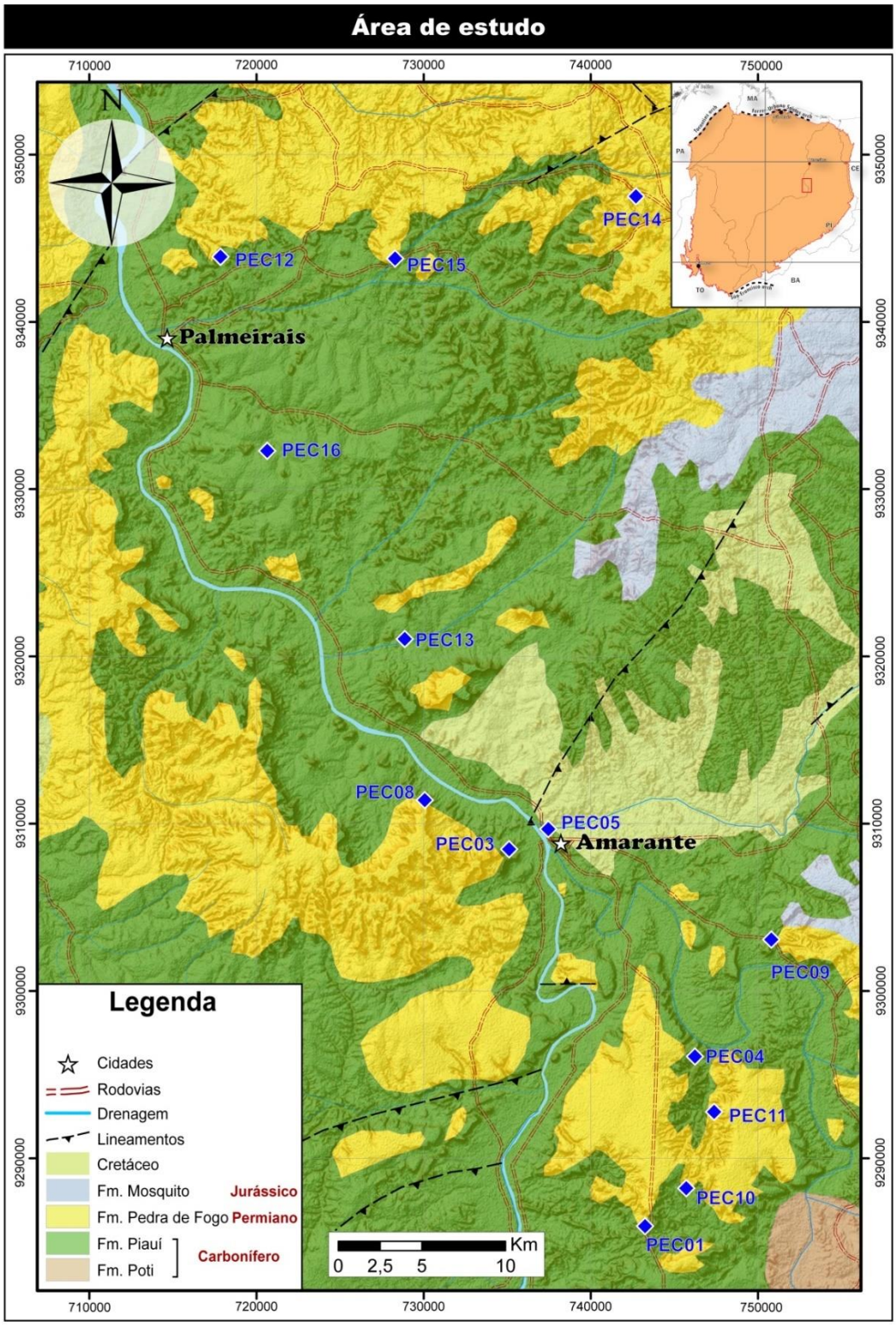

Figura 25: Mapa geológico da região de realização dos trabalhos de campo com a localização das seções colunares já levantadas. No canto superior esquerdo da figura está o mapa da bacia e a delimitação da área de estudo.

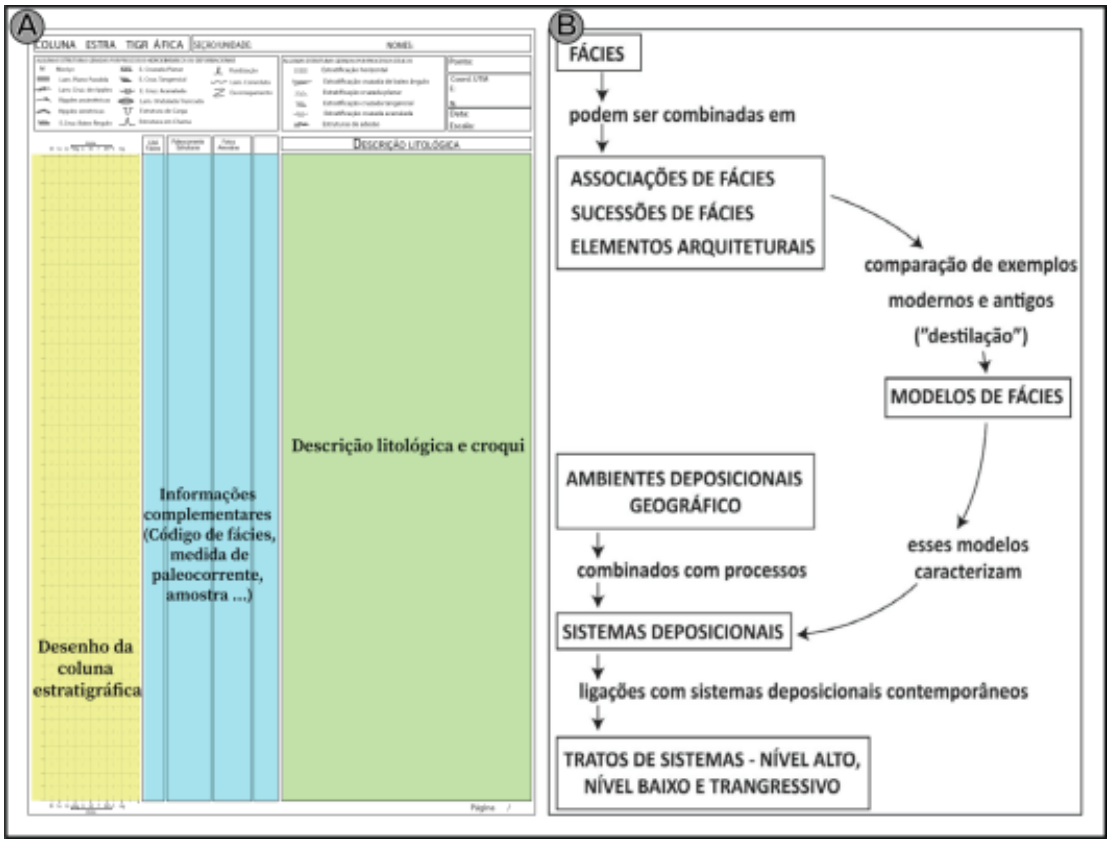

Figura 26: A) Exemplo de planilha base usada em campo. B) Esquema de “destilação” da análise de fácies (Modificado de Walker & James, 1992).

Devido ao declive acentuado de alguns morros testemunhos, não foi possível levantar seções colunares contínuas. Nestes casos, modelos virtuais de afloramento foram construídos a partir de imagens adquiridas com um drone. As imagens coletadas em campo foram processadas com *softwares* especializados a fim de extrair nuvens densas de pontos georreferenciados (Figura 27). Em seguida, por interpolação entre os pontos da nuvem densa, foi gerada uma malha sólida, à qual foi atribuída textura usando as cores originais das fotografias. Esses modelos virtuais tridimensionais permitiram a aquisição de informações indiretas como a espessura dos sets e o ângulo de mergulho das superfícies.

Vinte e nove amostras foram coletadas com a intenção de definir as estruturas e texturas, bem como as composições primárias e diagenéticas das fácies. A análise petrográfica foi realizada usando um microscópio Zeiss AXIO Imager 2 e as fotomicrografias foram obtidas com o software ZEN 2012.

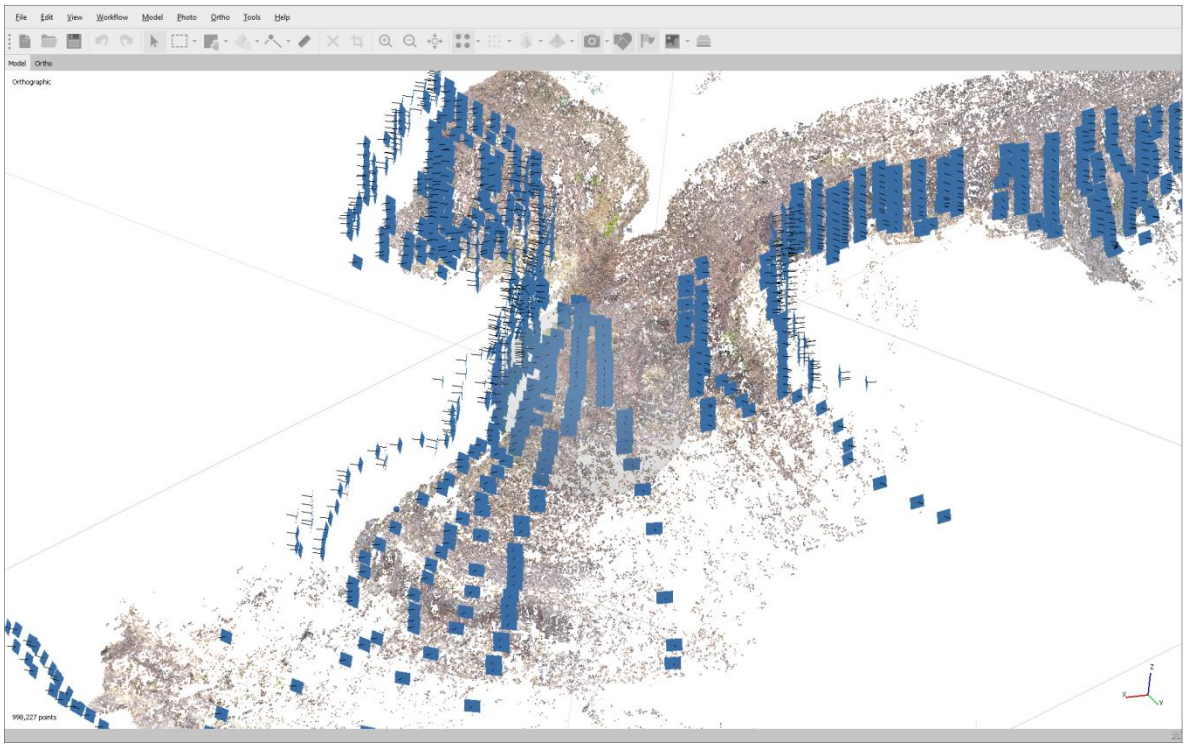

Figura 27: Os alvos azuis representam as posições de onde foram coletadas as fotos durante o voo vertical, buscando respeitar a sobreposição entre imagens.

Devido à intensa substituição da composição original por sílica microcristalina nos estromatólitos, optou-se por realizar análises geoquímicas de cromatografia gasosa-espectrometria de massa (GC-MS) visando a identificação dos biomarcadores que possibilitassem identificar o ambiente de deposição dos estromatólitos. Para estas análises foram selecionadas apenas as amostras de estromatólitos contendo lâminas escuras espessas por serem as que potencialmente contêm maior quantidade de matéria orgânica preservada (McKirdy, 1976). As amostras foram trituradas e aproximadamente 20 g do pó foram usados para a separação das frações alifática, aromática e polar em coluna com sílica gel ativada e alumina. Em seguida, as frações saturadas de hidrocarbonetos foram analisadas em um cromatógrafo gasoso equipado com amostrador automático e acoplado a espectrômetro de massa.

5 CONTEXTO GEOLÓGICO

A Bacia do Parnaíba, às vezes denominada de Bacia do Maranhão, Meio Norte ou Piauí-Maranhão é a terceira maior bacia sedimentar brasileira com aproximadamente de 600.000 km² (Vaz et al., 2007). A Bacia do Parnaíba é localizada geograficamente na região nordeste do Brasil (Figura 28), limitada das bacias de São Luís e Barreirinhas ao norte pelo Arco Ferrer-Urbano Santos, a nordeste é separada da Fossa de Marajó pelo Arco de Tocantins e ao sul e ao sudeste é limitada das bacias de São Francisco e Lençóis pelo Arco do Médio São Francisco (Figura 28). Os limites atuais da bacia compreendem todo o estado de Maranhão, Piauí e parte dos estados de Tocantins, Pará e Ceará.

Apesar do número crescente de estudos acerca da bacia do Parnaíba, a sua evolução estratigráfica permanece mal compreendida, principalmente no que diz respeito às regiões S e SE (estado do Piauí). Os principais estudos sobre a sedimentação permo-carbonífera na bacia são os de Lima & Leite (1978), e Lima Filho (1998), e por décadas o conhecimento atrelado a este intervalo estratigráfico se manteve estagnado. Este descaso dos pesquisadores foi consequência das campanhas de exploração de hidrocarboneto malsucedidas durante as décadas de 1970 e 1980 (Abelha *et al*., 2018) que levaram à conclusão de que não existisse reservas de hidrocarbonetos exploráveis. Contudo, os recentes investimentos na aquisição de dados têm levado à descoberta de novas jazidas de gás e aumentado as expectativas de descoberta de óleo.

Ainda não existe para esta bacia um estudo de estratigrafia de sequência que analisa a sucessão sedimentar Pensilvaniana do ponto de vista dos mecanismos autogênicos e alogênicos, que reconstrua a arquitetura de fácies e que crie um modelo evolutivo adaptado para o Permo-pensilvaniano da Bacia do Parnaíba. Considerando estes fatos, o estudo da evolução estratigráfica das formações Piauí se torna fundamental neste momento. Os depósitos eólicos Pensilvanianos afloram ao longo de dezenas de quilômetros no Sul e no Leste da bacia formando mesetas íngremes e

morros testemunhos correlacionáveis regionalmente (Figura 28). Estes depósitos constituem um estudo de caso ideal para entender os mecanismos de sedimentação eólica e a influência da glaciação do Pennsilvaniano na sedimentação eólica, e analisar a evolução da Bacia do Parnaíba neste período.

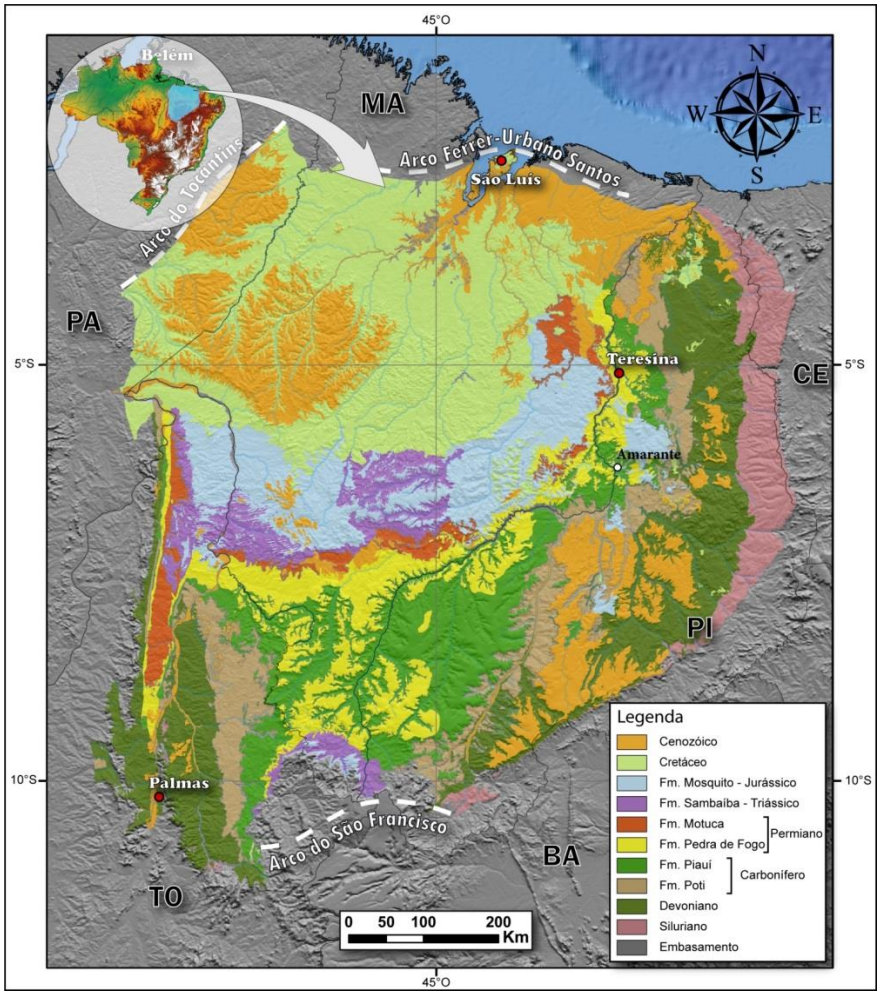

Figura 28: Mapa geológico da Bacia do Parnaíba com localização das áreas de estudo (Fonte do SIG Bizzi *et al.,* 2003).

5.1 Evolução tectono-estratigráfica

A Bacia do Parnaíba, localizada na província estrutural homônima, é limitada a norte pelo Cráton de São Luís, a oeste pelo Cráton Amazônico e a leste pelo Cráton de São Francisco-Congo (Almeida *e. al.,* 1981). O embasamento da bacia consiste em rochas metamórficas e ígneas pré-cambrianas acrecionadas que se estabilizaram depois da Orogenia Brasiliana

(Brito Neves *et al.,* 1984). Análises geofísicas evidenciam a compartimentação do substrato da bacia em três blocos (de Castro *et al.,* 2014; Daly *et al.,* 2014;Figura 29). No oeste, o bloco Amazônia/Araguaia é caracterizado por rochas metassedimentares, referente aos grupos Tocantins e Estrondo (Bizzi *et al.,* 2003), e ofiolíticas recobrindo o Cráton Amazônico. No centro, o bloco Parnaíba tem composição crustal desconhecida devido à ausência de afloramento, contudo, baseado na sua assinatura sísmica, Daly *et al.* (2014) supõem presença de rochas com afinidade granitoide. O bloco Borborema a leste é composto por gnaisses e migmatitos arqueanos (Araujo *et al.,* 2013). Da colisão entre estes blocos originaram-se cinturões e zonas de cisalhamentos: o bloco Parnaíba é separado do Cráton de São Luís pelo cinturão Gurupi; do Cráton Amazônico pela zona de falhas Araguaia, orientada segundo a direção N-S, a qual foi posteriormente reativada durante o Triássico superior e subsequentemente entre o Jurássico Superior e Cretáceo inferior; e o limite leste com o Cráton de São Francisco é uma zona de cisalhamento de direção NE-SW, relacionada ao lineamento Transbrasiliano (Araujo *et al.,* 2013).

Subsequentemente, durante o Cambriano, desenvolveram-se os riftes do Grupo Jaibaras, ao longo dos lineamentos transbrasilianos (Figura 29). Enquanto de Castro *et al .,* (2014) apontam para estes riftes como as estruturas que desencadearam a formação da bacia sedimentar. Daly *et al*., (2014) destacam na sísmica a existência de um contato abrupto entre a sequencia sedimentar cambriana e o resto da bacia. Os autores interpretam a superfície como resultado de aplainamento pós-brasiliano, argumentando que a estruturação do embasamento não tem relação com os mecanismos de subsidência desta. Consequentemente Rodríguez Tribaldos & White (2018), levantam a hipótese de uma subsidência lenta (250 Ma) como principal mecanismo de geração da Bacia do Parnaíba.

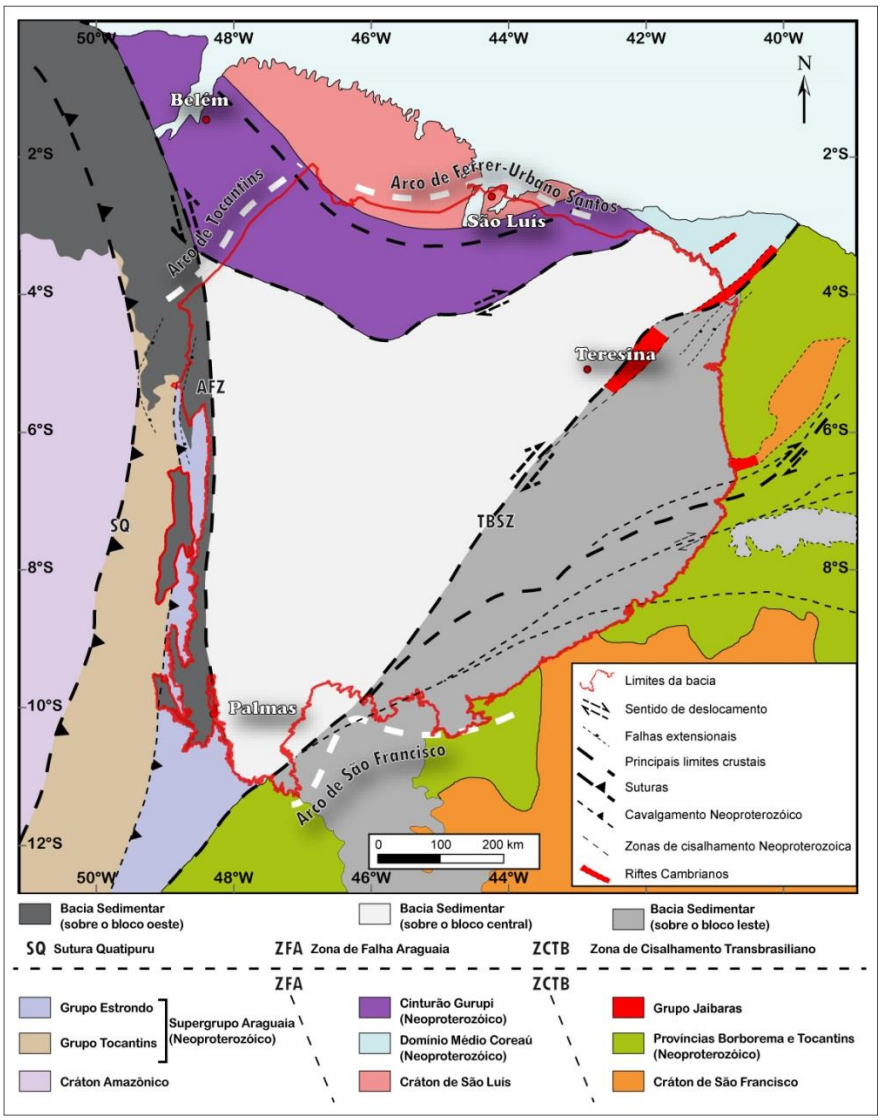

Figura 29: Mapa ilustrando a compartimentação tectônica do embasamento da Bacia do Parnaíba (Modificado de de Castro *et al.,* 2014 e Daly *et al.,* 2014).

5.2 Sucessão estratigráfica

Segundo Goés & Feijó (1994) e Vaz *et al.,* (2007), a sucessão sedimentar e magmática da Bacia do Parnaíba pode ser dividida em 5 supersequências: Siluriana, Mesodevoniana-Eocarbonífera, Neocarbonífera-Eotriássica, Jurrássica e Cretácea, sendo a Neocarbonífera-Eotriássica o foco do presente estudo.

A sucessão Pensilvaniana da Bacia do Parnaíba corresponde à formação Piauí. A denominação Série Piauí foi originalmente atribuída por Small (1914) para arenitos e folhelhos que ocorrem nos estados do Piauí e

Maranhão. O termo Formação Piauí foi subsequentemente usado para as camadas de idade Pensilvaniana cujos limites estratigráficos são os arenitos e siltitos da Formação Poti e o *sílex* da Formação Pedra de Fogo.

A Formação Piauí é subdividida em dois intervalos (Lima & Leite, 1978). A porção inferior da Formação Piauí, que aflora principalmente a leste da bacia, é caracterizada por raras camadas de folhelhos avermelhado e mais de 100 m de arenitos feldspáticos róseos, amarelados e esbranquiçados, variando de finos a grossos e por vezes conglomeráticos, mal a moderadamente selecionados e com grãos subangulares a subarredondados. O intervalo superior, foco desra tese, tem espessura de até 120 m e é constituída por arenitos creme a amarelados ou avermelhados, finos, bem selecionados, pouco feldspáticos com intercalação de siltitos, folhlelhos e *sílex* maciço ou oolítico.

O ambiente deposicional das rochas que constituem a sucessão superior da Formação Piauí é predominantemente fluvial com contribuição eólica. Nas regiões perto da cidade de Teresina os depósitos eólicos são sobrepostos por carbonatos ricos em fósseis (Carbonato de Mocambo) interpretados como tendo sido depositados em plataforma carbonática rasa adjacente a um campo de dunas costeiras (Medeiros et al., 2019). A idade de deposição da sucessão superior da Formação Piauí é restrita entre o Bashkiriano para a sucessão inferior e o Cisuraliano (Permiano) para a formação Pedra de Fogo sobrejacente (Mesner Wooldridge, 1964; Leite et al., 1975, Dino & Playford, 2002; Dino et al. ., 2002).

6 RESUMO DOS RESULTADOS

A análise estratigráfica de alta resolução da sucessão superior da Formação Piauí permitiu a identificação de vinte e uma litofácies que ocorrem em sete associações de fácies característicos de três ambientes deposicionais: (i) Os depósitos fluviais são compostos pelas associações de fácies de canal fluvial, inundações em lençóis e planícies de inundação; (ii) os depósitos eólicos compreendem as associações de fácies de dunas eólicas, depósitos de interdunas e de lençóis de areia; e (iii) os depósitos lacustres são representados essencialmente pela associação de fácies de margem de lago.

Com base na identificação de superfícies chave, a sucessão sedimentar foi dividida em três intervalos estratigráficos (Figura 30): (i) A base do primeiro intervalo estratigráfico (IS-1) é dominantemente composta por depósitos fluviais, enquanto o topo do intervalo é marcado por extensos pacotes de depósitos eólicos, ocasionalmente sobrepostos por depósitos de inundações em lençol. Os espessos pacotes de depósitos eólicos recobrindo depósitos fluviais indicam que a planície aluvial evoluiu progressivamente para um campo de duna; (ii) o segundo intervalo estratigráfico (IS-2) é caracterizado por uma camada delgada e extensão lateral de centenas de quilômetros, caracterizada por estromatólitos, arenitos ooidais e brechas conglomeráticas intensamente silicificados. Este intervalo foi interpretado como a inundação do campo de duna devido à expansão do lago adjacente; (iii) O terceiro intervalo é essencialmente composto por depósitos eólicos. A identificação de supersuperfícies neste intervalo permitiu a individualização de três unidades genéticas eólicas que sugerem fases de expansão e contração do campo de duna

Uma vez os principais intervalos definidos, resolvemos analisá-los em detalhe. O Artigo 1 foca no intervalo estratigráfico 3 (IS-3), tendo como objetivo desvendar a história estratigráfica embutida nos hiatos do registro eólico. A realização deste estudo foi motivada por uma observação intrigante. Embora o IS-3 seja constituído de ambos os sistemas eólicos seco e úmido,

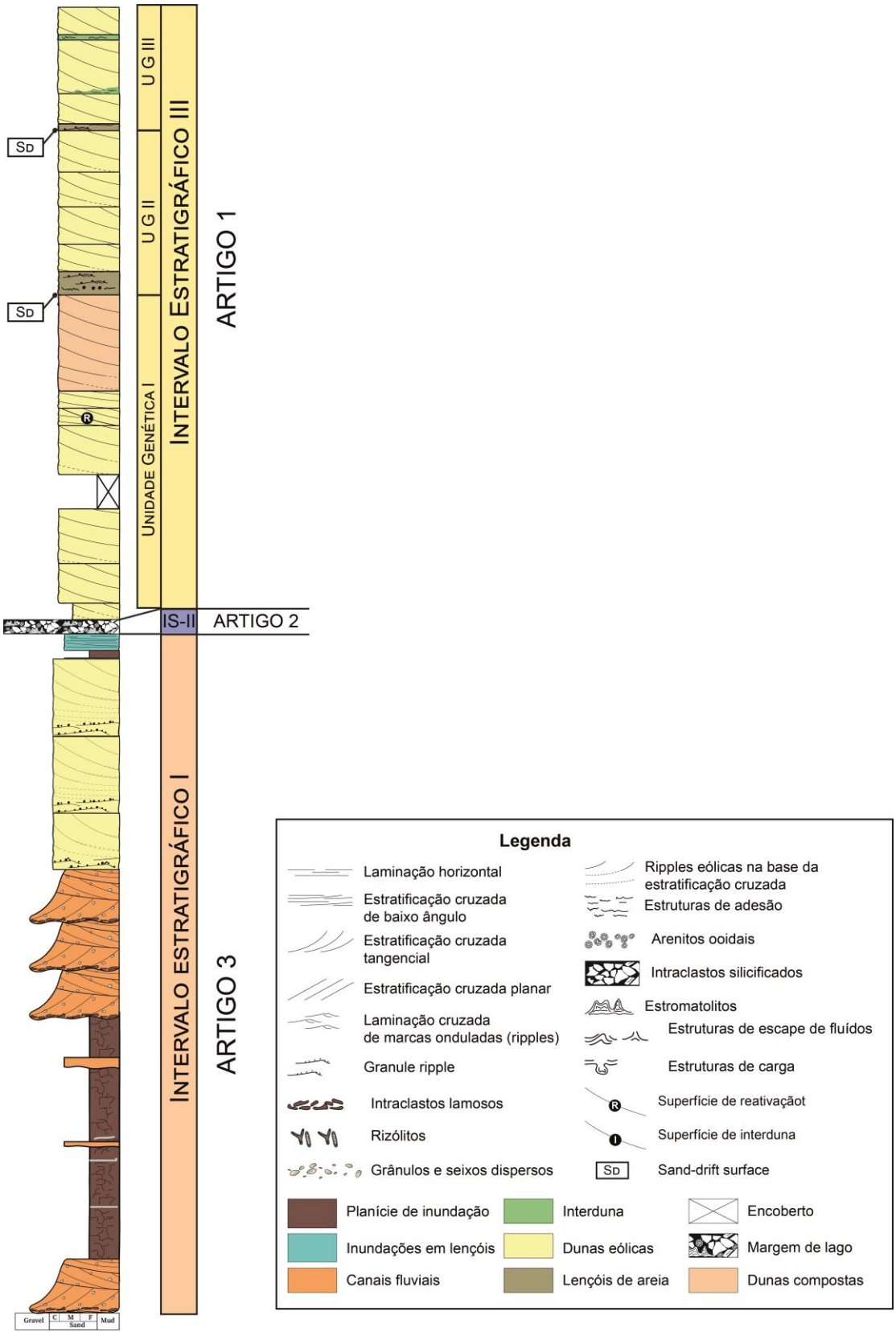

Figura 30: Seção estratigráfica idealizada doa sucessão superior da Formação Piauí.

em nenhum desses dois sistemas foram preservados os estágios embrionários nem terminais do campo de duna. Logo, através da análise quantitativa e a reconstrução das dimensões originais das dunas, foi possível demonstrar que: (i) Nos sistemas secos, a preservação dos estratos de protodunas é improvável porque durante a migração de dunas eólicas, as dunas maiores geram escavações profundas que erodem os estratos de protodunas (Paola & Borgman, 1991; Day & Kocurek, 2017; Swanson et al., 2019); (ii) Nos sistemas úmidos, a subida do freático é um fator que auxilia na preservação das protodunas. Porém, a reconstrução morfológica permitiu identificar que estratos eólicos de pequeno porte observados neste estudo não foram gerados por protodunas, mas por dunas de tipo barcanas a barcanóides; e (iii) A ausência dos estratos de estágios terminais foi causada pela exaustão do suprimento sedimentar e a redução da disponibilidade de areia, que contribuiram para o desenvolvimento de um ângulo de cavalgamento negativo ocasionando a canibalização e erosão das formas de leito finais.

O artigo 2 buscou identificar o ambiente deposicional do nível silicificado (IS-2) e entender as condições paleoclimáticas que possibilitaram a geração dessa significativa quantidade de sílica. Durante a redação do artigo 1, os resultados das análises químicas ainda não tinham sido obtidas e as análises sedimentológicas e petrográficas realizadas até então não eram conclusivas. Por esse conjunto de razões, o nível silisificado foi interpretado como sabkha no artigo 1. No entanto, uma vez recebidos os chromatogramas, foi possível identificar os hidrocarbonetos através de seus picos e interpretar os parâmetros dos biomarcadores. A análise das proporções de *n*-alcanos, terpanos e esteranos permitiu interpretar que os estromatólitos foram gerados por colônias de cianobactérias em um ambiente lacustre hipersalino com abundância de argilominerais. Esta interpretação é sustentada pelos dados de petrografia de arenitos ooidais onde se verificou que muitos ooides apresentam formas alongadas e deformadas, mesmo nas áreas de compactação leve. Estas deformações indicam que a composição original era argilosa e sugerem modificação da forma original dos ooides devido à desidratação. A ausência de feições originadas por exposição

subaérea nas brechas, nos ooides ou nos estromatólitos sugere que a desidratação ocorreu em ambiente subaquoso, por sinerese. A dissolução da composição original dos ooides (argilominerais) resultou na liberação de um grande volume de sílica que ocasionou a cimentação da camada.

Por fim, o artigo 3 consiste no estudo integrado dos três intervalos estratigráficos visando reconstruir a evolução paleoclimática das médias latitudes do Gondwana durante o Pensilvaniano. Como observado, a sucessão estratigráfica superior da Formação Piauí é caracterizada pela mudança de sistemas fluviais na base para essencialmente eólicos no topo, indicando condições climáticas cada vez mais áridas. Nessa sucessão, não foram encontrados depósitos glaciais nem estruturas geradas por processos glacígenos embora vários estudos sugiram que o Pensilvaniano foi marcado pelo período de *icehouse* mais importante do Carbonífero. Essa ausência pode ser explicada por duas alternativas: (i) a deposição da sucessão superior da Formação Piauí antecedeu ou sucedeu à glaciação, logo não houve simultaneidade: ou (ii) a glaciação do Pensilvaniano ocorreu simultaneamente à deposição, mas a cobertura de gelo não alcançou as médias latitudes. Para responder a estes questionamentos foi necessário revisar os modelos paleoclimáticos e de circulação atmosférica. Durante períodos glaciais, o aumento da cobertura de gelo permite a expansão das células de circulação polares para as latitudes médias (vento dominante para NW), enquanto a zona de convergência intertropical e as células de circulação de Hardley e de Ferrel encolhem. A posição da Bacia do Parnaíba durante o Pensilvaniano (cerca de 40°) e os dados de paleocorrentes coletados nos estratos eólicos (NW) sugerem que os campos de dunas eólicos se desenvolveram precisamente durante períodos glaciais. Por outro lado, durante períodos interglaciais o recuo da cobertura de gelo permite expansão da zona de convergência intertropical promovendo o aumento da umidade nas médias latitudes e causando assim a contração do campo de duna e o desenvolvimento das supersuperfícies. Desta forma, foi possível comprovar a simultaneidade entre o período glacial e a aridificação na Bacia do Parnaíba e mostrar de que forma a alternância entre períodos glaciais e interglaciais influenciou a sedimentação eólica.

7 CONCLUSÕES

A análise estratigráfica de alta resolução da sucessão superior da Formação Piauí possibilitou uma reconstrução precisa da evolução estratigráfica da bacia do Parnaíba durante o Pensilvaniano. Três unidades estratigráficas foram individualizadas com base na identificação de superfícies estratigráficas chaves. O primeiro intervalo estratigráfico é composto por depósitos fluviais recobertos por extensos pacotes de depósitos eólicos, e indica a transformação de uma planície aluvial para um campo de duna devido a condições climáticas áridas. O segundo intervalo estratigráfico representa a deflação do campo de duna e a subsequente inundação da área causada pela expansão de um lago hipersalino adjacente. A terceira unidade estratigráfica é essencialmente composta por depósitos eólicos e a identificação de supersuperfícies internas sugere que o campo de duna passou por fases de contração e expansão. Os períodos glaciais favoreceram a construção e a expansão do campo de duna enquanto os períodos interglaciais foram responsáveis por sua deflação e contração. Consequentemente, podemos afirmar que a alternância entre intervalos glaciais e interglaciais durante o período de *icehouse* do Pennsylvaniano controlou de forma significativa a dinâmica do campo de duna e a evolução estratigráfica da Bacia do Parnaíba.

8 REFERÊNCIAS

Abelha, M., Petersohn, E., Bastos, G., & Araújo, D. (2018). New insights into the Parnaíba Basin: results of investments by the Brazilian National Petroleum Agency. Geological Society, London, Special Publications, 472(1), 361-366.

Ahlbrandt, T. S., & Fryberger, S. G. (1981). Sedimentary features and significance of interdune deposits. In: Ethridge, F.G. & Flores, R.M. (eds). Recent and ancient nonmarine Depositional Environments. *Society of Economic Paleontologists and Miner*alogists, 31, pp.293-314.

Ahlbrandt, T. S., Andrews, S., & Gwynne, D. T. (1978). Bioturbation in eolian deposits. *Journal of Sedimentary Research*, *48*(3),839-948.

Al-Masrahy, M. A., & Mountney, N. P. (2015). A classification scheme for fluvial–aeolian system interaction in desert-margin settings. Aeolian Research, 17, 67-88.

Almeida, F. F. M., Y. Hasui, B. B. Brito Neves, and R. A. Fuck (1981), Brazilian structural provinces: An introduction, Earth Sci. Rev., 17, 1–29.

Allen, J. R. L. (1970). The avalanching of granular solids on dune and similar slopes. *The Journal of Geology*, *78*(3), 326-351.

Anthonsen, K. L., Clemmensen, L. B., & Jensen, J. H. (1996). Evolution of a dune from crescentic to parabolic form in response to short-term climatic changes: Råbjerg Mile, Skagen Odde, Denmark. *Geomorphology*, *17*(1-3), 63-77.

Araujo, C. E., R. F. Weinberg, and U. G. Cordani (2013), Extruding the Borborema Province (NE Brazil): A two-stage Neoproterozic collision process,Terra Nova, 26, 157–168.

Ash, J. E., & Wasson, R. J. (1983). Vegetation and sand mobility in the Australian desert dunefield. *Zeitschrift fur Geomorphologie*, *45*(Supp.), 7-25.

Bagnold, R. A. (1937). The transport of sand by wind. *The Geographical Journal*, *89*(5), 409-438.

Bagnold, R. A. (1941). The physics of blown sand and desert dunes. *Chapmann and Hall, Methuen, London*.

Bigarella, J. J. (1975). Structures developed by dissipation of dune and beach ridge deposits. *Catena*, *2*, 107-152.

Bigarella, J. J., Becker, R. D., & Duarte, G. M. (1969). Coastal dune structures from Parana (Brazil). *Marine Geology*, *7*(1), 5-55.

Bizzi, L. A., C. Schobbenhaus, R. M. Vidotti, and J. H. Goncalves (2003), Geologia, Tectonica e Rescursos Minerais do Brasil, 692 pp., CPRM,Ed., UnB, Brasilia.

Blakey, R. C. (1988). Superscoops: Their significance as elements of eolian architecture. *Geology*, *16*(6), 483-487.

Blakey, R. C., Havholm, K. G., & Jones, L. S. (1996). Stratigraphic analysis of eolian interactions with marine and fluvial deposits, Middle Jurassic Page Sandstone and Carmel Formation, Colorado Plateau, USA. *Journal of Sedimentary Research*, *66*(2), 324-342.

Blum, M. D., & Törnqvist, T. E. (2000). Fluvial responses to climate and sea-level change: a review and look forward. *Sedimentology*, *47*(s1), 2-48.

Brito Neves, B. B., R. A. Fuck, U. G. Cordani, and A. Thomas (1984), Influence of basement structures on the evolution of the major sedimentary basins of Brazil: A case of tectonic heritage, J. Geodyn., 1, 495–510.

Brookfield, M. E. (1977). The origin of bounding surfaces in ancient aeolian sandstones. *Sedimentology*, *24*(3), 303-332.

Bryant, G., & Miall, A. (2010). Diverse products of near-surface sediment mobilization in an ancient eolianite: outcrop features of the early Jurassic Navajo Sandstone. *Basin Research*, *22*(4), 578-590.

Catuneanu, O., Abreu, V., Bhattacharya, J. P., Blum, M. D., Dalrymple, R. W., Eriksson, P. G., ... & Giles, K. A. (2009). Towards the standardization of sequence stratigraphy. *Earth-Science Reviews*, *92*(1-2), 1-33.

Chan, M. A., & Kocurek, G. (1988). Complexities in eolian and marine interactions: processes and eustatic controls on erg development. *Sedimentary Geology*, *56*(1-4), 283-300.

Chakraborty, T., & Chaudhuri, A. K. (1993). Fluvial-aeolian interactions in a Proterozoic alluvial plain: example from the Mancheral Quartzite,

Sullavai Group, Pranhita-Godavari Valley, India. *Geological Society, London, Special Publications*, *72*(1), 127-141.

Chakraborty, T., & Sensarma, S. (2008). Shallow marine and coastal eolian quartz arenites in the Neoarchean-Palaeoproterozoic Karutola Formation, Dongargarh Volcano-sedimentary succession, central India. *Precambrian Research*, *162*(1-2), 284-301.

Christie-Blick, N., Mountain, G. S., & Miller, K. G. (1990). Seismic stratigraphic record of sea-level change. *Sea-level change*, 116-140.

Clemmensen, L. B., Olsen, H., & Blakey, R. C. (1989). Erg-margin deposits in the Lower Jurassic Moenave Formation and Wingate Sandstone, southern Utah. *Geological Society of America Bulletin*, *101*(6), 759-773.

Crabaugh, M., & Kocurek, G. (1993). Entrada Sandstone: an example of a wet aeolian system. *Geological Society, London, Special Publications*, *72*(1), 103-126.

Compagnucci, R. H. (2011). Atmospheric circulation over Patagonia from the Jurassic to present: a review through proxy data and climatic modelling scenarios. *Biological Journal of the Linnean Society*, *103*(2), 229-249.

Cosgrove, G. I., Colombera, L., & Mountney, N. P. (2021). Quantitative analysis of the sedimentary architecture of eolian successions developed under icehouse and greenhouse climatic conditions. GSA Bulletin.

Dalrymple, M., 2010. Interpreting sedimentary successions: facies, facies analysis and facies models. In: James, N.P., Dalrymple, R.W. (Eds.), Facies models 4, Geological Association of Canada. St. John's, Newfoundland, GEO text 6, pp. 3-18.

Daly, M.C., Andrade, V., Barousse, C.A., Costa, R., Mcdowell, K., Piggott, N. & Poole, A.J. 2014. Brasiliano crustal structure and the tectonic setting of the Parnaíba basin of NE Brazil: results of a deep seismic reflection profile. Tectonics, 33, 2102–2120.

de Castro, D. L., Fuck, R. A., Phillips, J. D., Vidotti, R. M., Bezerra, F. H., & Dantas, E. L. (2014). Crustal structure beneath the Paleozoic Parnaíba

Basin revealed by airborne gravity and magnetic data, Brazil. Tectonophysics, 614, 128-145.

Dickinson, W.R., Soreghan, G.S. and Giles, K.A., 1994, Glacio-eustatic origin of Permocarboniferous stratigraphic cycles: evidence from the southern Cordilleran foreland region, in Dennison, J.M. and Ettensohn, F.R., eds., Tectonic and Eustatic Controls on Sedimentary Cycles, Society for Sedimentary Geology Concepts in Sedimentology and Paleontology, v. 4,p. 25–34.

Dino, R., Playford, G., 2002. Stratigraphic and palaeoenvironmental significance of a Pennsylvanian (Upper Carboniferous) palynoflora from the Piauí Formation, Parnaíba Basin, northeastern Brazil. Paleontol. Res. 6, 23–40.

Dino, R., Antonioli, L., Braz, S.M.N., 2002. Palynological data from the Trisidela Member of Upper Pedra de Fogo Formation (“Upper Permian”) of the Parnaíba Basin, Northeastern Brazil. Rev. Bras. Paleontol. 24–35.

Doe, T. W., & Dott Jr, R. H. (1980). Genetic significance of deformed cross bedding--with examples from the Navajo and Weber Sandstones of Utah. *Journal of Sedimentary Research*, *50*(3), 93-811.

Driese, S., & Dott Jr, R. H. (1984). Model for sandstone-carbonate" cyclothems" based upon the Upper Morgan Formation (Pennsylvanian) of northern Utah and Colorado: Am. *Assoc. Petroleum Geologists Bull*, *58*, 574-597.

Edgett, K. S., & Lancaster, N. (1993). Volcaniclastic aeolian dunes: Terrestrial examples and application to Martian sands. *Journal of Arid Environments*, *25*(3), 271-297.

Eschner, T. B., & Kocurek, G. (1986). Marine destruction of eolian sand seas: origin of mass flows. *Journal of Sedimentary Research*, *56*(3), 401-411.

Forster A., Schouten S., Baas M. and Sinninghe Damsté J. S., 2007, Mid-Cretaceous (Albian-Santonian) sea surface temperature record of the tropical Atlantic Ocean, Geology, v. 35, p.919–922.

Frakes, L.A., Francis, J.E., and Syktus, J.I., 1992, Climate modes of the Phanerozoic, New York: Cambridge University Press, pp. 274.

Fryberger, S. G. (1984). The Permian Upper Minnelusa Formation, Wyoming: Ancient example of an offshore-prograding eolian sand sea with geomorphic facies, and system-boundary traps for petroleum In The Permian and Pennsylvanian Geology of Wyoming. *Wyoming Geological Association* 35,241-271.

Fryberger, S. G. (1986). Stratigraphic traps for petroleum in wind-laid rocks. *AAPG Bulletin*, *70*(12), 1765-1776.

Fryberger, S. G. (1990). Bounding surfaces in eolian sediments. . In: Fryberger, S.G., Krystinik, L.F., Schenk, C.J. (Eds.), Modern and Ancient Eolian Deposits: Petroleum Exploration and Production. Rocky Mountain Section SEPM, Denver, pp. 7.1 – 7.15.

Fryberger, S. G., & Schenk, C. (1981). Wind sedimentation tunnel experiments on the origins of aeolian strata. *Sedimentology*, *28*(6), 805-821.

Fryberger, S. G., & Schenk, C. J. (1988). Pin stripe lamination: a distinctive feature of modern and ancient eolian sediments. *Sedimentary Geology*, *55*(1-2), 1-15.

Fryberger, S. G., Ahlbrandt, T. S., & Andrews, S. (1979). Origin, sedimentary features, and significance of Low-Angle Eolian. *Journal of Sedimentary Research*, *49*(3), 733 – 746.

Fryberger, S. G., Al-Sari, A. M., & Clisham, T. J. (1983). Eolian dune, interdune, sand sheet, and siliciclastic sabkha sediments of an offshore prograding sand sea, Dhahran area, Saudi Arabia. *AAPG Bulletin*, *67*(2), 280-312.

Fryberger, S. G., Schenk, C. J., & Krystinik, L. F. (1988). Stokes surfaces and the effects of near-surface groundwater-table on Aeolian deposition. *Sedimentology*, *35*(1), 21-41.

Fryberger, S. G., Hesp, P., & Hastings, K. (1992). Aeolian granule ripple deposits, Namibia. *Sedimentology*, *39*(2), 319-331.

Fryberger, S. G., Krystinik, L. F., & Schenk, C. J. (1990). Tidally flooded back-barrier dunefield, Guerrero Negro area, Baja California, Mexico. *Sedimentology*, *37*(1), 23-43.

Glennie, K. W. (1987). Desert sedimentary environments, present and past—A summary. *Sedimentary Geology*, *50*(1-3), 135-165.

Glennie, K. W., & Buller, A. T. (1983). The Permian Weissliegend of NW Europe: the partial deformation of aeolian dune sands caused by the Zechstein transgression. *Sedimentary Geology*, *35*(1), 43-81.

Góes, A.M.O. & Feijó, F.J. 1994. Bacia do Parnaíba. Rio de Janeiro, PETROBRÁS, Boletim de Geociências da Petrobras, 8(1):57-67.

Hack, J. T. (1941). Dunes of the western Navajo country. *Geographical Review*, *31*(2), 240-263.

Handford, C. R. (1981). Coastal sabkha and salt pan deposition of the lower Clear Fork Formation (Permian), Texas. *Journal of Sedimentary Research*, *51*(3), 761-778.

Hesp, P. A. (1981). The formation of shadow dunes. *Journal of Sedimentary Research*, *51*(1), 101-112.

Hesp, P. (2002). Foredunes and blowouts: initiation, geomorphology and dynamics. *Geomorphology*, *48*(1-3), 245-268.

Hesp, P. A., & Hyde, R. (1996). Flow dynamics and geomorphology of a trough blowout. *Sedimentology*, *43*(3), 505-525.

Holbrook, J., Scott, R. W., & Oboh-Ikuenobe, F. E. (2006). Base-level buffers and buttresses: a model for upstream versus downstream control on fluvial geometry and architecture within sequences. *Journal of Sedimentary Research*, *76*(1), 162-174.

Horowitz, D. H. (1982). Geometry and origin of large-scale deformation structures in some ancient wind-blown sand deposits. *Sedimentology*, *29*(2), 155-180.

Hummel, G., & Kocurek, G. (1984). Interdune areas of the back-island dune field, North Padre Island, Texas. *Sedimentary Geology*, *39*(1-2), 1-26.

Hunter, R. E. (1969). Eolian microridges on modern beaches and a possible ancient example. *Journal of Sedimentary Research*, *39*(4).

Hunter, R. E. (1977). Basic types of stratification in small eolian dunes. *Sedimentology*, *24*(3), 361-387.

Hunter, R. E., & Richmond, B. M. (1988). Daily cycles in coastal dunes. *Sedimentary Geology*, *55*(1-2), 43-67.

Hunter, R. E., Richmond, B. M., & Rho Alpha, T. A. U. (1983). Storm-controlled oblique dunes of the Oregon coast. *Geological Society of America Bulletin*, *94*(12), 1450-1465.

Jervey, M. T. (1988). Quantitative geological modeling of siliciclastic rock sequences and their seismic expression. In: Wilgus, C.K., Hastings, B.S., Kendall, C.G.St.C., Posamentier, H.W., Ross, C.A., Van Wagoner, J.C. (Eds.), Sea Level Changes — An Integrated Approach. . Special Publication, vol. 42. *Society of Economic Paleontologists and Mineralogists* (SEPM), pp. 47–69.

Jordan, O. D., & Mountney, N. P. (2010). Styles of interaction between aeolian, fluvial and shallow marine environments in the Pennsylvanian to Permian lower Cutler beds, south-east Utah, USA. *Sedimentology*, *57*(5), 1357-1385.

Kamola, D. L., & Chan, M. A. (1988). Coastal dune facies, Permian Cutler Formation (White Rim Sandstone), Capitol Reef National Park area, southern Utah. *Sedimentary Geology*, *56*(1-4), 341-356.

Kinsman, D. J. (1969). Modes of formation, sedimentary associations, and diagnostic features of shallow-water and supratidal evaporites. *AAPG Bulletin*, *53*(4), 830-840.

Kocurek, G. (1981). Significance of interdune deposits and bounding surfaces in aeolian dune sands. *Sedimentology*, *28*(6), 753-780.

Kocurek, G. (1988). First-order and super bounding surfaces in eolian sequences—bounding surfaces revisited. *Sedimentary Geology*, *56*(1-4), 193-206.

Kocurek, G. (1991). Interpretation of ancient eolian sand dunes. *Annual Review of Earth and Planetary Sciences*, *19*(1), 43-75.

Kocurek, G. (1999). The aeolian rock record (Yes, Virginia, it exists, but it really is rather special to create one). *Aeolian environments, sediments and landforms*, 239-259.

Kocurek, G., 2003, Limits on extreme eolian systems: Sahara of Mauritania and Jurassic Navajo Sandstone examples, *in* Chan, M.A., and Archer, A.W., eds., Extreme depositional environments: Mega end members in

geologic time: Boulder, Colorado, Geological Society of America Special Paper 370, p. 43–52.

Kocurek, G. &jordan Day, M. (2018) What is preserved in the aeolian rock record? A Jurassic Entrada Sandstone case study at the Utah–Arizona border. Sedimentology, 65, 1301–1321.

Kocurek, G., & Dott Jr, R. H. (1981). Distinctions and uses of stratification types in the interpretation of eolian sand. *Journal of Sedimentary Research*, *51*(2), 579-595.

Kocurek, G., & Fielder, G. (1982). Adhesion structures. *Journal of Sedimentary Research*, *52*(4), 1229-1241.

Kocurek, G., & Havholm, K. G. (1993). Eolian Sequence Stratigraphy--A Conceptual Framework: Chapter 16: Recent Developments in Siliciclastic Sequence Stratigraphy. SEPM 52, 393-409.

Kocurek, G., & Hunter, R. E. (1986). Origin of polygonal fractures in sand, uppermost Navajo and Page sandstones, Page, Arizona. *Journal of Sedimentary Research*, *56*(6), 895-904.

Kocurek, G., & Lancaster, N. (1999). Aeolian system sediment state: theory and Mojave Desert Kelso dune field example. *Sedimentology*, *46*(3), 505-515.

Kocurek, G., & Nielson, J. (1986). Conditions favourable for the formation of warm-climate aeolian sand sheets. *Sedimentology*, *33*(6), 795-816.

Kocurek, G., Havholm, K. G., Deynoux, M. A. X., & Blakey, R. C. (1991). Amalgamated accumulations resulting from climatic and eustatic changes, Akchar Erg, Mauritania. *Sedimentology*, *38*(4), 751-772.

Kocurek, G., Townsley, M., Yeh, E., Havholm, K. and Sweet, M.L. (1992) Dune and dune-field development on Padre Island, Texas, with implications for interdune deposition and water-table- controlled accumulation. 62, 622–635.

Lancaster, N. (1980). The formation of seif dunes from barchans-supporting evidence for Bagnold's model from the Namib Desert. *Zeitschrift für Geomorphologie*, *24*(2), 160-167.

Lancaster, N. (1986). Grain-size characteristics of linear dunes in the southwestern Kalahari. *Journal of Sedimentary Research*, *56*(3). 395-400.

Lancaster, N. (1997). Response of eolian geomorphic systems to minor climate change: examples from the southern Californian deserts. *Geomorphology*, *19*(3-4), 333-347.

Langbein, W. B., & Schumm, S. A. (1958). Yield of sediment in relation to mean annual precipitation. *Eos, Transactions American Geophysical Union*, *39*(6), 1076-1084.

Langford, R. P. (1989). Fluvial-aeolian interactions: Part I, modern systems. *Sedimentology*, *36*(6), 1023-1035.

Langford, R. P., & Chan, M. A. (1989). Fluvial-aeolian interactions: Part II, ancient systems. *Sedimentology*, *36*(6), 1037-1051.

Leite, J.F., Aboarrage, A.M., Daemon, R.F., 1975. Projeto Carvão da Bacia do Parnaíba.

Lima Filho, F. P. (1998). A Sequência Permopensilvaniana da Bacia do Parnaíba. Tese de doutorado, Universidade de São Paulo, 155p.

Lima, E.A.M. & Leite, J.F. (1978). Projeto estudo global dos recursos Minerais da Bacia Sedimentar do Parnaíba. Integração geológico-metalogenética. DNPM-CPRM, Etapa III, Recife, Relatório Final, 16:212.

Loope, D. B. (1984). Eolian origin of upper Paleozoic sandstones, southeastern Utah. *Journal of Sedimentary Research*, *54*(2), 563-580.

Loope, D. B. (1985). Episodic deposition and preservation of eolian sands: A late Paleozoic example from southeastern Utah. *Geology*, *13*(1), 73-76.

Loope, D. B. (1988). Rhizoliths in ancient eolianites. *Sedimentary Geology*, *56*(1-4), 301-314.

Loope, D. B., Rowe, C. M., & Joeckel, R. M. (2001). Annual monsoon rains recorded by Jurassic dunes. *Nature*, *412*, 64-66.

Mainguet, M., & Chemin, M. C. (1983). Sand seas of the Sahara and Sahel: an explanation of their thickness and sand dune type by the sand budget principle. In *Developments in Sedimentology*. 38, 353-363.

Medeiros, R.S.P., Nogueira, A.C.R., Silva Junior, J.B.C., Sial, A.N., 2019. Carbonate-clastic sedimentation in the Parnaiba Basin, northern Brazil: Record of carboniferous epeiric sea in the Western Gondwana. J. South Am. Earth Sci. 91, 188–202.

McKee, E. D. (1966). Structures of dunes at White Sands National Monument, New Mexico (and a comparison with structures of dunes from other selected areas). *Sedimentology*, *7*(1), 3-69.

McKee, E. D. (1983). Eolian sand bodies of the world. In *Developments in Sedimentology*, 38, 1-25.

McKee, E. D., & Bigarella, J. J. (1972). Deformational structures in Brazilian coastal dunes. *Journal of Sedimentary Research*, *42*(3).

McKee, E. D., & Bigarella, J. J. (1979). Sedimentary structures in dunes. *McKee (Ed.), A Study of Global Sand Seas. US Geological Survey Professional Paper*, *1052*, 83-134.

McKee, E. D., & Moiola, R. J. (1975). Geometry and growth of the White Sands dune field, New Mexico. *J. Res. US Geol. Surv*, *3*(1), 59-66.

McKee, E. D., & Weir, G. W. (1953). Terminology for stratification and cross-stratification in sedimentary rocks. *Geological Society of America Bulletin*, *64*(4), 381-390.

McKee, E. D., Douglass, J. R., & Rittenhouse, S. (1971). Deformation of lee-side laminae in eolian dunes. *Geological Society of America Bulletin*, *82*(2), 359-378.

McKirdy, D.M., 1976. Biochemical Markers in Stromatolites, in: Stromatolites. pp. 163–191.

Mesner, J.C. and Wooldridge, L.C. (1964) Estratigrafia Das Bacias Paleozóica E Cretácea Do Maranhão. Bol. Téc. PETROBRÁS, 7, 137–164.

Miall, A.D.; (1984). Architectural-elements analysis: a new method of facies analysis applied to fluvial deposits. Earth-Science Review, v.22, p. 261-308.

Miall, A.D., 1996. The Geology of Fluvial Deposits: Sedimentary Facies, Basin Analysis and Petroleum Geology. New York, Springer-Verlag, 582 p.

Moretti, M. (2000). Soft-sediment deformation structures interpreted as seismites in middle-late Pleistocene aeolian deposits (Apulian foreland, southern Italy). *Sedimentary Geology*, *135*(1-4), 167-179.

Mountney, N. P. (2006). "Eolian Facies Models" in Posamentier, H. W., & Walker, R. G. (Eds.). Facies models revisited. 23-88.

Mountney, N. P. (2006b). Periodic accumulation and destruction of aeolian erg sequences in the Permian Cedar Mesa Sandstone, White Canyon, southern Utah, USA. *Sedimentology*, *53*(4), 789-823.

Mountney, N., & Howell, J. (2000). Aeolian architecture, bedform climbing and preservation space in the Cretaceous Etjo Formation, NW Namibia. *Sedimentology*, *47*(4), 825-850.

Mountney, N. P., & Jagger, A. (2004). Stratigraphic evolution of an aeolian erg margin system: the Permian Cedar Mesa Sandstone, SE Utah, USA. *Sedimentology*, *51*(4), 713-743.

Mountney, N. P., & Russell, A. J. (2004). Sedimentology of cold-climate aeolian sandsheet deposits in the Askja region of northeast Iceland. *Sedimentary Geology*, *166*(3-4), 223-244.

Nielson, J., & Kocurek, G. (1986). Climbing zibars of the Algodones. *Sedimentary Geology*, *48*(1-2), 1-15.

Olsen, H., Due, P. H., & Clemmensen, L. B. (1989). Morphology and genesis of asymmetric adhesion warts—a new adhesion surface structure. *Sedimentary Geology*, *61*(3-4), 277-285.

Parrish, J. T. (1993). Climate of the supercontinent Pangea. *The Journal of Geology*, *101*(2), 215-233.

Parrish, J. T., & Peterson, F. (1988). Wind directions predicted from global circulation models and wind directions determined from eolian sandstones of the western United States—A comparison. *Sedimentary Geology*, *56*(1-4), 261-282.

Plaziat, J. C., & Poisson, A. M. (1992). Mise en evidence de plusieurs seismes majeurs dans le Stampien superieur continental au sud de Paris; enregistrements sedimentaires de la tectonique oligocene. *Bulletin de la Société géologique de France*, *163*(5), 541-551.

Porter, M. L. (1986). Sedimentary record of erg migration. *Geology*, *14*(6), 497-500.

Price, W. A. (1950). Saharan sand dunes and the origin of the longitudinal dune: a review. *Geogr.Rev.* 40, 462–465.

Pye, K. (1982). Morphological development of coastal dunes in a humid tropical environment, Cape Bedford and Cape Flattery, North Queensland. *Geografiska Annaler: Series A, Physical Geography*, *64*(3-4), 213-227.

Pye, K. (1983). Coastal dunes. *Progress in Physical Geography*, *7*(4), 531-557.

Pye, K. (1983b). Dune formation on the humid tropical sector of the North Queensland Coast, Australia. *Earth surface processes and landforms*, *8*(4), 371-381.

Pye, K., & Tsoar, H. (2009). Aeolian Sand and Sand Dunes, 458 pp.

Rodríguez-López, J. P., Melendez, N., De Boer, P. L., & Soria, A. R. (2008). Aeolian sand sea development along the mid-Cretaceous western Tethyan margin (Spain): erg sedimentology and palaeoclimate implications. *Sedimentology*, *55*(5), 1253-1292.

Rodríguez-López, J. P., Melendez, N., De Boer., Poppe, L., & Soria, A. R. (2012). Controls on marine–erg margin cycle variability: aeolian–marine interaction in the mid-Cretaceous Iberian Desert System, Spain. *Sedimentology*, *59*(2), 466-501.

Rubin, D. M., & Hunter, R. E. (1982). Bedform climbing in theory and nature. *Sedimentology*, *29*(1), 121-138.

Rubin, D. M., & Hunter, R. E. (1983). Reconstructing bedform assemblages from compound crossbedding. In *Developments in Sedimentology*. 38, 407-427).

Sharp, R. P. (1963). Wind ripples. *The Journal of Geology*, *71*(5), 617-636.

Small, H.I. 1914. Geologia e supprimento d'agua subterranea no Piauhy e parte do Ceará. Inspectoria de Obras Contra as Seccas, Serie I.D, Geologia, 32:1-186.

Stokes, W. L. (1968). Multiple parallel-truncation bedding planes--a feature of wind-deposited sandstone formations. *Journal of Sedimentary Research*, *38*(2), 510-515.

Tirsgaard, H., & Øxnevad, I. E. (1998). Preservation of pre-vegetational mixed fluvio–aeolian deposits in a humid climatic setting: an example from the Middle Proterozoic Eriksfjord Formation, Southwest Greenland. *Sedimentary Geology*, *120*(1-4), 295-317.

Tribaldos, V. R., & White, N. (2018). Implications of preliminary subsidence analyses for the Parnaíba cratonic basin. Geological Society, London, Special Publications, 472(1), 147-156.

Tsoar, H. (1984). The formation of seif dunes from barchans—a discussion. *Z. Geomorphol*, *28*(1), 99-103.

Tsoar, H., & Blumberg, D. A. N. (2002). Formation of parabolic dunes from barchan and transverse dunes along Israel's Mediterranean coast. *Earth Surface Processes and Landforms*, *27*(11), 1147-1161.

Vaz, P.T., Resende, N.G.A.M., Wanderley Filho, J.R., Travassos, W.A. (2007). Bacia do Parnaíba. Rio de Janeiro, PETROBRÁS, Boletim de Geociências, 15(2):253-263.

Veiga, G. D., Spalletti, L. A., & Flint, S. (2002). Aeolian/fluvial interactions and high-resolution sequence stratigraphy of a non-marine lowstand wedge: the Avilé Member of the Agrio Formation (Lower Cretaceous), central Neuquén Basin, Argentina. *Sedimentology*, *49*(5), 1001-1019.

Vieira, L. V., & dos Santos Scherer, C. M. (2017). Facies architecture and high resolution sequence stratigraphy of an aeolian, fluvial and shallow marine system in the Pennsylvanian Piauí Formation, Parnaíba Basin, Brazil. Journal of South American Earth Sciences, 76, 238-256.

Walker, R. G. e James, N. P. (1992). Facies Models - In response to Sea Level Change.

Wanless, H.R. and Shepard, F.P., 1936, Sea level and climatic changes related to late Paleozoic cycles, Geological Society of America Bulletin, v. 47, p. 1177–1206.

Wilson, I. G. (1971). Desert sandflow basins and a model for the development of ergs. *Geographical Journal*, 180-199.

Wilson, I. G. (1972). Aeolian bedforms—their development and origins. *Sedimentology*, *19*(3-4), 173-210.

Wilson, I. G. (1973). Ergs. *Sedimentary geology*, *10*(2), 77-106.

9 ARTIGOS

9.1 ARTIGO 1

Dear Mr. Kifumbi:

Your manuscript entitled "Missing and preserved strata: keys for spatio-temporal variability in aeolian dune-field, Pennsylvanian Upper Piauí Formation (Parnaíba Basin), Brazil" has been successfully submitted online and is presently being given full consideration for publication in Sedimentology.

Your manuscript ID is SED-2021-OM-059.

Please quote the above manuscript ID in all future correspondence. If you have an existing user account for Sedimentology and there have been any changes to your contact details since you last used the website, please log in to Manuscript Central at https://mc.manuscriptcentral.com/sed and edit your user information as appropriate.

You can also view the status of your manuscript at any time by checking your Author Center after logging in to https://mc.manuscriptcentral.com/sed.

This journal offers a number of license options, information about this is available here: https://authorservices.wiley.com/author-resources/Journal-Authors/licensing/index.html. All co-authors are required to confirm that they have the necessary rights to grant in the submission, including in light of each co-author’s funder policies. For example, if you or one of your co-authors received funding from a member of Coalition S, you may need to check which licenses you are able to sign.

Thank you for submitting your manuscript to Sedimentology.

Yours sincerely
Elaine Richardson
Editorial Office Manager
Sedimentology

Missing and preserved strata: keys for spatio-temporal variability in aeolian dune-field, Pennsylvanian Upper Piauí Formation (Parnaíba Basin), Brazil

Carrel Kifumbi[1], Claiton Marlon dos Santos Scherer, Rossano Dalla Lana Michel, Felipe Guadagnin, Ezequiel Galvão de Souza, Adriano Domingos dos Reis, João Pedro Formolo Ferronatto, Fábio Herbert Jones
Programa de Pós-Graduação em Geociências, Universidade Federal do Rio Grande do Sul, P.O. Box 15001, CEP 91501-970 Porto Alegre, RS, Brazil
carrelkif@yahoo.fr

ABSTRACT

Although the preserved aeolian strata represent less time than the gaps, they have received more attention. Understanding the evolutionary history embedded within gaps requires a clear identification of the missing evolutionary stages and the mechanisms responsible for erosion. Through facies analysis of the Pennsylvanian to Permian Upper Piauí Formation four genetic units were identified. Time gaps are observed in both expansion and contraction phases. Units are organized in three drying-upward cycles that reflect climatic changes from relatively humid to dryer conditions. The first cycle is characterized by sabkha deposits at the base (Unit I), followed by a dry aeolian system (Unit II). Units I and II are separated by a sand-drift surface that marks a span between sabkha desiccation and dunefield expansion. The dry aeolian system is characterized by stacking of aeolian dunes and downwind increase in dimensions towards NW suggesting deceleration of saturated winds in a topographic depression. The second (Unit III) and third (Unit IV) drying-upward cycles are characterized by sandsheet elements at the base followed by progressively higher dunes and thinner interdunes. Furthermore, spatial change in wet system architecture is marked by a thickening of sandsheet deposits, reduction of dune/interdune ratio and reduction in dune dimensions towards NW. Such spatial changes suggest that the northwestern region represents dune margins where the water table level is close to the accumulation surface. Deposition of sandsheet suggests that the rate of sand availability was initially

equal to the rate of water table rise, and then the rate of sand availability became higher and allowed the formation of simple dunes. Aeolian units are capped by extensive supersurfaces that suggest deflation episodes triggered by exhaustion of sand availability. The expansion and contraction phases that characterize each drying-upward cycle are related to glacio-eustatic cycles characteristics of Pennsylvanian to Permian period.

1 INTRODUCTION

In aeolian sequences, the preserved sedimentary succession records only a small time span of the entire dune-field evolution. Significant volume of strata is removed and great periods of time are collapsed into bounding surfaces (Kocurek & Day, 2018). These time gaps are essentially caused by cannibalization of dunes during migration, either in expansion or contraction phases. During expansion phases, the earlier bedform strata (protodunes) are eroded by subsequent dune scours (Kocurek et al, 1992; Lancaster, 1996), whilst in contraction phases, dunes develop a negative angle of climb, cannibalize the ending stage bedforms and deflate part of the accumulation (Kocurek et al., 1992; Kocurek & Havholm, 1993). Although dune migration constitute an autogenic process, the resultant accumulation or deflation and the preservation are related to sand supply, availability and wind energy which define the sediment state (Kocurek & Lancaster, 1999). In turn, the sediment state is controlled by allogenic factors - tectonic, climatic and relative sea-level cycles (Kocurek, 1999). Any change in one of the key controlling factors triggers systematic changes in dune and interdune dimensions, rate of sand availability and rate of water table rise both spatially and temporally (Mountney, 2012). Despite the advanced knowledge on mechanisms of aeolian sedimentation, studies aiming to unveil the depositional history embedded in the gaps are rare (Kocurek & Day, 2018).

The late Pennsylvanian upper Piauí Formation aeolian succession is characterized by both dry and wet aeolian systems punctuated by bounding surfaces formed during expansion and contraction phases. The sedimentary record crops out over an area of ca. 400 km² as extensive hill tops and cliffs up

to 70 m high where architectural elements and bounding surfaces are reliably traced over the entire area.

This study aims to determine the evolutionary stage of the preserved aeolian strata and investigate the mechanisms responsible for the erosion of protodune and ending stage of dune-field evolution. These objectives are achieved through stratigraphic analysis and quantitative reconstruction of dune and interdune original dimensions to identify spatial and temporal variability across the erg. Moreover, the mechanisms for time gap generation are analyzed regarding the major global climatic, eustatic and tectonic changes that occurred during the Pennsylvanian in central-west Gondwana hinterland.

2 BACKGROUND

2.1 Origins of time gaps in accumulation and deflation phases

The onset of aeolian dune-field construction is characterized by sand patches emerging from the substrate as wind flows turn saturated due to flow deceleration. Sand patches then grow to protodunes (Kocurek et al., 1992), and subsequently protodunes evolve toward larger and more widely spaced dunes and eventually draas (Kocurek et al., 1992; Ewing & Kocurek, 2010a; Kocurek et al., 2010; Gao et al., 2015). Whilst sand patches are composed entirely of wind-ripple laminae (Swanson et al., 2019; Kocurek et al., 1992), protodunes are characterized by wind-ripple and grainfall laminae, dunes are characterized by grainflow avalanching on slipface; and draas are characterized by superimposed dunes (Kocurek et al., 1992).

During the onset of construction phases, protodune accumulation is unlikely to occur because deeper scours expected during migration of subsequent higher dunes usually erase previous bedforms (Paola & Borgman, 1991; Day & Kocurek, 2017; Swanson et al., 2019). Dry aeolian systems are specific case where protodunes do not accumulate unless in some special cases (Jerram et al., 2000; Scherer, 2002; Kocurek & Day, 2018). In these systems, the accumulation only begins when bedforms have grown to the point where interdune flats were eliminated (Wilson, 1971). Thus, protodunes are usually eroded and incorporated into higher bedforms. By contrast, in damp/wet aeolian systems protodunes are less likely to be deflated or eroded especially

when an absolute or relative rise in water table permit long-term accumulation and preservation (Kocurek & Havholm, 1993; Benan & Kocurek, 2000).

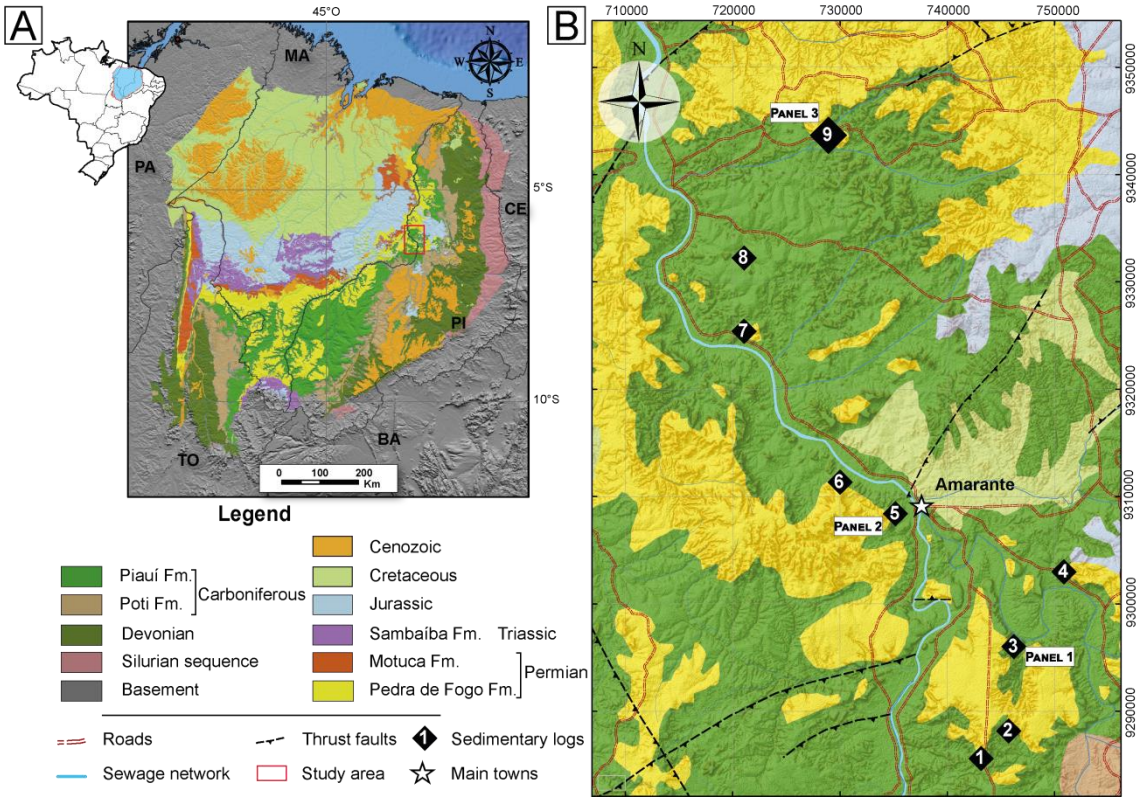

Figure 31: (A) Location of the Parnaíba basin and limits of the study area (in red). (B) Simplified geologic map of the studied area based on Brazilian Geologic Service (CPRM). Most of the regions colored in green represent the lower Piauí Fm. while aeolian deposits of upper Piauí Fm. are mostly observed at the borderline with Pedra de Fogo formation.

Conversely, during the final stages of dune-field evolution, the available sand is progressively exhausted and wind flow turns unsaturated in relation to its transport capacity (Mountey, 2006a). This condition leads to deflation of sand from dunes, reduction of dune dimensions and negative angle of climb. Deflation lowers the accumulation surface until a regional baseline of erosion is reached (Looope, 1985; Mountney, 2006). Because the depth of stabilization surface is significantly lower in dry aeolian systems, the amount of accumulation eroded in dry systems ranges from a few centimeters to several meters (Kocurek and Day, 2018). By contrast, in wet/damp aeolian systems the shallow water-table prevents deeper erosion. In sum, time gap during destruction phases is variable but can be estimated by the evolutionary stage of the preserved strata.

3 GEOLOGICAL SETTING

3.1 Tectonic framework

The Parnaíba Basin is a Paleozoic (Silurian to Cretaceous) intracratonic sag basin (Watts et al., 2018). The basin is located in the northeastern region of Brazil and covers an area of c. 660,000 km² (Fig. 1). The basin lies down unconformably on a basement built up from the collision of three Precambrian blocks: in the west, the Amazonian/Araguaia block is characterized by ophiolitic metasedimentary rocks; in the center, the Parnaíba block composition is uncertain yet is probably composed of granitoid rocks; and in the east, the Borborema block is formed by mylonitic gneisses (Daly et al., 2014). Rodriguéz Tribaldos and White (2018) investigated the subsidence history of the basin and proposed a gradual exponential decrease in subsidence over 340 Ma. The most rapid subsidence occurred within the first 100 Ma of the basin initiation (Silurian) later followed by slower rate from Carboniferous to Mesozoic.

3.2 Sedimentary succession

The sedimentary succession is nearly 3500 m thick, composed of five supersequences; this study focuses on the Pennsylvanian to Permian succession (Fig. 1). The Permo-Pennsylvanian succession of Parnaíba Basin includes Piauí and Pedra de Fogo formations. The Piauí Formation crops out in the south and east of the basin and is characterized by cyclic sedimentation. Each cycle initiated with fluvial and coastal aeolian deposits then overlain by shallow marine deposits (Vieira & Scherer, 2017). The studied aeolian succession occurs in the upper Piauí Formation, also refers to as Saraiva Sandstone (Mesner Wooldridge, 1964; Leite et al., 1975; Lima & Leite, 1978), and is separated from the underlying succession by a regionally extensive level of oolitic grainstone associated with stromatolites. The depositional age is constrained between Pennsylvanian age for the lower Piauí succession and Permian age for the overlying Pedra de Fogo formations (Mesner Wooldridge, 1964; Leite et al., 1975, Dino & Playford, 2002; Dino et al., 2002).

The Pedra de Fogo Formation is a Permian, plant- and vertebrate-rich unit (Iannuzzi et al., 2018) separated from the underlying Piauí Formation by a paraconformity. This formation consists of a cyclic sedimentation of sandstones,

mudstones, oolitic and concretionary limestones, and greenish fossiliferous shales. The sedimentation represents restricted shallow epeiric seas and coastal environments deposited during warm climatic conditions (Lima Filho, 1998) associated with coastal aeolian, lacustrine floodplain, and fluvial channel deposits (Araújo et al., 2016; Jones et al., 2021).

4 DATA AND METHODS

Stratigraphic analysis constitutes the main tool chosen to achieve our objectives. Field investigations were carried out in the eastern margin of the Parnaíba Basin. Localities around Amarante town of Piauí state were selected for detailed investigations because of the well exposed and laterally extensive cliffs that crop out over an area of 80 x 50 km (Fig. 1).

The main parameters considered for bedform reconstruction include (i) maximum set thickness, measured in cross-sections oriented both parallel and perpendicular to the mean aeolian transport; (ii) angle of climb calculated trigonometrically by the angle between interdune surface and the underlying supersurface; and (iii) dune wavelength calculated in cross-sections parallel to the mean aeolian transport (Mountney and Howell, 2000; Mountney, 2006; Romain and Mountney, 2014). The distance is calculated trigonometrically by the equation (1): $\lambda = s/\tan\delta$ where λ is dune wavelength, s represents set thickness, and δ is the angle of climb. Subsequently, the minimum bedform height was reconstructed using function (2) $D_h = c\ D^n_s$, where Dh is the minimum dune height, Ds is dune spacing, c and n are constants (Lancaster, 1988). Dune spacing as used by Lancaster (1988) is the same as dune wavelength used in this article.

The elevated slope of some cliffs precluded direct logging and measurements. For this reason, virtual outcrop models were built using images acquired with a remotely piloted aerial system (drone). Images were processed through the Structure from Motion with Multi-View Stereo workflow (Carrivick & Smith, 2016; Viana et al., 2018) to produce the low-resolution model - average ground sampling distances of 2 cm/pixel, and high resolution model - average ground sampling distances of 6 mm/pixel. Translation, rotation, and scaling were made using the coordinates of images to ensure that all models are at the same height level within a metric size accuracy tolerance. Finally, models were

interpreted in Move Petex software where identification of architectural element type and geometry, surface tracking, angle of climb calculation and paleocurrent measurement were achieved in three dimensions. Three two-dimensional orthomosaic panels are presented herein to depict sedimentary architecture and bounding surface nature. These panels occupy different positions within the area (south, center and northeast) to contemplate different regions within the dune-field (Fig. 1). Panels were used to construct regional correlation and also to compare quantitative data in order to identify sedimentation variability across the dune-field.

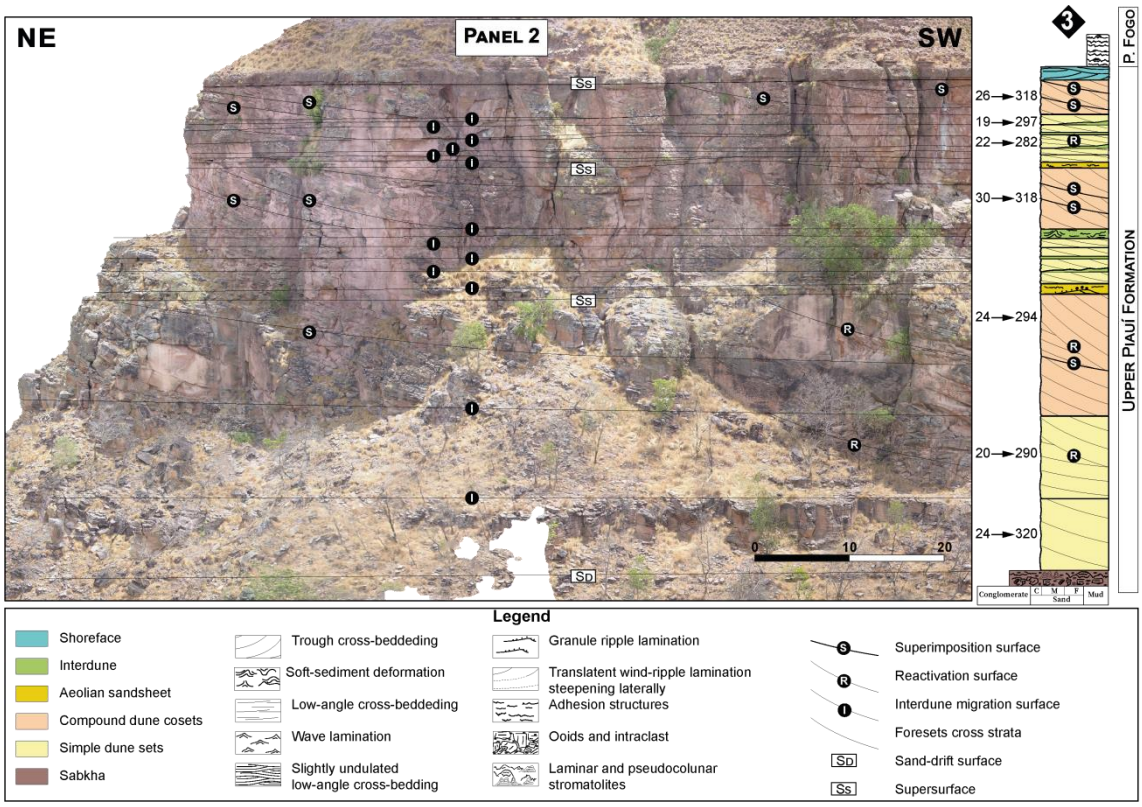

Figure 32: 2D orthomosaic panel of Morro da cruz cliff in São Francisco do Maranhão build from drone images. Aeolian deposits occur as vertical slope hilltops where architectural elements and bounding surfaces are easily identified.

Nine sedimentary logs were constructed detailing sedimentary facies and architectural elements relationships. The entire aeolian succession is bounded on the bottom and top by regionally extensive stratigraphic surfaces and ranges from 27 to 53 m thick (Fig. 2). Furthermore, seven samples were selected for petrologic and sedimentological analysis. Petrologic analyses were conducted using point count methods (Shutter et al., 1985).

The determination of wind regime during the Permo-Pennsylvanian were conducted using measurements of cross-bedded sets and bounding surfaces dip directions (simple dune sets n = 192, superimposed dunes n = 35). The mean azimuth was corrected to compensate for the clockwise rotation of Gondwana and then plotted on paleogeographic map.

5 RESULTS

The sedimentary succession studied is characterized by aeolian and subordinate non-aeolian deposits. Identification of facies associations and architectural elements was achieved based on architectural style, geometry, facies characteristics and relationships with adjacent units. Detailed descriptions and process interpretations are provided in this section.

5.1 Sabkha

Description: This facies association consists of thin (60 cm to 80 cm), yet regionally extensive microbialite (Burne & Moore, 1987) composed of columnar and laminated stromatolites interbedded with oolitic grainstone, and intraformational conglomerates (fig. 3). Macroscopic analysis of stromatolites allowed identification of millimeter-scale horizontal or undulated lamination and low-relief domes of up to 40 cm in wavelength and 10 cm in height, semi-circular to irregular in plan view. Columnar stromatolites occur overlying laminated ones, individual columns are typically 1 cm in diameter and 3 to 5 cm in height, and spaced a few millimeters (fig. 3). Both laminar and columnar stromatolites exhibit a disrupted and brecciated aspect. In thin section, horizontally laminated stromatolites are formed by millimetric irregular and lenticular lamination, predominantly replaced by microporous cryptocrystalline silica, and rhombohedral dolomite. The levels with a predominance of dolomite have more remnants of the original muddy matrix, partially replaced by silica and cryptocrystalline iron oxides. Fractures and vugular pores in silicified levels are filled with macrocrystalline dolomite. Mold pores from the dissolution of dolomite crystals were partially filled by iron oxides. Columnar stromatolites are characterized by digiform features that correspond to microbial colonies, replaced by cryptocrystalline and microcrystalline silica, microspherulitic chalcedony and rhombohedral crystals of dolomite. Dissolution of dolomite

crystals resulted in mold pores partially filled with iron oxides. The spaces between the “fingers” were filled with microporous microspherulitic chalcedony. Fractures through the “fingers” and interstitial chalcedony were partially filled with drusiform prismatic quartz and dolomite, later dissolved. Mold, vugular and channel pores generated by the dissolution of dolomite were partially filled by cryptocrystalline clay and oxides.

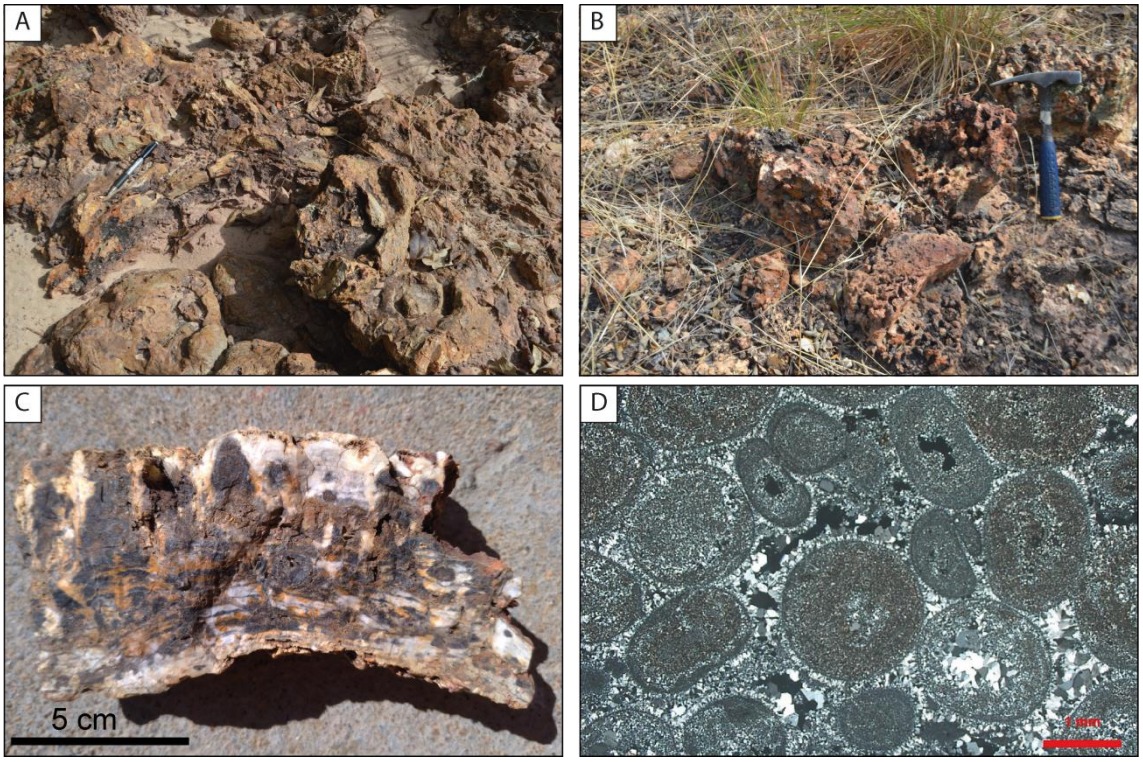

Figure 33: Characteristic features of sabkha element. (A) Brecciated and upturned blocks of microbialites. (B) Columnar stromatolites. (C) Centimeter-scale digiform colonies growing over horizontal and undulated laminae. (D) Photomicrography of oolitic grainstones. Note the oval and elongated shapes, moldic and intergranular pores and intense replacement by silica.

Oolitic grainstones are characterized by ooids that range from 0.15 to 2.5 mm in diameter, microcrystalline intraclasts, and smaller peloids completely replaced and cemented with cryptocrystalline to microcrystalline silica, with prismatic quartz and cryptocrystalline hematite. Ooids are generally oval, elongated or irregular in shape (fig. 3). Heterogeneous compaction can be inferred from areas of intense deformation of ooids and areas with only punctual inter-particle contacts. Dissolution of rhombohedral dolomite resulted in abundant heterogeneously disseminated mold pores filled by silica, hematite or iron oxide. Intra-particle and inter-particle pores of partial dissolution of ooids are partially or totally filled with drusiform prismatic quartz or radiated

chalcedony. Associated conglomerates are clast supported, massive and characterized by a brecciated aspect. They are dominantly composed of large (0.5 to 2.0 cm) angular cryptocrystalline to microcrystalline silica intraclasts and silicified ooids, cemented by drusiform prismatic quartz.

Interpretation: Stromatolite morphologies are essential criteria to investigate the depositional settings (Hoffman, 1976; Grotzinger, 1989). Microbial laminites with low-relief dome shapes are formed by bioherms and represent the accretion of stromatolite through time (Grotzinger, 1989). Low-relief domal stromatolites and centimeter-scale columnar stromatolites indicate development in a shallow-water depositional environment (Kah et al., 2017). The intense replacement by silica preclude identification of the original composition of ooid core essential for precise interpretation of environment energy. Nevertheless, the oval and irregular shapes and the wide variation in size of the ooids suggest that they did not originally correspond to carbonate oolites. The common occurrence of elongated forms even in poorly compacted areas suggests that ooids had original clay composition (chamosite or stevensite) characteristics of low energy environment. Hematite, clay coating and iron oxide filling mold, vugular and channel pores from the dissolution of dolomite suggest telodiagenetic infiltration in the vadose zone. Intense cementation by cryptocrystalline and microcrystalline silica and quartz overgrowths suggest early diagenesis (Goldberg et al., 2011). Early diagenesis would have caused heterogeneous compaction, as attested by areas of intense deformation and elongated ooids and others with only punctual interparticle contacts. Shallow water environments dominated by low energy currents with ooid formation and microbial activity resemble present sabkha environments. In these environments, stromatolite develops during periods of low terrigenous sediment influx and ooids formation are induced by microbial activity summed with wave agitation (Plee, 2008). Intraformational conglomerates reflect periods of high energy like storms and brecciated stromatolite laminae indicate subaerial exposure during water-lever lowering episodes (Buck, 1980).

5.2 Compound dune cosets

Description: Architectural elements composed of well-sorted, very fine- to medium grained sandstones, sometimes bimodal, are organized in large-scale,

planar and trough cross-stratified sets ranging from 3.0 to 19.5 m thick and several hundred meters in lateral extent. Cosets are limited by extensive, nearly horizontal erosive surfaces gently inclined upwind that can be traced laterally over hundreds of meters in cross-sections parallel to paleowind direction (Kocurek, 1981; Mountney and Howell,2000). Internally, cosets display low-angle planar surfaces inclined downwind bounded above and below by the previously cited horizontal surface (Fig. 4). These surfaces dip 3° to 19°, with a mean trend towards west (mean vector = 274°) with relatively low dispersion (between 230° and 320°). Cosets are punctuated by steep concave-up erosive surfaces that commonly dip towards NW (300°).

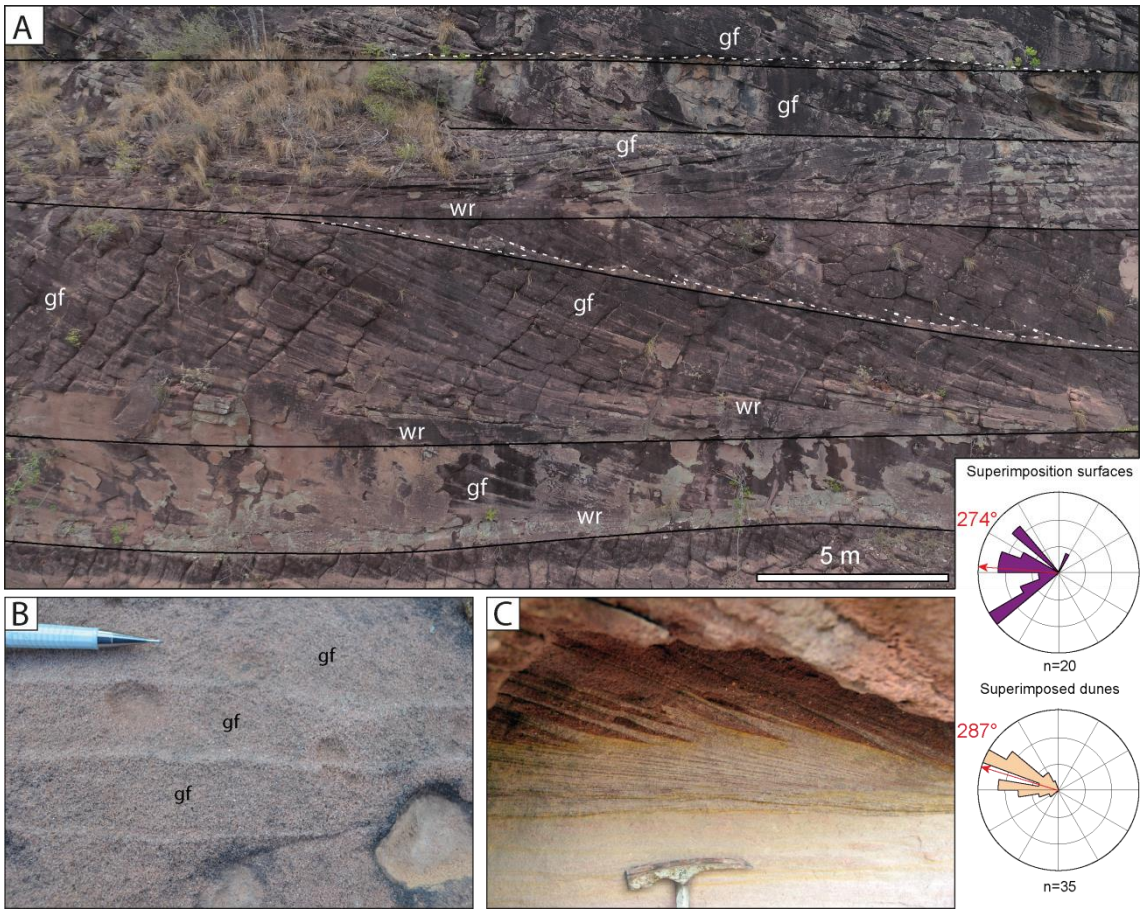

Figure 34: Facies architecture of aeolian dunes. (A) Alternation of simple dune sets and compound dune cosets. Dunes are internally composed of wind ripples laminae (wr) at the base interfingering with grainflow strata (gf). Dunes overlain each other or may be separated by interdune facies (wedge shape interdune between two simple dunes at the uppert part of the illustration). (B) Grainflow strata separated by grainfall laminae. Grainflow lenses interfingering with wind ripple. Observe the mean dip direction of superimposition surfaces towards W while superimposed dune direction of migration is slightly oblique NW.

Cross-strata are composed of progressively steeper forests, where wind ripple strata occur at the base and grainflow at the top. Wind-ripples strata are inversely-graded and arranged in 0.3 to 0.9 cm thick laminae. Grainflow strata have wedge shapes and form massive or inversely graded, medium-to-coarse grained sandstones strata 1 to 6 cm thick (Fig. 4). Grainfall strata are rare and occur as very fine-grained sandstones, of around 1 to 2 mm thick laminae, between grainflow strata. Where grainfall laminae are extremely thin, individual grainflow strata may appear as homogeneous stacked ones. For this reason, grainflows thickness was measured only where limits are well marked. Cross-strata have dip orientation towards west-northwest (mean vector = 287°) with relatively low dispersion (between 260° and 310°). In sections parallel to aeolian transports, cross-strata forests appear highly inclined, dipping from 7° to 25°, whilst sections perpendicular to transport exhibit trough geometries.

Interpretation: Well-sorted and bimodal sandstones arranged in cross-strata cosets composed of wind ripple, grainflow and grainfall strata are typical of aeolian dune deposits (Hunter, 1977; Kocurek, 1981, 1991, 1996). Horizontal to upwind inclined bounding surfaces that can be traced over several hundred meters are interdune migration surfaces (Brookfield, 1977; Kocurek 1981a). Internally, the low-angle down-wind inclined planar surfaces truncated by interdune surfaces are superimposition surfaces, originated by the migration of dunes on the lee slope of draas (Brookfield, 1977; Kocurek, 1991, 1996). Steep downwind-dipping surfaces truncated by interdune surfaces are reactivation surfaces generated through partial erosion of the bedform caused by changes in wind pattern or wind direction/strength (Brookfield, 1977; Fryberger, 1993). The progressive steepening of forests arises as a consequence of distinct processes that occur on the slipface of a dune: grainflow emerges from avalanche of non-cohesive sands on the brink of slipface where the slope angle is higher, and commonly alternate with grainfall; by contrast, the lee slope angle of the slipface is smoother due to wind-ripple migration in the plinths of aeolian dunes (Hunter, 1977). The unimodal direction and high dispersion (around 90°) of superimposition surface is suggestive of crescentic compound dunes. Similarly, the trough geometry of the cross-strata in cross section perpendicular to airflow suggests crescentic superimposed dunes. The unimodal direction of

superimposed surfaces suggests that while compound dunes migrated towards W, a secondary oblique airflow allowed the migration of superimposed dunes towards NW (Fig. 4).

5.3 Simple dune sets

Description: This architectural element is characterized by a series of trough-cross beddings defining sets of 0.6 to 2.9 m thick that extend laterally for hundreds of meters in cross-section oriented parallel to aeolian transport. When observed perpendicular to the mean paleowind, sets have highly inclined scoured bases. Sets are commonly separated by interdune deposits (next topic) and generate various types of interfingering relationships on the toeset. Less often these sets rest directly over one another, and are separated by erosive surfaces.

Foresets within trough cross strata are composed of grainflow lenses that reach the lowermost part of the set where they interfinger with wind-ripple laminae (Fig. 4). Cross-strata are inclined 10° to 22° and show dispersion of forest dip direction from 260° to 330° (mean vector = 270°). Deformation structures are often observed on the toeset where cross-strata show small-scale flame structures and convolute folds.

Interpretation: Aeolian dune sets characterized essentially by tangential/trough-cross strata suggest that bedforms had curved crest lines (Rubin, 1987). The lateral continuity of hundreds of meters in sections parallel to the prevailing paleowind direction, together with the wide dispersion of foreset-dip direction (around 70°) and the trough geometry of bounding surfaces between the sets indicate crescentic dunes with a sinuous crestline (Rubin, 1987; Paola & Borgman, 1991). The abundance of grainflow in the lower part of the sets indicate that avalanching processes reached the dune toeset, possibly facilitated by reduced dune height, because such features rarely reach the base in high slipfaces. The occurrence of deformation on the basal part of sets suggests liquefaction due to water escape caused by overload of water-saturated sand (McKee et al., 1971; Mountney & Thompson, 2002; Doe & Dott, 1980; Horowitz, 1982; Mountney & Thompson, 2002).

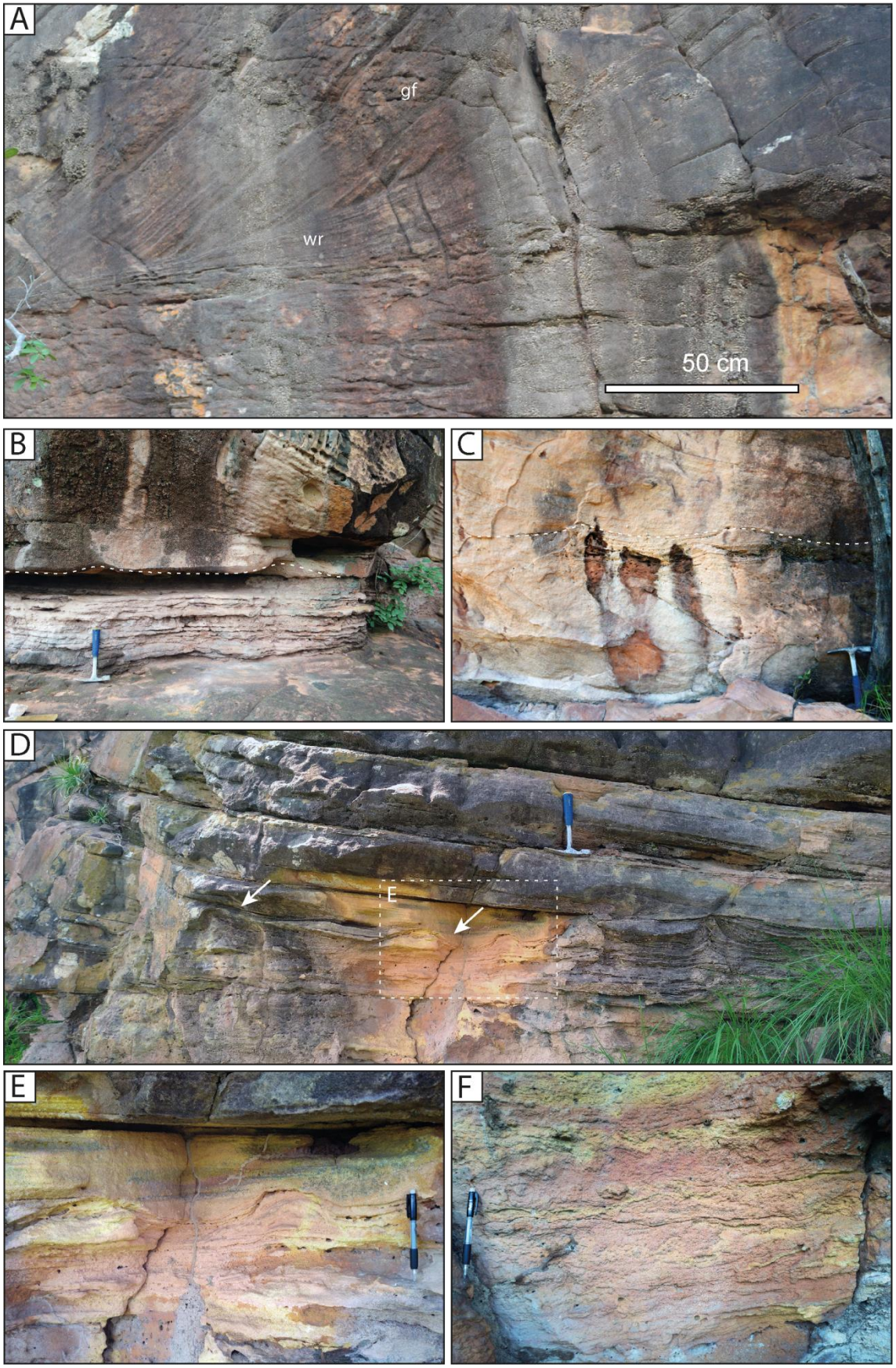

Figura 35: Type of architectural relationship between aeolian dunes and interdune. (A) Dune toeset passing downd-dip into interdune, suggestin migration of dune over dry interdune. (B) and (C) Cyclical

scours of dunes in damp interdunes indicate water table fluctuation and frequent erosion over dry surface. (D) Small-scale flame structures and convolute folds suggest high water table elevated pore pressure at time of dune advance. White arrows point deformations. (E) Detail of deformation structures. (F) Crinkly lamination and adhesion structures suggesting high water table.

5.4 Interdunes

Description: This facies association is composed of fine-grained sandstones and forms thin beds, ranging from 10 to 50 cm thick, though occasionally attaining a maximum thickness of 1.7m. These units are characterized by adhesion structures or near-horizontal translatent wind-ripple laminae.

Interdunes were observed sandwiched between dune sets or as tabular layers traced for hundreds of meters. These elements show a basal abrupt boundary with the underlying set, but the upper contact with the toeset of dune sets displays a series of interfingering relationship (Fig. 5): (i) Grainflow lenses pass down-dip into horizontal wind-ripple translatent strata or adhesion structures, (ii) Dune scours into interdune and (iii) Deformation of dune toesets.

Interpretation: Whilst adhesion structures and soft sediment deformations are indicative of accumulation under damp conditions, translatent wind-ripples laminae suggest drier substrate. The intertonguing relationship of both dry and damp interdune elements with small-scale dune sets indicates that interdune sedimentation was synchronous with dune migration and accumulation (Mountney & Thompson, 2002; Mountney, 2006a). Soft sediment deformation is due to liquefaction and upward fluid escape from water-saturated conditions of the substrate (Doe & Dott, 1980; Horowitz, 1982), hence implies a relatively high water-table level. Wind-ripple strata alternated with adhesion structure suggest fluctuations of water-table level (Mountney, 2012). Intertonguing types are generated by dune advance over dry or damp interdunes and are detailed in Mountey, (2006a).

5.5 Aeolian Sandsheet

Description: This facies association forms tabular sand bodies of 0.85 to 4.80 m thick and extend laterally for several hundreds of meters in sections both parallel and perpendicular to the mean aeolian transport direction. Aeolian sandsheets are limited at the base by extensive horizontal erosive surface and internally composed predominantly of near-horizontal to low-angle wind-ripple

strata of fine-grained inversely graded sandstones. In some cases granule ripples and coarse sand-grained wind-ripples occur alternating with fine sand-grained wind ripples (Fig. 6). Decimeter-scale (10 to 20 cm) trough-cross strata dominantly made of wind ripple occasionally occur encased within sandsheet element and pinch-out laterally within wind-ripple strata. Occasionally adhesion structures and flame structures are observed (Fig. 6).

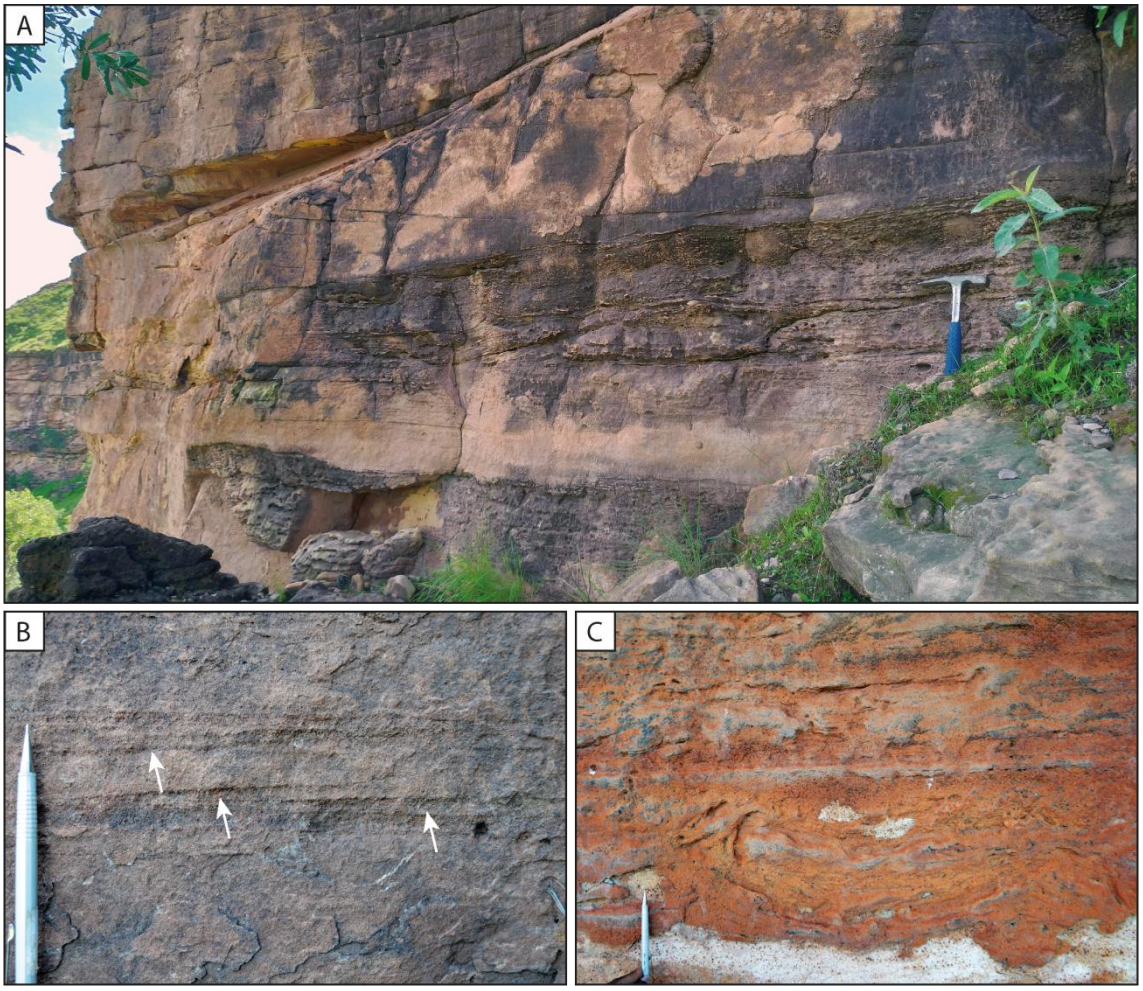

Figure 36: Sandsheet element. (A) Thick and laterally extensive sandsheet deposits dominated by near-horizontal to crinkly lamination. (B) Low-angle cross lamination characterized by inverse graded granule ripples. (C) Flame structures associated with horizontal lamination.

Interpretation: Low angle and near-horizontal wind-ripple strata suggest migration of wind ripples over a dry substrate. By contrast, adhesion structures and soft sediment deformations point to damp conditions. The predominance of wind-ripple strata and the significant thickness and lateral continuity of these deposits suggest limited sand availability and deposition in sandsheet environments (Fryberger et al., 1979; Fryberger & Scenk, 1981; Fryberger et

al., 1992 Kocurek & Lancaster, 1999). Decimeter-scale trough-cross strata dominantly characterized by wind-ripples represent bedforms without a well-developed slip face, characteristic of protodunes (Kocurek et al., 1992). The preservation of protodune within sandsheets suggests an absolute or relative rise in water table simultaneous to protodune migration (Kocurek & Havholm, 1993; Benan & Kocurek, 2000; Mountney & Russell, 2009; Mountney, 2012). The vertical alternation of coarse and fine grained wind ripple was the result of periodic introduction of coarse grains (Kocurek & Nielson, 1986) due to periodic shift in wind strength (Bagnold, 1941).

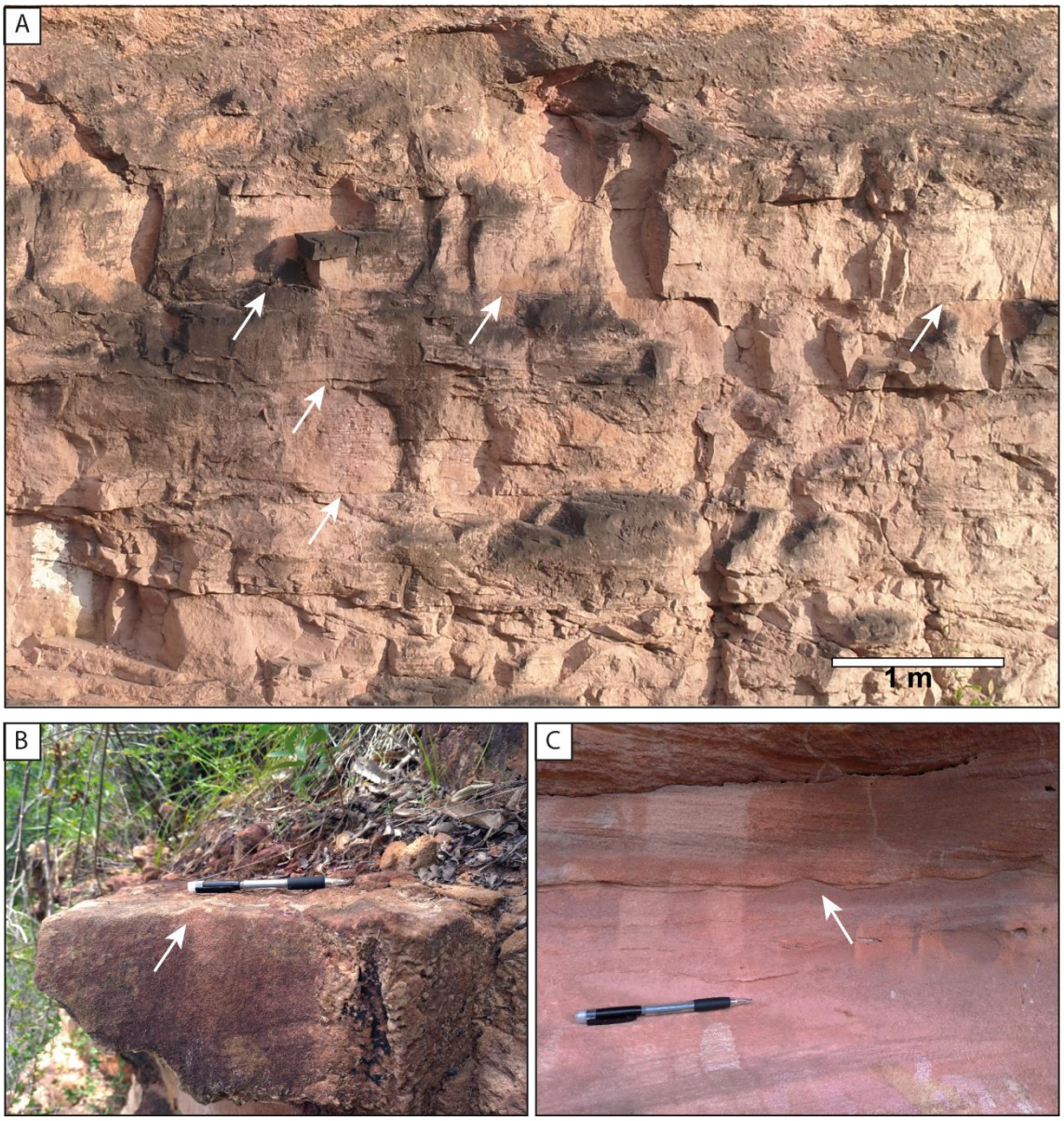

Figure 37: Shoreface elements. (A) Tabular bodies of well-sorted sandstones with low-angle lamination. White arrows point to undulated surface and symmetric ripples at the top of layers. (B) and (C) detail of symmetric wavy ripples commonly observed at the top of layers.

5.6 Shoreface

Description: This facies association is 1-2 m thick and laterally continuous over hundreds of meters. The basal boundary with the underlying aeolian dune sets is marked by a regionally extensive near-horizontal planar erosive surface. The facies association is composed of fine- to medium- grained, well-sorted sandstones. The most common structures are symmetrical wavy lamination and medium to large scale slightly undulated low-angle cross-bedding ranging from 60 cm to more than 2 m in wavelength (Fig. 7). Less frequently, trough-cross stratifications and massive sandstone are observed. Massive sandstones are composed of fine- to medium-grains and mud intraclasts.

Interpretation: Symmetrical wavy lamination and medium to large scale slightly undulated low-angle cross-bedding are generated by oscillatory flows (Dumas and Arnott, 2006). Medium and large wavy marks represent swaley cross-stratification while trough-cross bedded sandstones are interpreted as swash-zone deposits. The interpreted depositional environment for this unit is shallow-water to nearshore environments where both unidirectional currents and oscillatory flows occurs (Dumas & Arnott, 2006). The blocky aspect of massive sandstones suggests obliteration of the depositional structure.

6 GENETIC UNITS

Genetic units refer to deposits originated by a single depositional event, bounded at bottom and top by supersurfaces or sand drift surfaces (Clemmensen, 1989; Scherer, 2002). This section presents the depositional model of each genetic unit and discusses their spatial variability and temporal evolution base on quantitative measurements and stratigraphic correlation of three orthomosaic panels over a ca 50 km, SE-NW traverse (Fig. 8).

6.1 Genetic Unit I

Description: The GU I is composed of a unique 0.6 to 0.8 m thick layer essentially composed of microbialite deposits alternated with oolitic grainstones. The intense cementation by silica Progre. The unit is easily identified in the field by a near-horizontal, vegetated topographic level at the base of hilltops. The GU I is separated from the overlying GU II by a sharp and laterally extensive surface.

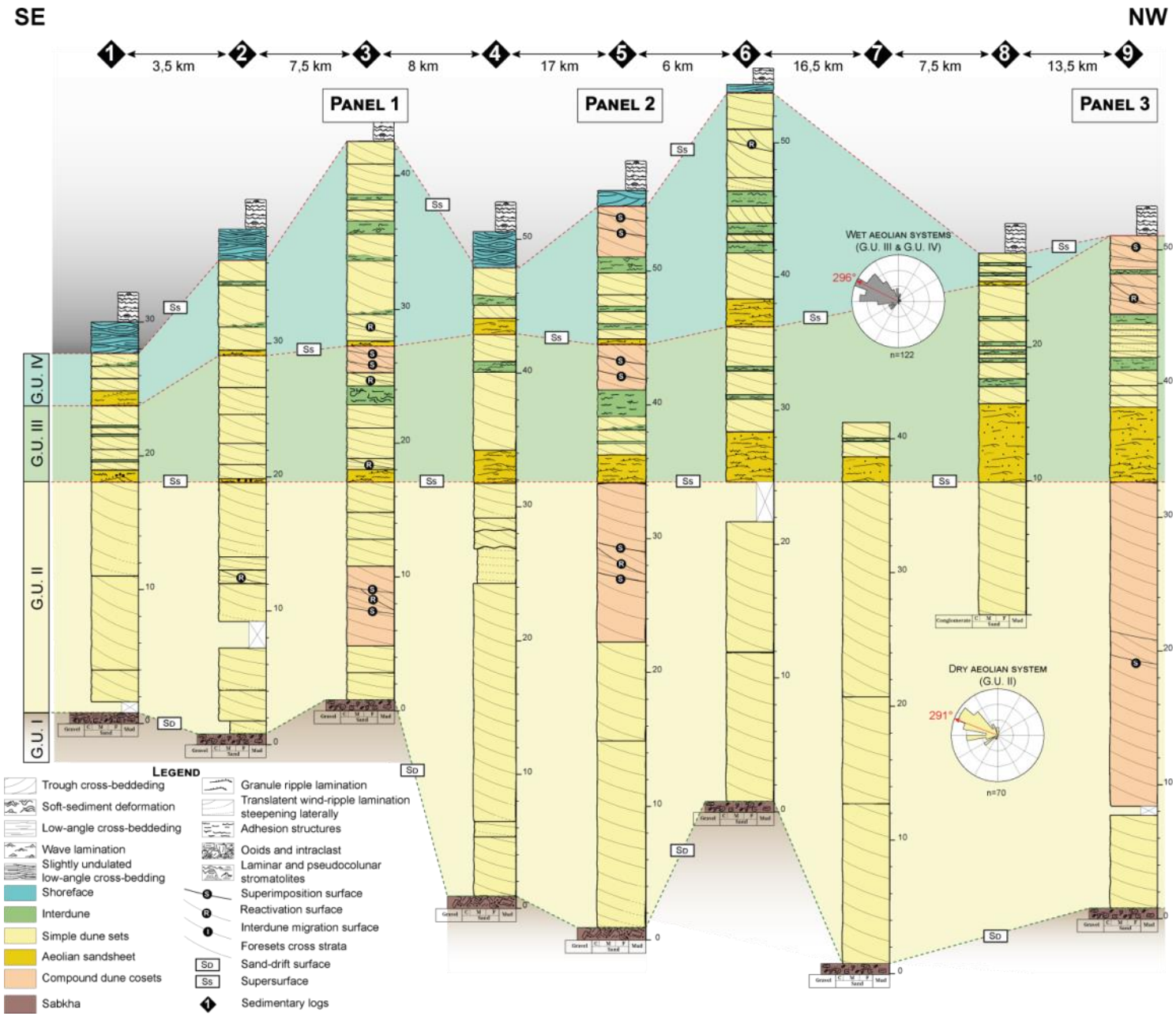

Figure 38: Lateral correlation of stratigraphic logs across a SE-NW traverse parallel to downwind transport.

Interpretation: Stromatolite and oolitic grainstones were deposited in a sabkha environment (see previous section for detailed interpretation). No evidence of interaction with dune-field has been encountered. Consequently the upper boundary surface with aeolian deposits represents a sand-drift surface (Clemmensen & Tirsgaard, 1990) that marks a hiatus before the onset of aeolian sedimentation. Facies analysis suggests that before the onset of aeolian sedimentation, a regional regression caused sabkha desiccation and formation a thin lag. This wide and shallow area constituted a topographic depression later filled by dune-field expansion.

6.2 GENETIC UNIT II

Description: The GU II is 16 to 36 m thick and is bounded at the bottom by a sand-drift surface and at the top by a supersurface (Fig. 8). The GU II is composed of simple dune sets and compound dune cosets separated by interdune migration surfaces. For the simple dune sets, the average thickness is 2.8 m in panel I (Fig. 9) and increases gradually to NW, with 3.9 m in panel II (Fig. 10) and 5.6 m in panel III (Fig. 11). The average 1.54° angle of climb (minimum of 0.42° and maximum of 3.01°) of GU II was used to reconstruct the dune size. Eq. 1 yields a dune wavelength of 105.3 m in panel I, 144.8 m in panel II and 208.0 m in panel III. With these values, the minimum dune heights reconstructed by Eq. 2 are 5.4 m in panel I, 8.5 m in panel II and 14.1 m in panel III (Table. 1).

On the other hand, compound dune cosets have an average set thickness of 6.8 m in panel I (Fig. 9), 14.4 m in panel II (Fig. 10) and 19.5 m in panel III (Fig. 11). No regional trend of change in climbing angle could be determined. Using the average GU II angle of climb, Eq. 1 yielded a dune wavelength of 250 m in panel I, 534.8 m in panel II and 724.1 m in panel III. Furthermore, the compound dune height was estimated using Eq. 2, resulting in average 18 m in panel I, 52 m in panel II and 80 m in panel III (Table. 1).

Interpretation: GU II, bounded at the bottom by sand drift surface and at the top by supersurface, constitutes a unique aeolian accumulation event. While sand-drift surface marks a span between sabkha desiccation and dune-field expansion, the supersurface marks the end of aeolian accumulation. The stacking of simple and composed crescentic dunes without evidence of water

table controlled features suggests dry aeolian system (Wilson, 1971; Kocurek & Havholm, 1993).

For simple dune sets, the reconstructed wavelength of 105 to 208 m suggests dune-scale bedforms, while compound dune cosets are characterized by thicknesses of 250 to 724 m, which correspond to draa-scale bedforms following classification of Wilson (1972).

Table 1: Quantitative data used for bedform reconstruction. Height column represent the estimation of the minimum dune height calculated from wavelength minimum, maximum and mean values.

				Set thickness (m)			Angle of climb (°)			Wavelength (m)			Height (m)		
				min.	max.	mean	min.	max.	mean	min.	max.	mean	min.	max.	mean
Wet aeolian system	G.U. IV	Panel III	Compound	-	-	-	-	-	-	-	-	-	-	-	-
			Simple	-	-	-	-	-	-	-	-	-	-	-	-
		Panel II	Compound	4.6	-	4.6	1.5	-	1.5	434.4	-	434.4	39.5	-	39.5
			Simple	0.7	1.8	0.8	0.8	1.0	0.9	66.1	170.0	79.3	2.8	10.6	3.7
		Panel I	Compound	-	-	-	-	2.4	2.4	-	-	-	-	-	-
			Simple	0.7	2.6	1.8	1.6	1.8	1.7	66.1	245.5	166.1	2.8	17.8	10.3
	G.U. III	Panel III	Compound	2.0	2.4	2.2	1.6	-	1.6	113.9	136.6	123.8	6.1	7.8	6.8
			Simple	0.6	1.6	0.8	1.0	1.2	1.1	34.2	91.1	47.3	1.1	4.4	1.8
		Panel II	Compound	5.8	-	5.8	0.6	-	0.6	330.2	-	330.2	26.9	-	26.9
			Simple	1.5	1.6	1.5	0.7	1.2	0.8	85.4	91.1	87.3	4.0	4.4	4.2
		Panel I	Compound	1.6	8.1	4.1	-	2.2	2.2	91.1	461.1	235.9	4.4	42.9	16.8
			Simple	0.7	3.4	1.5	0.5	3.1	1.8	39.8	193.6	82.7	1.4	12.7	3.9
Dry aeolian system	G.U. II	Panel III	Compound	19.5	-	19.5	-	-	-	724.1	-	724.1	80.7	-	80.7
			Simple	5.6	-	5.6	-	-	-	208.0	-	208.0	14.1	-	14.1
		Panel II	Compound	11.4	17.4	14.4	-	3.6	-	423.3	646.2	534.8	38.1	68.8	52.8
			Simple	3.9	-	3.9	0.4	1.0	0.7	144.8	-	144.8	8.5	-	8.5
		Panel I	Compound	3.9	9.0	6.8	1.3	-	1.3	144.8	334.2	250.7	8.5	27.3	18.3
			Simple	1.0	4.6	2.8	1.2	1.4	1.3	37.1	170.8	105.3	1.3	10.7	5.4

Both temporal and spatial variations in dune and draa size and angle of climb were interpreted from the vertical arrangement of GU II architectural elements and their spatial correlation (Fig. 8). Temporal variation in size is evidenced from the vertical alternation of dunes and draas. Such cyclic increase and reduction in bedform size reflects high-frequency expansion and contraction of the dune-field caused by periodic fluctuations in the saturation level of wind (Kocureck et al, 1992; Kocurek & Havholm, 1993). Basically a dune-field expands whenever wind turns saturated, due to flow deceleration

and contracts when wind gets undersaturated because of flow acceleration or reduction in sand availability (Bagnold, 1941; Hesp, 1981; Tsoar, 1989; Kocurek et al., 1992).

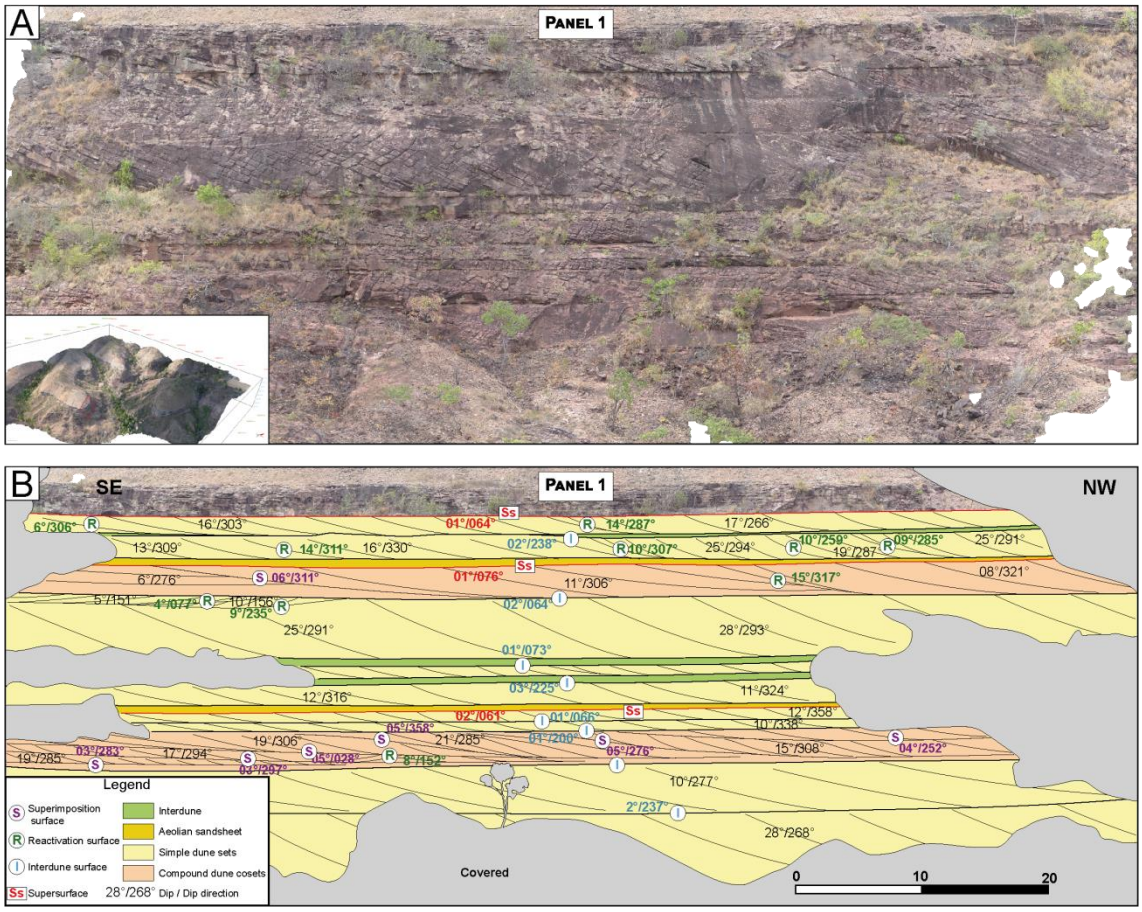

Figure 39: Panel 1 representative of the southern region. (A) 2D orthomosaic of outcrop. (B) Architectural element analysis panel showing geometry and bounding surface relationships.

Spatial variation in bedform size can be inferred from the absence of protodunes, the stacking of bedforms that were originally placed alongside and the increase in bedform dimensions from SE to NW (Fig. 8). Because GU II was deposited under dry conditions, the onset of bedform climbing was only possible after bedform growth progressed to the point where interdune flats were eliminated and the sediment surface was fully covered with dunes (Wilson, 1971). Consequently, protodunes that would have occurred just above the sand-drift surface were not preserved but were cannibalized by the lateral migration of higher bedforms (Kocurek & Havholm, 1993). Similar dry aeolian systems marked by the absence of the earlier stage protodune were widely documented. Among them, we mention the cretaceous Botucatu

Formation (Scherer, 2000) and the Jurassic Page Sandstone (Havholm & Kocurek, 1994). Additionally, the stacking of simple crescentic dunes over compound draas suggests lateral migration of erg margin bedforms over erg center during contraction phases (Porter, 1986; Lancaster, 1988, Sweet et al., 1988; Mountney & Jagger, 2004; Derickson et. Al., 2008). Conversely, compound draas overlying simple dunes indicates lateral migration during expansion periods. Finally, a net increase in set thickness, wavelength and height has been noted both in dunes and draas from panel I to III (Fig. 8). This increase in geometric parameters towards NW reflects bedform growth in the direction nearly along the mean aeolian transport (291° for GU I). In dry aeolian systems, downwind increase in bedforms size occurs in response to deceleration of airflow (Bagnold, 1941; Kocurek et al., 1992; Mountney & Jagger, 2004; Mountney, 2012). Similar downwind deceleration and consequent increase in bedform dimensions were documented in the ancient Cedar Mesa Sandstone (Mountney & Jagger, 2004) and in the recent Namib sand sea (Lancaster, 1988). Downwind deceleration in airflow suggests that a topographic depression was localized in the northern region of the study area. Our assumption is supported by stratigraphic correlation showing thicker aeolian successions towards NW (Fig. 8) and also by studies of deep reflection seismic data (Daly et al., 2014; Manenti et al., 2018), gravity and magnetic anomaly (Watts et al., 2018) and sediment isopachs (Leite et al., 1975; Watts et al., 2018). These studies show that the deeper area of the basin is located at northwest of the studied area.

Variations in angle of climb can be evidenced from the maximum 1.37° measured in simple dunes to a maximum of 3.60° for draas (Fig. 10). This difference was interpreted as related to the ratio between the rate of dune migration and the sediment accumulation of simple dune and draas (Mountney, 2012). For a constant rate of accumulation, a greater angle of climb is expected in draas because of their low rate of migration (Wilson, 1972).

The end of GU II is marked by a deflation supersurface lying abruptly above dunes or draas, without preservation of the final stage bedforms. The

final stage would be represented by progressively lower dunes suggesting a gradual decrease in sand availability. The absence of the final stage suggests

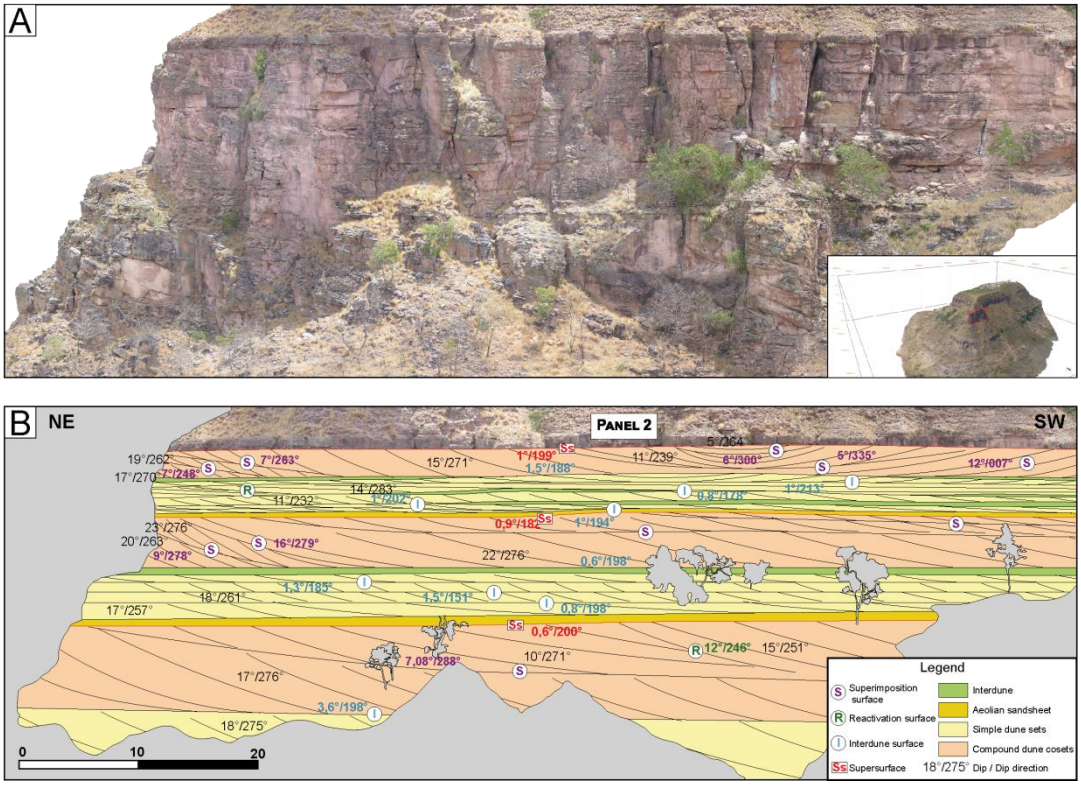

Figure 10: Panel 2 representative of the central region. (A) 2D orthomosaic of outcrop. (B) Architectural element analysis panel showing geometry and bounding surface relationships.

sand exhaustion, development of a negative angle of climb, cannibalization of dunes and deflation of the accumulation (Mountney, 2006).

6.3 Genetic Unit III

Description: The GU III is 6 to 18 m thick and is bounded at the bottom and top by supersurfaces. The facies succession indicates a drying-upward trend in which aeolian sandsheets deposits occur at the base and are overlain by progressively thicker simple dunes sets intercalated with interdunes, culminating with compound dune cosets to the top (Fig. 8).

A net increase of sandsheet thickness was noted from SE to NW. While the maximum aeolian sandsheet thickness in panel I is 1.0 m (Fig. 9), in panel II the measured thickness is 2.0 m (Fig. 10) and in panel III sandsheets reach 4.3 m (Fig. 11). Considering simple dunes, a small difference in set thickness can be observed from SE to NW. The mean set thickness measured in panel I is 1.45 m, in panel II the mean set thickness is 1.5 m and

in panel III 0.8 m. Although a wide variety of angle of climb was measured, no trend was identified. The minimum angle measured was 1° and the maximum 2.4°. Using the mean angle of climb 1.01° to estimate original dune wavelength, Eq. 1 yields 82.7 m wavelength in panel I, 87.2 m in panel II and 47.3 m in panel III. With Eq. 2, the minimum reconstructed dune height is 3.8 m in panel I, 3.1 m in panel II and 1.8 m in panel III (Table. 1).

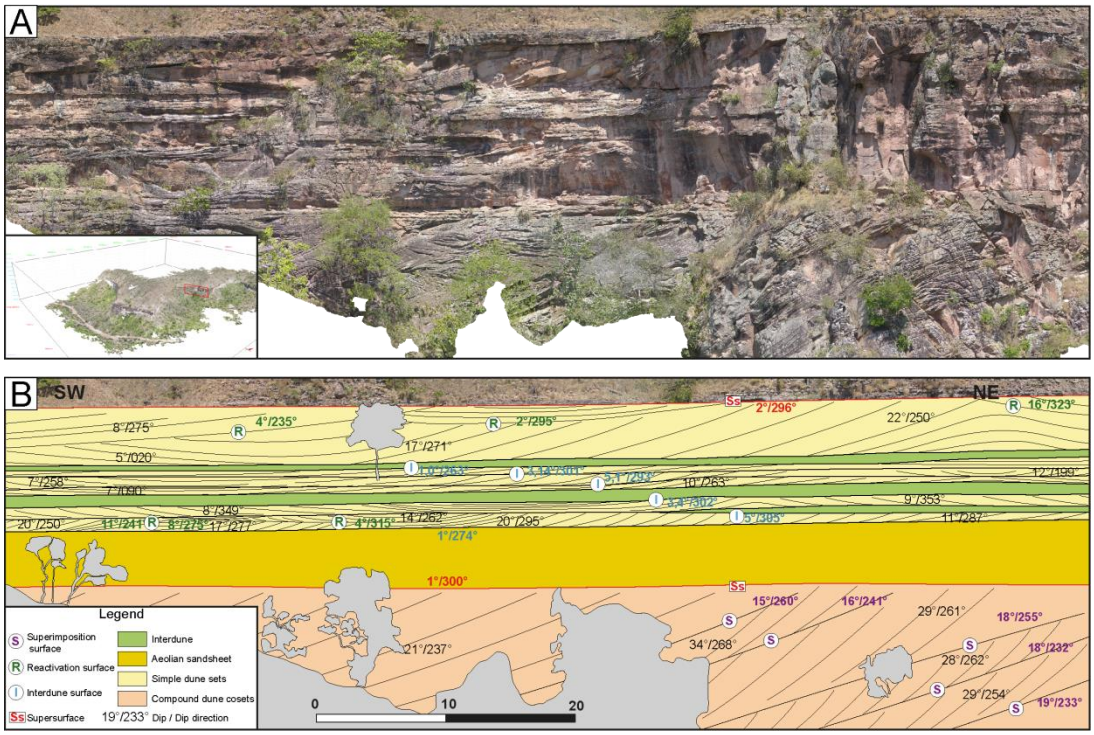

Figure 11: Panel 3 representative of the northern region. (A) 2D orthomosaic of outcrop. (B) Architectural element analysis panel showing geometry and bounding surface relationships.

For interdune elements, in panel I the maximum thickness is 0.35 m, and the ratio of thickness between interdunes and dunes is 12 %. Comparatively, interdunes are thicker and more numerous towards the north: the maximum thickness is 1.70 m in panel II and the ratio of interdune/dune thickness is 19 %, while the maximum thickness is 1.45 m in panel III and the ratio of interdune/dune thickness is 24 %.

Compound dune cosets occur at the top of GU III and have mean thickness of 4.1 m in panel I, 5.8 m in panel II and 2.2 in panel III. With an average angle of climb of 1.01° for GU III sets, Eq. 1 yields wavelength of 235.9 m in panel I, 330.1 m in panel II and 123.8 m in panel III. The original estimated height from Eq. 2 is 17.9 m in panel I, 26.8 m in panel II and 6.8 in panel III (Table. 1).

Interpretation: The GU III bounded at the bottom and top by supersurfaces constitutes the second aeolian accumulation event that was deposited in a wet aeolian system (Kocurek & Havholm, 1993). Using Wilson (1972) classification of aeolian bedforms, simple dune wavelengths fit in the category of dune-scale bedforms, while compound cosets mostly fit into the draa category.

The drying-upward trend represents a progressive increase in bedforms size through time and occurs when the rate of sand availability exceeds the rate of water table rise. The alternation of interdunes and dunes in the unit indicates fluctuations of the water table. During periods of high water table, sand availability was reduced and interdunes expanded; whenever the water table fell, sand availability increased causing dune growth (Kocurek & Havholm, 1993; Mountney & Jagger, 2004; Mountney & Russel, 2009).

Although bedforms grow over time, data show a downwind decrease in dune size, increase in sandsheet thickness and increase in interdune/dune thickness ratio (Fig. 8). According to Kocurek & Nielson (1986), the development of sandsheets is controlled by a series of factors that reduce the availability of sand for the construction of dunes. These factors include high water-table level, coarser grain size, periodic flooding or surface binding. In the case of GU III, the dominance of fine sand grain size and the abundance of adhesion structures, together with the absence of surface binding features and lack of facies indicative of periodic flooding, suggest that a high and rising water-table level were the factors that caused sandsheet development and accumulation. Accumulation of thick sandsheet deposits suggest that the rate of water table rise was equivalent to the rate of sand availability during a long period.

The increase in interdune/dune thickness ratio from SE to NW suggests that in the Southeastern region the rate of sand availability exceeds the rate of water table rise (Crabaugh & Kocurek, 1993). Thus, the northern region was more like recent dune margins (Fig. 12) (Porter, 1986; Mountney & Howell, 2000) where the water table level is close to the accumulation surface and the rate of sand availability is just a little higher than the rate of water

table rise, allowing only simple dunes to form (Kocurek & Havholm, 1993). The thicker interdunes observed in the northwestern area suggests longer periods of elevated water table level.

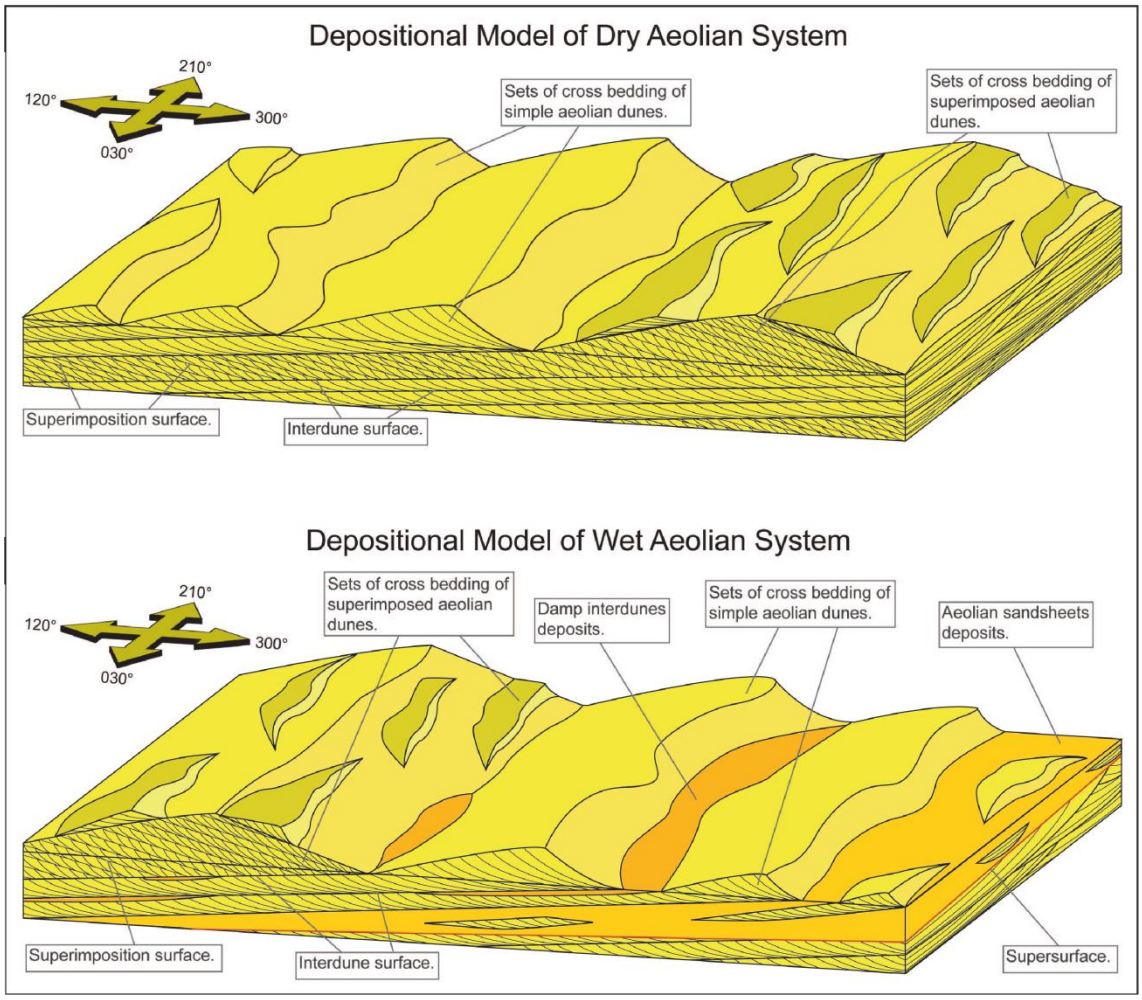

Figure 12: (A) Depositional model of dry aeolian system (GU II) depicting temporal and spatial variations in architectural elements. (B) Depositional model of wet aeolian system (GU III and IV) depicting temporal and spatial variations in architectural elements.

Unlike GU II where early and final stages of bedform evolution were erased, in GU III only the final stage is missing. The causes for final stage absence are related to supersurface developments. In wet aeolian systems, the supersurface forms because of a combination of falling water-table together and unsaturated wind flows (Kocurek and Havholm, 1993).

6.4 Genetic Unit IV

Description: The GU IV ranges from 4 to 18 m thick and is bounded at the bottom and top by supersurfaces. The G.U IV crops out in the southern and central region of the studied area which corresponds to panels I (Fig. 9) and II

(Fig. 10), but is absent in panel III (Fig. 11) of the northern region. Similar to the previous unit, GU IV exhibits a drying-upward trend with aeolian sandsheet occurring at the base, overlain by simple dunes intercalated with interdunes, and compound dune cosets at the top (Fig. 8).

A slight downwind increase in sandsheet thickness is noted: In panel I the maximum thickness is 0.65 m and in panel II sandsheet reaches 0.80 m (Fig. 8). Interdunes have a maximum thickness of 0.30 m in panel I and the ratio of interdune/dune thickness is 5%, while the maximum thickness in panel II is 0.70 m and the ratio interdune/dune is 12 %. The mean set thickness measured of simple dunes is 1.8 m in panel I and 1.5 in panel II mean while the mean angle of climb is 0.61°. Using Eq. 1 the estimated wavelength in panel I is 166.1 m and 87.2 m in panel II. With Eq. 2, the minimum dune height estimated is 10.3 in panel I and 4.2 m in panel II. Compound dune cosets were identified only in panel II, where the coset thickness is 4.6 m, the reconstructed wavelength is 434.4 and the minimum dune height estimated is 39.5 m (Table. 1).

Interpretation: The GU IV is bounded at the bottom and top by supersurfaces and represents the third aeolian accumulation event. The estimated wavelength for simple dunes best fits to dune-scale bedforms while compound cosets wavelength are indicative of draa-scale bedforms (Wilson, 1972). Variations in geometric parameters in GU IV are very similar to those documented for the previous unit.

The vertical alternation of dunes and interdunes suggests fluctuations of the water table over time. The drying-upward trend observed in this unit indicates that over time the rate of sand availability was progressively higher than the rate of water table rise, allowing expansion of the dune-field (Crabaugh & Kocurek, 1993; Kocurek & Havholm, 1993; Mountney & Russel, 2009).

Conversely, the lateral increase in sandsheet thickness from south to center suggest that the rate of water table rise is nearly equal to the rate of sand availability at the dune-field center (Kocurek & Nielson, 1986). Moreover, the northward increase in interdune maximum thickness suggest that periods of elevated water table lasted longer in the dune-field center. These

observations are consistent with reduction of simple dune size from south to center, which suggests reduction in sand availability towards the center (Fig. 12).

The GU IV is capped by a near-horizontal regionally extensive deflation supersurface that separates the aeolian succession from the overlying shoreface deposits. Supersurface was generated because of water table fall and unsaturated airflows, due to sand exhaustion (Mountey, 2006). The absence of GU IV in the north suggests that while the dune-field was accumulating at the center and southern regions, the northern region was deflating or the minimum conditions for dune construction were not met. The similarity between GU III and GU IV interpretations highlights the predictable character of sedimentation when the controlling factors are known.

7 DISCUSSION

7.1 Controlling factors of sediment state

Climatic, eustatic and tectonic changes have significant effects on the sediment state of an aeolian system (Kocurek, 1999). The upper Piauí Formation represents three dynamic erg sequences within which every expansion and contraction phase, and the depositional architecture was intrinsically related to climatic-eustatic change, similarly to most erg systems of Permian-Pennsylvanian age (Chan & Kocuren, 1988; Howell & Mountney, 1997; Mountney & Jagger, 2004; Mountney, 2006; Jordan & Mountney, 2010, Jordan & Mountney, 2012). On the other hand, tectonic activity controlled the creation of accommodation space for accumulation and preservation of aeolian units, but had no direct impact on sedimentation cyclicity. The upper Piauí Formation accumulated in an intracontinental sag basin characterized by long-term thermal-flexural subsidence of low frequency and low rate of variation (Daly et al., 2014, Watts et al., 2018), that is unlikely to have caused high-frequency fluctuations of the water table.

The sabkha deposits occurring at the base of the studied succession (GU I) was deposited in a context of humid phase and high water table level. As result, the sediment supply was not transported by wind but remained stored (sediment stored because it is availability limited - S_{AL}) (Fig. 13).

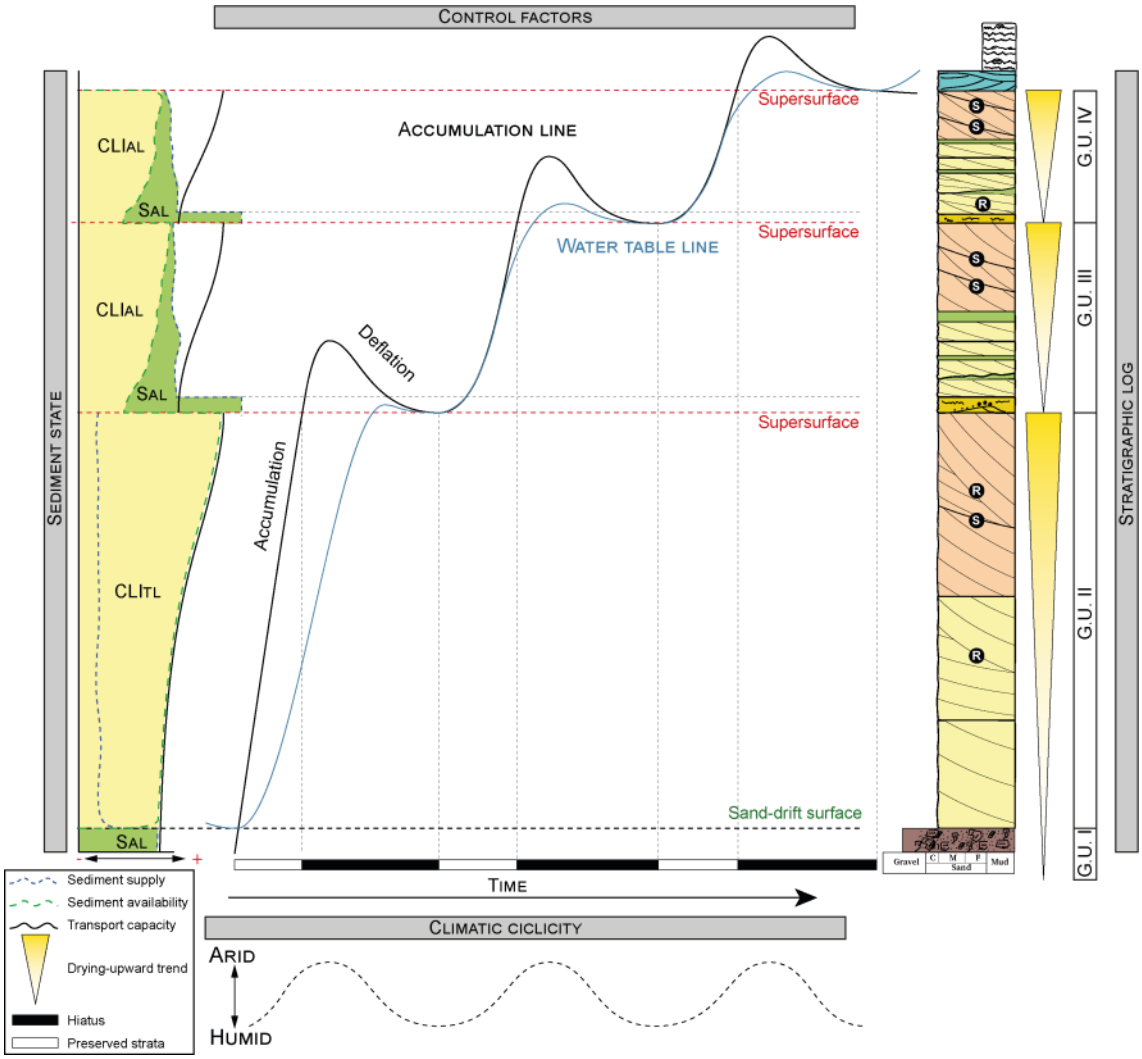

Figura 13: Integrate diagram of relationship between accumulation curve, water table oscillation, sediment state, climatic cycles and stratigraphic log. Note that the preserved strata represent less time than the hiatus.

As climate shifted to more arid conditions, the water table lowered and the sediment availability increased (Kocurek & Lancaster, 1999; Kocurek, 1999). Sediments that were originally stored were progressively entrained by winds and the onset of aeolian deflation generated a sand-drift surface. Because the sediment supply was generated at a rate greater than the wind transport capacity (contemporaneous and lagged influx, transport limited – CLI_{TL}) (Fig. 13) the airflow became saturated (Kocurek & Lancaster, 1999; Kocurek, 1999). This condition of elevated sand availability, saturated winds and low groundwater table favored accumulation of a dry aeolian system (GU II) and allowed the gradual growth and subsequent climbing of dunes without damp interdune flats. Nevertheless, fluctuations of the wind saturation are

evidenced by temporal alternation of simple dunes and draas, which suggests high frequency contractions and expansions of the dune-field.

The GU II is bounded on top by an extensive supersurface that indicates exhaustion or significant reduction of the contemporaneous and lagged sedimentary influx due to availability limitations (CLI_{AL}), resulting in deflation during periods of maximum aridity (Kocurek, 1999).

Both GU III and GU IV are characterized by drying upward cycles composed of basal aeolian sandsheets followed by progressively thicker dunes intercalated with interdunes. The base of cycles marks the return of more humid conditions during which the rise of groundwater level accompanied the sediment availability at an equivalent rate. This configuration indicates that although the rate of sand availability is positive, the elevated water table limits sand availability and most of the sediment is not available for wind transport but is stored (S_{AL}). The progressive increase in dune occurrence and dimensions to the top suggests an increase in sediment availability although the high water table still limits contemporaneous and lagged influx availability (CLI_{AL}). The facies succession of GU III and IV marks climatic cycles characterized by more humid conditions at the base and drier at the top.

The supersurfaces on top of both units were formed during a climax of aridity when sediment influx was exhausted leading to availability-limited conditions (CLI_{AL}) and aeolian deflation. The supersurface marks a span between the end of aeolian sedimentation and a later flooding of the area that deposited shoreface facies and culminated with the formation of Pedra de Fogo lake.

7.2 Paleogeographic and paleoclimate reconstruction

The Late Carboniferous was characterized by the presence of expressive continental ice cap on high to medium latitudes of Gondwana, as attested by the systematic occurrence of glacial deposits in different sedimentary basins, e.g., Paraná Basin in Brazil (Caputo, 1984; Vesely et al., 2015; Mottin et al 2018), Paganzo Basin in Argentina (Gulbranson et al., 2015), Karoo, Kalahari and Congo basins (Kar & Bose, 1978; Veevers, 1994; Visser, 1997), basins of western Australia (Veevers 1984).

Several models suggest that the peak of glaciation caused an intense aridification in Gondwana low latitudes (Heckel 1980, 1994; Maynard and Leeder 1992; Blakey 2003, Jordan & Mountney, 2012). Paleogeographic reconstructions of late Pennsylvanian suggest that the collision of Gondwana with Laurasia resulted in the closure of the Rheic Ocean and caused a progressive withdrawal of epeiric seas (Golonka & Ford, 2000; Gibbs et al., 2002; Tabor & Poulsen, 2008). Due to extreme continentality, the monsoonal circulation intensified and resulted in long-term aridification across Gondwana (Kutzbach and Gallimore, 1989; Parrish, 1993, Loope et al. 2004). In addition to climate aridity, the great extension of ice cap compressed climatic belts and enhanced surface airflow velocities that contributed for dune-field construction (Roscher & Schneider, 2006).

The extensive occurrence of aeolian systems at the top of the Piauí Formation reflects the Late Carboniferous intense aridification process resulting from the glaciation in the high latitudes of Gondwana. However, within this icehouse period, we note an alternation of glacial and interglacial intervals, which altered the climatic conditions in the low and medium latitudes. The four genetic units interpreted in the Piauí Formation reflect distinct climatic cycles possibly induced by Milankovitch orbital forcing that prevailed in Gondwana during Pennsylvanian to Permian (Wanless & Shepard, 1936; Ziegler et al., 1979; Dickinson et al., 1994). The GU I was deposited during humid period and may represent the extension of epeiric seas. The dry aeolian system of the UG II corresponds to the first aridification event in the studied interval, probably corresponding to the peak of the Pensilvanian glacial event in high latitudes (Fig. 13). Alternatively, the wet systems (GU III and IV) record periods of subhumid climate and rising relative sea level. The change to more humid conditions is mostly attributed to melting of Gondwana ice cap (Roscher & Schneider, 2006). The reduction in ice cap extent triggered the shrinking of polar high-pressure cells and expansion of the Intertropical Convergence Zone to higher latitudes causing more humid climate conditions (Perlmutter & Matthews, 1989). Sandsheet deposits that occur at the base of each cycle occurred during interglacial intervals, whilst the drying-upward trends represent progressively more arid conditions to the

top (Fig. 13). The supersurfaces that separate genetic units III and IV were formed at the peak of aridization, representing the moments of maximum glaciation. Finally, the shoreface deposits that occur on top of the Piauí Formation, followed by the deposition of the siliciclastic carbonate mixed platform of the Pedra de Fogo Formation, represent humid conditions, probably linked to progressive decrease in the extent of the ice cap during early Permian age.

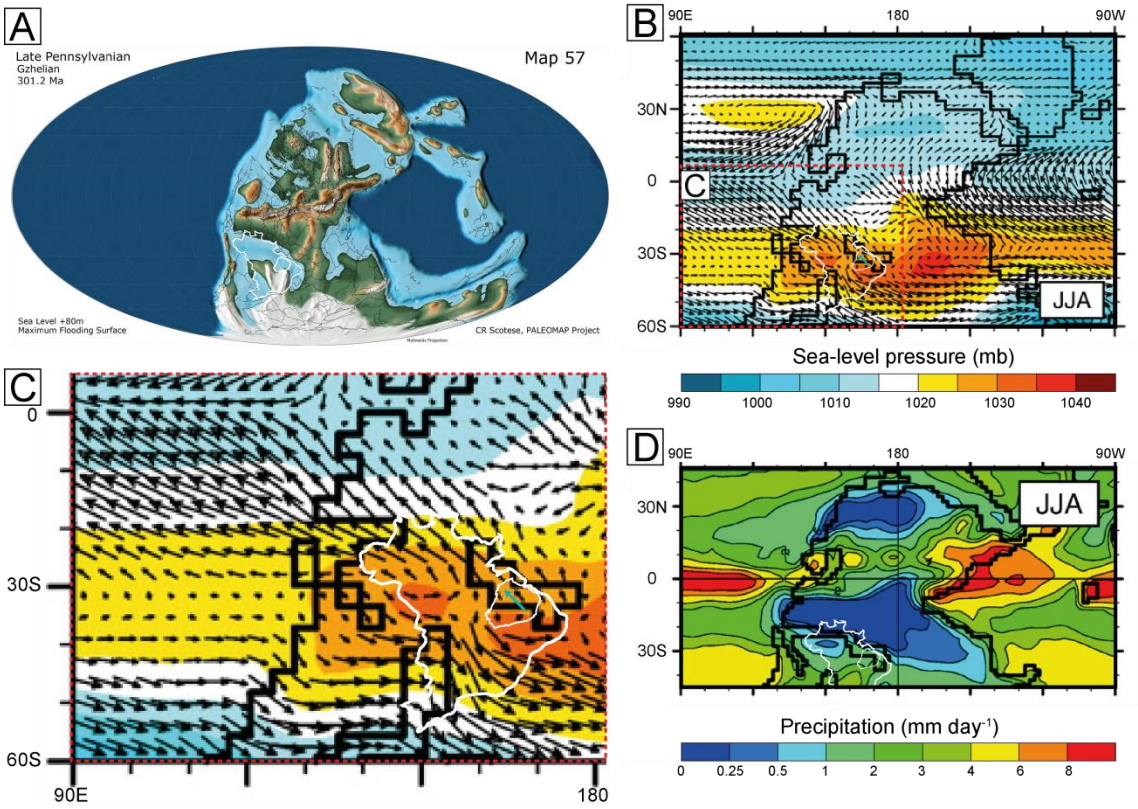

Figura 14: (A) Paleogeographic map of Late Pennsylvanian, 301Ma (from Scotese, 2014). Observe the position of the Parnaiba Basin completely covered by water simultaneously with glaciation. (B) Surface wind pattern simulations during June – July and August from Peyser & Poulsen (2008). (C) Close-up on Brazil and Parnaíba Basin. Note the prevailing NW wind across the basin. (D) June-July-August average precipitation rates (mm day $^{-1}$) for simulations considering no ice sheets at high latitudes from Peyser & Poulsen (2008).

The aeolian cross-bedding paleocurrent collected were corrected considering the present position of the basin. The mean azimuth was compared with late Paleozoic paleogeographic maps and surface wind pattern simulations (Fig. 14). The maximum transgression proposed in Scotese (2014) Late Pennsylvanian map is probably responsible for the deposition of the sabkha deposit, however the subsequent development of

dune-field suggest that during glaciation interval the eastern region of the basin was essentially characterized by continental sedimentation. Among the series of surface wind pattern simulations presented by Peyser & Poulsen (2008), our field observations (prevailing NW wind directions) suggest aeolian accumulation during southern hemisphere winter (June – July – August). According to the simulations, during wintertime the prevailing wind blew towards northwest, whilst during summer (December – January - February) the prevailing East-southeast wind would be responsible for development of reactivation surfaces (Jones et al., 2021).

8 CONCLUSIONS

The aeolian sedimentary record of upper Piauí formation contributes to the understanding of the complex dynamics that involves aeolian sedimentation and highlights the predictive nature of what will in fact be preserved in both a dry e.g. Sahara dune-field and wet aeolian system e.g. Algodones dune-field. The study shows how the evolutionary stage of a dune-field can be estimated from the quantitative reconstruction of the original bed forms dimensions. Once the evolutionary stage was set, we observed that in dry system neither the early stage protodunes nor the ending stages bedforms are preserved. By contrast, in a wet system protodunes have greater potential of preservation, especially during water table rise, while the final stages preservation are commonly rare. The main process responsible for erosion of these evolutionary stages is the autogenic process of dunes migration. In dry systems the initial stages are eroded by the migration of subsequently larger dunes, while the final stages in both dry and wet systems are eroded when the sand availability is exhausted, triggering airflow subsaturation and development of a negative angle of climb. Finally this study detailed how climatic, eustatic and tectonic conditions in Late Pannsylvanian affected the sediment state of the aeolian system.

9 ACKNOWLEDGMENTS

This research is part of the project of research and development named “Facies architecture and high resolution stratigraphy of coastal aeolian systems” funded by Petrobras S.A. and executed in partnership with the

Federal University of Rio Grande do Sul. The first authors thank IAS for postgraduate research grant. Authors thank Raimundo Nonato for accomodation at Amarante.

10 REFERENCES

Araújo, D.B. de (2017) Bacia do Parnaíba - Sumário Geológico e Setores em Oferta. Bras. -14ª Rodada Licitações Petróleo e Gás - Agência Nac. do Petróleo, Gás Nat. e Biocombustivel 21.

Araújo, R.N., Nogueira, A.C.R., Bandeira, J. and Angélica, R.S. (2016) Shallow lacustrine system of the Permian Pedra de Fogo Formation, Western Gondwana, Parnaíba Basin, Brazil. *J. South Am. Earth Sci.*, 67, 57–70.

Bagnold, R.A. (1941) The physics of blown sand and desert dunes. 302 pp.

Benan, C.A.A. and Kocurek, G. (2000) Catastrophic flooding of an aeolian dune-field: Jurassic Entrada and Todilto formations, Ghost Ranch, New Mexico, USA. *Sedimentology*, 47, 1069–1080.

Blakey, R.C. (2003) Carboniferous-Permian paleogeography of the assembly of Pangaea. In: *Proceedings of the XVth International Congress on Carboniferous and Permian Stratigraphy* (Ed. T.E. Wong), Utrecht, Netherlands, 443–456.

Brookfield, M.E. (1977) The origin of bounding surfaces in ancient aeolian sandstones. *Sedimentology*, 24, 303–332.

Bryant, G., Cushman, R., Nick, K. and Miall, A. (2016) Paleohydrologic controls on soft-sediment deformation in the Navajo Sandstone. *Sediment. Geol.*, 344, 205–221.

Buck, S.G. (1980) Stromatolite and ooid deposits within the fluvial and lacustrine sediments of the Precambrian Ventersdorp Supergroup of South Africa. *Precambrian Res.*, 12, 311–330.

Burne, R. V. and Moore, L.S. (1987) Microbialites: Organosedimentary Deposits of Benthic Microbial Communities. Palaios 241–254.

Carrivick, J. L., Smith, M. W., & Quincey, D. J. (2016). Structure from Motion in the Geosciences. John Wiley & Sons.

Chan, M.A. and Kocurek, G. (1988) Complexities in eolian and marine interactions: Processes and eustatic controls on erg development.

Sediment. Geol., 56, 283–300.

Clemmensen, L.B. (1989) Preservation of interdraa and plinth deposits by the lateral migration of large linear draas (Lower Permian Yellow Sands, northeast England). *Sediment. Geol.*, 65, 139–151.

Clemmensen, L.B. and Tirsgaard, H. (1990) Sand-drift surfaces: A neglected type of bounding surface. *Geology*, 18, 1142–1145.

Crabaugh, M. and Kocurek, G. (1993) Entrada Sandstone: An example of a wet aeolian system. *Geol. Soc. Spec. Publ.*, 72, 103–126.

Daly, M.C., Andrade, V., Barousse, C.A., Costa, R., McDowell, K., Piggott, N. and Poole, A.J. (2014) Brasiliano crustal structure and the tectonic setting of the Parnaíba basin of NE Brazil: Results of a deep seismic reflection profile. *Tectonics*, 33, 2102–2120.

Day, M. and Kocurek, G. (2017) Aeolian dune interactions preserved in the ancient rock record. *Sediment. Geol.*, 358, 187–196.

Derickson, D., Kocurek, G., Ewing, R.C. and Bristow, C. (2008) Origin of a complex and spatially diverse dune-field pattern, Algodones, southeastern California. *Geomorphology*, 99, 186–204.

Dickinson, W.R., Soreghan, G.S. and Giles, K.A. (1994) Glacio-eustatic origin of Permo-Carboniferous stratigraphic cycles: evidence from the southern cordilleran foreland region. In: *Tectonic And Eustatic Controls on Sedimentary Cycles*, *SEPM (Society for Sedimentary Geology)*, 25–34.

Dino, R., Antonioli, L. and Braz, S.M.N. (2002) Palynological Data From The Trisidela Member of Upper Pedra de Fogo Formation (“Upper Permian”) of The Parnaíba Basin, Northeastern Brazil. *Rev. Bras. Paleontol.*, 24–35.

Dino, R. and Playford, G. (2002) Stratigraphic and palaeoenvironmental significance of a Pennsylvanian (Upper Carboniferous) palynoflora from the Piauí Formation, Parnaíba Basin, northeastern Brazil. *Paleontol. Res.*, 6, 23–40.

Doe, T.W. and Dott, R.H. (1980) Genetic significance of deformed cross bedding - with examples from the Navajo and Weber sandstones of Utah. *J. Sediment. Petrol.*, 50, 793–812.

Dumas, S. and Arnott, R.W.C. (2006) Origin of hummocky and swaley cross-

stratification - The controlling influence of unidirectional current strength and aggradation rate. *Geology*, 34, 1073–1076.

Ewing, R.C. and Kocurek, G. (2010) Aeolian dune-field pattern boundary conditions. *Geomorphology*, 114, 175–187.

Fryberger, S.G. (1993) A review of aeolian bounding surfaces, with examples from the Permian Minnelusa Formation, USA. *Geol. Soc. Spec. Publ.*, 73, 167–197.

Fryberger, S.G., Ahlbrandt, T.S. and Andrews, S. (1979) Origin, sedimentary features, and significance of low-angle eolian ' sand sheet' deposits, Great Sand Dunes National Monument and vicinity, Colorado. *J. Sediment. Petrol.*, 49, 733–746.

Fryberger, S.G., Hesp, P. and Hastings, K. (1992) Aeolian granule ripple deposits, Namibia. *Sedimentology*, 39, 319–331.

Fryberger, S.G. and Schenk, C.J. (1981) Wind sedimentation tunnel experiments on the origins of aeolian strata. *Sedimentology*, 28, 805–821.

Gao, X., Narteau, C. and Rozier, O. (2015) Development and steady states of transverse dunes: A numerical analysis of dune pattern coarsening and giant dunes. *J. Geophys. Res. Earth Surf.*, 120, 2200–2219.

Gibbs, M.T., Rees, P.M.A., Kutzbach, J.E., Ziegler, A.M., Behling, P.J. and Rowley, D.B. (2002) Simulations of Permian climate and comparisons with climate-sensitive sediments. *J. Geol.*, 110, 33–55.

Goldberg, K., Morad, S., Al-Aasm, I.S. and De Ros, L.F. (2011) Diagenesis of Paleozoic playa-lake and ephemeral-stream deposits from the Pimenta Bueno Formation, Siluro-Devonian (?) of the Parecis Basin, central Brazil. *J. South Am. Earth Sci.*, 32, 58–74.

Golonka, J. and Ford, D. (2000) Pangean (Late Carboniferous-Middle Jurassic) paleoenvironment and lithofacies. *Palaeogeogr. Palaeoclimatol. Palaeoecol.*, 161, 1–34.

Grotzinger, J.P. (1989) Facies and evolution of Precambrian carbonate depositional systems: emergence of the modern platform archetype. In: *Controls on Carbonate Platform and Basin Development*, 44th edn. (Ed. P.D. Crevello, J.L. Wilson, J.F. Sarg, and J.F. Read), *SEPM Spec. Publ.*,

79–106.

Gulbranson, E. L., Montañez, I. P., Tabor, N. J., & Limarino, C. O. (2015). Late Pennsylvanian aridification on the southwestern margin of Gondwana (Paganzo Basin, NW Argentina): a regional expression of a global climate perturbation. Palaeogeography, Palaeoclimatology, Palaeoecology, 417, 220-235.

Havholm, K.G. and Kocurek, G. (1994) Factors controlling aeolian sequence stratigraphy: clues from super bounding surface features in the Middle Jurassic Page Sandstone. *Sedimentology*, 41, 913–934.

Heckel, P.H. (1980) Paleogeography of Eustatic Model for Deposition of Midcontinent Upper Pennsylvanian Cyclothems. 197–215.

Heckel, P.H. (1994) Evaluation of evidence for glacio-eustatic control over marine Pennsylvanian cyclothems in North America and consideration of possible tectonic effects. In: *Tectonic And Eustatic Controls on Sedimentary Cycles*, *SEPM (Society for Sedimentary Geology)*, 65–87.

Hesp, P.A. (1981) The formation of shadow dunes. *J. Sediment. Petrol.*, 51, 101–112.

Hoffman, P. (1976) Environmental Diversity of Middle Precambrian Stromatolites. In: *Developments in Sedimentology - Stromatolites* (Ed. M.R. Walter), *Elsevier*, 20, 599–611.

Horowitz, D.H. (1982) Geometry and origin of large-scale deformation structures in some ancient wind-blown sand deposits. *Sedimentology*, 29, 155–180.

Howell, J. and Mountney, N. (1997) Climatic cyclicity and accommodation space in arid to semi-arid depositional systems: an example from the Rotliegend Group of the UK southern North Sea. *Geol. Soc. Spec. Publ.*, 123, 63–86.

Hunter, R.E. (1977) Basic types of stratification in small eolian dunes. *Sedimentology*, 24, 361–387.

Iannuzzi, R., Neregato, R., Cisneros, J.C., Angielczyk, K.D., Rößler, R., Rohn, R., Marsicano, C., Fröbisch, J., Fairchild, T., Smith, R.M.H., Kurzawe, F., Richter, M., Langer, M.C., Tavares, T.M.V., Kammerer, C.F., Conceição, D.M., Pardo, J.D. and Roesler, G.A. (2018) Re-evaluation of the Permian

macrofossils from the Parnaíba Basin: Biostratigraphic, palaeoenvironmental and palaeogeographical implications. *Geol. Soc. Spec. Publ.*, 472, 223–249.

Jerram, D.A., Mountney, N.P., Howell, J.A., Long, D. and Stollhofen, H. (2000) Death of a sand sea: An active aeolian erg systematically buried by the Etendeka flood basalts of NW Namibia. *J. Geol. Soc. London.*, 157, 513–516.

Jones, F.H., dos Santos Scherer, C.M. and Kifumbi, C. (2021) Aeolian dunes morphodynamics and wind regime reconstruction in mid-latitudes of the Gondwana during Early Permian, Aracaré Formation, Sergipe-Alagoas Basin, Brazil. *Aeolian Res.*, 50, 100672.

Jordan, O.D. and Mountney, N.P. (2012) Sequence stratigraphic evolution and cyclicity of an ancient coastal desert system: The pennsylvanian-permian lower cutler beds, paradox basin, Utah, U.S.A. *J. Sediment. Res.*, 82, 755–780.

Jordan, O.D. and Mountney, N.P. (2010) Styles of interaction between aeolian, fluvial and shallow marine environments in the Pennsylvanian to Permian lower Cutler beds, south-east Utah, USA. *Sedimentology*, 57, 1357–1385.

Kah, L.C., Bartley, J.K., Frank, T.D. and Lyons, T.W. (2006) Reconstructing sea-level change from the internal architecture of stromatolite reefs: An example from the Mesoproterozoic Sulky Formation, Dismal Lakes Group, arctic Canada. *Can. J. Earth Sci.*, 43, 653–669.

Kocurek, G. (1999) The Aeolian Rock Record (Yes, Virginia, it Exists, But it Really is Rather Special to Create One). *Aeolian Environ. Sediments Landforms*, 239–259.

Kocurek, G. (1991) Interpretation of ancient eolian sand dunes. *Annu. Rev. Earth Planet*, 33.

Kocurek, G. (1981) Significance of interdune deposits and bounding surfaces in aeolian dune sands. *Sedimentology*, 28, 753–780.

Kocurek, G. and Day, M. (2018) What is preserved in the aeolian rock record? A Jurassic Entrada Sandstone case study at the Utah–Arizona border. *Sedimentology*, 65, 1301–1321.

Kocurek, G. and Dott, R.H. (1981) Distinctions and uses of stratification types in the interpretation of eolian sand. *J. Sediment. Petrol.*, 51, 579–596.

Kocurek, G., Ewing, R.C. and Mohrig, D. (2010) How do bedform patterns arise? New views on the role of bedform interactions within a set of boundary conditions. *Earth Surf. Process. Landforms*, 35, 51–63.

Kocurek, G. and Havholm, K.G. (1993) Eolian sequence stratigraphy - a conceptual framework. Siliciclastic Seq. Stratigr. Recent Dev. Appl. 393–409.

Kocurek, G. and Lancaster, N. (1999) Aeolian system sediment state: Theory and Mojave Desert Kelso dune-field example. *Sedimentology*, 46, 505–515.

Kocurek, G., Townsley, M., Yeh, E., Havholm, K. and Sweet, M.L. (1992) Dune and dune-field development on Padre Island, Texas, with implications for interdune deposition and water-table- controlled accumulation. 62, 622–635.

Kocurek, G.A. (1996) Desert aeolian systems. In: *Sedimentary Environments: Processes, Facies and Stratigraphy.*, 3rd edn. (Ed. H.G. Reading), *Oxford, Blackwell Science*, London, 125–153.

Kocurek, G.A. and Nielson, J. (1986) Conditions favourable for the formation of warm-climate aeolian sand sheets. *Sedimentology*, 33, 795–816.

Kutzbach, J.E. and Gallimore, R.G. (1989) Pangaean climates: Megamonsoons of the megacontinent. *J. Geophys. Res.*, 94, 3341.

Lancaster, N. (1988a) Controls of eolian dune size and spacing. *Geology*, 16, 972–975.

Lancaster, N. (1988b) The development of large aeolian bedforms. *Sediment. Geol.*, 55, 69–89.

Lancaster, N. (1996) Field studies of sand patch initiation processes on the northern margin of the Namib Sand Sea. *Earth Surf. Process. Landforms*, 21, 947–954.

Leite, J.F., Aboarrage, A.M. and Daemon, R.F. (1975) Projeto Carvão da Bacia do Parnaíba. 55 pp.

Lima, E. de A.M. and Leite, J.F. (1978) Projeto estudo global dos recursos minerais da bacia sedimentar do Parnaíba. 413.

Lima Filho, F.P. (1998) A sequencia Permo-Pensilvaniana da Bacia do Parnaiba. 155.

Loope, D.B. (1985) Episodic deposition and preservation of eolian sands: a late Paleozoic example from southeastern Utah (Canyonlands National Park, USA). *Geology*, 13, 73–76.

Loope, D.B., Steiner, M.B., Rowe, C.M. and Lancaster, N. (2004) Tropical westerlies over Pangaean sand seas. *Sedimentology*, 51, 315–322.

Maynard, J.R. and Leeder, M.R. (1992) On the periodicity and magnitude of late Carboniferous glacio- eustatic sea-level changes. *J. - Geol. Soc.*, 149, 303–311.

McKee, E.D., Douglass, J.R. and Rittenhouse, S. (1971) Deformation of lee-side laminae in eolian dunes. *Bull. Geol. Soc. Am.*, 82, 359–378.

Mesner, J.C. and Wooldridge, L.C. (1964) Estratigrafia Das Bacias Paleozóica E Cretácea Do Maranhão. *Bol. Téc. PETROBRÁS*, 7, 137–164.

Mottin, T. E., Vesely, F. F., de Lima Rodrigues, M. C. N., Kipper, F., & de Souza, P. A. (2018). The paths and timing of late Paleozoic ice revisited: new stratigraphic and paleo-ice flow interpretations from a glacial succession in the upper Itararé Group (Paraná Basin, Brazil). Palaeogeography, palaeoclimatology, palaeoecology, 490, 488-504.

Mountney and Howell (2000) Aeolian architecture, bedform climbing and preservation space in the Cretaceous Etjo Formation, NW Namibia. *Sedimentology*, 47, 825–849.

Mountney, N.P. (2006a) Periodic Accumulation And Destruction Of Aeolian Erg Sequences In The Permian Cedar Mesa Sandstone, White Canyon, Southern Utah, USA. *Sedimentology*, 53(4), 789–823.

Mountney, N.P. (2006b) Eolian Facies Models. In: *Facies Models Revisited*, *SEPM (Society for Sedimentary Geology)*, 19–83.

Mountney, N.P. (2012) A stratigraphic model to account for complexity in aeolian dune and interdune successions. *Sedimentology*, 59, 964–989.

Mountney, N.P. and Jagger, A. (2004) Stratigraphic evolution of an aeolian erg margin system: The Permian Cedar Mesa Sandstone, SE Utah, USA. *Sedimentology*, 51, 713–743.

Mountney, N.P. and Russell, A.J. (2009) Aeolian dune-field development in a water table-controlled system: Skeiðarársandur, Southern Iceland. *Sedimentology*, 56, 2107–2131.

Mountney, N.P. and Thompson, D.B. (2002) Stratigraphic evolution and preservation of aeolian dune and damp/wet interdune strata: An example from the Triassic Helsby Sandstone Formation, Cheshire Basin, UK. *Sedimentology*, 49, 805–833.

Paola, C. and Borgman, L. (1991) Reconstructing random topography from preserved stratification. *Sedimentology*, 38, 553–565.

Parrish, J.T. (1993) Climate of the supercontinent Pangea. *J. Geol.*, 101, 215–233.

Perlmutter, M.A. and Matthews, M.D. (1989) Global cyclostratigraphy – A model. In: *Quantitative Dynamic Stratigraphy* (Ed. T.A. Cross), *Prentice Hall*, Englewood, 233–260.

Peyser, C.E. and Poulsen, C.J. (2008) Controls on Permo-Carboniferous precipitation over tropical Pangaea: A GCM sensitivity study. *Palaeogeogr. Palaeoclimatol. Palaeoecol.*, 268, 181–192.

Plee, K., Ariztegui, D., Martini, R. and Davaud, E. (2008) Unravelling the microbial role in ooid formation - results of an in situ experiment in modern freshwater Lake Geneva in Switzerland. *Geobiology*, 6, 341–350.

Porter, M.L. (1986) Sedimentary record of erg migration. *Geology*, 14, 497–500.

Romain, H.G. and Mountney, N.P. (2014) Reconstruction of three-dimensional eolian dune architecture from one-dimensional core data through adoption of analog data from outcrop. *Am. Assoc. Pet. Geol. Bull.*, 98, 1–22.

Roscher, M. and Schneider, J.W. (2006) Permo-Carboniferous climate: Early Pennsylvanian to Late Permian climate development of central Europe in a regional and global context. *Geol. Soc. Spec. Publ.*, 265, 95–136.

Rubin, D.M. (1987) Formation of scalloped cross-bedding without unsteady flows. *J. Sediment. Petrol.*, 57, 39–45.

Scherer, C.M.S. (2000) Eolian dunes of the Botucatu Formation (Cretaceous) in southernmost Brazil: Morphology and origin. *Sediment. Geol.*, 137, 63–

84.

Scherer, C.M.S. (2002) Preservation of aeolian genetic units by lava flows in the Lower Cretaceous of the Paraná Basin, southern Brazil. *Sedimentology*, 49, 97–116.

Scotese, C.R. (2014) Atlas of Permo-Carboniferous Paleogeographic Maps (Mollweide Projection), Maps 53 – 64, Volumes 4, The Late Paleozoic, PALEOMAP Atlas for ArcGIS, PALEOMAP Project, Evanston, IL.

Suttner, L.J., Basu, A., Ingersoll, R. V., Bullard, T.F., Ford, R.L. and Pickle, J.D. (1985) The effect of grain size on detrital modes: a test of the Gazzi-Dickinson point-counting method - DISCUSSION AND REPLY. *J. Sediment. Petrol.*, 55, 616–627.

Swanson, T., Mohrig, D., Kocurek, G., Cardenas, B.T. and Wolinsky, M.A. (2019) Preservation of autogenic processes and allogenic forcings in set-scale aeolian architecture I: Numerical experiments. *J. Sediment. Res.*, 89, 728–740.

Sweet, M.L., Nielson, J., Havholm, K. and Farrelley, J. (1988) Algodones dune-field of southeastern California: case history of a migrating modern dune-field. *Sedimentology*, 35, 939–952.

Tabor, N.J. and Poulsen, C.J. (2008) Palaeoclimate across the Late Pennsylvanian-Early Permian tropical palaeolatitudes: A review of climate indicators, their distribution, and relation to palaeophysiographic climate factors. *Palaeogeogr. Palaeoclimatol. Palaeoecol.*, 268, 293–310.

Tribaldos, V.R. and White, N. (2018) Implications of preliminary subsidence analyses for the Parnaíba cratonic basin. In: *Geological Society Special Publication*, *Geological Society of London*, 472, 147–156.

Tsoar, H. (1989) Linear dunes - forms and formation. *Prog. Phys. Geogr. Earth Environ.*, 13, 507–528.

Viana, C.D., Grohmann, C.H., Busarello, M.S.T. and Garcia, G.P.B. (2018) Structural analysis of clastic dikes using Structure from Motion - Multi-View Stereo: A case-study in the Paraná Basin, southeastern Brazil. *Brazilian J. Geol.*, 48, 839–852.

Vesely, F. F., Trzaskos, B., Kipper, F., Assine, M. L., & Souza, P. A. (2015). Sedimentary record of a fluctuating ice margin from the Pennsylvanian of

western Gondwana: Paraná Basin, southern Brazil. Sedimentary Geology, 326, 45-63.

Vieira, L.V. and Scherer, C.M. dos S. (2017) Facies architecture and high resolution sequence stratigraphy of an aeolian, fluvial and shallow marine system in the Pennsylvanian Piauí Formation, Parnaíba Basin, Brazil. *J. South Am. Earth Sci.*, 76, 238–256.

Wanless, H.R. and Shepard, F.P. (1936) Sea level and climatic changes related to late Paleozoic cycles. *Bull. Geol. Soc. Am.*, 47, 1177–1206.

Watts, A.B., Tozer, B., Daly, M.C. and Smith, J. (2018) A comparative study of the Parnaíba, Michigan and Congo cratonic basins. *Geol. Soc. Spec. Publ.*, 472, 45–66.

Wilson, I.G. (1972) Aeolian Bedforms—Their Development and Origins. *Sedimentology*, 19, 173–210.

Wilson, I.G. (1971) Desert Sandflow Basins and a Model for the Development of Ergs. *Geogr. J.*, 137, 180–199.

Ziegler, A.M., Scotese, C.R., McKerrow, W.S., Johnson, M.E. and Bambach, R.K. (1979) Paleozoic Paleogeography. *Annu. Rev. Earth Planet. Sci.*, 7, 473–502.

9.2 ARTIGO 2

This is an automated message.

A Pennsylvanian saline-alkaline lake in Gondwana mid-latitude: Evidence from the Piauí Formation, Parnaíba Basin, NE Brazil

Dear Mr Kifumbi,

We have received the above referenced manuscript you submitted to Palaeogeography, Palaeoclimatology, Palaeoecology.

To track the status of your manuscript, please log in as an author at https://www.editorialmanager.com/palaeo/, and navigate to the "Submissions Being Processed" folder.

Thank you for submitting your work to this journal.

Kind regards,

Palaeogeography, Palaeoclimatology, Palaeoecology

More information and support

You will find information relevant for you as an author on Elsevier’s Author Hub: https://www.elsevier.com/authors

FAQ: How can I reset a forgotten password?

https://service.elsevier.com/app/answers/detail/a_id/28452/supporthub/publishing/

For further assistance, please visit our customer service site: https://service.elsevier.com/app/home/supporthub/publishing/

Here you can search for solutions on a range of topics, find answers to frequently asked questions, and learn more about Editorial Manager via interactive tutorials. You can also talk 24/7 to our customer support team by phone and 24/7 by live chat and email

---

In compliance with data protection regulations, you may request that we remove your personal registration details at any time. (Use the following URL: https://www.editorialmanager.com/palaeo/login.asp?a=r). Please contact the publication office if you have any questions.

A Pennsylvanian saline-alkaline lake in Gondwana mid-latitude: Evidence from the Piauí Formation, Parnaíba Basin, NE Brazil

Carrel Kifumbi[1], Claiton Marlon dos Santos Scherer[1], Luiz Fernando De Ros[1], Tais Freitas Da Silva[1], Elias Cembrani Da Rocha[1], Bruno Silverston Angonese[1]

Programa de Pós-Graduação em Geociências, Universidade Federal do Rio Grande do Sul, P.O. Box 15001, CEP 91501-970 Porto Alegre, RS, Brazil
carrelkif@yahoo.fr

Key words: Saline-alkaline lake, Biomarkers, Piauí Formation, Parnaíba Basin, Pennsylvanian reconstruction

ABSTRACT

The Pangaea assemblage resulted in significant tectonic and eustatic changes, but also a well-known increasing desertification triggered by the increasing continentalization. While northern hemisphere basins have been thoroughly studied, recent studies on southern hemisphere basins bring new insight on how these events affected the Gondwana hinterlands. In the present study, new evidence is added to take this discussion ahead. Through sedimentological and geochemical analysis of chert deposits from the Parnaíba Basin, the onset of aridification in Gondwana mid-latitudes can reliably be positioned during Pennsylvanian age. The chert deposits are composed of three facies (stromatolites, ooidal arenites and intraformational breccias) deposited in a shallow-water environment characterized by high organic matter productivity and seasonal changes, typical of saline-alkaline lakes. Biomarkers analysis allowed identification of number of evidence that suggest predominance of planktonic organic matter productivity from cyanobacterial in an environment characterized by high salinity, elevated pH and anoxic conditions. These evidence suggest that the Piauí Formation saline-alkaline lake is a remnant from the progressive withdrawal of the Panthalassa ocean due to the ongoing continentalization and increasing aridification.

1 INTRODUCTION

The development of lacustrine environments with high pH and salinity is favored by closed (endorheic) drainage and arid or semiarid climate conditions (Hammer, 1986; Oduor and Schagerl, 2007; Stenger-Kovács et al., 2014). Their physical and chemical features depend on both tectonic setting and climatic factors (Yuretich and Cerling, 1983). Although modern saline-alkaline lakes are geographically widespread, most of them occur in tropical or subtropical latitudes (Ventosa and Arahal, 2009). Among the most documented are the lakes of the East African Rift (Butturini et al., 2020), central and western Asia (Clauer et al., 1998), central Europe (Stenger-Kovács et al., 2014), and Brazilian Pantanal wetland (Andreote et al., 2014). In these lakes, the water composition is essentially controlled by river input and weathering of the surrounding areas (Jones and Deocampo, 2003), while salinity is mainly controlled by the evaporation rate, which is a function of rainfall intensity. Although their elevated salinity and alkalinity limit faunal and floral diversity (Andreote et al., 2014; Yuretich and Cerling, 1983), cyanobacteria productivity is usually very high, because cyanobacteria are among the few organisms capable to survive in such extreme conditions (López-Archilla et al., 2004; López-Cortés et al., 2001; Oduor and Schagerl, 2007; Ventosa and Arahal, 2009; Wang and Fu, 1997).

This study presents the first evidence of a Pennsylvanian (Late Carboniferous) saline-alkaline lacustrine environment in tropical central Gondwana, recorded in the chert deposits of the still poorly studied Piauí Formation of the Parnaíba Basin, northeastern Brazil. Much attention has been directed to the overlaying, fossil-rich Pedra de Fogo Formation, which records a major southern hemisphere Permian aridification event (Cisneros et al., 2015; Iannuzzi et al., 2018, Abrantes et al., 2019). However, the onset of aridification can reliably be positioned during the late Pennsylvanian period, when the collision of Gondwana and Laurasia triggered the withdrawal of epeiric seas and the uplift of Central Pangean mountains, which resulted in increasing monsoonal circulation and enhanced arid conditions in the Gondwana (Becker et al., 1997; Gibbs et al., 2002; Golonka and Ford, 2000). The formation of epeiric seas during arid periods caused the deposition of stromatolites and clay ooids that

reveal specific sedimentological and geochemical conditions of the depositional environment.

The stromatolites and chert deposits of the Parnaíba Basin offer an opportunity to understand the climatic and environmental conditions prevailing in the still poorly known mid-latitudes of Gondwana hinterland during Pennsylvanian. This study aims to: (1) identify the depositional environment of these deposits based on sedimentological and geochemical analysis and; (2) unravel the paleoclimatic conditions of the central, tropical Gondwana during the Pennsylvanian.

2 GEOLOGICAL SETTING

2.1 Regional geology

The Parnaíba basin is a c.a. 600,000 km² Paleozoic basin with Silurian to Cretaceous infill, located in northeastern Brazil. The basin shows a decreasing tectonic subsidence evolution (Rodríguez Tribaldos and White, 2018), with a faster subsidence phase occurring during the first 100 Ma (Silurian) followed by slower rate from Carboniferous to Mesozoic. The basin is a near-circular intracratonic sag, with a basement made up from assemblage of three Precambrian blocks. In the west, the Amazonian/Araguaia block is characterized by ophiolitic metasedimentary rocks. At the center, the Parnaíba block composition is uncertain, but presumably composed of granitoid rocks. In the east, the Borborema block is formed by mylonitic gneisses (Daly et al., 2014). The collision between these blocks gave rise to major shear zones, which was reactivated by subsequent orogenies (Zalan, 1991).

During the Pennsylvanian, the Parnaíba basin suffered significant tectonic and environmental changes (Góes and Feijó, 1994). Depocenters changed from elongated to circular, and open marine environments were replaced by shallow epeiric sea under arid climate (Caputo, 1984). Subsequently, the rupture of the Pangea mega-continent during the Mesozoic led to distensional tectonics, reactivation of shear zones and intense basic magmatism. Two main pulses of magmatism activity occurred in the Parnaíba basin, the first (215 - 150 Ma) related to the Central Atlantic rifting and the second (149 – 87 Ma), to the South Atlantic rifting (Milani and Thomaz Filho, 2000).

2.2 Stratigraphic framework

The sedimentary record of the Parnaíba basin is about 3500 m thick and can be divided into 5 supersequences (Vaz et al., 2007). This study focuses on the Pennsylvanian succession, which corresponds to the Piauí Formation (Fig. 1; Mesner and Wooldridge, 1964; Small, 1914). The Piauí Formation is dominantly composed of sandstones, with rare carbonates (Lima and Leite, 1978), and represents deposition under continental context (fluvial and eolian environments) with some rare marine invasions (Fig. 1; Lima Filho, 1999; Vieira and Scherer, 2017).

Chert deposits were documented for the first time in the Parnaíba basin by Plummer (1946). The author reported abundant chert deposits in the Permian succession and proposed the name Pedra de Fogo (“Flint”) Formation for the Permian rocks. Later, Lima and Leite (1978) documented a thin, yet regionally extensive, chert level within the Pennsylvanian Piauí Formation. The Piauí and Pedra de Fogo cherts show different associated deposits. While the Piauí chert occurs at the base of aeolian deposits (Fig.1; Santos and Carvalho, 2004), the Pedra de Fogo cherts are intercalated with - lacustrine mudstones rich in plants and vertebrates (Faria, 1979; Iannuzzi et al., 2018). Both the Piauí and Pedra de Fogo cherts show a wide variety of textures and compositions, including ooids, intraformational breccias and silicified stromatolites (Faria, 1979).

According to Faria (1979) the significant volume of dissolved silica required for formation of the Pedra de Fogo cherts may be related to: (i) silica supply from continental sources;(ii) inorganic silica precipitation caused by intense evaporation and elevated pH in environments with restricted connection with sea water; and (iii) diagenetic replacement of carbonate by microcrystalline silica. The author also described columnar and pseudocolumnar stromatolites organized in domal and undulated biostromes, and suggested their formation in shallow marine environments (supratidal to intertidal), with subaerial exposure. While the Pedra de Fogo chert deposits have received much interest, especially from paleontologists, the Piauí Formation chert deposits are hardly reported in literature, even though their occurrence has significant implications on paleoclimatic conditions of central Gondwana during the Pennsylvanian period.

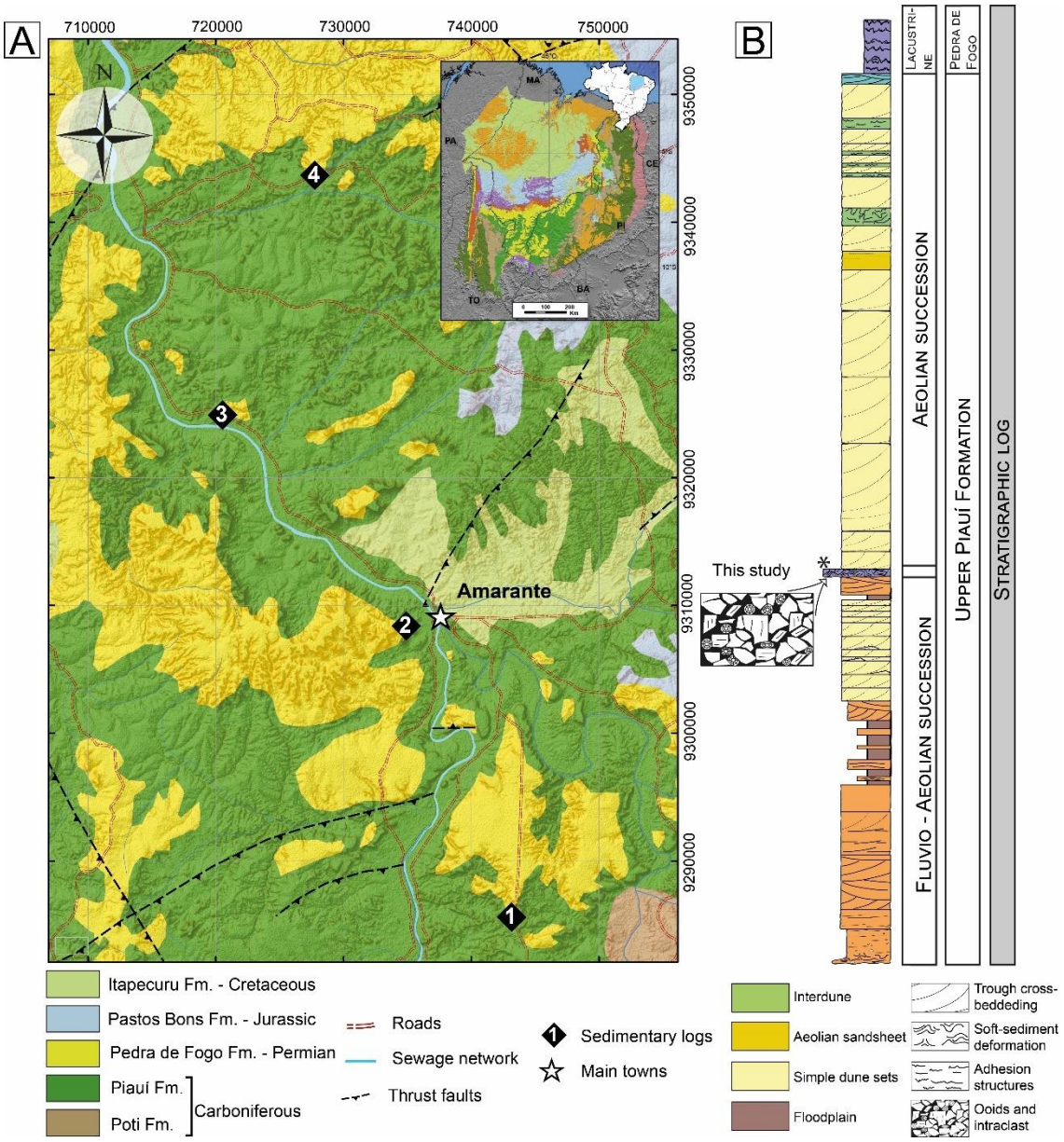

Figure 1: (A) Detailed geologic map of the studied area with location of the four outcrops where studied samples were collected. (B) Stratigraphic log of the upper Piauí Formation. The studied deposits are thin, yet regionally continuous over the entire area.

3 MATERIALS AND METHODS

Field investigations were carried out around the Amarante town, where nine sedimentologic logs were recorded. Among these, four localities stand out for their well-preserved chert deposits (Fig. 1). Detailed sedimentologic analysis allowed identification of three facies: Stromatolites, ooidal arenites and intraformational breccias (next section).

Eleven samples of stromatolites and ooidal arenites were collected from these four locations to account for possible variations in facies composition or structure. Stromatolite analysis was conducted in macroscale using field and laboratory methods proposed by Preiss (1976), and at microscale through the petrographic descriptions of thin sections (Awramik, 1991; Hofmann, 1973; Riding, 2011). Twelve thin sections were prepared from the collected samples to characterize structure, texture, fabric, primary and diagenetic composition. Thin section petrography was performed using a Zeiss AXIO Imager 2 microscope and the photomicrographs were obtained with ZEN 2012 software.

Because original mineral composition was completely replaced by silicification and dolomitization, biomarker identification was used to determine the depositional environment through identification of environmental conditions such as salinity, pH, etc. Three samples of stromatolites containing thicker dark laminae were selected for gas chromatography-mass spectrometry (GC-MS), because of their potentially high organic matter preservation (McKirdy, 1976). Powdered core (20 g) samples were extracted using a Soxtec^{TM} 2050 equipment with 83-ml dichloromethane and 7 ml of methanol during 4 hours at 125 °C, then left to evaporate until constant weight was reached. Aliquots of total extract were separated into aliphatic, aromatic and polar fractions using a column with activated silica gel and alumina. About 75% of hexane were added to fill the glass column (30 cm, Ø = 0.5 cm). Then, 1.5 g of silica and 3.0 g of alumina, previously heated for 3 hours (200 °C - 400 °C), and 0.5 g of sodium sulfate were added to the column to remove all possible remaining water. Elution proceeded with 20 ml of hexane (saturated fraction), 12 ml hexane + 8 ml of toluene (aromatic fraction), and 12 ml of toluene + 8 ml of methanol (polar fraction).

The saturated hydrocarbons fractions were analyzed using an Agilent Technologies gas chromatograph (Palo Alto, CA, USA) model 7890 A, equipped with an automatic sampler and coupled to quadrupole 5975 MDS mass spectrometer. The carrier gas was helium (He) at 1.2 mL/min., in constant flow mode. Capillary column Agilent Technologies (USA) DB-5 (5% phenyl, 95% methylsilicone, 30 m x 0.25 mm ID, and film thickness 0.25 lm) were used. The injector temperature was 290 °C. The analyzes were performed in scanning

(SCAN) with an acquisition time of 50 ms for the analytes, and selective ion monitoring (SIM) mode using *m/z* 191, *m/z* 177, *m/z* 217, *m/z* 218, *m/z* 259, and *m/z* 85. In the SCAN mode, the GC temperature programming was: 40 ºC (1 min) to 300 ºC to 6 ºC/min (25 min). In the SIM mode the GC temperature programming was: 80 ºC (3 min) to 150 ºC at 35 ºC/min and 310 °C at 3 °C/min (hold 15 min). The operating conditions of the MS were ion source temperature of 280 ºC; interface temperature was 300 ºC and quadrupole temperature 150 ºC. The ionization voltage was 70 eV.

4 RESULTS

The studied chert deposits comprise stromatolites, ooidal arenites and intraformational breccias. Detailed description of macro- and micro-scale structures are provided in section 4.1. Biomarker profiles are interpreted in section 4.2.

4.1 Facies

Stromatolites

Description: Stromatolites form low-relief coalescent domes of up to 40 cm in wavelength and 10 cm in height, with irregular shapes and disrupted aspect in plan view. Domes are composed of columnar stromatolites growing over horizontal laminae. The laminations are formed by mm-thick, irregular and lenticular laminae (Fig. 2), characterized by alternation of light and dark laminae. Light laminae are composed of dolomitized and silicified matrix, while dark laminae contain high organic mat concentration. The primary composition has been nearly completely replaced by cryptocrystalline and microcrystalline silica, and rhombohedral dolomite. Columnar stromatolites are composed of elongated structures with c.a. 1 cm in diameter and 3 to 5 cm in height (Fig. 2). The columns are replaced by cryptocrystalline and microcrystalline silica, microspherulitic chalcedony and rhombohedral dolomite crystals. The inter-column spaces are filled with microporous microspherulitic chalcedony. Fractures through columns and interstitial chalcedony are partially filled with drusiform prismatic quartz and dolomite, which was later dissolved. Fractures and vugular pores in silicified levels were filled with macrocrystalline dolomite.

Moldic and vugular pores generated by the dissolution of dolomite were partially filled by iron oxides.

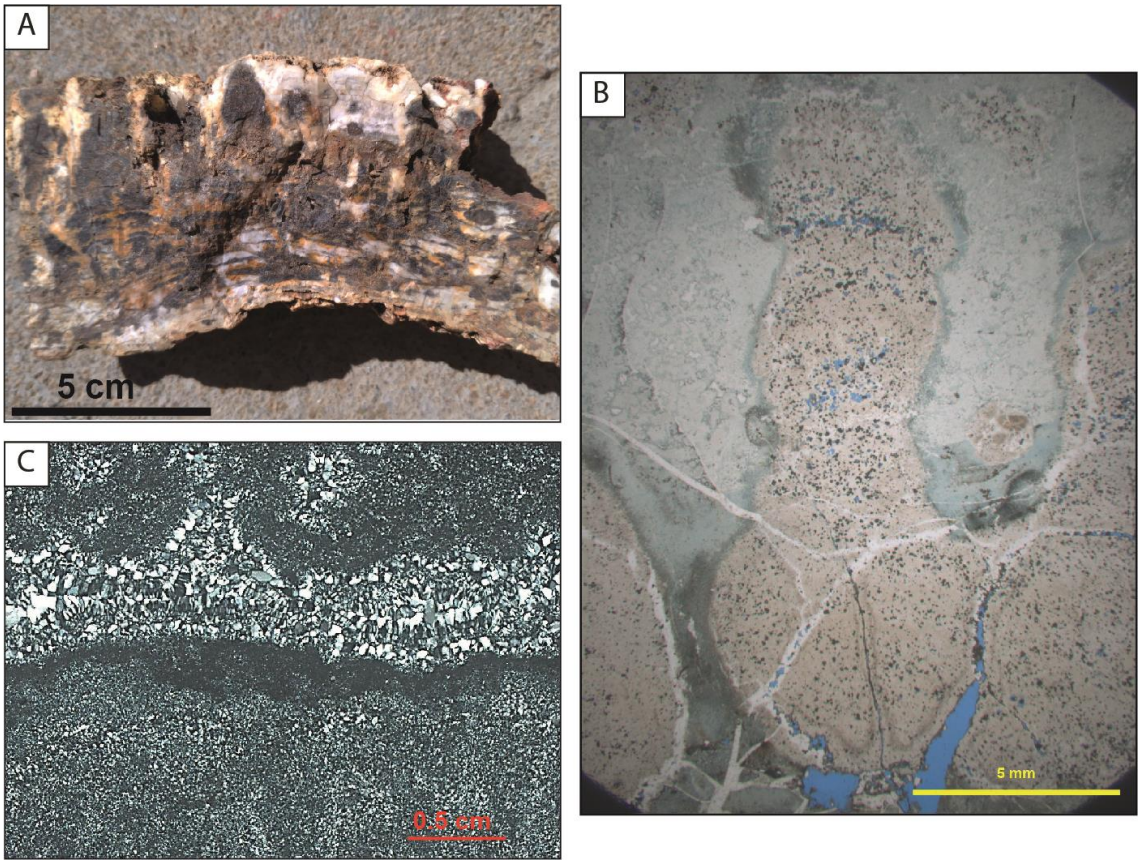

Figure 2: (A) Stromatolite hand sample. Observe that columnar stromatolites grow over sub-horizontal laminations (lower part of the sample). (B) Photomicrograph of a columnar stromatolite thin section, with “inter-finger” space filled with microporous microspherulitic chalcedony. Uncrossed polarizers (//P). (C) Photomicrograph of silicified ooidal arenite covering a silicified stromatolite with clotted texture, indicative of microbial deposition. Note the intense silicification of both ooids and stromatolite, and intergranular chalcedony cementation. Crossed polarizers (XP).

Interpretation: Decimeter-scale domes were formed by bioherms and represent the accretion of stromatolite through time (Grotzinger, 1989). An alternation of light and dark laminae similar to that of the studied stromatolites was documented in sabkha-associated microbialites from the Upper Permian Platy dolomite, in which the light laminae are composed of micrite matrix and the dark laminae are characterized by remnants of filamentous cyanobacteria (Brehm et al., 2002; Gasiewicz et al., 1987). Such dark and light stromatolite

laminations usually reflect seasonal changes. The lighter laminae usually contain very few or no fossilized microorganisms and are deposited during wetter periods, while the dark laminae contain high organic matter derived from microbial ecosystems and forms in drier periods (Brehm et al., 2002; Gasiewicz et al., 1987; Maliński et al., 2009).

The low-relief and centimeter-scale size of columnar stromatolites indicate development in a shallow-water depositional environment (Kah et al., 2006). The evolution from horizontal lamination to columnar structure reflects hydrodynamic conditions of the water column (Grotzinger and Knoll, 1999; Hofmann, 1973; Walter, 1977). Horizontal laminations represent fair-weather periods of shallow water environment, while columnar structures represent vertical accretion linked to the 'light-driven' growth of microbial mats caused by progressive increase in water depth (Hofmann, 1973). The progressive increase in water depth enhanced the vertical growth of stromatolite.

Ooidal arenites

Description: Ooidal arenites are dominantly characterized by ooids that range from 0.15 to 2.5 mm in diameter, together with rare peloids and siliceous microcrystalline intraclasts. The ooids exhibit oval, elongated and irregular shapes, and a wide size variation (Fig. 3). Internally, the ooids concentric structure is poorly-preserved, owing to intense silicification (Fig. 3). Their primary composition was partially dissolved and/or replaced by dolomite, cryptocrystalline and microcrystalline silica and prismatic quartz, which also affected the peloids and intraclasts. Cementation by chalcedony rims, quartz mosaic and blocky dolomite filled most of the interparticle pores (Fig. 3). Interparticle contacts between ooids vary heterogeneously between point, longitudinal and concavo-convex. Locally, dolomite crystals replaced the ooids and cement, and were later oxidized, dissolved and/or replaced by microcrystalline silica (Fig. 3). Moldic pores formed by dissolution of dolomite crystals were partially filled with hematite and clay coatings. Additionally, silicified crusts are found in some of the sample between layers of ooids and show clotted texture borders. Secondary porosity generated by dissolution of dolomite, ooids and intraparticle cement is scarce.

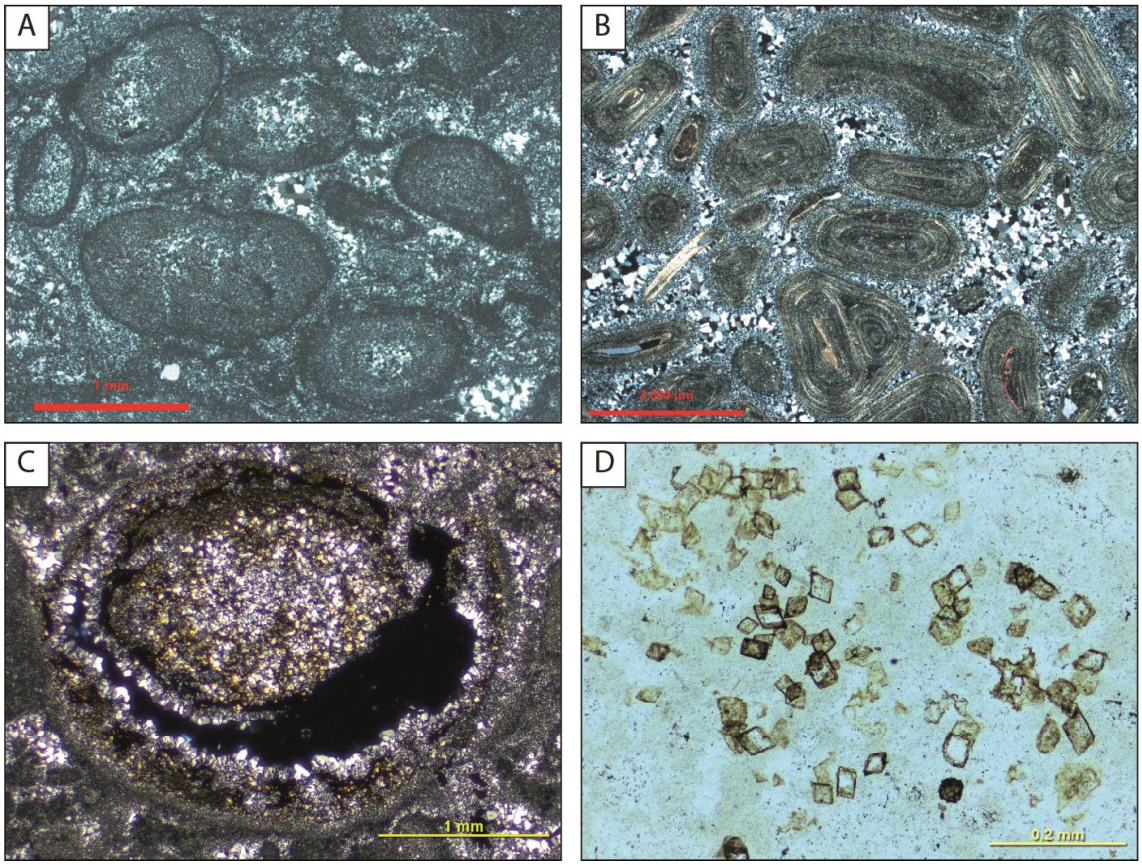

Figure 3: Photomicrographs of : (A) Piauí ooids partially deformed before silicification and silica cementation. Note the wide variation in grain size, and the oval and deformed shape of many ooids. XP. (B) Similar, deformed and partially silicified stevensite ooids of the Cretaceous 'pre-salt' rift section of Campos Basin (Goldberg et al, 2017). (C) Photomicrograph of silicified ooidal arenite covering a silicified stromatolite with clotted texture, indicative of microbial deposition. Note the intense silicification of both ooids and stromatolite, and intergranular chalcedony cementation. Crossed polarizers (XP). (D) Photomicrograph of a poorly-sorted ooidal arenite. Note the wide variation in grain size, and the oval and deformed shape of many ooids. XP.

Interpretation: The variable nature of interparticle contacts among ooids grains suggests heterogeneous compaction caused by partial early cementation, which inhibited further compaction. The oval and irregular shapes of the ooids, even in areas with early cementation and little compaction (Fig. 3), suggest that this deformation was not caused only by the ductile behavior of grains during burial compaction. Such irregular deformation and the presence of shrinkage-

like porosity within the concentric ooids structure was in part probably promoted by early dehydration of ooids originally composed by smectitic clays. This is suggested by their similar morphology with the stevensite ooids of the ‘pre-salt’ Cretaceous section of Campos and Santos basins of Brazil (Fig. 3; Armelenti et al., 2016; Herlinger et al., 2017; Leite et al., 2020) and of the Eocene Green River Formation of central Utah, USA (Tettenhorst and Moore, 1978). Although the original clay composition of the Piauí ooids was not preserved, owing to their intense silicification, the widespread occurrence of dolomite ($MgCO_3$) in the cherts suggests that early diagenetic waters were Mg-rich, what could be related to the dissolution of stevensite.

According to Tosca and Wright (2015), stevensite is formed after a Mg-silicate gel under strongly alkaline conditions. Mg-clays such as stevensite are highly sensible to changes in water chemistry, what may promote their dissolution and replacement by silica (Tosca and Wright, 2015). Dissolution of Mg-silicates such as stevensite may release a significant volume of Si and Mg, what could explain the pervasive dolomitization and silicification and the common occurrence of dolomite in the studied deposits (Tosca and Wright, 2015). This set of evidence support the interpretation of an original Mg-rich clay composition for the ooids.

The presence of hematite and clay coatings within dolomite dissolution pores can be interpreted as a telodiagenetic process that resulted from the infiltration of meteoric waters into the exposed rocks.

Intraformational breccia

Description: This facies consists of angular and irregular intraclasts of stromatolites and fragments of ooidal rocks, ranging from 0.3 to 2 cm (Fig. 4). Intraclasts are completely replaced by microcrystalline silica, and most primary textures are obliterated by recrystallization (Fig. 4). However, remnants of primary lamination are observed in some intraclasts. Interparticle primary porosity is totally cemented by microcrystalline silica. The dissolution of intraclasts resulted in vugular and moldic pores cemented by clay minerals, iron oxides, and microcrystalline and prismatic quartz.

Interpretation: The very angular shape of the clasts suggest disruption of stromatolitic and ooidal facies during high-energy events, with very limited transportation (Harwood and Sumner, 2011). The extremely angular and sharp

edges of the intraclasts suggests that they were not subjected to transportation and reworking. The poor sorting indicates that events of erosion and stromatolite disruption were episodic and related to periods of high energy wave action, like storms. Clay and iron oxide precipitation in some pores are product of telodiagenesis owing to later exposure.

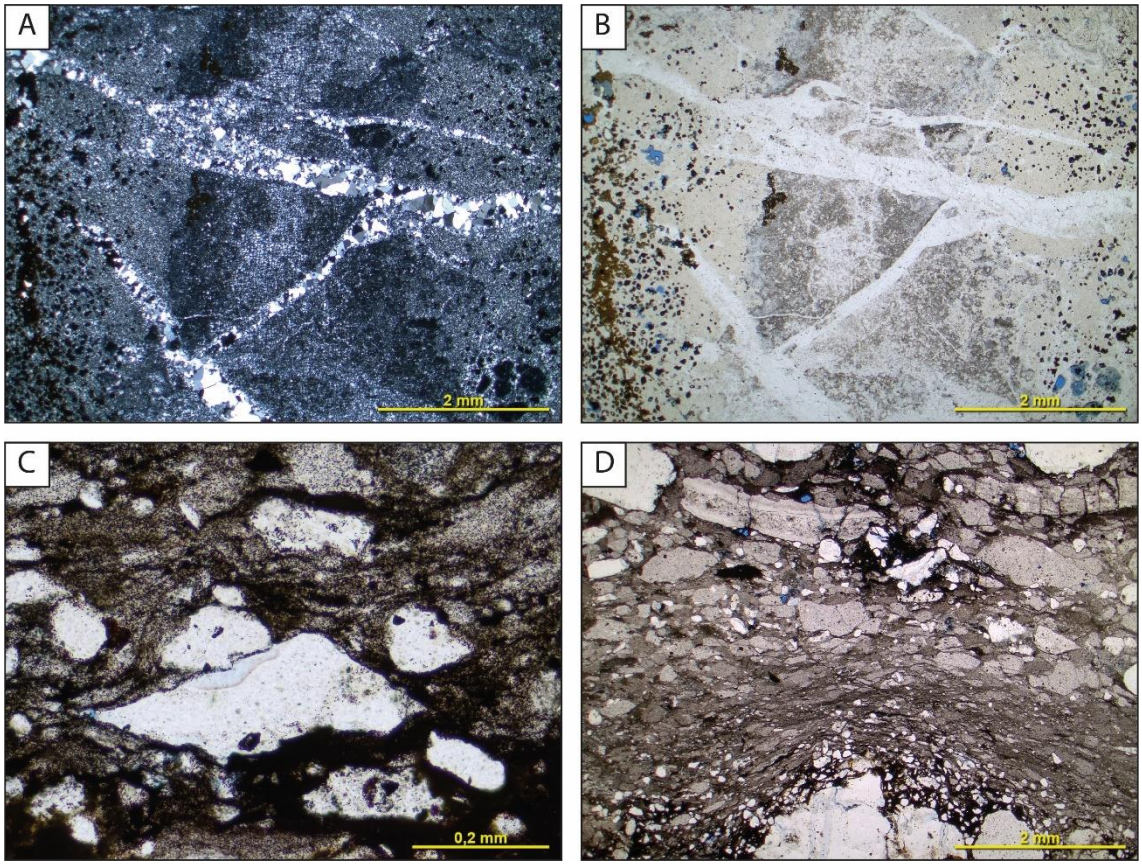

Figure 4: Photomicrographs of intraformational breccias. (A) and (B) Angular microcrystalline silica clasts under crossed and uncrossed polarizers. Note the interparticle porosity completely cemented by quartz. Observe iron oxides replacing dolomite crystals at the right and left borders of the (B). (C) Texture of a deformed breccia. //P. (D) Breccia with some clasts showing remnants of original lamination. //P.

4.2 Biomarkers

n-Alkanes and isoprenoids

The gas chromatograms of the saturate fraction of the three samples are characterized by an unimodal distribution as shown in Figure 5; the identification of peaks is listed in Table. 1**.** The identification of *n*-alkanes and

isoprenoids was performed using the *m/z* = 57 ion (Fig. 5). The *n*-alkanes are present over the range *n*-C_{17} to *n*-C_{37} and there is a predominance of even carbon number over odd numbers within the range of C_{20} to C_{30} and the carbon preference index (CPI) value ranges from 1.04 to 1.12. Because the even over odd predominance may be obscured by the input of continental matt, ten Haven

Table 2: Hydrocarbons identified by GC–MS in the extracts from microbialite deposits

Peak	Structure
Tr20	C_{20} Tricyclic Terpane
Tr21	C_{21} Tricyclic Terpane
Tr23	C_{23} Tricyclic Terpane
Tr24	C_{24} Tricyclic Terpane
Tr25	C_{25} Tricyclic Terpane
TT24	C_{24} Tetracyclic Terpane
Tr26	C_{26} Tricyclic Terpane
Ts	C_{27} 18α(H)-22,29,30-Trisnorneohopane
Tm	C_{27} 17α(H)-22,29,30-Trisnorhopane
H29	C_{29} 17α (H), 21β(H)−30-Norhopane
M29	C_{29} 17β (H), 21α(H)− Normoretane
H30	C_{30} 17α (H), 21β(H)− Hopane
M30	C_{30} 17β (H), 21α(H)− Moretano
H31S	C_{31} 17α (H), 21β(H)-30-Homohopane (22S)
H31R	C_{31} 17α (H), 21β(H)-30-homohopane (22R)
Gam	Gammacerane
H32S	C_{32} 17α (H), 21β(H)-30-Bishomohopane (22S)
H32R	C_{32} 17α (H), 21β(H)-30-Bishomohopane (22R)
H33S	C_{33} 17α (H), 21β(H)-30-trishomohopano (22S)
H33R	C_{33} 17α (H), 21β(H)-30-trishomohopane (22R)
H34S	C_{34} 17α (H), 21β(H)-30-tetrakishomohopane (22S)
H34R	C_{34} 17α (H), 21β(H)-30-tetrakishomohopane (22R)
H35S	C_{35} 17α (H), 21β(H)-30-pentakishomohopane (22S)
DIA 27 S	C_{27} 13β(H), 17α(H)- Diacholestane (20S)
DIA 27 R	C_{27} 13β(H), 17α(H)- Diacholestane (20R)
C_{27}aaa S	C_{27} 5α(H), 14 α(H), 17 α(H)- Cholestane (20S)
C_{27} abb R	C_{27} 5α(H), 14 β(H), 17 β(H)- Cholestane (20R)
C_{27} abb S	C_{27} 5α(H), 14β(H), 17β(H)- Cholestane (20S)
C_{27} aaa R	C_{27} 5α(H), 14α(H), 17α(H)- Cholestane (20R)

C_{28} aaa S	C_{28} 5α(H), 14β(H), 17β(H)- 24-ethyl Cholestane (20S)
C_{28} aaa R	C_{28} 5α(H), 14α(H), 17α(H)- 24- ethyl Cholestane (20R)
C_{29} aaa S	C_{29} 5α(H), 14α(H), 17α(H)- 24- ethyl Cholestane (20S)
C_{29} abb R	C_{29} 5α(H), 14β(H), 17β(H)- 24- ethyl Cholestane (20R)
C_{29} abb S	C_{29} 5α(H), 14β(H), 17β(H)- 24- ethyl Cholestane (20S)
C_{29} aaa R	C_{29} 5α(H), 14α(H), 17α(H)- 24- ethyl Cholestane (20R)

et al (1985) proposed the use of R_{22} index, defined as 2 x C_{22} /(C_{21}+C_{23}). The R_{22} index is 0.9 in sample 1, 1.05 in sample 2 and 1.08 in sample 3 and in sample 2 and 3 the R_{22} index is greater than 1. There is a gradual increase in abundance from*n*-C_{16} to *n*-C_{31}. Isoprenoid alkanes are abundant and phytane is the most abundant compound in the saturate fraction of all samples. The pristane/phytane ratio is applied as indicator of redox conditions and provides reliable information on the source rock. In the collected samples the Pr/Ph ratio is low, ranging between 0.17 and 0.33. Long chain isoprenoids, especially regular C_{25} and tail-to-tail C30 alkanes are also abundant.

Terpanes and Steranes

Terpanes and steranes are shown in in *m/z* 191 and *m/z* 217 mass chromatogram (Fig. 5). Peak identification on *m/z* 191 and *m/z* 217 chromatograms are given in Table 1 and geochemical parameters are show in the Table 2. The *m/z* 191 mass chromatogram of the saturated hydrocarbon fractions show high relative abundance of pentacyclic triterpanes compared to tricyclic terpanes. In all samples analyzed, Ts (C_{27} 18-(H)-22,29,30-trisnorneohopane) is more abundant than Tm (C_{27} 17-(H)-22,29,30-trisnorhopane) (Figure 5). The ratio H_{29}/H_{30} shows values of 1.00, 1.11 and 0.96 respectively for samples 1, 2 and 3. The tricyclic diterpenoid detected are C_{20}, C_{21}, C_{22}, C_{23}, C_{24}, and C_{26} (Fig. 5). Results showed that concentrations of C_{23}tricyclic terpanes are significantly high.

Hopanes hydrocarbons observed are 17α(H), 21β(H) and 17β(H), 21α(H) hopane. The C27 hopanes are represented by 17α(H)- and 17β(H)-22, 29, 30-trisnorhopanes with the latter in higher concentration. The 17α(H), 21β(H) hopanes are represented by C_{29} to C_{35} homologues, with the C30 as the biggest peak. Extended hopanes are dominated by the C_{31} homohopane and decreasing towards the C35 homohopane (Fig. 5). The C_{35} Homohopane Index are 0.12 , 0.07 and 0.09 (Table 2). The analysis of the *m/z* 191 mass

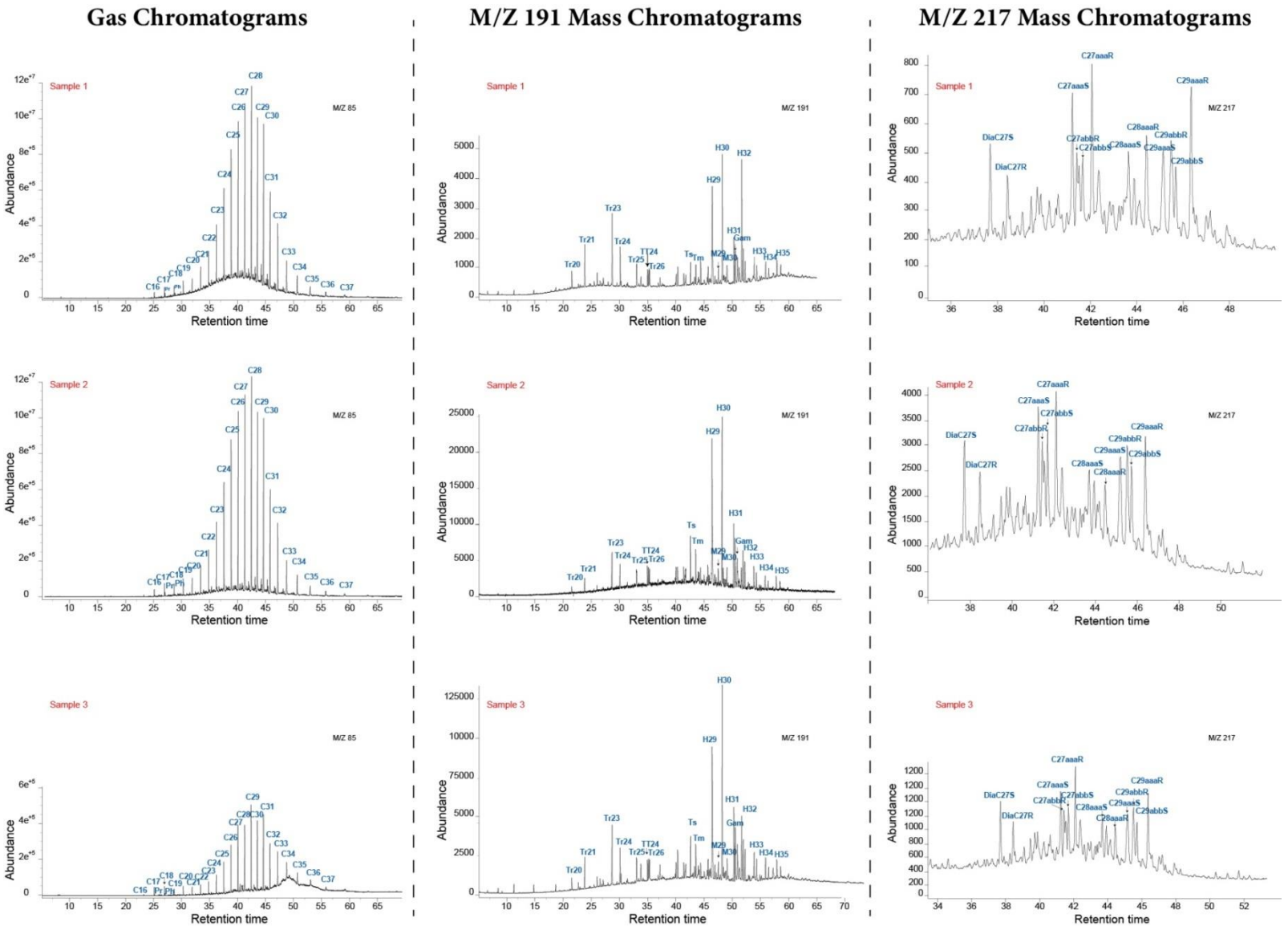

Figure 5: Gas chromatograms and mass chromatogram of the extracted.

fragmentogram also revealed series of pairs of peaks over the C_{31}–C_{35} hopane, which correspond to the 22S and 22R epimers of C31–C35 17α(H), 21β(H) and 17β(H), 21α(H) hopanes. There is a predominance of 22S epimer of both the 17α(H), 21β(H) and 17β(H), 21α(H) hopanes. High content of gammacerane is detected in all samples and Gammacerane index (gammacerane/C30αβ hopane x100) are 25 in sample 1, 22 in sample 2 and 23 in sample 3 (Table 2). Hopane/sterane ratios in the sample are 3.98, 5.11 and 5.3.

Steranes composition are shown in Fig. 5 and peak identification of the compounds is shown in Table 1. From the m/z 217 mass chromatograms (Fig. 5), we noted that the distributions of C_{27}-C_{28}-C_{29} regular steranes for all samples are very similar, generally characterized by C_{27} > C_{29} > C_{28}. The C27/C29 sterane ratio is 0.94 in sample 1, 1.02 in sample 2 and 1.02 in sample 3 (Table 2). Diasterane/sterane ratios (DIA/DIA+REG) show values of 0.13 in sample 1, 0.13 in sample 2 and 0.14 in sample 3 (Table 2). The significance of biomarker parameters will be discussed in the geochemical properties section.

Table 3: Biomarker parameters used in the interpretation.

Biomarker parameters	Sample 1	Sample 2	Sample 3
Alkanes			
Pr/Ph	0,33	0,23	0,17
Pr/C_{17}	0,47	0,29	0,06
C_{17}/(C_{17}+C_{27})	0,04	0,03	0,14
CPI	1,09	1,04	1,12
Ph/C_{18}	1,41	0,67	0,33
C_{17}/C_{18}	0,98	0,54	0,93
R22	0,9	1,05	1,08
Terpanes			
Tric/H30	1,78	0,71	1,08
Ts/Tm	1,04	1,34	1,30
Tetr24/H30	0,11	0,10	0,11
Gam/H30	25	22	23
Tr24/Tr23	0,56	0,67	0,60
H34/H35	1,02	1,16	1,21
H31R/H30	0,31	0,29	0,31
H29/H30	1,00	1,11	0,96

Tetr24/(Tr26+Tetr24)	0,30	0,37	0,37
Tr26/Tr25	0,91	1,17	0,90
Hom Index	0,12	0,07	0,09
Tr23/(Tr23+H30)	0,33	0,14	0,21
Hopane/Sterane	3,98	5,11	5,30
Tr23/H30	0,49	0,17	0,27
Tr25/Tr26	1,10	0,85	1,12
Tr25/Tetr24	2,52	1,48	1,93
Steranes			
%27 aaa R	35,79	39,48	39,60
%28 aaa R	26,12	21,74	21,52
%29 aaa R	38,09	38,79	38,87
C27 Dia/ C27 aaa (R+S)	0,54	0,60	0,61
Dia/(DIA+REG)	0,13	0,13	0,14
S / R (C29 ααα)	0,79	1,09	1,04
S / (S + R) (C29 ααα)	0,44	0,52	0,51
ββ / (αα + ββ) (C29)	0,40	0,46	0,42
C27/C29	0,94	1,02	1,02

5 DEPOSITIONAL ENVIRONMENT

5.1 Sedimentological evidence

Sedimentological features described in the previous section suggest that the Piauí Formation chert facies was deposited in a shallow-water environment that periodically experienced storms events. During fair-weather periods, stromatolites grew by vertical accretion, forming horizontal lamination and centimeter-scale columns, whilst events of high energy, probably storms, caused fragmentation of the stromatolites and generated intraformational breccias.

The ooids would be formed during fair-weather periods, from precipitation of stevensite or similar Mg-silicate under mildly agitation, such as in the Cretaceous Brazilian Pre-salt (Goldberg et. al, 2017; Armelenti et al., 2017; Leite et al, 2020), or in the Eocene Green River Formation of USA (Tettenhorst and Moore, 1978). The common deformation of the ooids suggests dehydration and shrinkage of an original clay composition. In the absence of clear evidence of subaerial exposure, we assume that such dehydration took place in subaqueous environment, occasioned by salinity variations.

The preservation of organic-rich dark laminations in the stromatolites suggests that the environment was characterized by high organic matter productivity and seasonal changes. Gąsiewicz et al., (1987) noted that high salinity may contribute to the preservation of microbial mats. As grazing metazoans are unable to survive in extreme salinity conditions, cyanobacteria flourishes and dominates the ecosystem. Saline-alkaline lakes are the ideal sedimentary environments to allow the association of the described deposits (Andreote et al., 2014; Butturini et al., 2020; Clauer et al., 1998; Jones and Deocampo, 2003; Stenger-Kovács et al., 2014; Yuretich and Cerling, 1983).

5.2 Geochemical evidence

The composition of the *n*-alkane fraction is characterized by a net predominance of even over odd numbers, which is commonly interpreted as typical of hypersaline environments (e.g. de Leeuw et al., 1985; Dembicki et al., 1976; Ten Haven et al., 1985). However, we also noticed high content of odd number long chain *n*-alkanes, which suggests a mixture of higher-plant detritus (Peters et al., 2004). As suggested by ten Haven et al (1985), input of continental derived matt may obliterate the predominance of even numbers. In these cases, the R_{22} index is a better criterion for hypersaline environments. The R_{22} index greater than 1 in samples 2 and 3 suggests predominance of docosane (Table 2), a marker of hypersaline environments (ten Haven et al., 1988; Ten Haven et al., 1985).

Hypersaline condition is additionally supported by the Pristane/Phytane (Pr/Ph) ratio < 0.8 (e.g. Benalioulahj et al., 1994; Giani et al., 1984; Peters et al., 2004), and the ratios of tricyclic terpanes (Huang et al., 2015; Seifert and Michael Moldowan, 1978). The Pr/Ph of ratio the studied samples ranges from 0.17 to 0.33, characteristics of saline environments and deposition under anoxic conditions (Table 2), possibly related to intense methanogenic activity (Didyk et al., 1978; Giani et al., 1984). The cross plot of Pr/*n*-C_{17} versus Ph/*n*-C_{18} show that the extracts analyzed concentrated in the reducing (anoxic) area typical of marine or saline lakes (Fig. 6). Tao et al. (2015) reported that C_{24}TeT/(C_{24}TeT + C_{26}TT) values > 5 suggest terrigenous/freshwater lacustrine environments and < 5 suggest saline lacustrine environments. The samples collected are

characterized by C_{24}TeT/(C_{24}TeT + C_{26}TT) values that range from 0.32 to 0.37, indicative of saline lacustrine environment. The cross plots of C_{24}TeT/(C_{24}TeT + C_{26}TT) versus C_{23}TT/ (C_{23}TT + C_{30}H) have been successfully used for source rock in Tarim Basin, China (Hanson et al. 2000; Tao et al. 2015), and clearly show concentration of samples in the field of saline lacustrine environment (Fig. 6).

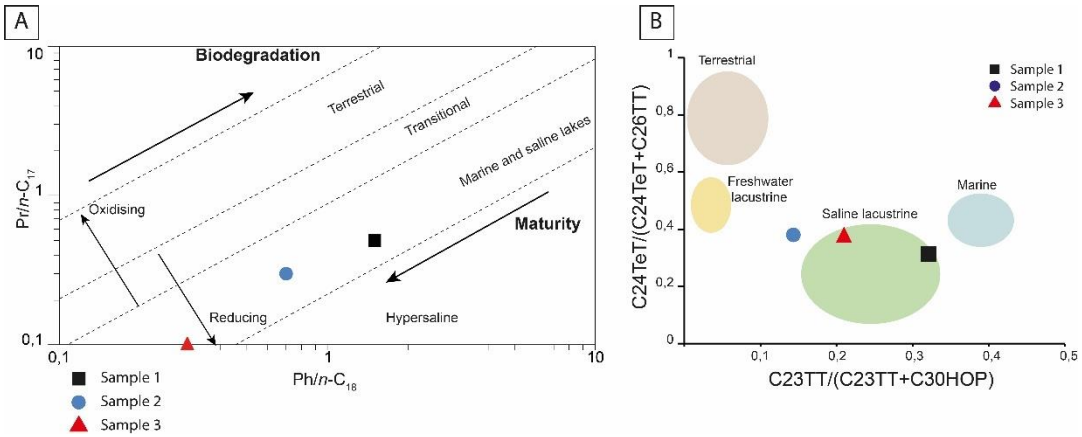

Figure 6: (A) cross plot of Pr/*n*-C_{17} versus Ph/*n*-C_{18}. (B) cross plots of C24TeT/(C24TeT + C26TT) versus C23TT/ (C23TT + C30H)

The most ubiquitous indicator in saline environment is the gammacerane, a major biomarker in many arid or semi-arid setting (Peters et al., 2004). The *m/z* 191 fragmentograms of all samples are characterized by gammacerane peak (Fig. 5) and high gammacerane index (Table 2), which indicates a stratified water column, commonly resulting from hypersaline conditions during deposition of the organic matter (Jiamo et al., 1990, 1988; Moldowan et al., 1985; Peters et al., 2004; Sinninghe Damsté et al., 1995). While saline environments are usually characterized by absent or extremely low abundance of diasteranes (Jiamo et al., 1990; Mello et al., 1988; Wang and Fu, 1997), the presence of diasterane in all our samples suggest high amounts of clay minerals resulting from terrigenous input (Mello et al., 1988; van Kaam-Peters et al., 1998). This interpretation corroborate with sedimentological evidences which suggested that clay ooids formation required clay-rich conditions in water composition.

The characterization of depositional environment was realized through differentiation of terrigenous, lacustrine and marine input. A common *n*-alkane

ratio used in identification of depositional environment is the carbon preference index (CPI), which compare the nC_{25}–nC_{35} odd carbon numbers with nC_{24}–nC_{34} even numbers. The low CPI values (~ l) observed in our extracted rule out the possibility of terrigenous input; typically >3 (Peters et al., 2004). Such low CPI values may indicate marine/lacustrine environment or extensive diagenetic alteration, related to microbial reworking (Meyers, 1993). The distinction of lacustrine and marine systems is more complex because few geochemical indicators are distinctive of lacustrine environments. Among the most common indicators, hopane/sterane, C_{31}/C_{30} and C_{34}/C_{35} have been successfully used to identify lacustrine environments (Mello et al., 1988). High values of hopane/sterane (>1), C_{34}/C_{35} (>1) and C_{31}/C_{30} (>0.30) observed in this study (Table 2) are suggestive of lacustrine environments rather than marine settings (Mello et al., 1988).

The *n*-alkane distribution is also useful to identify microorganism responsible for mat productivity. The extracted studied herein were plotted in the triangular sterane diagram (Huang and Meinschein, 1978; Hunt, 1995), and all sample are grouped in the planktonic field with bacterial and land plant contributions (Fig. 7). The predominance of even numbered *n*-alkanes is indicative of organic matter originated from cyanobacterial remains in high temperature settings (Bubela et al., 1984; Dembicki et al., 1976; Peters et al., 2004). The presence of long chain C_{25} (squalane) isoprenoid indicate halophilic cyanobacteria (Mello et al., 1988; ten Haven et al., 1988; Wang and Fu, 1997). According to de Rosa et al (1982), the abundance of C_{25} isoprenoid is a specific indicator of halophilic alkaliphilic bacteria, hence the presence of C_{25} isoprenoid not only suggest high salinity, but also high pH (alkalinity). There is also a positive correlation between gammacerane and alkaline hypersaline environments rather than sulfate or acidic hypersaline environments (Wang and Fu, 1997).

In conclusion, the distribution and compositions of alkanes, terpanes and steranes in the extracts supports the idea that cyanobacteria were the most important contributor to the Piauí microbialite deposit. Geochemical evidences suggest predominance of planktonic (bacterial) organic matter while terrigenous

input (plant debris) quantitatively contributed only a small proportion in the depositional environment. The depositional environment was characterized by high salinity and anoxic conditions typically favorable for flourishment of cyanobacteria ecosystem (Brehm et al., 2002; Gasiewicz et al., 1987). This is in agreement with results from sedimentological analysis, which defined the environment as saline-alkaline lake.

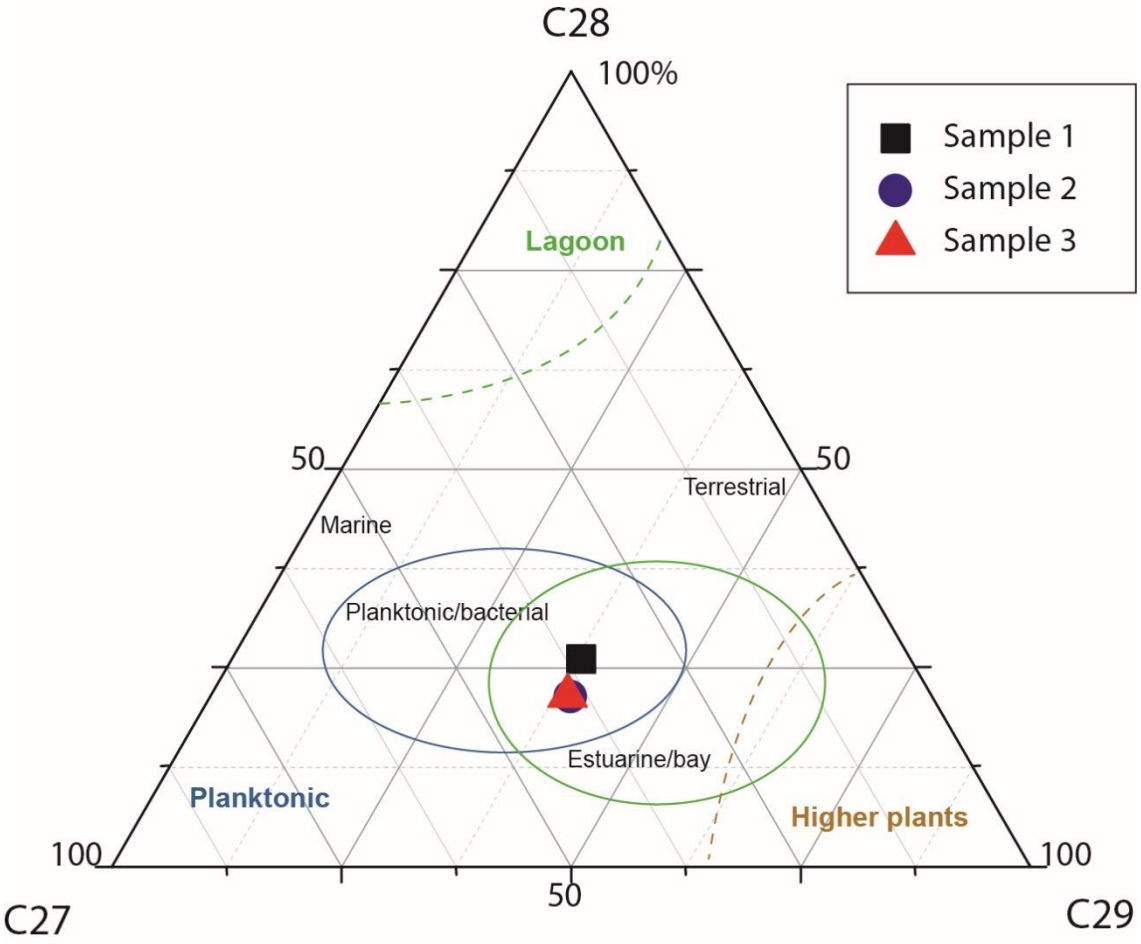

Figure 7: Ternary plots of C27–C28–C29 for Piauí Formation.

6 PALAEOENVIRONMENTAL RECONSTRUCTION

The Piauí Formation was deposited during the Pennsylvanian, a period characterized by major climatic and tectonic changes caused by the assembly of the supercontinent Pangea (Golonka and Ford, 2000). During this time, the Gondwana progressively moved northward and the Parnaíba Basin was placed in mid-latitudes (between 30° and 40°). As result of these changes, the Pangean hinterland experienced an increasing continentalization, which lead to

the well-known Permian-Triassic aridification (Benison et al., 1998; Scotese et al., 1999; Zharkov and Chumakov, 2001). In their reconstruction of the paleogeographic evolution of the Parnaíba Basin from the Permian to the Jurassic, Abrantes et al., (2019) observed that the Pedra de Fogo Formation

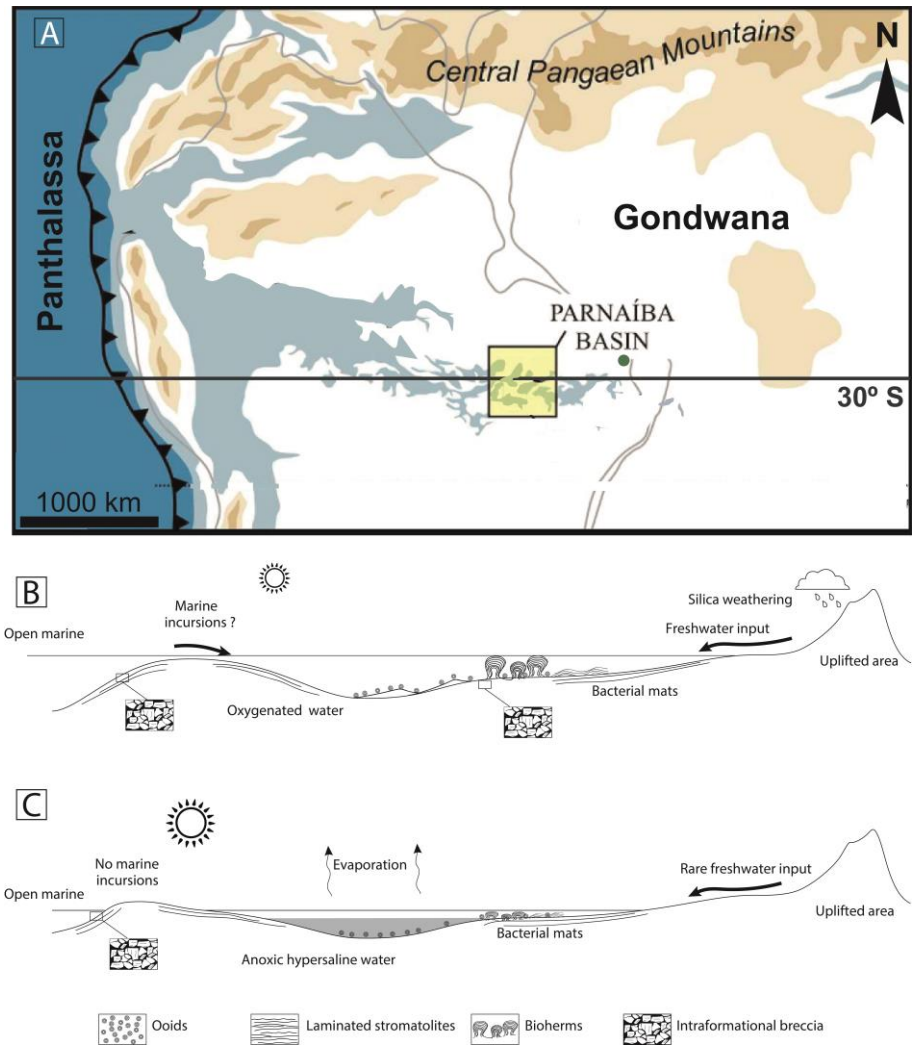

Figure 8: (A) Palaeoenvironmental reconstruction of west-central Pangaea modified from Abrantes et al., 2019. (B) Depositional model of Piauí Formation saline lake during wet periods. (C) Depositional model of Piauí Formation saline lake during dry periods.

was deposited in extensive, ephemeral, evaporitic lakes surrounded by dune fields. The authors suggest that that the Pedra de Fogo lakes probably represent remnant of a Pennsylvanian epeiric sea from the progressive withdrawal of the Panthalassa Ocean (Fig. 8) (Ford and Golonka, 2003; Zharkov and Chumakov, 2001). In this sense, the Piauí Formation saline-

alkaline lake most likely represents epeiric conditions precursor of the Pedra de Fogo evaporitic lake, characterized by endorheic drainage, as suggested by high salinity and pH, associated to the continuous retraction of epicontinental sea. The volume of dissolved Si, and Mg cation required for the formation of stevensite ooids and the intense silicification may have been sourced from the uplift of Central Pangean Mountain chain caused by the collision of Gondwana and Laurasia (Gibbs et al., 2002; Golonka and Ford, 2000; Tabor et al., 2008; Ziegler et al., 1979). The palaeogeographic location of the Parnaíba Basin during the Pennsylvanian period was approximately 20° S, and the intense continentalization would favor this setting (Abrantes et al., 2016; Góes and Feijó, 1994; Jaju et al., 2018; Vaz et al., 2007; Zharkov and Chumakov, 2001). While the high latitudes of Pangea were covered with ice caps, the mid-latitudes areas experienced intense aridification, evidenced both by the biomarkers and the sedimentological features presented herein, and by the deposition of an extensive eolian succession overlying the chert deposits (Lima Filho, 1991). The terrigenous input would be supplied during wet periods, with increased runoff in the continental areas and resulted in the formation of light, organic-poor stromatolite laminations (Fig. 8). Conversely, during dry periods, increased salinity and pH reaches would favor the flourishment of cyanobacteria and preservation of organic-rich stromatolite laminations (Fig. 8).

7 CONCLUSIONS

The analysis of biomarker and sedimentological features in combination with paleogeographic information allowed a reconstruction of conditions of deposition of the silicified microbialites, ooidal arenites and breccias of the Piauí Formation. The integration of petrographic, sedimentologic and geochemical evidence revealed the existence of saline alkaline lacustrine environments in mid-latitude areas of Gondwana. The arid conditions contributed to the formation of microbial deposits in lacustrine saline shallow-water environments that frequently experienced storms events. Geochemical features allowed identification of productivity from cyanobacteria in saline to hypersaline anoxic conditions. Intraformational breccias associated with the stromatolites are probably a product of their episodic fragmentation by the action of storms. The associated silicified ooidal arenites were probably originally constituted by Mg-

clays, such as stevensite, as indicated by their deformation, pervasive silicification or dissolution, and by the common occurrence or early diagenetic dolomite. The paleoenvironmental reconstruction indicate that during the Pennsylvanian tectonic, climatic and geographic conditions promoted the development of saline-alkaline lacustrine systems favorable for the flourishment of cyanobateria and deposition of Mg-silicate ooids.

8 AKNOWLEDGMENTS

This paper is part of the PhD thesis funded by Petrobras S.A executed in partnership with the Federal University of Rio Grande do Sul. The first authors thank IAS for postgraduate research grant. Authors thank Raimundo Nonato for accomodation at Amarante and the local guide Rommulo for the assistance and friendship during fieldwork.

9 REFERENCES

Abrantes, F.R., Nogueira, A.C.R., Andrade, L.S., Bandeira, J., Soares, J.L., Medeiros, R.S.P., 2019. Register of increasing continentalization and palaeoenvironmental changes in the west-central pangaea during the Permian-Triassic, Parnaíba Basin, Northern Brazil. J. South Am. Earth Sci. 93, 294–312. https://doi.org/10.1016/j.jsames.2019.05.006

Abrantes, F.R., Nogueira, A.C.R., Soares, J.L., 2016. Permian paleogeography of west-central Pangea: Reconstruction using sabkha-type gypsum-bearing deposits of Parnaíba Basin, Northern Brazil. Sediment. Geol. 341, 175–188. https://doi.org/10.1016/j.sedgeo.2016.06.004

Andreote, A.P.D., Vaz, M.G.M.V., Genuário, D.B., Barbiero, L., Rezende-Filho, A.T., Fiore, M.F., 2014. Nonheterocytous cyanobacteria from Brazilian saline-alkaline lakes. J. Phycol. 50, 675–684. https://doi.org/10.1111/jpy.12192

Armelenti, G., Goldberg, K., Kuchle, J., De Ros, L.F., 2016. Deposition, diagenesis and reservoir potential of non-carbonate sedimentary rocks from the rift section of Campos Basin, Brazil. Pet. Geosci. 22, 223–239. https://doi.org/10.1144/petgeo2015-035

Awramik, S.M., 1991. Archaean and Proterozoic Stromatolites, in: Calcareous Algae and Stromatolites. Springer Berlin Heidelberg, Berlin, Heidelberg, pp.

289–304. https://doi.org/10.1007/978-3-642-52335-9_15

Becker, L., Glavin, D.P., Bada, J.L., 1997. Polycyclic aromatic hydrocarbons (PAHs) in Antarctic Martian meteorites, carbonaceous chondrites, and polar ice. Geochim. Cosmochim. Acta 61, 475–481. https://doi.org/10.1016/S0016-7037(96)00400-0

Benalioulhaj, S., Schreiber, B.C., Philp, R.P., 1994. RELATIONSHIP OF ORGANIC GEOCHEMISTRY TO SEDIMENTATION UNDER HIGHLY VARIABLE ENVIRONMENTS, LORCA BASIN, SPAIN: PRELIMINARY RESULTS, in: Sedimentology and Geochemistry of Modern and Ancient Saline Lakes. SEPM (Society for Sedimentary Geology), pp. 315–324. https://doi.org/10.2110/pec.94.50.0315

Benison, K.C., Goldstein, R.H., Wopenka, B., Burruss, R.C., Pasteris, J.D., 1998. Extremely acid Permian lakes and ground waters in North America. Nature 392, 911–914. https://doi.org/10.1038/31917

Brehm, U., Gasiewicz, A., Gerdes, G., Krumbein, W., 2002. Biolaminoid facies in a peritidal sabkha: Permian Platy Dolomite of northern Poland. Int. J. Earth Sci. 91, 260–271. https://doi.org/10.1007/s005310100207

Bubela, B., Philp, P., Gilbert, T., 1984. Effect of microbial activity on buried cyanobacterial organic matter. Geomicrobiol. J. 3, 231–244. https://doi.org/10.1080/01490458409377800

Butturini, A., Herzsprung, P., Lechtenfeld, O.J., Venturi, S., Amalfitano, S., Vazquez, E., Pacini, N., Harper, D.M., Tassi, F., Fazi, S., 2020. Dissolved organic matter in a tropical saline-alkaline lake of the East African Rift Valley. Water Res. 173, 115532. https://doi.org/10.1016/j.watres.2020.115532

Caputo, M.V., 1984. Stratigraphy, tectonics, paleoclimatology and paleogeography of northern basins of Brazil.

Cisneros, J.C., Marsicano, C., Angielczyk, K.D., Smith, R.M.H., Richter, M., Fröbisch, J., Kammerer, C.F., Sadleir, R.W., 2015. New Permian fauna from tropical Gondwana. Nat. Commun. 6, 8676. https://doi.org/10.1038/ncomms9676

Clauer, N., Zuppi, G.M., Blanc, G., Toulkeridis, T., Gasse, F., 1998. Compositions chimiques et isotopiques d’eaux de la mer Caspienne et de

tributaires de la région de Makachkala (Russie): premières données sur le fonctionnement d'un système endoréïque particulier. Comptes Rendus l'Académie des Sci. - Ser. IIA - Earth Planet. Sci. 327, 17–24. https://doi.org/10.1016/S1251-8050(98)80013-X

Daly, M.C., Andrade, V., Barousse, C.A., Costa, R., McDowell, K., Piggott, N., Poole, A.J., 2014. Brasiliano crustal structure and the tectonic setting of the Parnaíba basin of NE Brazil: Results of a deep seismic reflection profile. Tectonics 33, 2102–2120. https://doi.org/10.1002/2014TC003632

de Leeuw, J.W., Damsté, J.S.S., Klok, J., Schenck, P.A., Boon, J.J., 1985. Biogeochemistry of Gavish Sabkha Sediments. pp. 350–367. https://doi.org/10.1007/978-3-642-70290-7_20

De Rosa, M., Gambacorta, A., Nicolaus, B., Ross, H.N.M., Grant, W.D., Bu'Lock, J.D., 1982. An Asymmetric Archaebacterial Diether Lipid from Alkaliphilic Halophiles. Microbiology 128, 343–348. https://doi.org/10.1099/00221287-128-2-343

Dembicki, H., Meinschein, W.., Hattin, D.E., 1976. Possible ecological and environmental significance of the predominance of even-carbon number C20-C30n-alkanes. Geochim. Cosmochim. Acta 40, 203–208. https://doi.org/10.1016/0016-7037(76)90177-0

Didyk, B.M., Simoneit, B.R.T., Brassell, S.C., Eglinton, G., 1978. Organic geochemical indicators of palaeoenvironmental conditions of sedimentation. Nature 272, 216–222. https://doi.org/10.1038/272216a0

Faria, L.E. do C., 1979. Estudo sedimentológico da formação Pedra de Fogo-Permiano: Bacia do Maranhão.

Ford, D., Golonka, J., 2003. Phanerozoic paleogeography, paleoenvironment and lithofacies maps of the circum-Atlantic margins. Mar. Pet. Geol. 20, 249–285. https://doi.org/10.1016/S0264-8172(03)00041-2

Gasiewicz, A., Gerdes, G., Krumbein, W.E., 1987. The peritidal sabkha type stromatolites of the platy dolomite (Ca3) of the Leba Elevation (north Poland), in: The Zechstein Facies in Europe. Springer-Verlag, Berlin/Heidelberg, pp. 253–272. https://doi.org/10.1007/BFb0011382

Giani, D., Giani, L., Cohen, Y., Krumbein, W.E., 1984. Methanogenesis in the hypersaline Solar Lake (Sinai). FEMS Microbiol. Lett. 25, 219–224.

Gibbs, M.T., Rees, P.M., Kutzbach, J.E., Ziegler, A.M., Behling, P.J., Rowley, D.B., 2002. Simulations of Permian Climate and Comparisons with Climate-Sensitive Sediments. J. Geol. 110, 33–55. https://doi.org/10.1086/324204

Góes, A.M.O., Feijó, F.J., 1994. Bacia do Parnaíba. Bol. Geociências da Petrobrás 57–67.

Goldberg, K., Kuchle, J., Scherer, C., Alvarenga, R., Ene, P. L., Armelenti, G., & De Ros, L. F. (2017). Re-sedimented deposits in the rift section of the Campos Basin. Marine and Petroleum Geology, 80, 412-431.

Golonka, J., Ford, D., 2000. Pangean (Late Carboniferous–Middle Jurassic) paleoenvironment and lithofacies. Palaeogeogr. Palaeoclimatol. Palaeoecol. 161, 1–34. https://doi.org/10.1016/S0031-0182(00)00115-2

Grotzinger, J.P., 1989. FACIES AND EVOLUTION OF PRECAMBRIAN CARBONATE DEPOSITIONAL SYSTEMS: EMERGENCE OF THE MODERN PLATFORM ARCHETYPE, in: Controls on Carbonate Platforms and Basin Development. SEPM (Society for Sedimentary Geology), pp. 79–106. https://doi.org/10.2110/pec.89.44.0079

Grotzinger, J.P., Knoll, A.H., 1999. STROMATOLITES IN PRECAMBRIAN CARBONATES: Evolutionary Mileposts or Environmental Dipsticks? Annu. Rev. Earth Planet. Sci. 27, 313–358. https://doi.org/10.1146/annurev.earth.27.1.313

Hammer, U.T., 1986. Saline lake ecosystems of the world. Springer Science & Business Media.

Harwood, C.L., Sumner, D.Y., 2011. Microbialites of the Neoproterozoic Beck Spring Dolomite, Southern California. Sedimentology 58, 1648–1673. https://doi.org/10.1111/j.1365-3091.2011.01228.x

Herlinger Jr., R., Zambonato, E.E. & De Ros, L.F., 2017. Influence of diagenesis on the quality of Lower Cretaceous Pre-Salt lacustrine carbonate reservoirs from northern Campos Basin, offshore Brazil. Journal of Sedimentary Research, v. 87(12), p. 1285-1313. DOI: http://dx.doi.org/10.2110/jsr.2017.70

Hofmann, H.J., 1973. Stromatolites: Characteristics and utility. Earth-Science Rev. 9, 339–373. https://doi.org/10.1016/0012-8252(73)90002-0

Huang, H., Zhang, S., Su, J., 2015. Geochemistry of Tri- and Tetracyclic

Terpanes in the Palaeozoic Oils from the Tarim Basin, Northwest China. Energy & Fuels 29, 7014–7025. https://doi.org/10.1021/acs.energyfuels.5b01613

Huang, W.-Y., Meinschein, W.G., 1978. Sterols in sediments from Baffin Bay, Texas. Geochim. Cosmochim. Acta 42, 1391–1396. https://doi.org/10.1016/0016-7037(78)90044-3

Hunt, J.M., 1995. Petroleum geochemistry and geology.

Iannuzzi, R., Neregato, R., Cisneros, J.C., Angielczyk, K.D., Rößler, R., Rohn, R., Marsicano, C., Fröbisch, J., Fairchild, T., Smith, R.M.H., Kurzawe, F., Richter, M., Langer, M.C., Tavares, T.M. V., Kammerer, C.F., Conceição, D.M., Pardo, J.D., Roesler, G.A., 2018. Re-evaluation of the Permian macrofossils from the Parnaíba Basin: biostratigraphic, palaeoenvironmental and palaeogeographical implications. Geol. Soc. London, Spec. Publ. 472, 223–249. https://doi.org/10.1144/SP472.14

Jaju, M.M., Mort, H.P., Nader, F.H., Mário Filho, L., Macdonald, D.I.M., 2018. Palaeogeographical and palaeoclimatic evolution of the intracratonic Parnaíba Basin, NE Brazil using GPlates plate tectonic reconstructions and chemostratigraphic tools. Geol. Soc. London, Spec. Publ. 472, 199–222.

Jiamo, F., Guoying, S., Dehan, L., 1988. Organic geochemical characteristics of major types of terrestrial petroleum source rocks in China. Geol. Soc. London, Spec. Publ. 40, 279–289. https://doi.org/10.1144/GSL.SP.1988.040.01.22

Jiamo, F., Guoying, S., Jiayou, X., Eglinton, G., Gowar, A.P., Rongfen, J., Shanfa, F., Pingan, P., 1990. Application of biological markers in the assessment of paleoenvironments of Chinese non-marine sediments. Org. Geochem. 16, 769–779. https://doi.org/10.1016/0146-6380(90)90116-H

Jones, B.F., Deocampo, D.M., 2003. Geochemistry of Saline Lakes, in: Treatise on Geochemistry. Elsevier, pp. 393–424. https://doi.org/10.1016/B0-08-043751-6/05083-0

Kah, L.C., Bartley, J.K., Frank, T.D., Lyons, T.W., 2006. Reconstructing sea-level change from the internal architecture of stromatolite reefs: an example from the Mesoproterozoic Sulky Formation, Dismal Lakes Group, arctic Canada. Can. J. Earth Sci. 43, 653–669. https://doi.org/10.1139/e06-013

Leite, C.O.N., Silva, C.M.A. & De Ros, L.F., 2020. Depositional and diagenetic processes in the Pre-salt rift section of a Santos Basin Area, SE Brazil. Journal of Sedimentary Research, v. 90, p. 584–608. http://dx.doi.org/10.2110/jsr.2020.27

Lima Filho, F.P., 1999. A seqüência permo-pensilvaniana da Bacia do Parnaíba. Universidade de São Paulo, São Paulo. https://doi.org/10.11606/T.44.1999.tde-11112015-164411

Lima Filho, F.P., 1991. Fácies e ambientes deposicionais da Formação Piauí (Pensilvaniano), Bacia do Parnaíba. Universidade de São Paulo, São Paulo. https://doi.org/10.11606/D.44.1991.tde-25092015-155651

Lima, M.A.E., Leite, F.J., 1978. Estudo global dos recursos minerais da Bacia Sedimentar do Parnaíba, Companhia de Pesquisa de Recursos Minerais: Superintendência Regional de Recife.

López-Archilla, A.I., Moreira, D., López-García, P., Guerrero, C., 2004. Phytoplankton diversity and cyanobacterial dominance in a hypereutrophic shallow lake with biologically produced alkaline pH. Extremophiles 8, 109–115. https://doi.org/10.1007/s00792-003-0369-9

López-Cortés, A., García-Pichel, F., Nübel, U., Vázquez-Juárez, R., 2001. Cyanobacterial diversity in extreme environments in Baja California, Mexico: a polyphasic study. Int. Microbiol. 4, 227–236. https://doi.org/10.1007/s10123-001-0042-z

Maliński, E., Gąsiewicz, A., Witkowski, A., Szafranek, J., Pihlaja, K., Oksman, P., Wiinamäki, K., 2009. Biomarker features of sabkha-associated microbialites from the Zechstein Platy Dolomite (Upper Permian) of northern Poland. Palaeogeogr. Palaeoclimatol. Palaeoecol. 273, 92–101. https://doi.org/10.1016/j.palaeo.2008.12.005

McKirdy, D.M., 1976. Biochemical Markers in Stromatolites, in: Stromatolites. pp. 163–191. https://doi.org/10.1016/S0070-4571(08)71136-1

Mello, M.R., Gaglianone, P.C., Brassell, S.C., Maxwell, J.R., 1988. Geochemical and biological marker assessment of depositional environments using Brazilian offshore oils. Mar. Pet. Geol. 5, 205–223. https://doi.org/10.1016/0264-8172(88)90002-5

Mesner, J.C., Wooldridge, L.C.P., 1964. Maranhao Paleozoic Basin and

Cretaceous Coastal Basins, North Brazil. Am. Assoc. Pet. Geol. Bull. 48. https://doi.org/10.1306/BC743D99-16BE-11D7-8645000102C1865D

Meyers, P.A., 1993. Origin of the Plio-Pleistocene Vrica laminites: Organic geochemical evidence. Mar. Geol. 115, 117–127. https://doi.org/10.1016/0025-3227(93)90077-9

Milani, E., Filho, A., 2000. Sedimentary basins of South America, in: Tectonic Evolution of South America.

Moldowan, J.M., Seifert, W.K., Gallegos, E.J., 1985. Relationship Between Petroleum Composition and Depositional Environment of Petroleum Source Rocks1. Am. Assoc. Pet. Geol. Bull. 69, 1255–1268. https://doi.org/10.1306/AD462BC8-16F7-11D7-8645000102C1865D

Oduor, S.O., Schagerl, M., 2007. Phytoplankton primary productivity characteristics in response to photosynthetically active radiation in three Kenyan Rift Valley saline alkaline lakes. J. Plankton Res. 29, 1041–1050. https://doi.org/10.1093/plankt/fbm078

Peters, K.E., Walters, C.C., Moldowan, J.M., 2004. The Biomarker Guide. Cambridge University Press. https://doi.org/10.1017/CBO9780511524868

Plummer, F.D., 1946. Report on Maranhão and Piauí geosyncline. Rio de Janeiro.

Preiss, W. V., 1976. Basic Field and Laboratory Methods for the Study of Stromatolites, in: Developments in Sedimentology. pp. 5–13. https://doi.org/10.1016/S0070-4571(08)71124-5

Riding, R., 2011. Microbialites, stromatolites, and thrombolites. Encycl. Earth Sci. Ser. 635–654. https://doi.org/10.1007/978-1-4020-9212-1_196

Rodríguez Tribaldos, V., White, N., 2018. Implications of preliminary subsidence analyses for the Parnaíba cratonic basin. Geol. Soc. London, Spec. Publ. 472, 147–156. https://doi.org/10.1144/SP472.3

Santos, M.C.M., Carvalho, M.S.S., 2004. Paleontologia das bacias do Parnaíba, São Luís e Grajaú. Reconstituições paleobiológicas. CPRM, Rio Janeiro 1, 212.

Scotese, C.R., Boucot, A.J., McKerrow, W.S., 1999. Gondwanan palaeogeography and pal1oclimatology. J. African Earth Sci. 28, 99–114. https://doi.org/10.1016/S0899-5362(98)00084-0

Seifert, W.K., Michael Moldowan, J., 1978. Applications of steranes, terpanes and monoaromatics to the maturation, migration and source of crude oils. Geochim. Cosmochim. Acta 42, 77–95. https://doi.org/10.1016/0016-7037(78)90219-3

Sinninghe Damsté, J.S., Kenig, F., Koopmans, M.P., Köster, J., Schouten, S., Hayes, J.M., de Leeuw, J.W., 1995. Evidence for gammacerane as an indicator of water column stratification. Geochim. Cosmochim. Acta 59, 1895–1900. https://doi.org/10.1016/0016-7037(95)00073-9

Small, H.L., 1914. Geologia e suprimento d'água subterrânea no Piauí e parte do Ceará, Brasil. Instituto e Obras Contra Secas, Série ID. Publicação.

Stenger-Kovács, C., Lengyel, E., Buczkó, K., Tóth, F., Crossetti, L., Pellinger, A., Zámbóné Doma, Z., Padisák, J., 2014. Vanishing world: alkaline, saline lakes in Central Europe and their diatom assemblages. Inl. Waters 4, 383–396. https://doi.org/10.5268/IW-4.4.722

Tabor, N.J., Montañez, I.P., Scotese, C.R., Poulsen, C.J., Mack, G.H., 2008. Paleosol archives of environmental and climatic history in paleotropical western Pangea during the latest Pennsylvanian through Early Permian, in: Special Paper 441: Resolving the Late Paleozoic Ice Age in Time and Space. Geological Society of America, pp. 291–303. https://doi.org/10.1130/2008.2441(20)

Ten Haven, H.L., De Leeuw, J.W., Schenck, P.A., 1985. Organic geochemical studies of a Messinian evaporitic basin, northern Apennines (Italy) I: Hydrocarbon biological markers for a hypersaline environment. Geochim. Cosmochim. Acta 49, 2181–2191. https://doi.org/10.1016/0016-7037(85)90075-4

ten Haven, H.L., de Leeuw, J.W., Sinninghe Damsté, J.S., Schenck, P.A., Palmer, S.E., Zumberge, J.E., 1988. Application of biological markers in the recognition of palaeohypersaline environments. Geol. Soc. London, Spec. Publ. 40, 123–130. https://doi.org/10.1144/GSL.SP.1988.040.01.11

Tettenhorst, R., Moore, G.E., 1978. Stevensite Oolites from the Green River Formation of Central Utah. SEPM J. Sediment. Res. Vol. 48. https://doi.org/10.1306/212F74DC-2B24-11D7-8648000102C1865D

Tosca, N.J., Wright, V.P., 2015. Diagenetic pathways linked to labile Mg-clays

in lacustrine carbonate reservoirs: a model for the origin of secondary porosity in the Cretaceous pre-salt Barra Velha Formation, offshore Brazil. Geol. Soc. London, Spec. Publ. 435, 33–46. https://doi.org/10.1144/SP435.1

van Kaam-Peters, H.M.., Köster, J., van der Gaast, S.J., Dekker, M., de Leeuw, J.W., Sinninghe Damsté, J.S., 1998. The effect of clay minerals on diasterane/sterane ratios. Geochim. Cosmochim. Acta 62, 2923–2929. https://doi.org/10.1016/S0016-7037(98)00191-4

Vaz, P.T., Resende, N.G.A.M., Wanderley Filho, J.R., Travassos, W.A., 2007. Bacia do Parnaíba. Bol. Geociências da Petrobrás 253–263.

Ventosa, A., Arahal, D.R., 2009. Physico-chemical characteristics of hypersaline environments and their biodiversity. Extremophiles 2, 247–262.

Vieira, L.V., Scherer, C.M. dos S., 2017. Facies architecture and high resolution sequence stratigraphy of an aeolian, fluvial and shallow marine system in the Pennsylvanian Piauí Formation, Parnaíba Basin, Brazil. J. South Am. Earth Sci. 76, 238–256. https://doi.org/10.1016/j.jsames.2017.03.009

Walter, M.R., 1977. Interpreting Stromatolites: These fossils can tell us much about past organisms and environments if we can learn to decode their message. Am. Sci. 65, 563–571.

Wang, R., Fu, J., 1997. Variability in biomarkers of different saline basins in China. Int. J. Salt Lake Res. 6, 25–53. https://doi.org/10.1007/BF02441867

Yuretich, R.F., Cerling, T.E., 1983. Hydrogeochemistry of Lake Turkana, Kenya: Mass balance and mineral reactions in an alkaline lake. Geochim. Cosmochim. Acta 47, 1099–1109. https://doi.org/10.1016/0016-7037(83)90240-5

Zalan, P.V., 1991. Influence of Pre-Andean Orogenies on the Paleozoic Intracratonic Basins of South America, in: 4th Simposio Bolivariano - Exploracion Petrolera En Las Cuencas Subandinas. European Association of Geoscientists & Engineers. https://doi.org/10.3997/2214-4609-pdb.115.008eng

Zharkov, M.A., Chumakov, N.M., 2001. Paleogeography and sedimentation settings during Permian–Triassic reorganizations in biosphere. Stratigr. Geol. Correl. 9, 340–363.

Ziegler, A.M., Scotese, C.R., McKerrow, W.S., Johnson, M.E., Bambach, R.K., 1979. Paleozoic Paleogeography. Annu. Rev. Earth Planet. Sci. 7, 473–502. https://doi.org/10.1146/annurev.ea.07.050179.002353

9.3 ARTIGO 3

This is an automated message.

Late Pennsylvanian aridification in Gondwana mid-latitudes contemporaneous to high-latitudes ice cap expansion. Upper Piauí Formation. Brazil

Dear Mr Kifumbi,

We have received the above referenced manuscript you submitted to Journal of South American Earth Sciences.

To track the status of your manuscript, please log in as an author at https://www.editorialmanager.com/sames/, and navigate to the "Submissions Being Processed" folder.

Thank you for submitting your work to this journal.

Kind regards,

Journal of South American Earth Sciences

More information and support

You will find information relevant for you as an author on Elsevier’s Author Hub: https://www.elsevier.com/authors

FAQ: How can I reset a forgotten password?

https://service.elsevier.com/app/answers/detail/a_id/28452/supporthub/publishing/

For further assistance, please visit our customer service site: https://service.elsevier.com/app/home/supporthub/publishing/

Here you can search for solutions on a range of topics, find answers to frequently asked questions, and learn more about Editorial Manager via interactive tutorials. You can also talk 24/7 to our customer support team by phone and 24/7 by live chat and email

#AU_SAMES#

To ensure this email reaches the intended recipient, please do not delete the above code

---

In compliance with data protection regulations, you may request that we remove your personal registration details at any time. (Use the following URL: https://www.editorialmanager.com/sames/login.asp?a=r). Please contact the publication office if you have any questions.

Late Pennsylvanian aridification in Gondwana mid-latitudes contemporaneous to high-latitudes ice cap expansion. Upper Piauí Formation. Brazil

Carrel Kifumbi[1], Claiton Marlon dos Santos Scherer[1], Ezequiel Galvão de Souza[2], Adriano Domingos dos Reis[1], João Pedro Formolo Ferronatto[1], Rossano Dalla Lana Michel[1]

[1]Programa de Pós-Graduação em Geociências, Universidade Federal do Rio Grande do Sul, P.O. Box 15001, CEP 91501-970 Porto Alegre, RS, Brazil

[2] Universidade Federal do PAMPA, CEP 96570-000 Caçapava do Sul, RS, Brazil

Corresponding author: carrelkif@yahoo.fr

Key words: Late Pennsylvanian aridification, Piauí Formation, Parnaíba Basin, Pennsylvanian reconstruction

ABSTRACT

The Pennsylvanian age was marked by a well-known glaciation period documented in several basins on Gondwana. However, stratigraphic data from the Parnaíba Basin suggest that mid-paleolatitudes was dominated by drier climate conditions simultaneously to the glaciation. To investigate the possible time equivalence and the causes of aridification in mid-paleolatitudes, high-resolution stratigraphic analysis of the upper Piauí Formation has been conducted in the eastern margin of the Parnaíba Basin. As a result three stratigraphic intervals separated by key stratigraphic surfaces have been identified: The first stratriraghic interval is dominantly composed of fluvial deposits progressively overlain by aeolian facies; the second stratigraphic unit is essentially composed of lacustrine deposits and represent a period of lake expansion and regional flooding; finally, the third stratigraphic unit is characterized by three aeolian genetic units and depicts cyclic expansion and contraction of a dune field. The overall vertical stratigraphic succession represents a progressive change from original fluvial sedimentation to essentially aeolian accumulation and constitutes a drying upward trend that

reflects an increasing aridification in the Parnaíba Basin during the late Pennsylvanian age. A detailed analysis of the paleoclimatic conditions and the atmospheric circulation evidenced that waning and waxing of the high-latitudes ice sheets was the main responsible for the development, expansion and contraction of the upper Piauí Formation dune-field.

1 INTRODUCTION

The late Paleozoic stratigraphy of Gondwana basins records a well-known long-term transition from icehouse to extreme greenhouse conditions (Limarino et al, 2014). This long-term climate change encompasses the late Devonian (Frasnian) icehouse period that progressively shifted to drier conditions and culminated with semi-arid to arid climate in late Permian (Loopingian) (Díaz-Martínez et al., 1993; Caputo et al., 2008; Grader et al., 2008; Isaacson et al., 2008, Limarino et al., 2014). Although the Gondwana glaciation was initially thought to have occurred over an uninterrupted interval of time from the Carboniferous to early Permian (Frakes et al., 1992), subsequent studies identified up to three glacial episodes (Frasnian, Namurian and Stephanian) separated by inter-glacial intervals (Isbell et al., 2003).

Concerning the upper Pennsylvanian period, glacigenic deposits of Stephanian age have been essentially documented in Kalahari and Karoo basins basins located at high-paleolatitudes and Paraná basin of mid- to high-paleolatitudes (Fig. 1). By contrast, number of evidence suggests contemporaneous arid conditions in low- to mid-latitudes. Among the most documented evidence, we highlight: extinction of land plants and collapse of the rainforests (DiMichele et al., 2009; Sahney et al., 2010; Cascales-Miñana and Cleal, 2014), and widespread aeolian deposits reported in Solimões (Wanderley Filho et al., 2007), Amazonas (Cunha et al., 2007; Costa et al., 2020), Parnaíba (Lima & Leite, 1978; Lima Filho, 1998; Vaz et al., 2007) and Paganzo (Gulbranson et al., 2015) basins, all positioned at low- to mid-latitudes (Fig. 1). Such observations suggest that the upper Pennsylvanian period was characterized by a marked difference between high- to low-latitude paleoclimate. In order to refine the understanding of the Late Paleozoic climate change and contribute to the discussion about synchronism between high-

paleolatitude ice cover and low-paleolatitude aridification, this study brings new data from the Parnaíba Basin, based on high-resolution stratigraphy analysis.

In the Parnaíba Basin, the upper Pennsylvanian period is marked by the deposition of the upper Piauí Formation, which records a progressive shift from fluvial-aeolian sedimentary succession at the base, to an interval essentially composed of aeolian deposits at the top. This significant change in the sedimentation represents an increasing aridification in mid-latitudes. This study aims to reconstruct the paleoclimate evolution of Gondwana mid-latitude during the upper Pennsylvanian period in the light of recent stratigraphic information. Because, the analysis of the wind pattern suggests that aridification was triggered by the expansion of polar ice sheets, here we also discuss the effects of glaciation on the aeolian sedimentation

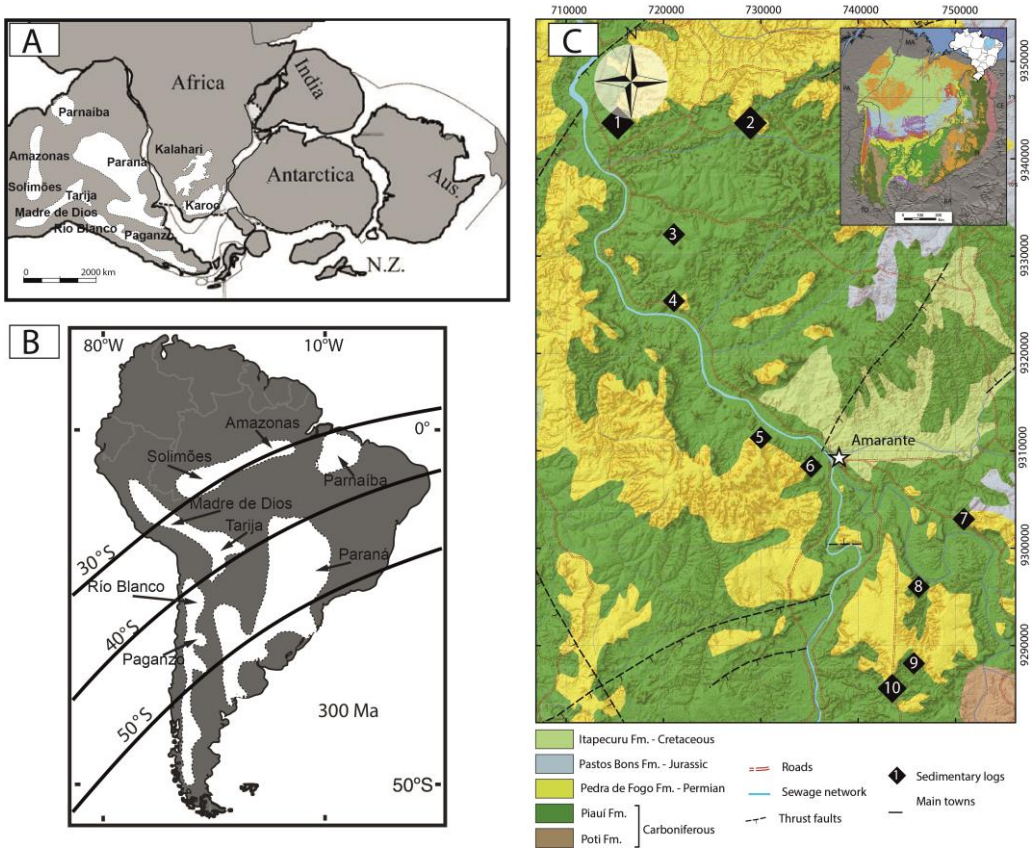

Figure 1: A) Reconstruction of Gondwana showing South America basins and Southern Africa basins. Reconstruction and polar wander path are from Powell and Li (1994) (B) Map of South America highlighting the location of late Paleozoic basins in white and paleolatitudes for 300 Ma. (C) Detailed geologic

map of the studied area with location of the outcrops where stratigraphic sections were logged.

2 GEOLOGICAL SETTING

2.1 Tectonic framework

The Parnaíba basin is a c.a. 600,000 km² Paleozoic (Silurian to Cretaceous) intracratonic sag basin (Watts et al., 2018) located in the northeastern region of Brazil (Fig. 1). The basin developed on a basement built up from the collision of Precambrian blocks composed of granitoid, mylonitic gneisses and ophiolitic metasedimentary rocks (Daly et al., 2014; Daly et al., 2018). During the Braziliano orogenesis (Cambrian to Ordovician), a series of graben and half-graben formed along the thrust belts originated by the assemblage of the Precambiran blocks. The rifting processes then evolved and triggered thermal-mechanical subsidence that resulted in the formation of the Parnaíba Basin. Rodriguéz Tribaldos and White (2018) proposed a gradual exponential decrease in subsidence over 340 Ma characterized by a rapid subsidence during the first 100 Ma of the basin initiation (Silurian) followed by slower rate from Carboniferous to Mesozoic. During the Carboniferous age, the Eo-Hercinian orogeny (late Mississipian) resulted in the uplift of the basin and the formation of the unconformity that limits the Piauí Formation from the underlying Poti Formation (Caputo, 1984; Vaz et al., 2007).

2.2 Stratigraphic framework and chronostratigraphy

The Parnaíba Basin sedimentary succession is nearly 3500 m thick and was separated in five supersequences (Góes & Feijó, 1994; Vaz et al., 2007). The Pennsylvanian stratigraphic succession, focus of this study, is part of the Balsas Group and crops out at the eastern and southern regions of the Parnaíba Basin.

The Piauí formation can be divided in two stratigraphic successions (Lima & Leite, 1978; Fig. 2): The lower Piauí Formation deposited during the Bashkirian (Melo et al., 1998; Souza et al., 2010) consists of a cyclic sedimentation of fluvial and coastal aeolian deposits interbedded with marine deposits (Vieira & Scherer, 2017). According to the authors, the cyclic

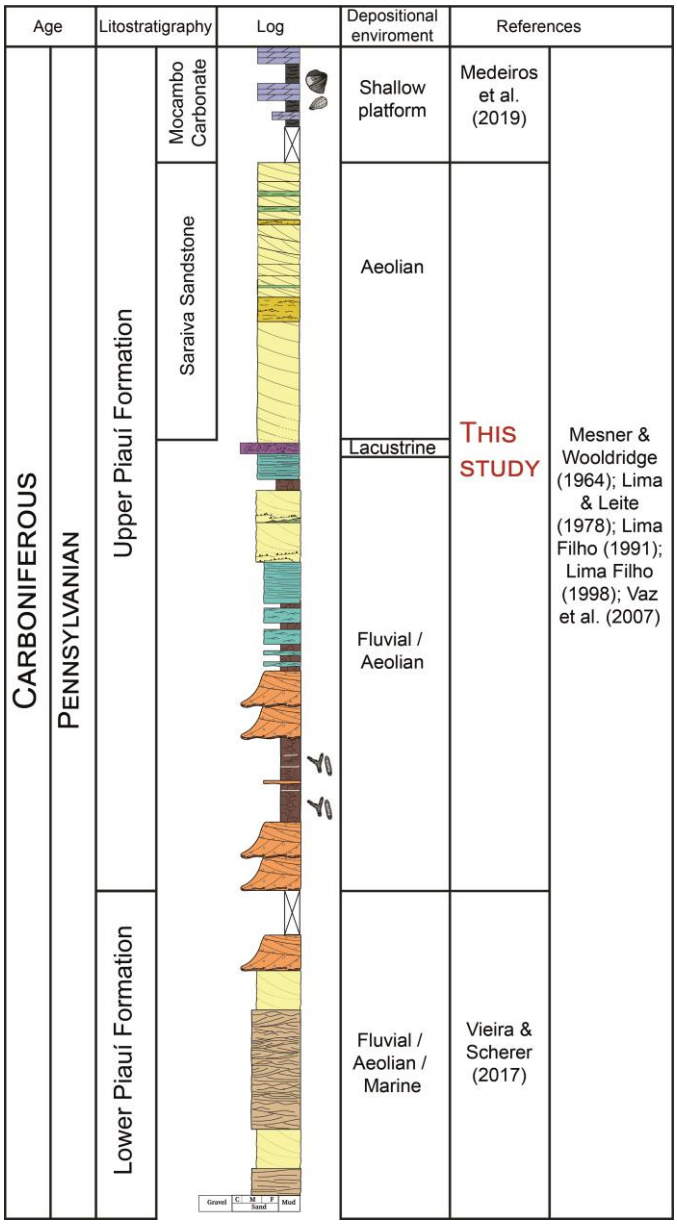

Figure 2: Chronostratigraphy and composite column of the Piauí Formation.

sedimentation represents transgressive-regressive cycles related to the fluctuation of the sea level. On the other hand, the upper Piauí formation studied here is essentially composed of continental deposits, and is characterized by basal fluvial deposits passing upwards to thick aeolian succession (Fig. 2). In some restricted areas the aeolian facies are overlain by fossil-rich carbonates (Mocambo Carbonate) interpreted to have been deposited in shallow carbonate platform system adjacent to a coastal dune field (Medeiros et al., 2019; Fig. 2). The depositional age of the upper Piauí Formation is constrained between Bashkirian age for the lower Piauí

succession and Cisuralian age for the overlying Pedra de Fogo formation (Mesner Wooldridge, 1964; Leite et al., 1975, Dino & Playford, 2002; Dino et al., 2002).

3 DATASET AND METHODS

The field investigations were carried out in the eastern margin of the Parnaíba Basin (Fig. 1). The selected area for this high-resolution study is an 60 km x 40 km area around Amarante town where well-exposed and laterally extensive cliffs and canyons allowed detailed vertical logging and facies description, and also permitted correlation of the stratigraphic intervals and bounding surfaces. Two topographic levels have been used as datum to correlate the stratigraphic sections. The first datum consists of a silicified breccia that can be tracked in the entire study area. The intense silicification confers to this layer elevated resistances to weathering, which results in a near-horizontal, vegetated topographic level that occurs at the base of hilltops. The second datum is the upper bounding surface of the studied stratigraphic succession, and represents an abrupt contact with the overlying Pedra de Fogo Formation. This surface forms a near-horizontal and vegetated topographic level at the top of the cliffs. The Mocambo Carbonate has not been observed in the studied area, suggesting that its occurrence is restricted the north of the area studied here, near Teresina town.

Ten stratigraphic sections were measured with a detailed description of facies composition, sedimentary structures and architecture (Fig. 3). The facies were grouped in facies associations, which correspond to genetically related facies that represent sub-environment within a depositional system (Collinson, 1996; Dalrymple, 2010). Additionally, fifteen samples were selected for petrologic and sedimentological analysis. Virtual outcrop models were also built using geo-referenced photographs acquired with a drone. These models allowed indirect logging of stratigraphic section in high- slope cliffs, characterization of sedimentary bodies, as well as lateral tracking of bounding surfaces

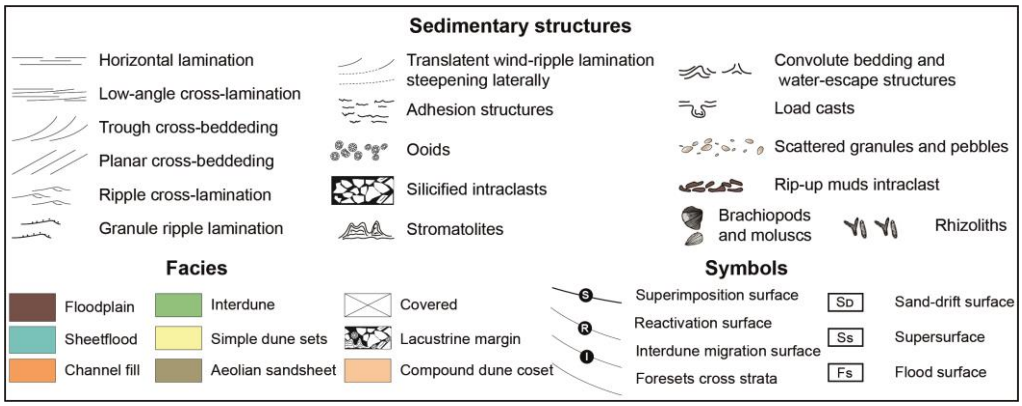

Figure 3: Set of symbols used in stratigraphic logs.

Table 1: Summary of lithofacies observed in the upper Piauí Formation

Facies	Code	Description	Interpretation
Trough cross-stratified conglomerate	Gt	Clast-supported, poorly-sorted, intraformational sandy conglomerate. Sandy matrix composed of fine- to medium-grained grains. Trough cross-stratification forming sets ranging from 0.2 to 0.3 m. Intraclasts vary from granule to cobble (< 0.15 m), subangular, usually imbricated. This lithofacies occurs as basal lags with lenticular geometry and erosive base.	Migration of subaqueous, sinuous-crested gravel dunes under unidirectional flow (Rust, 1978; Todd, 1996).
Massive conglomerate	Gm	Clast-supported, poorly-sorted, massive intraformational sandy conglomerate. Sandy matrix composed of very fine- to medium-grained sand, subangular to subrounded. Intraclasts vary from granule to cobble (< 0.1 m), subangular to rounded, usually with elongated shape. This lithofacies occurs as basal lags with lenticular geometry and erosive base.	Bedload deposition as diffuse gravel sheets (Hein and Walker, 1977) or rapid sedimentation of coarse sediments from hyperconcentrated gravity flows (Miall, 1977; Nemec and Postma, 1993).
Horizontally-laminated sandstone	Sh	Fine- to medium-grained, moderately- to well-sorted sandstone, with horizontal lamination. Intraclasts are common. Sets are < 0.15 m thick, with erosive base.	Planar-bedded deposits originated via upper flow regime (Miall, 1977; Best and Bridge, 1992).
Low angle Cross-laminated sandstone	Sl	Fine- to medium-grained, moderately- to well-sorted sandstone, with low angle lamination (< 15°). Intraclasts are common. Sets vary from 0.2 m to 1.2 m thick beds, with erosive base.	Washed-out dunes and humpback dunes (transition between subcritical and supercritical flows) (Harms et al., 1982; Bridge and Best, 1988).
Sigmoidal cross-stratified sandstone	Ssg	Fine- to medium-grained, moderate to poorly sorted, small-scale (< 0.5 m thick) sigmoidal cross-stratification. Intraclasts are common. Sets vary from 0.2 to 0.5 m and exhibit erosive base.	Lower- to upper-flow regime transitional bedform (Wizevich, 1992).
Trough cross-stratified sandstone	St	Fine- to medium-grained, poorly-sorted, small- to medium-scale trough cross-stratified sandstone (0.2 to 1.4 m thick), may form amalgamated sets (2 – 5 m thick). Mudclasts, granules and pebbles are concentrated along the bedform foresets and bottomsets.	Migration of sinuous-crested subaqueous bedforms under unidirectional (Allen, 1963; Harms et al., 1982; Todd, 1996; Collinson et al., 2006)

Planar cross-stratified sandstone	Sp	Fine- to medium-grained, poorly-sorted, small- to medium-scale planar cross-stratified sandstone (0.2 to 0.6 m thick). Mudclasts, granules and pebbles are concentrated along the bedform foresets and bottomsets.	Migration of straight-crested subaqueous bedforms under unidirectional (Allen, 1963; Harms et al., 1982; Todd, 1989; Collinson et al., 2006).
Ripple cross-laminated sandstone	Sr	Very fine- to fine-grained, moderately sorted sandstone, with small-scale asymmetric ripple cross-lamination (< 9 cm) forming up to 1,4 m thick beds. The climbing angle varies from subcritical to critical.	Migration of ripples under unidirectional lower flow regime (Allen, 1963; Miall, 1977).
Massive sandstone	Sm	Fine- to very coarse-grained sandstones; moderately- to well-sorted; massive; sparse granules and pebbles; 20 to 80 cm thick beds.	Rapid deposition of hyperconcentrated flows, fluidization (Miall, 1978, 1996).
Massive mudstone	Fm	Mudstones to siltstone; massive; purple to brownish gray; 20 cm to 8 m thick beds. Horizons of color variations; mottling structures; root traces traces and rhizoliths; slickensides; 20 cm to 3.5 m thick beds.	Suspension settling from standing water; lack of lamination due to (i) pedogenesis or (ii) loss of lamination associated intensive bioturbation; post-depositional graying under reducing conditions (Miall, 1977; Foix et al., 2013); mottling, slickensides and rhizoliths suggest subaerial exposure and paleosol development (Wright, 1992).
Laminated mudstone	Fl	Mudstones to siltstone; horizontal lamination ; purple to brownish gray; 20 cm to 8 m thick beds. Horizons of color variations; mottling structures; root traces and rhizoliths; slickensides; 20 cm to 3.5 m thick beds.	Suspension settling from weak currents or standing water; post-depositional graying under reducing conditions (Miall, 1977; Foix et al., 2013); mottling, slickensides and rhizoliths suggest subaerial exposure and paleosol development (Wright, 1992).
Low-angle laminated aeolian sandstone	Sl (e)	Very fine- to medium-grained sandstones; bimodal; well-sorted; well-rounded grains; low angle cross bedding; rare coarse grains	Migration of translatent wind ripples. The millimetrically-spaced laminations result from the relatively low-angle of climbing and the high index of ripples (10-20) (Hunter, 1977; Mountney, 2006).
Trough cross-stratified aeolian sandstone	St (e)	Fine- to coarse-grained sandstones; bimodal; inversely-graded; well- to moderately-sorted; well-rounded grains trough cross-bedding. Wedge-shaped packages of homogeneous sand pinching-out towards the toesets, intercalated with structureless fine-grained sandstones laminae of 1 to 3 mm. Foresets dip steepening from the base to the top of set.	Migration of aeolian dune characterized by alternation of grain flow avalanche and grain fall settling on the lee face of dunes (Hunter, 1977; Kocurek, 1981; Rubin & Hunter, 1982).
Planar cross-stratified aeolian sandstone	Sp (e)	Fine to coarse-grained sandstones; bimodal; inversely-graded; well- to moderately-sorted; well-rounded grains trough cross-bedding. Wedge-shaped packages of homogeneous sand pinching-out towards the toesets, intercalated with structureless fine-grained sandstones laminae of 1 to 3 mm.	Migration of aeolian dune characterized by alternation of grain flow avalanche and grainfall settling on the lee face of dunes (Hunter, 1977; Kocurek, 1981; Rubin & Hunter, 1982).

Ripple-laminated aeolian sandstone	Sr (e)	Fine- to coarse-grained sandstone; bimodal; inversely-graded; well- to moderately-sorted; millimetrically-spaced asymmetric ripple cross-lamination (pinstripe lamination); sometimes with coarse-grained or granule ripple cross-lamination	Migration and climbing of translatent wind ripples (Mountney, 2006). The granule ripples are formed due to the removal of fine sand causing the concentration of coarse sand (Ahlbrandt & Fryberger, 1981).
Aeolian sandstone with adhesion structures	Sa (e)	Very fine to medium-grained sandstones; well- to moderately-sorted; bimodal; adhesion structures.	Adhesion of wind-transported grains on a damp surface or its capillary fringe (Hummel & Kocurek, 1984; Kocurek & Fielder, 1982).
Massive aeolian sandstone	Sm (e)	Very fine to medium-grained sandstones; wel-sorted and well-rounded grains; massive; generally fluidized.	Obliteration of aeolian dune structure due to liquefaction and overpressured pore water caused by the overload of water-saturated sand (Doe & Dott, 1980; Horowitz, 1982).
Horizontally laminated stromatolite	STh	Millimeter-thick; sub-horizontal to wrinkle lamination; alternation of light and dark laminae. Light laminae are composed of dolomitized and silicified matrix, while dark laminae contain high organic mat concentration.	Organosedimentary deposits formed by benthic microbial in shallow-water environment during fair-weather periods (Kah et al., 2006).
Columnar stromatolite	STc	Columns are c.a. 1 cm in diameter and 3 to 5 cm in height; replaced by cryptocrystalline and microcrystalline silica, microspherulitic chalcedony and rhombohedral dolomite crystals. The inter-column spaces are filled with microporous microspherulitic chalcedony.	Organosedimentary deposits formed by benthic microbial growth through trapping and bidding of particles allowing 'light-driven' vertical accretion (Hofmann, 1973).
Deformed ooids	Od	Ooids range 0.15 to 2.5 mm in diameter; oval, elongated and irregular shapes; internal concentric structure poorly-preserved; intense silicification; primary composition partially dissolved and/or replaced by dolomite, cryptocrystalline and microcrystalline silica and prismatic quartz. Cementation by chalcedony rims, quartz mosaic and blocky dolomite filling interparticle pores.	Ooids formation suggests wave agitation (Plee, 2008) Deformation of ooids suggests shrinkage of original clay ooids due to dehydration and salinity variations (Tettenhorst and Moore, 1978; Goldberg et. al, 2017; Armelenti et al., 2017; Leite et al, 2020).
Intraformational breccia	Gcm	Clast supported silicified conglomerate, composed of large (0.5 to 2.0 cm) angular clasts of silicified ooids, brecciated stromatolites and cryptocrystalline to microcrystalline silica.	Brecciation of stromatolites during high energy events like storms (Buck, 1980).

4 FACIES AND FACIES ASSOCIATION

The detailed facies analysis of the upper Piauí formation stratigraphic succession allowed identification of twenty-one lithofacies (Table 1) that occur within seven facies association characteristics of three subenvironments: (i) The fluvial deposits are composed of channel-fill, sheetflood and floodplain facies association; (ii) the aeolian deposits comprise aeolian dune, interdune and sandsheet facies associations; and (iii) the lacustrine deposit is represented by lacustrine margin facies association (Fig. 4).

Facies association	Vertical log	Description	Lithofacies	Interpretation
Channel-fill	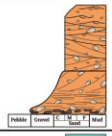	Lenses-shaped sandstone bodies limited by erosive concave-up surface; organized in fining-upward successions of 0,2 to 2 m thick; basal lenticular lags, passing vertically into poorly sorted cross-bedded sandstones and sometimes ending with ripple laminated sandstones at the top. Pebbles and granules are scattered.	Gt, Gm, Sh, Sl, Ssg, St, Sp, Sr,	Deposition of subaqueous dunes within a low-sinuosity fluvial channel.
Sheetflood	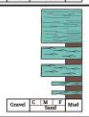	Moderately-sorted fine to medium-grained sandstones interlayered with mudstone layers; tabular sheet-like bodies, 2 to 6 m thick; coarsening and thickening-upward succession	Sh, Sl, St, Sp, Sr, Sm, Fm, Fl	Terminal plays and poorly-confined to unconfined streams at distal portion of fluvial channels.
Floodplain		Massive and laminated mudstones, purple or red, sometimes bleached to cream or white. Rhizoliths and calcrete nodules are common. Rare fine-grained sandstone laterally discontinuous. Successions of 1 to 19 m in thickness and lateral extension of hundreds of meters.	Sh, Sr, Sm, Fm, Fl	Deposition within a standing water floodplain area under reducing condition and episodic flood events.
Aeolian dunes	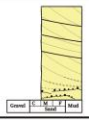	Bimodal, inversely graded, fine to medium-grained sandstones arranged in small to large-scale sets; reactivation and superimposition surfaces are common; low angle wind ripples at the base; Progressive steepening of foreset dip; Tabular bodies of 0,6 to 19 m in thickness and lateral extension of hundreds of meters.	Sl(e), St(e), Sp(e)	Migration of sinuous-crest aeolian dunes and draas.
Interdunes		Fine-grained sandstones arranged into thin beds of 10 to 50 cm thick; Adhesion structures, near-horizontal translatent wind-ripple laminae, soft-sediment deformations; Interfingering relationship with aeolian dunes; Lense-shaped bodies encased between aeolian dune sets, rarely tabular.	Sr(e), Sa(e), Sm(e)	Deposition of sediments in dry to damp interdune areas.
Aeolian Sandsheet		Fine to coarse-grained sandstones; bimodal grain-size distribution. Inversely graded, near-horizontal translatent wind-ripple laminae, and rare wedge-shaped decimeter-scale cross-strata. Tabular bodies of 0.85 m to 4.80 m thick and hundreds of meters laterally.	Sl(e), St(e), Sr(e), Sa(e)	Migration of wind ripples and sediment adhesion in sandsheet environment.
Lacustrine margin		Stromatolites, ooids and intraformational conglomerate: Stromatolites form millimetrically-spaced columns or millimeter-scale horizontal lamination; Ooids are poorly sorted, deformed and irregular in shape, and completely replaced and cemented by cryptocrystalline to microcrystalline silica. The intraformational conglomerates are composed of angular clasts of silicified ooids, brecciated stromatolites and cryptocrystalline to microcrystalline silica.	STh, STc, Od, Gcm	Microbial growth in shallow water environment periodically affected by storms.

Figure 4: Description and interpretation of facies association observed in the upper Pìauí Formation.

4.1 Fluvial deposits

Channel-fill facies association

Description. This unit is composed of grey, poorly sorted arkosic very fine- to coarse-grained sandstones, arranged into several sandstone bodies up to 3 m thick. Mudclasts, granules and pebbles are scattered and concentrated along the bedform foresets (Fig. 5). Internally the sandstones bodies exhibit planar (Sp) and trough cross-bedding (St) and, less commonly, sigmoidal cross-bedding (Ss), horizontal lamination (Sh), low-angle cross lamination (Sl) and ripple cross-lamination (Sr). Units of this facies association are bounded at the base by a sharp and erosive concave-up surface with low relief (up to 1.5 m deep). The basal surface is immediately overlain by massive, intraformational conglomerates (Gm) or trough cross-bedded, sandy conglomerates (Gt) that

form lenticular lags up to 1 m thick and a few meters wide, composed of angular to sub-angular quartz clasts and mudstone rip-up clasts (Fig. 5).

The basal lags pass vertically into trough (St) and planar (Sp) cross-beds and sometimes ending with ripple laminated sandstones (Sr) at the top resulting in poorly- to well-defined fining-upward trends. Two types of architectural elements have been recognized on the basis of lithofacies assemblage, geometry and orientation of the boundary surfaces: (1) Simple, large-scale cross-strata forming isolated sets of cross-strata (0.8–2.1 m thick), that extend laterally a few meters (maximum of 10 m). Foresets are planar to sigmoidal with uniform dip directions throughout the sets. (2) Amalgamated cross-strata composed of grouped small-scale sets (0.2 to 0.4 m thick) of trough and planar cross-strata, forming storeys of 1.2 to 3.0 m thick. Sets are bounded by flat surfaces dipping at low angles (5 to 15°), in the same direction as the cross-bedding. Soft sediment-deformation structures (flame structures and contorted bedding) have been observed at the base of some sand bodies. The fluvial paleocurrents show a prevailing direction towards NW (mean vector = 300°), with low dispersion (270° to 340°).

Interpretation. The occurrence of poorly sorted sand bodies composed of cross-bedded sets is indicative of subaqueous dunes deposited within a channel (Chagas, 2006). The lenticular lags at the base of the channel result from the deposition of hyper-concentrated flows (Miall, 1978, 1996). The planar cross-bedding (Sp) represents migration of straight-crested and the trough cross-bedding (St) results from the migration of sinuous-crested subaqueous bedforms under unidirectional to combined flow regime (Allen, 1963; Harms et al., 1982; Todd, 1989; Collinson et al., 2006). Sigmoidal cross-bedding (Ss) represent migration of transitional subaqueous bedforms under lower- to upper-flow regime (Wizevich, 1992). Horizontally (Sh), and low-angle laminated sandstones (Sl) are indicative of deposition under high energy and transitional flow regime respectively and may be associated to flooding event, while smaller-scale ripple cross-lamination (Sr) are indicative of lower flow regime (Allen, 1982; Baas, 1993). Hence, the alternation of horizontally and low-angle cross-bedded sandstones with ripple cross-laminated sandstones suggest

alternation of flow energy. The fining-upward trend suggests progressive decrease of current velocity during the channel filling (Hughes & Lewin, 1982; Kumar et al., 2004). The presence of siltstone and mudstone rip-up clasts, indicate erosion of overbank deposits (Kumar et al., 2004). The simple, large-scale, isolated cross strata are interpreted as formed by downstream migration of sand bars with well-developed slipfaces, such as transverse bars, alternate bars or tributary mouth bars (Wizevich, 1992; Bridge, 1993; Jo and Chough, 2001). The stacked cross-strata bounded by surfaces dipping at low angles, in the same direction as the cross-bedding represent the downstream accretion of compound sand bars with superimposed dunes, similar with mid-channel bars (Allen, 1983; Haszeldine, 1983; Wizevich, 1992; Miall, 1996). The low dispersion of paleocurrents suggests low-sinuosity fluvial channel pattern.

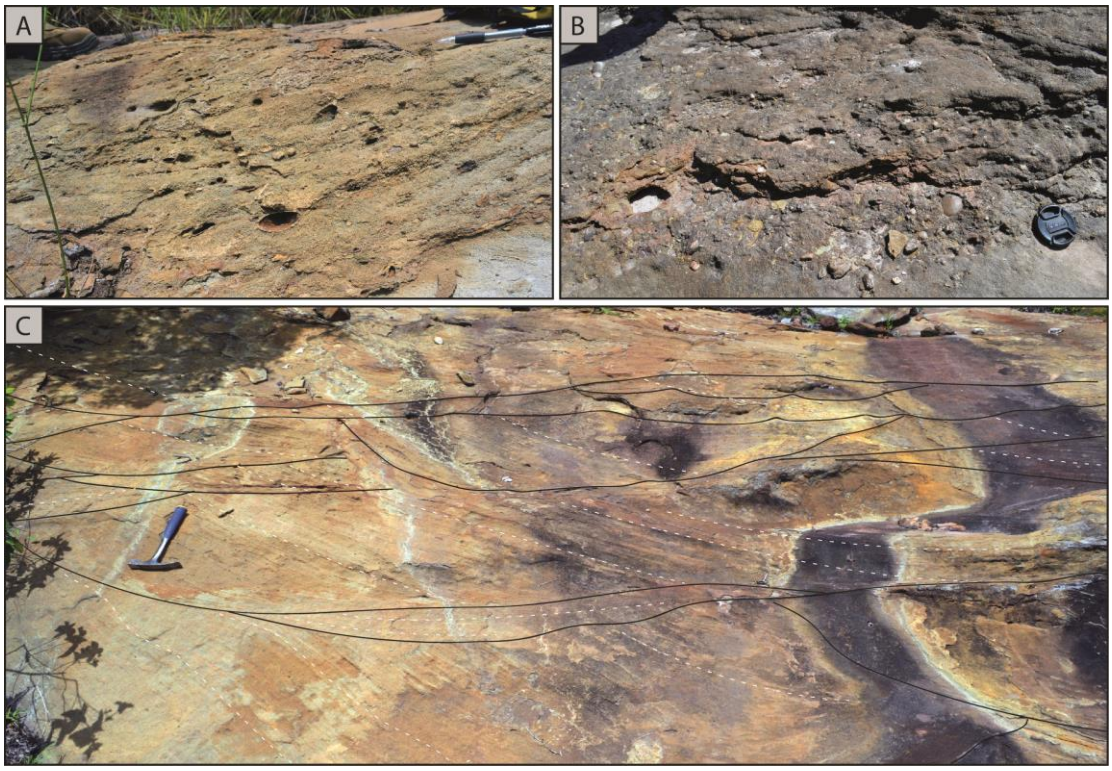

Figure 5: (A) Granules and pebbles concentrated along the bedform foresets. (B) intraformational conglomerate lags with angular to sub-angular quartz clasts and mudstone rip-up clasts. (C) Small-scale trough cross-strata bounded at the base by erosive concave-up surface and lateral extension of a few decimeters.

Sheetflood facies association

Description. This facies association is composed of fine to medium-grained, moderately sorted, grey arkosic sandstones occasionally interbedded with red to brown mudstones. This facies association forms: (1) thick (up to 4 m thick) sandstone bodies with sheet-like geometries, lateral extension of tens to hundreds of meters, composed essentially of ripple cross-lamination (Sr), bounded by non-erosive surfaces or (2) alternated sandstones and mudstones beds arranged in coarsening-upward trends of up to 24 m thick bounded by erosive basal surfaces with lenticular lags (Fig. 6) of massive conglomerates (Gm) or trough cross-bedded, sandy conglomerates (Gt);. The sandstone beds are dominantly composed of horizontal lamination (Sh), low-angle cross-lamination (Sl) and ripple cross-lamination (Sr), and less commonly exhibit massive (Sm), planar (Sp) and trough cross-bedding (St) (Fig. 6). The mudstones are massive (Fm) or horizontally laminated (Fl) (Fig. 6). These sandstones beds are bounded by sharp non-erosive bases and occur as thinner (up to 1.2 m thick) tabular beds that extend laterally tens of meters or as smaller lenses-shaped sandstone beds (0.1 to 0.3 m thick) encased within mudstone packages, and extend laterally only a few meters (maximum of 5 m measured). Soft-sediment deformation (load cast, pseudonodules, ball-and-pillow and flame structures) are abundant (Fig. 6).

Interpretation. Sandstone bodies characterized by sheet-like geometry and unidirectional tractive structures, are interpreted as deposition from poorly-confined to unconfined streams as terminal plays that represent the distal portion of fluvial channels (Bridge, 2003). The abundance of ripples lamination and the scarce occurrence of cross-bedding are further evidence of episodic flows (Tunbridge, 1984; Hampton and Horton, 2007). On the other hand, the alternated sandstones and mudstones beds arranged in coarsening-upward trends indicate alternate sedimentation linked to energy variations. The horizontal and low-angle cross-lamination represents waning flow within upper and transitional flow regimes respectively (Harms et al., 1982; Bridge and Best, 1988), whereas the ripple lamination results from unidirectional currents under lower flow regime conditions (Miall, 1977; Collinson et al., 2006). The rare

occurrence of planar or trough cross-bedded sandstone suggest rapid variation in flow energy, between supercritical to subcritical flow regimes, and suggests

Figure 6: (A) Outcrop panoramic view of sheetflood facies association. Note the net erosive contact between the basal reddish mudstones and siltone and the overlying sandstones. . White dotted box point out the position of close-up pictures. Black arrow for pseudonodules. (B) Close-up of intraformational massive conglomerate gradding upward to trough cross-bedded sandy conglomerates. (C) Sandstone alternating horizontal lamination (Sh) and ripple

cross-lamination (Sr). (D) Close-up of ripple cross-lamination. (E) Laminated sandstone pseudonodules within mudstone package. (F) Close-up of sandstone pseudonodule.

deposition by ephemeral streams, typical of sheetflood deposits (Bridge, 2003). The laminated and massive mudstones indicates deposition in a zone where settling was a common process. Therefore, the coarsening-upward packages are interpreted as distal portions of high energy short-lived sheetfloods deposits (Spalletti & Piñol, 2005; Hampton & Horton, 2007; Cain & Mountney, 2009). The soft-sediment deformation can be interpreted as result of high sediment load over water-saturated sediment, leading to liquefaction (Owen, 2003; Collinson et al., 2006).

Floodplain facies association

Description. This facies association is composed of intercalated mudstones, siltstones and very fine-grained sandstones. Mudstones are dominantly purple or red in color, but also occur bleached almost cream or white (Fig. 7). Internally, mudstones and siltstones are structureless (Fm) or horizontally laminated (Fl) (Fig. 7). Rhizoliths and calcrete nodules are common and are usually associated with mottling and discoloration of mudstones. The fine-grained sandstone are thin (1 to 25 cm) and laterally discontinuous. Sandstones are typically massive although rare horizontal laminations (Sh) and ripple cross-laminations (Sr) may also occur (Fig. 7). This facies normally occurs as thick packages of up to 19 m in thickness and lateral extension of hundreds of meters, immediately overlying thicker fluvial channel or sheetflood units.

Interpretation. The mudstone-rich character of this facies association, its alternation with fine-grained sandstones and its close association with fluvial channel and sheetflood deposits suggest subaqueous deposition in floodplain area marked by repeated flood events (Bridge, 2003). The thin and discontinuous sandstones record multiple events of lateral spilling of fluvial channel (Bristow et al., 1999). Horizontal lamination within sandstones suggests upper flow regime condition, whereas ripple cross-laminations result from reduction of flow velocity. The bleaching of the purple-colored sediment suggest

reducing effect caused by decay of vegetation within an anoxic environment and support the interpretation of standing water like floodplain (Retallack, 2001). The intense mottling combined with rhizoliths and calcrete nodules suggest subaerial exposure and paleosol development (Wright, 1992). Similar paleosol development has been related to semi-arid climate (Mack, 1977; Mack et al., 1993; Loope, 1981), and has been reported in several sedimentary successions with fluvial-aeolian interactions (Langford & Chan, 1988; Mountney & Thompson, 2002; Taagart et al., 2010).

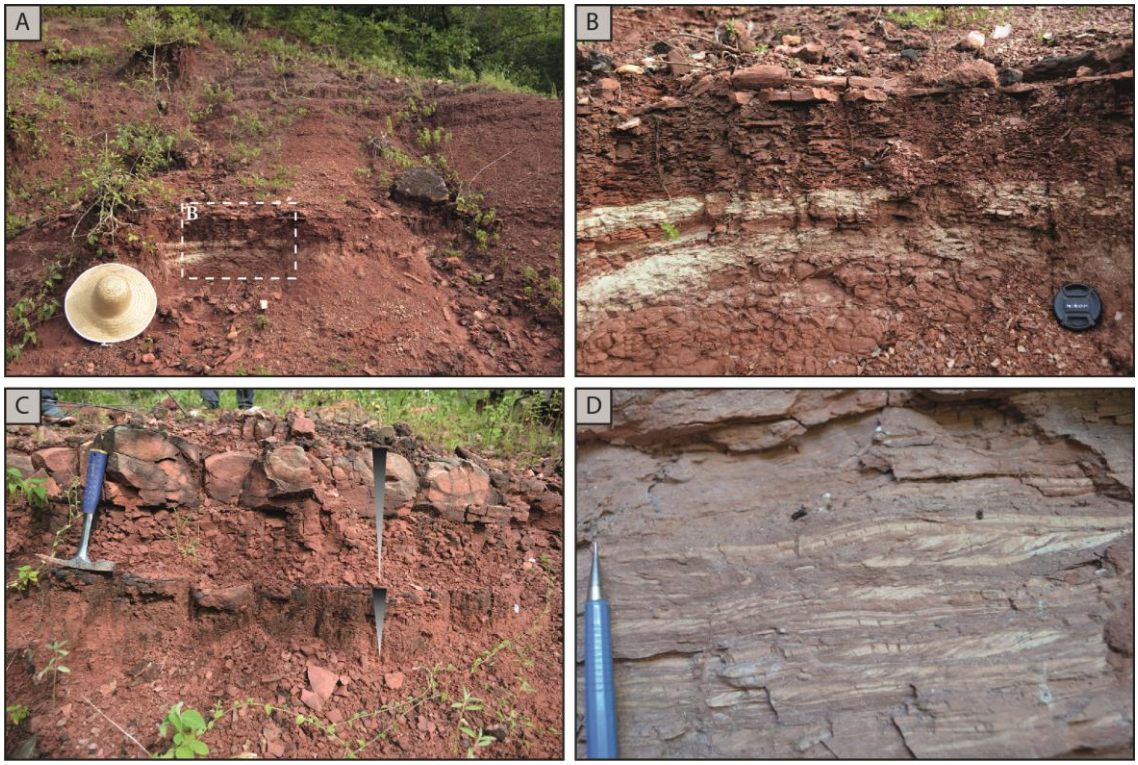

Figure 7: (A) Thick package of reddish mudstone. (B) Blocky massive mudstone at the base, gradding vertically to laminated mudstone. Mudstone are bleached to cream or white color. (C) Thin beds of fine-grained sandstone defining centimeter-scale coarsening-upward cycles. (D) Lenses of very-fine grained sandstone with ripple-cross lamination.

4.2 Aeolian deposits

Aeolian sandsheet facies association

Description: This facies association comprise fine to medium-grained, well sorted sandstones characterized by bimodal grain-size distribution. Less

commonly coarse-grained and granule also occur (Fig. 8). Units of this facies form tabular sand bodies of 0.85 m to 4.80 m thick, with planar top and base and extend laterally for several hundreds of meters in sections both parallel and perpendicular to the mean aeolian transport direction (Fig. 8). These units are predominantly composed of inversely graded low-angle translatent wind-ripple laminae (Sl (e)). However wedge-shaped decimeter-scale (10 to 20 cm) trough cross-strata (St (e)) have also been observed encased within these units. Granule ripples and coarse-grained wind-ripples (Sr (e)) are rare and occur alternating with fine-grained wind ripples (Fig. 8). Adhesion (Sa (e)) and flame structures (Sm (e)) have also been observed (Fig. 8).

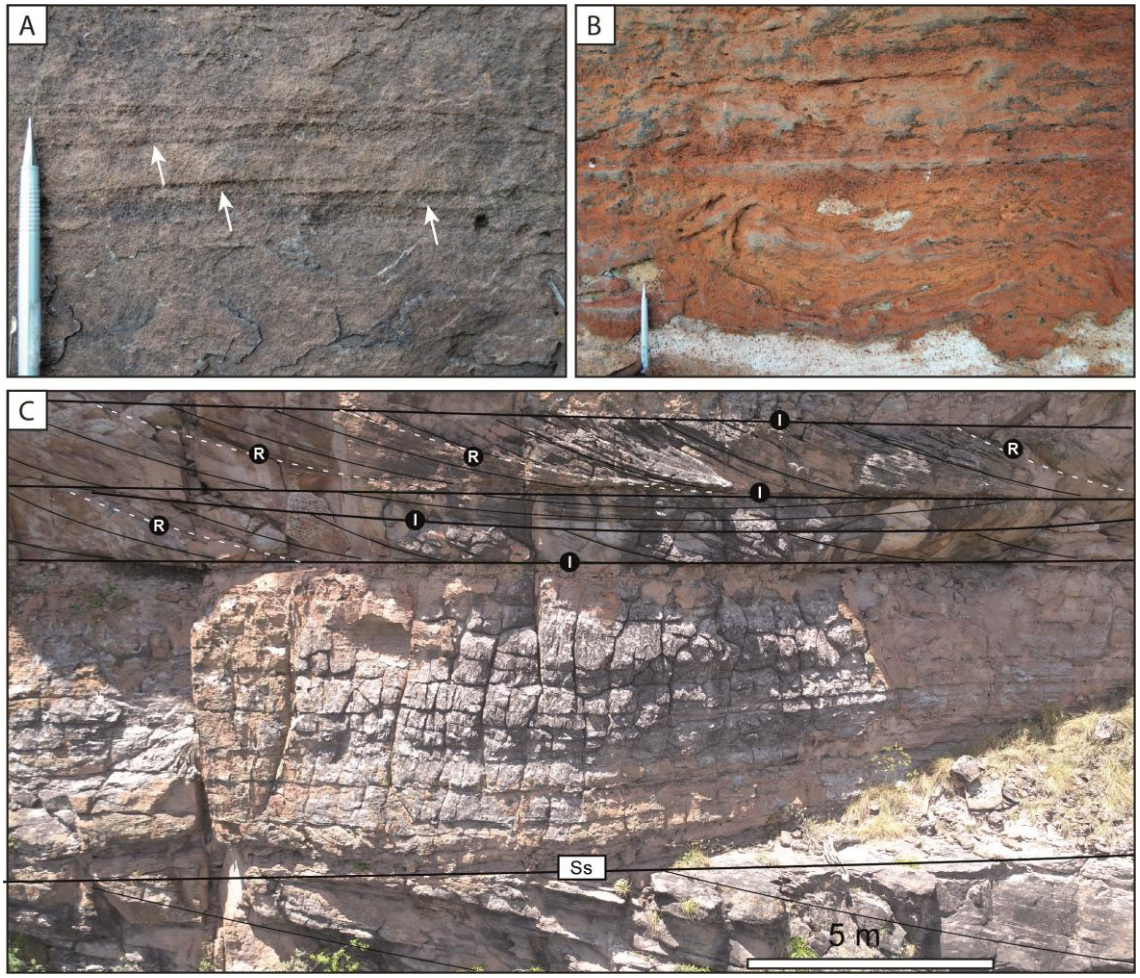

Figure 8: Granule ripples intercalated with wind ripples. (B) Flame structures and wavy to crinkly lamination at the uppermost part reflecting adhesion structures. (C) Thick and laterally extensive aeolian sandsheet deposit separated from underlying and overlying aeolian dune sets by sharp sug-

horizontal surface. R for reactivation surfaces, I for interdune surfaces and Ss for supersurface.

Interpretation: Whist low-angle wind-ripple strata suggest migration of wind ripples over a dry substrate, adhesion structures and soft-sediment deformations point to damp conditions (Mountney, 2006). The significant thickness and lateral continuity of this facies characterized by the lack of well-developed dune sets suggest limited sand availability and deposition in aeolian sandsheet environments (Fryberger et al., 1979; Fryberger & Scenk, 1981; Fryberger et al., 1992 Kocurek & Lancaster, 1999). Decimeter-scale trough-cross strata represent protodunes migration within aeolian sandsheets (Kocurek et al., 1992). The presence of granule ripples is indicative of episodic introduction of coarse grains during periods of higher wind strength (Bagnold, 1941; Kocurek & Nielson, 1986).

Aeolian dune facies association

Description: This facies association consists of well sorted fine to medium-grained (rarely coarse-grained) sandstones arranged in medium to large-scale sets of trough (St (e)) and planar cross-strata (Sp (e)). This unit forms tabular bodies that extend laterally for hundreds of meters in cross-section oriented parallel to aeolian transport and scoured bases in cross-sections perpendicular to the mean paleowind. Individual sets range from 0,6 to 19 m in thickness (Fig. 9), and usually interfinger at the base with interdune deposits and eventually exhibit soft-sediment structures (flame structures and convolute bedding) on the toeset. Foreset laminations consist of wedge-shaped packages of homogeneous sand that pinch out towards the toesets, intercalated with structureless fine-grained sandstones laminae of 1 to 3 mm (Fig. 9).

This unit typically has sharp planar horizontal to upwind inclined upper surface and is internally punctuated by steep downwind-dipping concave-up erosive surfaces (Fig. 9). In some cases units of this facies display low-angle planar surfaces inclined downwind truncated above and below by the previously cited horizontal surface. These surfaces dip 3° to 19°, with a mean trend towards west (mean vector = 274°) (Fig. 9).The lowermost part of the sets is

commonly characterized by fine- to medium-grained, bimodal and inversely-graded sandstones with sub-horizontal to low-angle cross lamination. Foresets dip 10° to 22° and cross-bedding shows wide dispersion of dip direction from 260° to 330° (mean vector = 270°). When aeolian dunes overlie fluvial deposits, the toeset of aeolian dunes generally appear contorted or exhibits fluid escape structures. Occasionally the set immediately above fluvial deposits is structureless or the internal stratifications are deformed (Sm (e)).

Interpretation: The presence of medium to large-scale cross-strata formed by well sorted grains suggests deposition via migration of aeolian dunes (Kocurek, 1981; Rubin & Hunter, 1982). The homogeneous medium to coarse-grained wedge-shaped sand packages wiithin the forests are grain flow deposits, whereas the fine-grained structureless laminae represent grain fall deposits on the lee face of dunes (Hunter, 1977). The low-angle cross-lamination in inversely-graded laminae, occurring preferentially at the base of sets, are deposited by subcritically climbing translatent wind ripples (Hunter, 1977). The lateral continuity of hundreds of meters in sections parallel to the prevailing paleowind direction, together with the wide dispersion of foreset-dip direction (around 70°) and the trough geometry of basal bounding surfaces indicate crescentic dunes with a sinuous crestline (Rubin, 1987; Paola & Borgman, 1991). The horizontal to upwind inclined upper bounding surfaces are interdune migration surfaces (Brookfield, 1977; Kocurek 1981). The erosional steep downwind-dipping surfaces that occur inside the dune sets are reactivation surfaces (Brookfield, 1977; Fryberger, 1993). This kind of surface are common in dunes of sinuous crest lines and reflects changes in changes in dune asymmetry, local fluctuations in wind direction and/or speed wind (Hunter and Rubin, 1983; Kocurek et al., 1991; Mountney and Howell, 2000; Loope et al., 2001; Scherer and Lavina, 2005; Scherer and Goldberg, 2010; Jones et al., 2016), but may also be generated by partial erosion of the lee face in the aeolian dunes during periods of reverse winds (Rubin and Hunter, 1983). Finally, the low-angle down-wind inclined planar surfaces truncated by horizontal interdune surfaces are interpreted as superimposition surfaces (Brookfield, 1977; Kocurek, 1991, 1996). The trough geometry of the cross-strata separated by superimposition surfaces suggests that these surfaces were

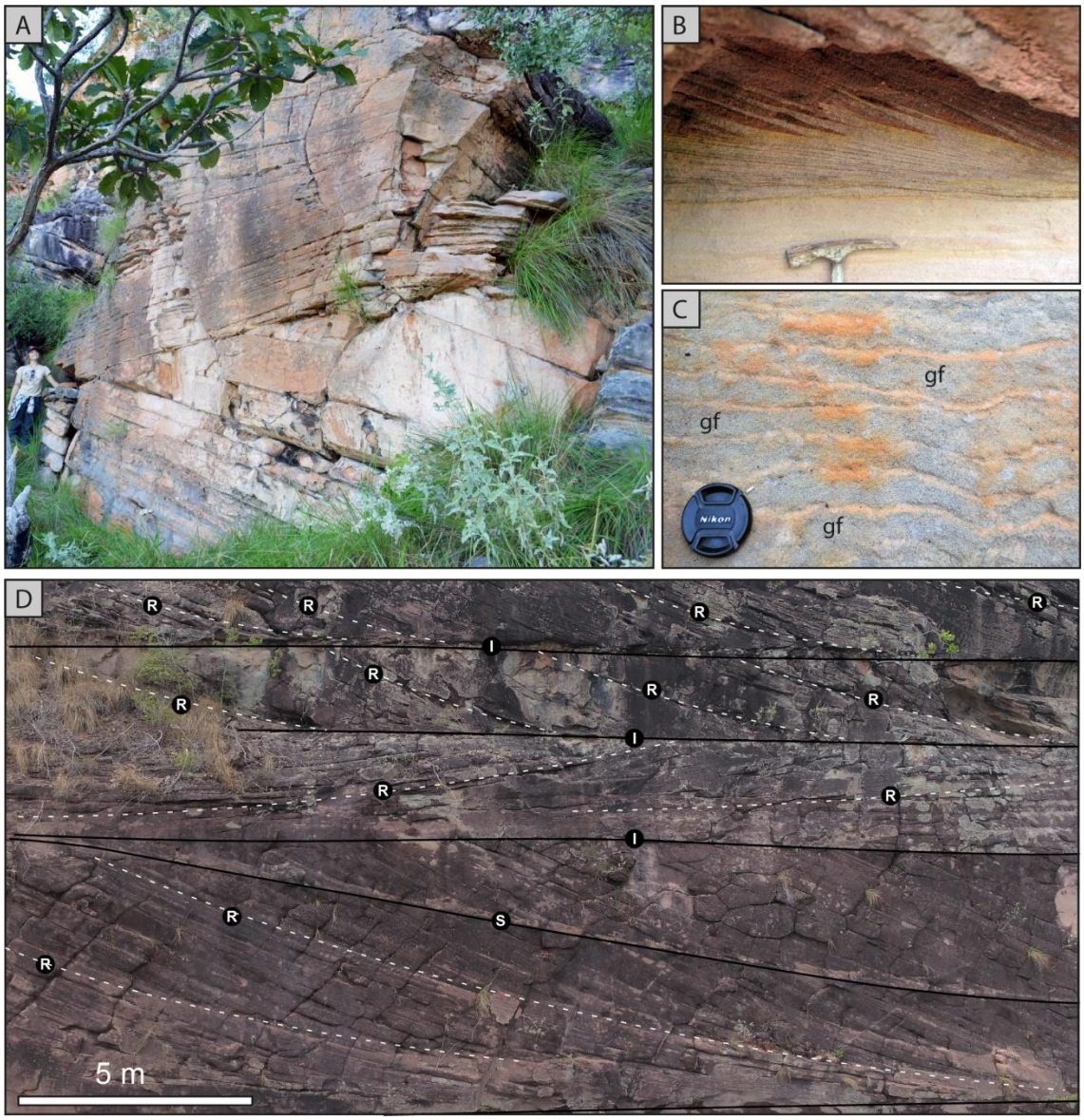

Figure 9: (A) Large-scale trough cross-strata separated by interdune surface. (B) Wedge shaped grain flow strata pinhcing out laterally and interfingering with wind ripples. (D) Homogeneous grain flow strata “gf” intercalated with milimeter-thick grain fall deposits. (D) Outcrop panoramic view of aeolian succession. Note the steep downwind-dipping reactivation surfaces “R”, truncated by superimposed surface “S”.

originated by migration of crescentic bedforms on the lee face of draas. The low angle of superimposition surfaces, their climbing nature and the divergent orientation existing between the cross-bedding (287°) and the surfaces (274°) suggest that the superimposed dunes migrated slightly obliquely relative to the main bedforms crestlines (Rubin, 1987; Scherer. 2000). The presence of soft-

sediment deformation structures at the base of sets suggests liquefaction due to overpressured pore water, generally caused by the overload of water-saturated sand (McKee et al., 1971; Mountney & Thompson, 2002; Doe & Dott, 1980; Horowitz, 1982; Mountney & Thompson, 2002). Thus, the presence of soft-sediment deformation structures indicates high water table at the time of dune migration (Mountney, 2006).

Interdune area facies association

Description: This facies association is composed of well-sorted and well-rounded fine-grained sandstones with adhesion structures (Sa (e)) or low-angle translatent wind-ripple laminae (Sl (e)) arranged into thin beds of 10 to 50 cm thick, though occasionally attaining a maximum thickness of 1.7 m. These sand bodies were observed encased between dune sets, yet occasionally form tabular layers that can be traced for tens of meters. Differently from aeolian sandsheets deposits, the interdune area deposits show a sharp basal surface with the underlying dune sets, but the upper contact with the toeset of dune sets displays a series of interfingering relationship and soft-sediment deformations (Fig. 10). Additionally, the interdune area deposits are usually identified by a lateral variation in thickness.

Interpretation: Deposits characterized by sand bodies of well-sorted and well-rounded fine-grained sandstones, encased and frequently interfingered with aeolian dune toeset suggest deposition in interdune areas (Mountney, 2006). Adhesion structures indicate close proximity of water table or its capillarity fringe triggering adhesion of aeolian sediments in transport (Olsen et al., 1989). Both adhesion structures and soft-sediment deformations at the contact with aeolian dune sets suggest accumulation under damp conditions (Kocurek & Fielder, 1982). Conversely, translatent wind-ripples laminae suggest drier substrate. Thus, the alternation of wind-ripple strata with adhesion structure suggests fluctuations of water-table level, allowing period of dry and damp interdune formation (Mountney, 2012). The intertonguing relationship with aeolian dune sets suggests dune migration over dry to damp interdune (Mountney & Thompson, 2002; Mountney, 2006).

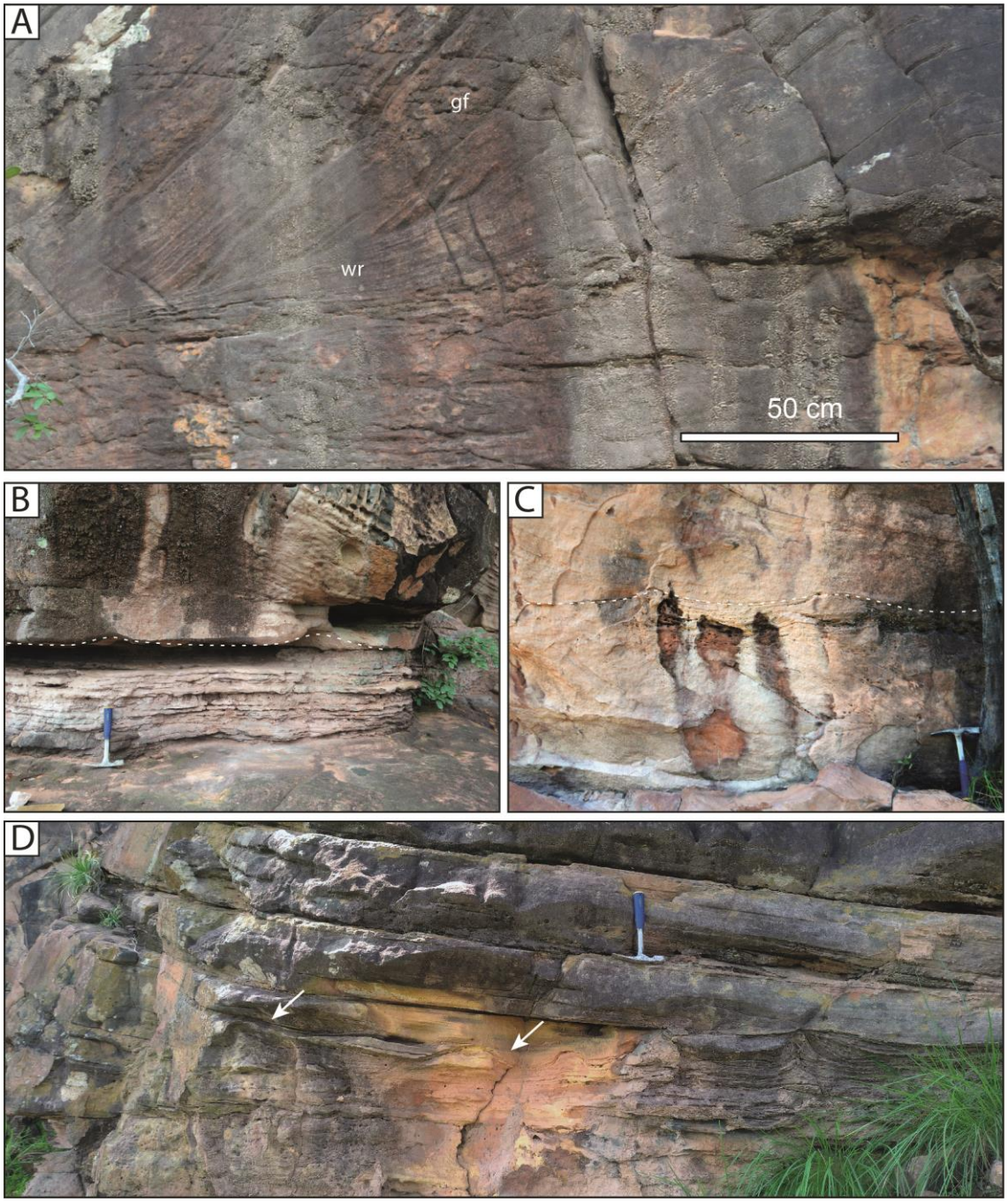

Figure 10: Different relationships between aeolian dune and deposits of interdune area. (A) Grain flow “gf”strata on aeoluan dune passing down-dip into wind ripple “wr” of dune toeset and wawy crinkly laminations of interdune area. (B) and (C) Cyclical scours resulting from erosion of interdune deposits during dune migration. (D) Flame structures and contorted lamination caused by overpressured pore water.

4.3 Lacustrine deposits

Lacustrine margin facies association

Description: This facies association consists of stromatolites associated to ooids, and intraformational conglomerate, and occur as a thin (60 cm to 80 cm), yet regionally extensive chert deposits. The stromatolites are composed of horizontally laminated (STh) (Fig. 11) and columnar (STc) structures arranged in low-relief domes of up to 40 cm in wavelength and 10 cm in height. The laminated stromatolites are characterized by millimeter-scale horizontal or undulated lamination, alternating organic-rich dark laminations and light grey laminations poor in organic matter. On the other hand, the columnar stromatolites are characterized by elongated features, typically 1 cm in diameter and 3 to 5 cm in height, spaced a few millimeters. Both laminar and columnar stromatolites exhibit a disrupted and brecciated aspect.

Ooids are poorly sorted, ranging in diameter from 0.15 to 2.5 mm, elongated or irregular in shape (Od), and are completely replaced and cemented with cryptocrystalline to microcrystalline silica or prismatic quartz (Fig. 11). In thin sections, the interparticle contacts between ooids vary heterogeneously between point, longitudinal and concavo-convex. The associated intraformational conglomerates are clast supported, massive (Gcm), composed of large (0.5 to 2.0 cm) angular clasts of silicified ooids, brecciated stromatolites and cryptocrystalline to microcrystalline silica (Fig. 11).

Interpretation: The low-relief domal stromatolites and centimeter-scale columnar stromatolites indicate development in a shallow-water environment (Kah et al., 2006). Ooids formation suggests wave agitation (Plee, 2008) and the presence of intraformational conglomerates composed of brecciated stromatolite reflect periods of high energy like storms (Buck, 1980). The common occurrence of elongated ooids suggests plastic deformation due to ductil behavior of grains and indicates original clay composition. The variable nature of interparticle contacts among ooids grains suggests early cementation, which inhibited further compaction. Therefore, the deformation of ooids, even in areas of light compaction, suggests dehydration and shrinkage of original clay ooids very similar to the Mg-silicate ooids reported in the Cretaceous Brazilian Pre-salt

(Goldberg et. al, 2017; Armelenti et al., 2016; Leite et al, 2020), and in the Eocene Green River Formation of USA (Tettenhorst and Moore, 1978). Since no evidence of subaerial exposure was observed, the most likely cause of dehydration may be salinity variations. This variation of salinity is further indicated by the alternation of organic-rich black and light grey lamination poor in organic matter, which suggests that the environment was characterized by seasonal changes that affected the productivity of organic matter. The shallow water nature of this environment, the high productivity of organic matter and the variation of salinity suggest saline lacustrine environment.

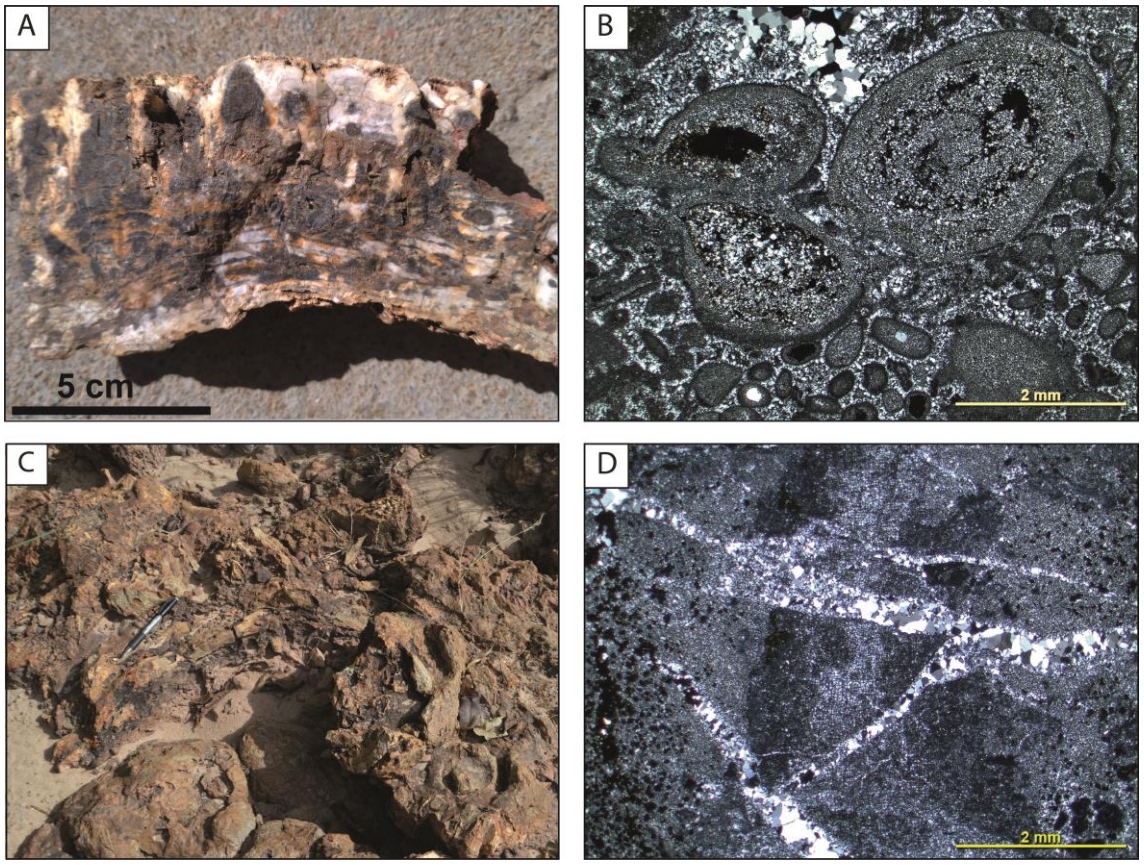

Figure 11: Centimeter-scale columnar stromatolites growing over horizontal and undulated stromatolite. (B) Poorly sorted ooids replaced and cemented with cryptocrystalline to microcrystalline silica. (C) Brecciated aspect in plan-view. (D) Brecciated angular clasts replaced and cemented by cryptocrystalline to microcrystalline silica.

5 STRATIGRAPHIC EVOLUTION

The following section describes three stratigraphic intervals (Fig. 12) defined from the overall vertical stacking of the sedimentary succession and interprets each stage in terms of the evolution of depositional model. The individual stratigraphic intervals are characterized by lateral and vertical relationship between laterally disposed depositional environments and are bounded by key stratigraphic surfaces that represent abrupt change in the depositional style (Fig. 12). The recognition of surfaces is fundamental to the development of a model for the stratigraphic evolution of the Upper Piauí Formation. The key surface tracing allowed correlation of stratigraphic intervals across the entire region, c.a. 60 km x 40 km (Fig. 12).

5.1 Stratigraphic Interval 1: Fluvial-Aeolian interaction

Description: The first stratigraphic interval (SI-1) dominantly crops out at the south of the region where drainage excavation exposes thicker sedimentary successions (c.a. 343 m of vertical section). This interval is characterized by fluvial deposits (channel-fill, sheetflood and floodplain facies associations) interbedded with aeolian deposits (aeolian dunes and interdune facies associations). The basal bounding surface with the underlying lower Piauí Formation does not crop out in the studied area. The upper bounding surface is a sharp and regionally extensive erosive surface marked by an abrupt contact between fluvial or aeolian facies with the overlying lacustrine deposits (Fig. 12).

The fluvial deposits make up the largest portion of the succession (73 % of the SI-1 thickness) and occur dominantly at the base of this interval (Fig. 12). Floodplain facies association is the most abundant fluvial deposit (c.a. 33% of the SI-1 section) and is represented by thick mudstone packages. The channel fill facies association is the second most abundant fluvial deposit (c.a. 36% of the measured section) and is represented by isolated or amalgamated sandbodies. Both isolated and stacked channel-fill sand bodies usually occur at the top of floodplain or sheetflood facies association. Finally, the sheetflood deposits are less common (c.a. 13% of the SI-1 section) and are characterized by sandstone bodies with sheet-like geometries, or alternated sandstones and

mudstones beds arranged in coarsening-upward trends. The mean paleocurrent direction for fluvial facies is 300° (NW).

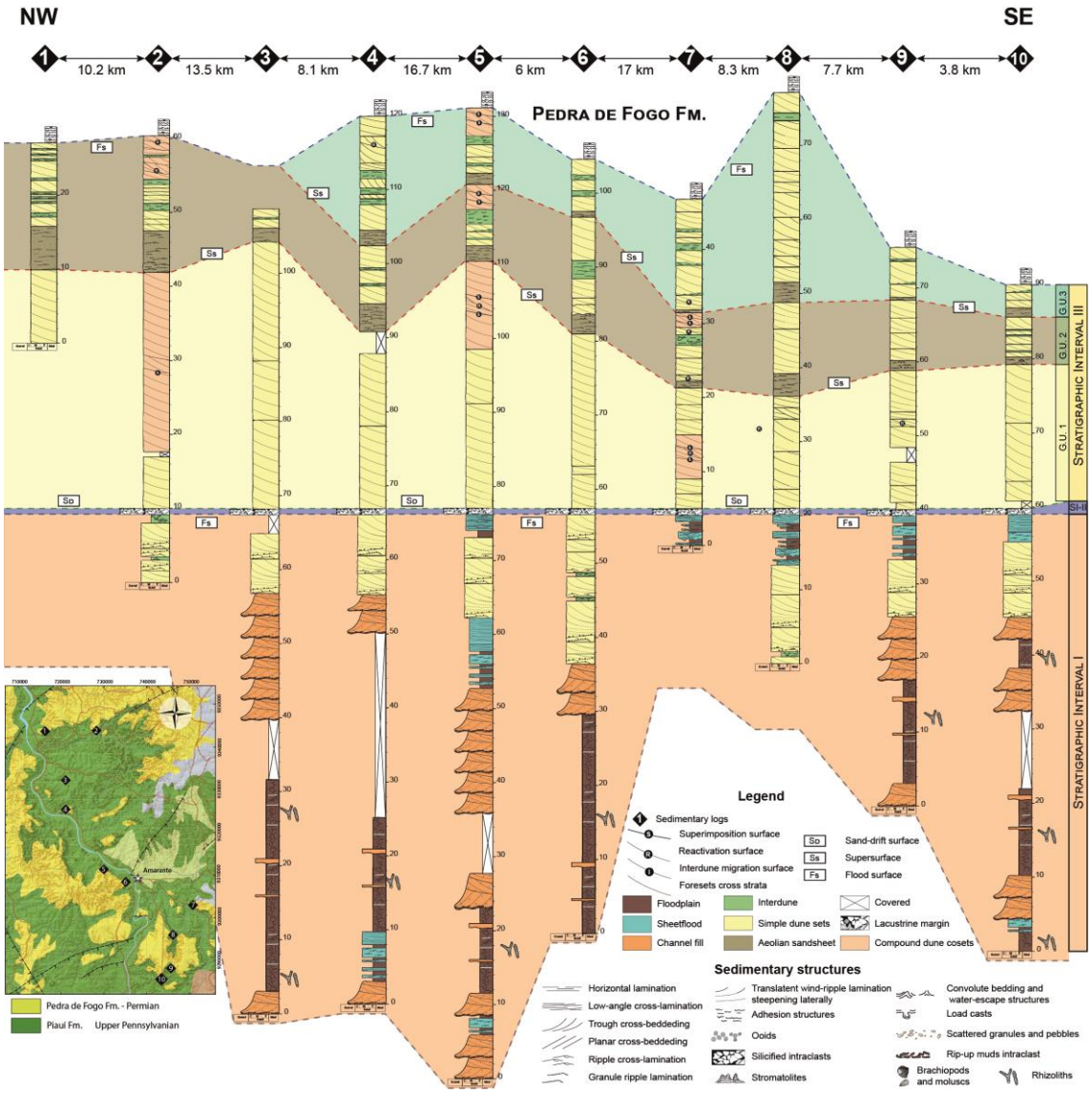

Figure 12: Lateral correlation of stratigraphic logs across a NW-SE traverse parallel to downwind transport. The lacustrine deposits have been used as stratigraphic datum for correlation

The uppermost part of the SI-1is marked by the appearance of an extensive aeolian succession (c.a. 27% of the SI-1 section) that can be correlated in almost all outcrops of the southern region (Fig. 12). The basal contact of aeolian dunes with the underlying fluvial deposits is marked an irregular surface characterized by soft-sediment structures at the toeset of aeolian dune sets.The aeolian deposits are composed of aeolian dune sets and

interdune facies associations. The aeolian dune forms tabular sets of 0.3 to 1.2 m thick that extend laterally for hundreds of meters, and interdune deposits form thin (0.1 to 0.3 m) discontinuous sandbodies with adhesion structures or low-angle wind ripple lamination. The aeolian deposits are occasionally overlain by sheetflood facies association that show paleocurrents direction towards 350°, in high angle relative to aeolian cross-strata that display dip orientation towards west-northwest (mean vector = 291°).

Interpretation. The vertical and lateral association of facies allowed a better definition of the depositional model in the SI-1. The significant thickness and lateral extension of mudstone packages suggest that these mudstones were not deposited in small interdune ponds between aeolian dunes, but rather in floodplain regions at the distal portion of fluvial system where settling of material in suspension was the most common process (Collinson et al., 2006). The unconfined sheetflood sandstones bodies are indicative of repeated pulses of high energy streams at the distal portion of fluvial system (Bridge, 2003). Furthermore, the channel-fill deposits associated with unconfined sheetflood represent ephemeral fluvial processes characterized by episodic high energy flash flood currents. The overall predominance of fluvial facies at the base of the interval suggests a position close to alluvial plain or a greater penetration of fluvial system into the margins of the dune field (Jagger, 2003).

The thick and extensive aeolian succession occurring at the uppermost part of SI-1suggests expansion of the aeolian dune field and dune migration over the alluvial plain. The presence of soft-sediment deformation structures at the base of aeolian deposits indicates high water table at the time of dune migration (Mountney, 2006). Moreover, the lack of features such as paleosols, polygonal fractures or deflation lag suggest that the basal bounding surface does not imply a hiatus in the erg development, thus does not represent a super surface (Kocurek, 1981; Kocurek & Hunter, 1986; Kocurek, 1988). Based upon the presence of water-influenced structures within interdune deposits, the aeolian succession of interval 1 may be classified as “wet” aeolian system (Kocurek & Havholm, 1993). The sheetflood deposits observed on top of the aeolian succession represent terminal lobes of fluvial system that reached the

dune-field margin, and indicate greater penetration of fluvial currents into the dune field during episodes of flash flood (Jagger. 2003; Al-Masrahy & Mountney, 2015). While the fluvial deposits at the base of SI-1 were oriented towards north-west (mean vector = 300°) nearly parallel to the mean wind direction (mean vector = 305°), the sheetflood deposits overlying aeolian dune deposits show a high angle relative to aeolian directions (mean vector = 350°), suggesting that the fluvial steams may have been reoriented into interdune corridors (Al-Masrahy & Mountney, 2015).

5.2 Stratigraphic Interval 2: Lacustrine deposits

Description. The second stratigraphic interval (SI-2) is characterized by a thin (40 to 60 cm) yet regionally extensive silicified unit, composed by lacustrine margin facies association that crops out in the entire studied area (Fig. 12). This interval directly overlies the sharp and regionally extensive erosive at the top of SI-1, and is bounded by an abrupt contact with aeolian units. Despite the reduced thickness, this layer is usually well preserved and easily identified in the field owing to its pervasive cementation by microcrystalline and criptocrystalline silica. This deposit is composed of stromatolites, ooids, and intraformational conglomerate whose primary composition has been completely replaced by cryptocrystalline and microcrystalline silica. No evidence of interaction with the adjacent deposits has been observed.

Interpretation. The lack of evidence indicating interaction between lacustrine unit and the underlying fluvial-aeolian units suggests a span between the end of accumulation of SI-1 and the lake expansion. Furthermore, the regional extension of the basal surface covering the entire studied area suggests an allogenic forcing on lake expansion and represents a regional transgression over the SI-1dune field and alluvial plain. The shallow nature of this lake, the seasonal productivity of organic matter, the variation of salinity and the pervasive silica cementation are suggestive of arid climate conditions.

5.3 Stratigraphic Interval 3: Aeolian sedimentation

Description: The upper stratigraphic interval (SI-3) crops-out in the entire studied area and is essentially composed of aeolian units that range from 33 m

to 56 m in thickness (Fig. 12). The basal bounding surface is abrupt and separates this interval from the underlying lacustrine unit, while the upper surface is an erosive contact with the overlying lacustrine Pedra de Fogo Formation.

Three aeolian genetic units separated by sandsheet facies have been recognized (Fig. 12). The first genetic unit (GU 1) is composed of stacked simple dune sets and compound dune cosets separated by interdune migration surfaces with no features suggesting groundwater influence. The second and third genetic units (GU 2 & 3) are characterized by a basal aeolian sandsheet deposits overlying a regionally extensive erosional surface, followed by progressively thicker simple dunes sets, occasionally culminating with compound dune cosets, and intercalated with damp interdunes deposits (Fig. 12).

Interpretation. The presence of aeolian succession overlying lacustrine deposits of SI-2 without evidence of interaction suggests that the lower bounding surface represents a sand-drift surface (Clemmensen & Tirsgaard, 1990) that marks a hiatus before the onset of aeolian sedimentation. The upper bounding surface, characterized by a regionally extensive erosional contact with the overlying Pedra de Fogo Formation, is interpreted as an allogenic-forced flood surface (Langford & Chan, 1988), and represents a new transgression event.

Based upon the absence of any sedimentary feature that indicate influence of ground-water level, the first aeolian genetic unit has been classified as a dry eolian system , typical of erg center (Wilson, 1971; Kocurek & Havholm, 1993). In contrast, the damp interdune deposits interbedded with dunes sets and cosets of the second and third units are indicative of wet aeolian system, commonly associated to erg margin (Kocurek & Havholm, 1993).

The progressive increase in set thickness observed in the second and third genetic unit represents drying-upward cycles and suggests an increase in bedforms size, occasionally culminating with draa development. Such increase in bedform size results from an increase in sediment availability. The erosive surfaces that separate the genetic unit are deflation surfaces and represent

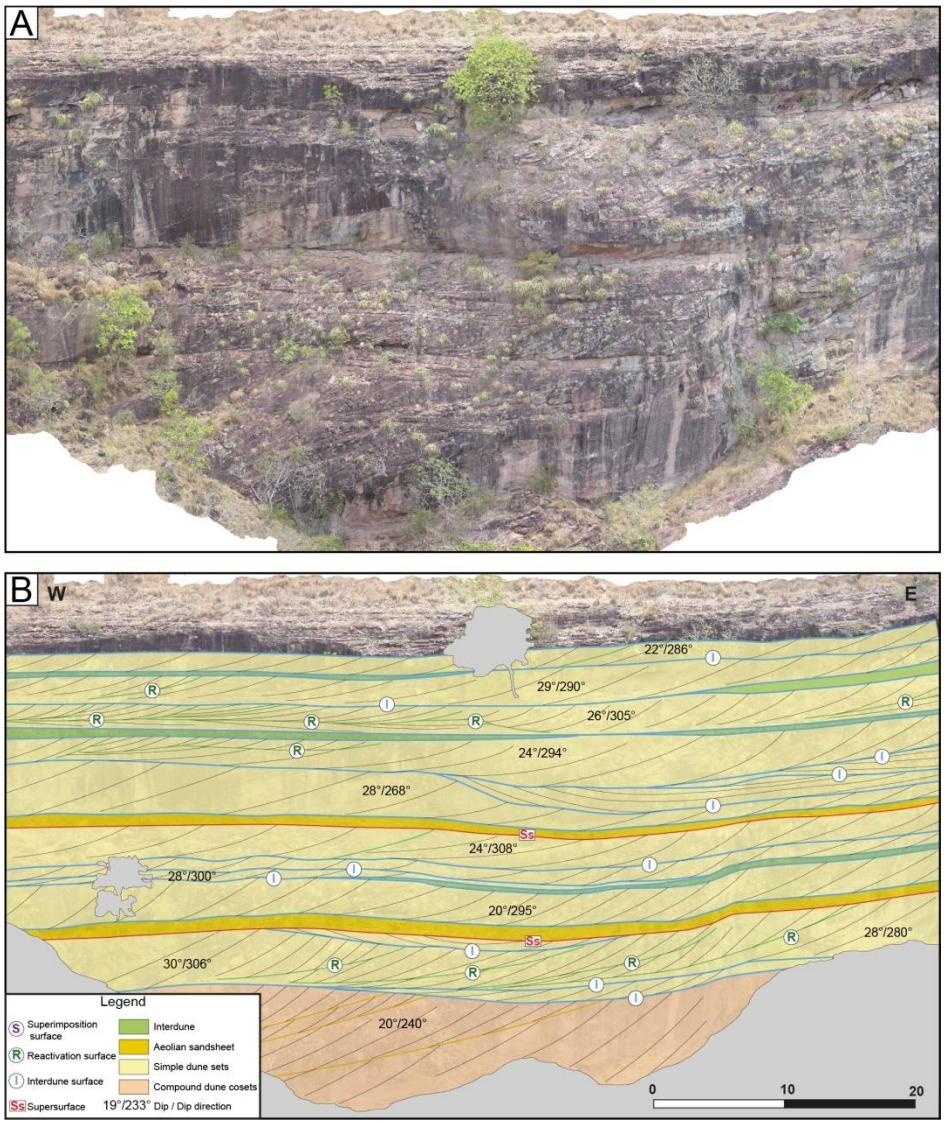

Figure 13: Outcrop panoramic view of stratigraphic interval 3, in W-W direction. Note the descontinuous interdune area deposits encased between aeolian dunes sets.

periods of erg contraction (Loope, 1985), which occurs because of a reduction in sand availability triggering unsaturated wind flows that progressively deflate the accumulation (Kocurek & Lancaster, 1999; Kocurek, 1999). For these reasons the deflation surfaces have been interpreted as supersurfaces (Loope, 1985; Kocurek, 1988) and each of the three genetic units represent an aeolian sequence (Mountney, 2006). The presence of damp sandsheet units immediately above the deflation surfaces suggests specific condition of limited sand availability (Kocurek & Nielson, 1986), in which the rise of groundwater

level accompanied the sediment availability at an equivalent rate, precluding the construction of bedforms with well-developed slip faces.

6 DEPOSITIONAL MODEL

The overall vertical stacking of the three stratigraphic intervals and their bounding surfaces allows for the reconstruction of the evolution. The relationships of the fluvial, aeolian and lacustrine sedimentary systems in the study area can be best explained by facies models for erg-margins in which interactions of the dune-field and adjacent systems are common (Mountney, 2006). In these models, the erg center is characterized by a dry aeolian system whereas the erg margin is damp to wet, in which interdune areas are periodically flooded and dune accumulation is controlled by the water table (Langford and Chan, 1989; Havholm and Kocurek, 1993; Mountney and Jagger, 2004; Mountney, 2006). In this sense, the depositional model suggests that the vertical variations in facies association are driven by contractions and expansions of an erg-system.

The vertical succession of SI-1 depicts a progressive change in the depositional environment from a dominant fluvial system to mostly aeolian processes. This change represents a drying-upward trend indicative of progressively drier climate conditions. The base of the succession represents a period dominated by fluvial sedimentation in an alluvial plain. However, as the climate progressively shifted to drier conditions, a dune-field started to develop and expanded to a point when the entire study area was covered by aeolian dunes and interdunes. The fluvial influence was restricted to episodic flash flood events invading interdunes areas (Fig. 14).

Subsequently, the fluvial-aeolian deposits of SI-1 were eroded, and then the entire region got flooded due to the expansion of SI-2 lake. However, the lack of features indicative interaction with the overlying aeolian deposits of SI-3 suggests a regional lowering and desiccation of the lake before the dune-field expansion. The dune-field expanded in such way that the entire studied area was completely covered by aeolian dunes and draas of the erg center. The absence of interdune area deposits in the first genetic unit suggests that the

interdune areas were completely and the entire erg center was covered of aeolian bedforms. Subsequently, the exhaustion of sand availability triggered deflation and contraction of the dune-field, and the erg-center was replaced by small dunes and damp interdunes of the erg margin (Havholm and Kocurek, 1993; Mountney, 2006). The third genetic units of the SI-3 indicate that the erg expanded and contracted once more and finally, a major transgression caused the complete flooding of the area and the deposition of the Pedra de Fogo Formation.

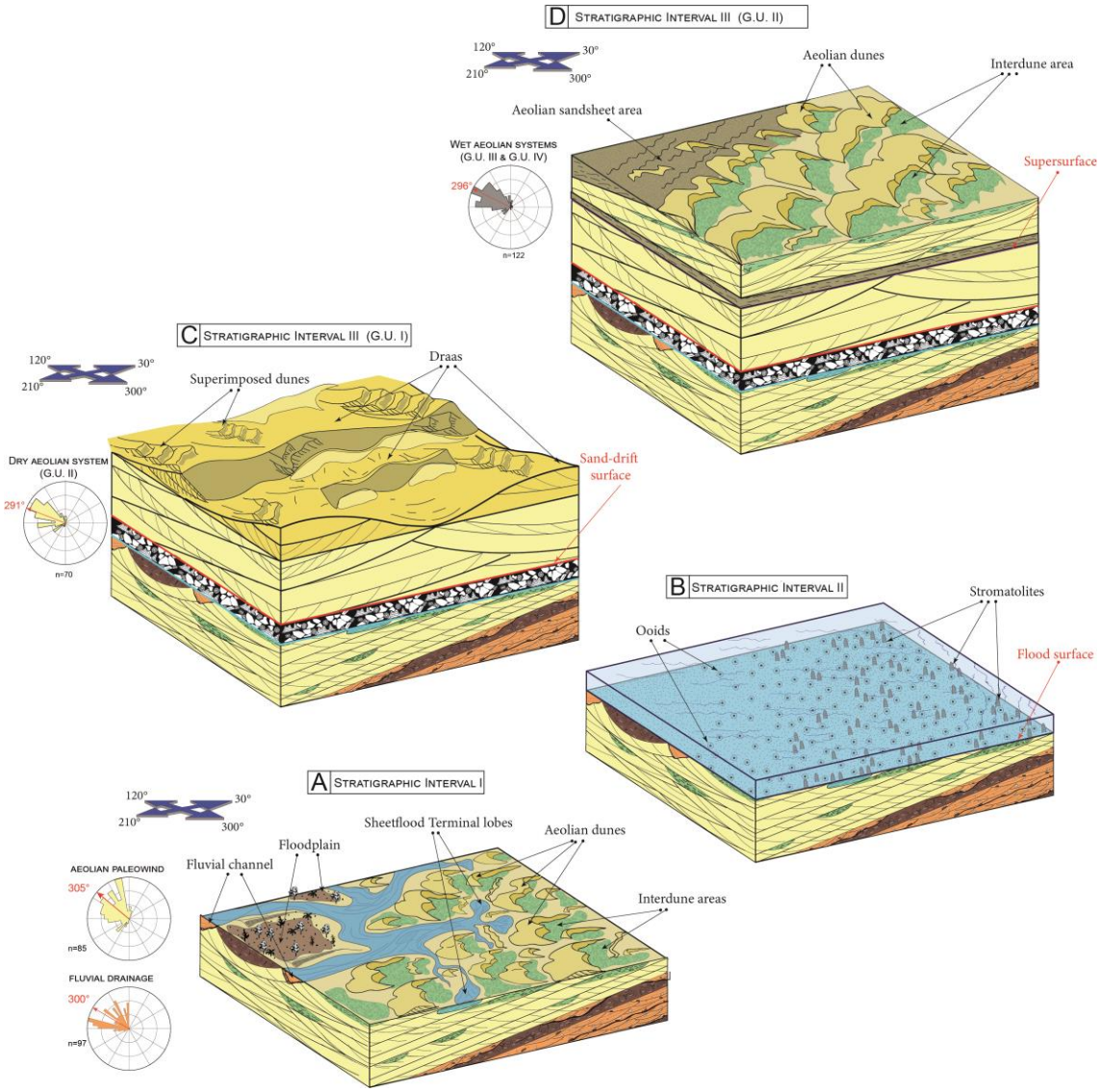

Figure 14: Depositional models. (A) Stratigraphic interval 1. Fluvial and aeolian rose diagram indicate similar orientation towards NW. The dune-field expansion reduced the alluvial plain area. (B) Stratigraphic interval 2. Complete flooding of

the area during lake expansion. (C) Stratigraphic interval 3, genetic unit 1. The area is completely covered by dunes and draas of erg center. (D) Stratigraphic interval 3, genetic unit 2. The erg of GU 1 deflated and triggered supersurface development. The dune field then expanded and the area is cover by erg margin.

7 DISCUSSION

The stratigraphic succession presented herein depicts a gradual change from original fluvial sedimentation to essentially aeolian accumulation in the upper Piauí Formation. This progressive change constitutes a low-frequency drying upward trend that reflects an increasing aridification in the Parnaíba Basin during the late Pennsylvanian age.

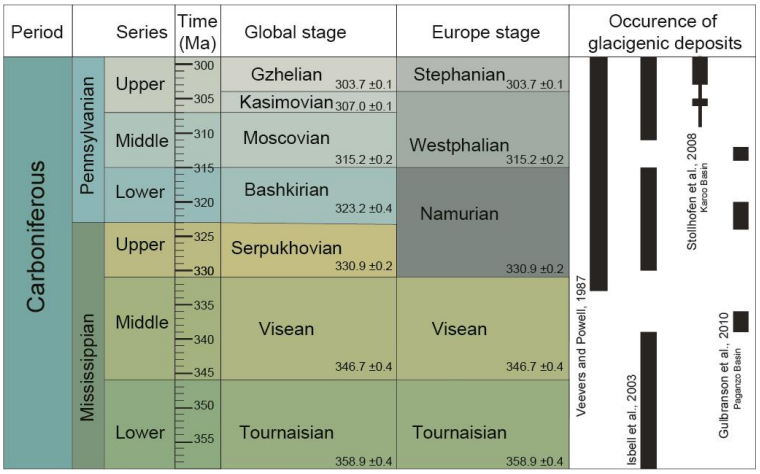

Figure 15: Correlation of global and European regional stages of Carboniferous and occurrence of glacigenic deposits (Gulbranson et al., 2010). Chronostratigraphic chart modified from Cohen et al. (2013).

The paleoclimatic evolution of the Late Paleozoic is characterized by a well-known long-term transition from icehouse conditions (late Visean) to extreme greenhouse conditions (Lopingian) in the Gondwana (Limarino et al., 2014). The Permian stratigraphic record of Gondwana is dominated by lithological indicators of arid conditions (eg. eolian deposits, evaporates and playa lake successions), suggesting that arid conditions would have succeeded to Carboniferous glaciation (Limarino et al., 2014; Abrantes et al., 2019). Although, the stratigraphic record of Piauí Formation studied here suggest that

the onset of aridification in the Parnaíba Basin occurred simultaneously with the glaciation.

The Carboniferous glaciation was originally thought to have occurred over an uninterrupted interval of time (Veevers & Powell, 1987; Crowell, 1999). However, Isbell et al. (2003) recognized three different glacial periods separated by inter-glacial intervals: Glacial I (Frasnian to possibly Tournaisian), Glacial II (Namurian to lowermost Westphalian), and Glacial III from upper Carboniferous (Stephanian) to Lower Permian (Sakmarian-Artinskian). Later, using high-precision U-Pb calibration, Stolhofen et al. (2008) and Gulbranson et al. (2010) established a precise timing of glaciation episodes in high- and mid-paleolatitudes respectively (Fig. 15). Despite minor differences in glaciation age, two main conclusions can be highlighted from the correlation of glacigenic deposits (Fig. 15): (i) Glacial diamictites, rhythmites of glacial origin and glacial-related structures of Visean age are widespread and have been described in basins of the northern region of South America (Caputo, 1985; Cunha et al., 2007;Caputo et al., 2008), as well as southern South America basins (Limarino et al., 2014) and high latitudes (Isbell et al., 2003). (ii) By contrast, during the upper Pennsylvanian age, evidence of glacial conditions completely disappeared in the northern South America basins (Caputo, 1985), but several glacigenic deposits of Pennsylvanian age (Bashkirian) have been documented in the southern South America: Paraná (Vesely et al., 2015), Chaco-Paraná (Assine et al., 2018) and Tarija basins (Limarino et al., 2014); and also in southern Africa: Kalahari and Karoo basins (Isbell et al., 2003; Stollhofen et al., 2008). Such difference in the stratigraphic record between Northern and southern basins suggests that ice cover was restricted to higher paleolatitudes (Fig. 16).

The absence of glacial-related structures in the stratigraphic succession studied here supports the interpretation of ice sheet restricted at high-paleolatitudes. Moreover, the progressive change from fluvial-aeolian sedimentation to essentially aeolian accumulation suggests time equivalence and coexistence between ice cap cover in high-paleolatitudes and increasing aridity in the mid-paleolatidudes. Similar conclusions have been reported in

Paganzo and Río Blanco Basins (Gulbranson et al., 2010). Therefore, the onset of arid climate conditions in Gondwana mid-paleolatidudes can reliably be positioned in Pennsylvanian.

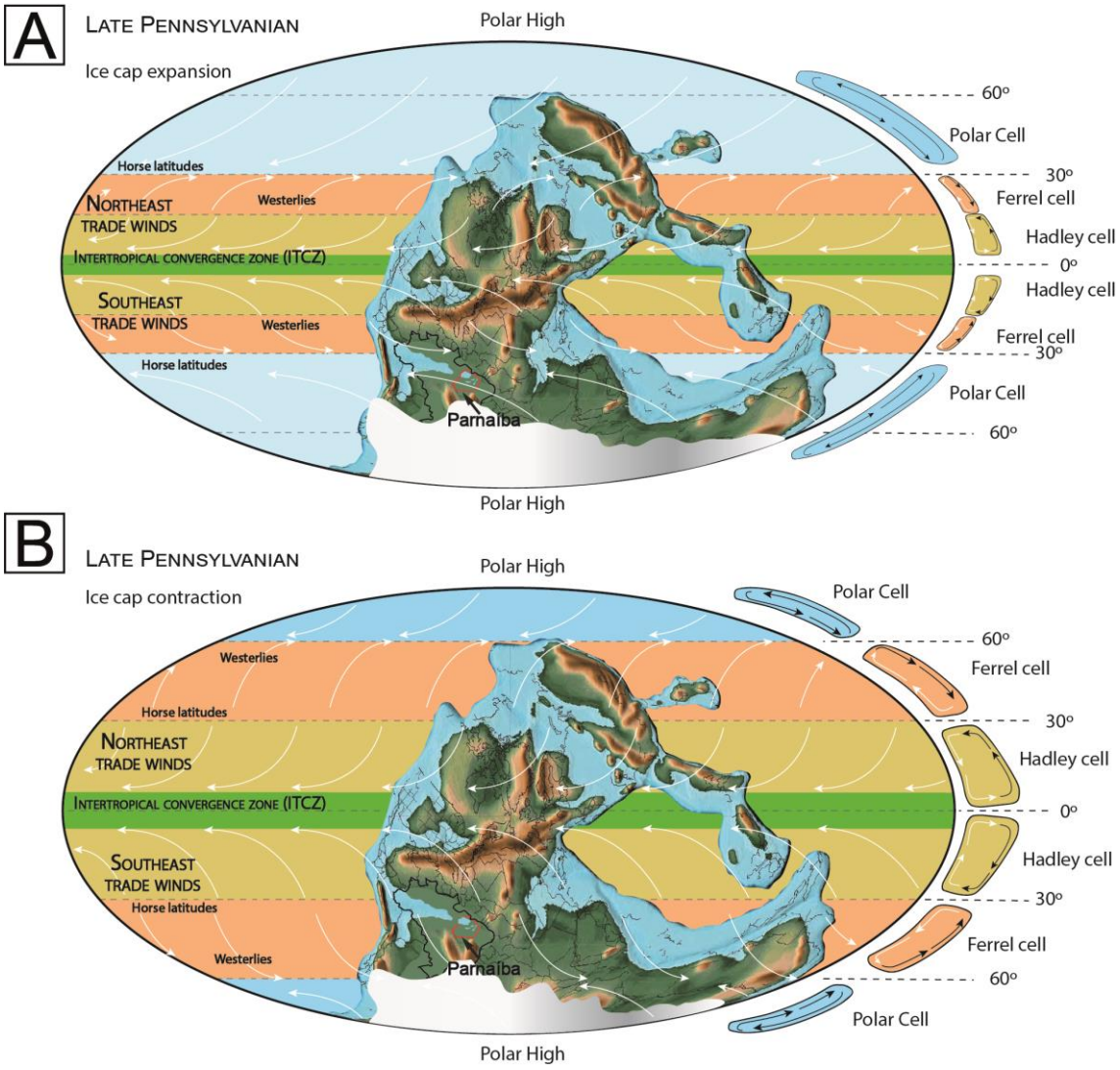

Figure 16: Paleoclimatic reconstruction of Pennsylvanian age. (A) During glacial periods the ITCZ shrink to lower latitudes and drier winds from high paleolatitudes allowed the development of Piauí dune-field. (B) During interglacial periods the ITCZ expands and bring moisture to the basin, causing reduction of sand availability. Paleogeographic reconstruction from Scotese (2014) and atmospheric circulation modified from Compagnucci (2011).

In this study we assume that the periods of dune-field development resulted from episodes of ice cover expansion at high-latitudes, and periods of dune-field contraction and supersurface development are related to interglacial

intervals (Fig. 16). Several studies proved that the Pennsylvanian glaciation was characterized by short-term events of ice sheet waxing and waning, which resulted in high-frequency eustatic changes of short durations (~1 to 8 m.y.)

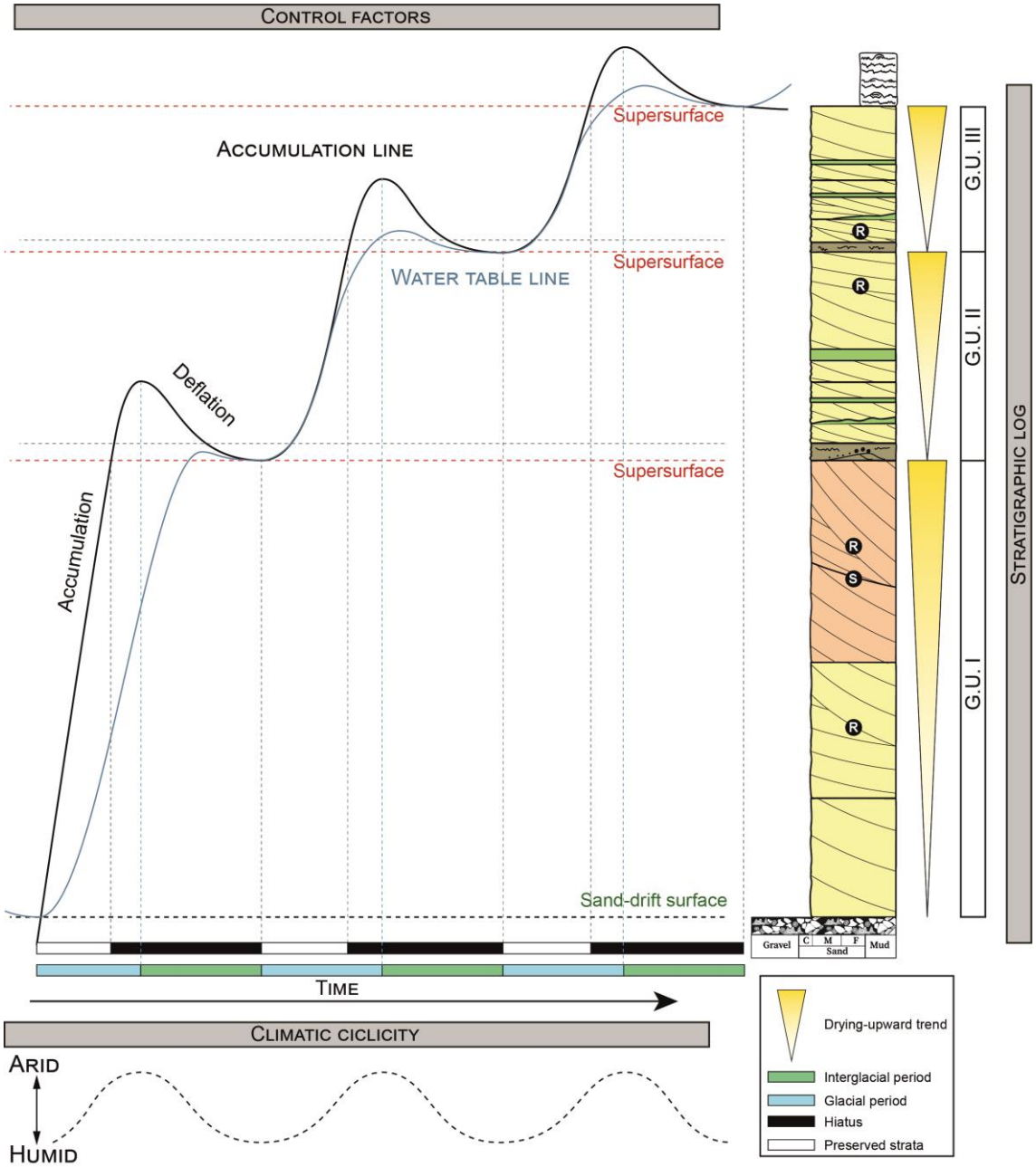

Figure 17: Schematic sedimentary log of SI-3 showing high-resolution drying-upward cycles bounded by supersurfaces. The supersurface development resulted from a decrease in sand availability during humid climate conditions related to interglacial periods.

responsible for the cyclothems of Pennsylvanian age reported in North America (Dickinson et al., 1994; Isbell et al., 2003; Fielding et al., 2008; Heckel, 2008). Although the absence of marine deposits in the upper Piauí Formation indicates that glacio-eustasy did not directly affect the sedimentation, the transgression event recorded in the SI-2 might represent a period of sea-level rise that permitted intermittent connection and expansion of the lake. According to Medeiros et al. (2019) a similar transgressive event allowed the deposition of the Mocambo carbonate.

The direct influence of short-term waxing and waning of ice sheets are high-frequency climate changes that resulted in the drying-upward cycles observed in the genetic unit II and III of SI-3 (Fig. 17). During glacial periods the extension of ice cover increases and the polar high-pressure cells expand. As a consequence, Hadley and Ferrel cells move towards lower latitudes causing the Intertropical Convergence Zone (ITCZ) to shrink to a thin humid region near the equator (Perlmutter and Matthews, 1989). Consequently, glacial episodes result in drier and cooler tropical environments and allow dune-field expansion registered in Piauí Formation. The mean aeolian paleocurrent towards NW observed in this study represent polar easterlies dominating mid-latitudes during glacial periods. In turn, during inter- and nonglacial episodes the ITCZ expands towards higher latitudes and Hadley and Ferrel cells expand. As a result, westerlies winds bring moisture into the continent and humid to subhumid climate conditions cause decrease in sand availability that triggers dune-field deflation and supersurface development.

8 CONCLUSION

The detailed facies analysis of the upper Piauí Formation allowed a precise reconstruction of the stratigraphic evolution of the Parnaíba basin during the Pennsylvanian. Three stratigraphic units have been identified based on the lateral and vertical relationships of architectural elements and the correlation of key stratigraphic surfaces. The first stratigraphic interval is composed of an interaction of fluvial and aeolian deposits in which the aeolian facies overlie fluvial deposits. The second stratigraphic interval represents an abrupt transgression of the area by the expansion of a saline lake, and the third

stratigraphic unit is composed of three aeolian genetic units that indicate cyclic expansions and contractions of the dune-field. Consequently, the stratigraphic succession of the upper Piauí Formation records a progressive change from fluvial-aeolian systems to essentially aeolian sedimentation, suggesting a progressive aridification in Gondwana mid-latitudes.

While several authors suggest that the Pennsylvanian age was marked by a glacial age, the evidence of arid climate conditions in the Parnaíba Basin prove that the Pennsylvanian glacial period was marked by a significant difference in climate conditions between high- to mid-latitude paleoclimate. Careful analysis of atmospheric circulation evidenced that ice sheet expansion during glacial periods usually result in drier and cooler tropical environments owing to the ITCZ shrinkage to a thin band near the equator. This configuration favored the development and expansion of Piauí Formation dune field. By contrast, during interglacial periods the ITCK expanded and the basin experienced more humid conditions that caused reduction of sand availability and triggered the development of supersurfaces.

9 ACKNOWLEDGMENTS

This research is part of the project of research and development named “Facies architecture and high resolution stratigraphy of coastal aeolian systems” funded by Petrobras S.A. and executed in partnership with the Federal University of Rio Grande do Sul. The first authors thank IAS for postgraduate research grant. Carrel Kifumbi thank Raimundo Nonato for accomodation at Amarante, and Romulo, the local guide at São Francisco do Maranhão.

10 REFERENCES

Ahlbrandt, T.S., Fryberger, S.G., 1981. Sedimentary features and significance of interdune deposits. Recent Anc. nonmarine Depos. Environ. Model. Explor. 293–314. https://doi.org/10.2110/pec.81.31.0293

Allen, J.R.L., 1963. The classification of cross-stratified units. With notes on their origin. Sedimentology 2, 93–114. https://doi.org/10.1111/J.1365-3091.1963.TB01204.X

Allen, J.R.L., 1983. Studies in fluviatile sedimentation: Bars, bar-complexes and sandstone sheets (low-sinuosity braided streams) in the brownstones (L. devonian), welsh borders. Sediment. Geol. 33, 237–293. https://doi.org/10.1016/0037-0738(83)90076-3

Allen, P.A., 1982. Cyclicity of Devonian fluvial sedimentation, Cunningsburgh Peninsula, SE Shetland. J. Geol. Soc. London. 139, 49–58. https://doi.org/10.1144/GSJGS.139.1.0049

Al-Masrahy, M.A., Mountney, N.P., 2015. A classification scheme for fluvial-aeolian system interaction in desert-margin settings. Aeolian Res. 17, 67–88. https://doi.org/10.1016/j.aeolia.2015.01.010

Araújo, R.N., Nogueira, A.C.R., Bandeira, J., Angélica, R.S., 2016. Shallow lacustrine system of the Permian Pedra de Fogo Formation, Western Gondwana, Parnaíba Basin, Brazil. J. South Am. Earth Sci. 67, 57–70. https://doi.org/10.1016/j.jsames.2016.01.009

Armelenti, G., Goldberg, K., Kuchle, J., Ros, L.F. De, 2016. Deposition, diagenesis and reservoir potential of non-carbonate sedimentary rocks from the rift section of Campos Basin, Brazil. Pet. Geosci. 22, 223–239. https://doi.org/10.1144/PETGEO2015-035

Assine, M. L., de Santa Ana, H., Veroslavsky, G., & Vesely, F. F. (2018). Exhumed subglacial landscape in Uruguay: Erosional landforms, depositional environments, and paleo-ice flow in the context of the late Paleozoic Gondwanan glaciation. Sedimentary Geology, 369, 1-12. https://doi.org/10.1016/j.sedgeo.2018.03.011

Baas, J.H., 1993. Dimensional analysis of current ripples in recent and ancient depositional environments 199.

Bagnold, R.A., 1941. The physics of blown sand and desert dunes.

Best, J., Bridge, J., 1992. The morphology and dynamics of low amplitude bedwaves upon upper stage plane beds and the preservation of planar laminae.

Sedimentology 39, 737–752. https://doi.org/10.1111/J.1365-3091.1992.TB02150.X

Bridge, J.S., 1993. Description and interpretation of fluvial deposits: a critical perspective. Sedimentology 40, 801–810. https://doi.org/10.1111/J.1365-3091.1993.TB01361.X

Bridge, J.S., 2003. Rivers and floodplains : forms, processes, and sedimentary record 491.

Bridge, J.S., Best, J.L., 1988. Flow, sediment transport and bedform dynamics over the transition from dunes to upper-stage plane beds: implications for the formation of planar laminae. Sedimentology 35, 753–763. https://doi.org/10.1111/J.1365-3091.1988.TB01249.X

Bristow, C.S., Smith, N., Rogers, J., 1999. Gradual avulsion, river metamorphosis and reworking by underfit streams: a modern example from the Brahmaputra River in Bangladesh and a possible ancient example in the Spanish Pyrenees. Fluv. Sedimentol. VI 28, 221e230.

Brookfield, M.E., 1977. The origin of bounding surfaces in ancient aeolian sandstones. Sedimentology 24, 303–332. https://doi.org/10.1111/J.1365-3091.1977.TB00126.X

Buck, S.G., 1980. Stromatolite and ooid deposits within the fluvial and lacustrine sediments of the Precambrian Ventersdorp Supergroup of South Africa. Precambrian Res. 12, 311–330. https://doi.org/10.1016/0301-9268(80)90033-9

Cain, S.A., Mountney, N.P., 2009. Spatial and temporal evolution of a terminal fluvial fan system: the Permian Organ Rock Formation, South-east Utah, USA. Sedimentology 56, 1774–1800.

Caputo, M. V., 1984. Stratigraphy, Tectonics, Paleoclimatology and Paleogeography of Northern Basins of Brazil. Dissertation. University of California.

Caputo, M.V., 1985. Late Devonian glaciation in South America. Palaeogeogr. Palaeoclimatol. Palaeoecol. 51, 291–317. https://doi.org/10.1016/0031-0182(85)90090-2

Caputo, M.V., Melo, J.H.G., Streel, M., Isbell, J.L., 2008. Late Devonian and Early Carboniferous glacial records of South America. Spec. Pap. Geol. Soc. Am. 441, 161–173. https://doi.org/10.1130/2008.2441(11)

Cascales-Miñana, B., Cleal, C.J., 2014. The plant fossil record reflects just two great extinction events. Terra Nov. 26, 195–200. https://doi.org/10.1111/TER.12086

Chagas, D.B. das, 2006. Litoestratigrafia da Bacia do Araripe: reavaliação e propostas para revisão.

Clemmensen, L.B., Tirsgaard, H., 1990. Sand-drift surfaces: A neglected type of bounding surface. Geology 18, 1142–1145.

Collinson, J.D., 1996. Alluvial sediments. Sediment. Environ. Process. facies, Stratigr. 37–82.

Collinson, J.D., Mountney, N.P., Thompson, D.B., 2006. Sedimentary Structures, Third Edit. ed. Terra Publishing, Hertfordshire, England.

Compagnucci, R. H. (2011). Atmospheric circulation over Patagonia from the Jurassic to present: a review through proxy data and climatic modelling scenarios. Biological Journal of the Linnean Society, 103(2), 229-249. https://doi.org/10.1111/j.1095-8312.2011.01655.x

Costa, M.S., Oliveira, R.S., Barbosa, R.C.M., Mota, C.B., 2020. Early Pennsylvanian fluvial-Aeolian interplay in the Amazonas Basin (central-western Gondwana) and its relation to marine transgression. J. South Am. Earth Sci. 104, 102857.

Crowell, J. C. (1999). Pre-Mesozoic ice ages: their bearing on understanding the climate system (Vol. 192). Geological Society of America.

Cunha, P.R.C., Melo, J.H.G., Silva, O.B., 2007. Bacia do Amazonas. Bol. Geociências da PETROBRAS 15, 227–251.

Dalrymple, R.W., 2010. Interpreting sedimentary successions: facies, facies analysis and facies models. In: Facies Model. 4, 3–18.

Daly, M.C., Andrade, V., Barousse, C.A., Costa, R., McDowell, K., Piggott, N., Poole, A.J., 2014. Brasiliano crustal structure and the tectonic setting of the Parnaíba basin of NE Brazil: Results of a deep seismic reflection profile. Tectonics 33, 2102–2120. https://doi.org/10.1002/2014TC003632

Daly, M.C., Fuck, R.A., Julià, J., Macdonald, D.I.M., Watts, A.B., 2018. Cratonic basin formation: A case study of the Parnaíba Basin of Brazil. Geol. Soc. Spec. Publ. 472, 1–15. https://doi.org/10.1144/SP472.20

Díaz Martínez, E., Isaacson, P.E., Sablock, P.E., 1993. Late Paleozoic latitudinal shift of Gondwana : stratigraphic/sedimentologic and biogeographic evidence from Bolivia. Trav. Doc. des Lab. Géologie Lyon 125, 119–138.

Dickinson, W.R., Soreghan, G.S., Giles, K.A., 1994. Glacio-eustatic origin of Permo-Carboniferous stratigraphic cycles: evidence from the southern cordilleran foreland region, in: Tectonic And Eustatic Controls on Sedimentary Cycles. SEPM (Society for Sedimentary Geology), pp. 25–34. https://doi.org/10.2110/csp.94.04.0025

DiMichele, W.A., Montañez, I.P., Poulsen, C.J., Tabor, N.J., 2009. Climate and vegetational regime shifts in the late Paleozoic ice age earth. Geobiology 7, 200–226. https://doi.org/10.1111/J.1472-4669.2009.00192.X

Dino, R., Antonioli, L., Braz, S.M.N., 2002. Palynological data from the Trisidela Member of Upper Pedra de Fogo Formation (“Upper Permian”) of the Parnaíba Basin, Northeastern Brazil. Rev. Bras. Paleontol. 24–35.

Dino, R., Playford, G., 2002. Stratigraphic and palaeoenvironmental significance of a Pennsylvanian (Upper Carboniferous) palynoflora from the Piauí Formation, Parnaíba Basin, northeastern Brazil. Paleontol. Res. 6, 23–40.

Doe, T.W., Dott, R.H., 1980. Genetic significance of deformed cross bedding - with examples from the Navajo and Weber sandstones of Utah. J. Sediment. Petrol. 50, 793–812. https://doi.org/10.1306/212F7AEF-2B24-11D7-8648000102C1865D

Fielding, C. R., Frank, T. D., Birgenheier, L. P., Rygel, M. C., Jones, A. T., & Roberts, J. (2008). Stratigraphic imprint of the Late Palaeozoic Ice Age in eastern Australia: a record of alternating glacial and nonglacial climate regime. Journal of the Geological Society, 165(1), 129-140. https://doi.org/10.1144/0016-76492007-036

Foix, N., Paredes, J.M., Giacosa, R.E., 2013. Fluvial architecture variations linked to changes in accommodation space: Río Chico Formation (Late Paleocene), Golfo San Jorge basin, Argentina. Sediment. Geol. 294, 342–355. https://doi.org/10.1016/J.SEDGEO.2013.07.001

Fryberger, S.G., 1993. A review of aeolian bounding surfaces, with examples from the Permian Minnelusa Formation, USA. Geol. Soc. Spec. Publ. 73, 167–197. https://doi.org/10.1144/GSL.SP.1993.073.01.11

Fryberger, S.G., Ahlbrandt, T.S., Andrews, S., 1979. Origin, sedimentary features, and significance of low-angle eolian ' sand sheet' deposits, Great Sand Dunes National Monument and vicinity, Colorado. J. Sediment. Petrol. 49, 733–746. https://doi.org/10.1306/212F782E-2B24-11D7-8648000102C1865D

Fryberger, S.G., Hesp, P., Hastings, K., 1992. Aeolian granule ripple deposits, Namibia. Sedimentology 39, 319–331. https://doi.org/10.1111/j.1365-3091.1992.tb01041.x

Fryberger, S.G., Schenk, C.J., 1981. Wind sedimentation tunnel experiments on the origins of aeolian strata. Sedimentology 28, 805–821. https://doi.org/10.1111/j.1365-3091.1981.tb01944.x

Góes, A.M.O., Feijó, F.J., 1994. Bacia do Parnaiba. Bol. Geociências da Petrobras 8, 57–67.

Goldberg, K., Kuchle, J., Scherer, C., Alvarenga, R., Ene, P.L., Armelenti, G., De Ros, L.F., 2017. Re-sedimented deposits in the rift section of the Campos Basin. Mar. Pet. Geol. 80, 412–431. https://doi.org/10.1016/J.MARPETGEO.2016.11.022

Grader, G.., Isaacson, P., Díaz-Martínez, E., Pope, M.., 2008. Pennsylvanian and Permian sequences in Bolivia: Direct responses to Gondwana glaciation. Spec. Pap. Geol. Soc. Am. 441, 143–159. https://doi.org/10.1130/2008.2441(10)

Gulbranson, E.L., Montañez, I.P., Schmitz, M.D., Limarino, C.O., Isbell, J.L., Marenssi, S.A., Crowley, J.L., 2010. High-precision U-Pb calibration of Carboniferous glaciation and climate history, Paganzo Group, NW Argentina. GSA Bull. 122, 1480–1498. https://doi.org/10.1130/B30025.1

Gulbranson, E.L., Montañez, I.P., Tabor, N.J., Limarino, C.O., 2015. Late Pennsylvanian aridification on the southwestern margin of Gondwana (Paganzo Basin, NW Argentina): A regional expression of a global climate perturbation. Palaeogeogr. Palaeoclimatol. Palaeoecol. 417, 220–235. https://doi.org/10.1016/J.PALAEO.2014.10.029

Hampton, B.A., Horton, B.K., 2007. Sheetflow fluvial processes in a rapidly subsiding basin, Altiplano plateau, Bolivia. Sedimentology 54, 1121–1148. https://doi.org/10.1111/J.1365-3091.2007.00875.X

Harms, J.C., Southard, J.B, Walker, R.G., 1982. Structures and sequences in clastic rocks.

Haszeldine, R.S., 1983. Fluvial bars reconstructed from a deep, straight channel, Upper Carboniferous coalfield of northeast England (sandstones). J. Sediment. Petrol. 53, 1233–1247. https://doi.org/10.1306/212F8350-2B24-11D7-8648000102C1865D

Heckel, P. H. (2008). Pennsylvanian cyclothems in Midcontinent North America as far-field effects of waxing and waning of Gondwana ice sheets. Resolving the Late Paleozoic Ice Age in Time and Space; Fielding, CR, Frank, TD, Isbell, JL, Eds, 275-290.

Hein, F.J., Walker, R.G., 1977. Bar evolution and development of stratification in the gravelly, braided, Kicking Horse river, British Columbia. Can J Earth Sci 14, 562–570. https://doi.org/10.1139/E77-058

Hofmann, H.J., 1973. Stromatolites: Characteristics and utility. Earth-Science Rev. 9, 339–373. https://doi.org/10.1016/0012-8252(73)90002-0

Horowitz, D.H., 1982. Geometry and origin of large-scale deformation structures in some ancient wind-blown sand deposits. Sedimentology 29, 155–180.

Hughes, D.A., Lewin, J., 1982. A small-scale flood plain. Sedimentology 29, 891–895.

Hummel, G., Kocurek, G., 1984. Interdune areas of the back-island dune field, North Padre Island, Texas. Sediment. Geol. 39, 1–26. https://doi.org/10.1016/0037-0738(84)90022-8

Hunter, R.E., 1977. Basic types of stratification in small eolian dunes. Sedimentology 24, 361–387. https://doi.org/10.1111/j.1365-3091.1977.tb00128.x

Hunter, R.E., Rubin, D.M., 1983. Interpreting Cyclic Crossbedding, with An Example from the Navajo Sandstone. Dev. Sedimentol. 38, 429–454. https://doi.org/10.1016/S0070-4571(08)70808-2

Iannuzzi, R., Neregato, R., Cisneros, J.C., Angielczyk, K.D., Rößler, R., Rohn, R., Marsicano, C., Fröbisch, J., Fairchild, T., Smith, R.M.H., Kurzawe, F., Richter, M., Langer, M.C., Tavares, T.M.V., Kammerer, C.F., Conceição, D.M., Pardo, J.D., Roesler, G.A., 2018. Re-evaluation of the Permian macrofossils from the Parnaíba Basin: Biostratigraphic, palaeoenvironmental and palaeogeographical implications. Geol. Soc. Spec. Publ. 472, 223–249. https://doi.org/10.1144/SP472.14

Iannuzzi, R., Pfefferkorn, H.W., 2002. A pre-glacial, warm-temperate floral belt in Gondwana (Late Visean, early carboniferous). Palaios 17, 571–590. https://doi.org/10.1669/0883-1351(2002)017<0571:APGWTF>2.0.CO;2

Isaacson, P.E., Díaz-Martínez, E., Grader, G.W., Kalvoda, J., Babek, O., Devuyst, F.X., 2008. Late Devonian–earliest Mississippian glaciation in Gondwanaland and its biogeographic consequences. Palaeogeogr. Palaeoclimatol. Palaeoecol. 268, 126–142. https://doi.org/10.1016/J.PALAEO.2008.03.047

Isbell, J.L., Miller, M.F., Wolfe, K.L., Lenaker, P.A., 2003. Timing of late Paleozoic glaciation in Gondwana: Was glaciation responsible for the development of northern hemisphere cyclothems? Spec. Pap. Geol. Soc. Am. 370, 5–24. https://doi.org/10.1130/0-8137-2370-1.5

Jagger, A., 2003. Sedimentology and Stratigraphic Evolution of the Permian Cedar Mesa Sandstone, Paradox Basin, SE Utah.

Jo, H.R., Chough, S.K., 2001. Architectural analysis of fluvial sequences in the northwestern part of Kyongsang Basin (Early Cretaceous), SE Korea. Sediment. Geol. 144, 307–334.

Jones, F.H., Scherer, C.M.S,, Kifumbi, C., 2021. Aeolian dunes morphodynamics and wind regime reconstruction in mid-latitudes of the Gondwana during Early Permian, Aracaré Formation, Sergipe-Alagoas Basin, Brazil. Aeolian Res. 50, 100672. https://doi.org/10.1016/j.aeolia.2021.100672

Jones, F.H., Scherer, C.M.S., Kuchle, J., 2016. Facies architecture and stratigraphic evolution of aeolian dune and interdune deposits, Permian Caldeirão Member (Santa Brígida Formation), Brazil. Sediment. Geol. 337, 133–150. https://doi.org/10.1016/J.SEDGEO.2016.03.018

Kah, L.C., Bartley, J.K., Frank, T.D., Lyons, T.W., 2006. Reconstructing sea-level change from the internal architecture of stromatolite reefs: an example from the Mesoproterozoic Sulky Formation, Dismal Lakes Group, arctic Canada. Can. J. Earth Sci. 43, 653–669.

Kocurek, G., 1981. Significance of interdune deposits and bounding surfaces in aeolian dune sands. Sedimentology 28, 753–780. https://doi.org/10.1111/j.1365-3091.1981.tb01941.x

Kocurek, G., 1988. First-order and super bounding surfaces in eolian sequences-Bounding surfaces revisited. Sediment. Geol. 56, 193–206. https://doi.org/10.1016/0037-0738(88)90054-1

Kocurek, G., 1991. Interpretation of ancient eolian sand dunes. Annu. Rev. Earth Planet. Sci. 19 43–75. https://doi.org/10.1146/ANNUREV.EA.19.050191.000355

Kocurek, G., 1996. Desert aeolian systems, in: Reading, H.G. (Ed.), Sedimentary Environments: Processes, Facies and Stratigraphy. Oxford, Blackwell Science, London, pp. 125–153.

Kocurek, G., 1999. The Aeolian Rock Record (Yes, Virginia, it Exists, But it Really is Rather Special to Create One). Aeolian Environ. Sediments Landforms 239–259.

Kocurek, G., Fielder, G., 1982. Adhesion structures. J. Sediment. Petrol. 52, 1229–1241. https://doi.org/10.1306/212f8102-2b24-11d7-8648000102c1865d

Kocurek, G., Havholm, K.G., 1993. Eolian sequence stratigraphy - a conceptual framework. Siliciclastic Seq. Stratigr. Recent Dev. Appl.

Kocurek, G., Havholm, K.G., Deynoux, M., Blakey, R.C., 1991. Amalgamated accumulations resulting from climatic and eustatic changes, Akchar Erg, Mauritania. Sedimentology 38, 751–772. https://doi.org/10.1111/j.1365-3091.1991.tb01018.x

Kocurek, G., Lancaster, N., 1999. Aeolian system sediment state: Theory and Mojave Desert Kelso dune field example. Sedimentology 46, 505–515. https://doi.org/10.1046/j.1365-3091.1999.00227.x

Kocurek, G., Nielson, J., 1986. Conditions favourable for the formation of warm-climate aeolian sand sheets. Sedimentology 33, 795–816. https://doi.org/10.1111/j.1365-3091.1986.tb00983.x

Kocurek, G., Townsley, M., Yeh, E., Havholm, K., Sweet, M.L., 1992. Dune and dune-field development on Padre Island, Texas, with implications for interdune deposition and water-table- controlled accumulation. 62, 622–635.

Kumar, R., Sangode, S.J., Ghosh, S.K., 2004. A multistorey sandstone complex in the Himalayan Foreland Basin, NW Himalaya, India. J. Asian Earth Sci. 23, 407–426. https://doi.org/10.1016/S1367-9120(03)00176-7

Langford, R.P., Chan, M.A., 1988. Flood surfaces and deflation surfaces within the Cutler Formation and Cedar Mesa Sandstone (Permian), southeastern Utah. GSA Bull. 100, 1541–1549.

Langford, R.P., Chan, M.A., 1989. Fluvial-aeolian interactions: Part II, ancient systems. Sedimentology 36, 1037–1051.

Leite, C.O.N., Silva, C.M.A., de Ros, L.F., 2020. Depositional and diagenetic processes in the pre-salt rift section of a Santos Basin area, SE Brazil. J. Sediment. Res. 90, 584–608. https://doi.org/10.2110/JSR.2020.27

Leite, J.F., Aboarrage, A.M., Daemon, R.F., 1975. Projeto Carvão da Bacia do Parnaíba.

Lima Filho, F.P., 1998. A sequencia Permo-Pensilvaniana da Bacia do Parnaiba 155.

Lima, E.A.M., Leite, J.F., 1978. Projeto estudo global dos recursos minerais da bacia sedimentar do Parnaíba.

Limarino, C.O., Césari, S.N., Spalletti, L.A., Taboada, A.C., Isbell, J.L., Geuna, S., Gulbranson, E.L., 2014. A paleoclimatic review of southern South America during the late Paleozoic: A record from icehouse to extreme greenhouse conditions. Gondwana Res. 25, 1396–1421. https://doi.org/10.1016/J.GR.2012.12.022

Loope, D.B., 1981. Deposition, deflation, and diagenesis of upper Paleozoic eolian sediments, Canyonlands National Park, Utah. University of Wyoming.

Loope, D.B., 1985. Episodic deposition and preservation of eolian sands: a late Paleozoic example from southeastern Utah (Canyonlands National Park, USA). Geology 13, 73–76. https://doi.org/10.1130/0091-7613(1985)13<73:EDAPOE>2.0.CO;2

Loope, D.B., Rowe, C.M., Joeckel, R.M., 2001. Annual monsoon rains recorded by Jurassic dunes. Nat. 2001 4126842 412, 64–66. https://doi.org/10.1038/35083554

Loope, D.B., Steiner, M.B., Rowe, C.M., Lancaster, N., 2004. Tropical westerlies over Pangaean sand seas. Sedimentology 51, 315–322. https://doi.org/10.1046/j.1365-3091.2003.00623.x

Mack, G.H., 1977. Depositional environments of the Cutler-Cedar Mesa facies transition (Permian) near Moab, Utah.

Mack, G.H., James, W.C., Monger, H.C., 1993. Classification of paleosols: Gological Society of America Bulletin, v. 105.

McKee, E.D., Douglass, J.R., Rittenhouse, S., 1971. Deformation of lee-side laminae in eolian dunes. Bull. Geol. Soc. Am. 82, 359–378. https://doi.org/10.1130/0016-7606(1971)82[359:DOLLIE]2.0.CO;2

Medeiros, R.S.P., Nogueira, A.C.R., Silva Junior, J.B.C., Sial, A.N., 2019. Carbonate-clastic sedimentation in the Parnaiba Basin, northern Brazil: Record of carboniferous epeiric sea in the Western Gondwana. J. South Am. Earth Sci. 91, 188–202. https://doi.org/10.1016/J.JSAMES.2019.01.018

Melo, J.H.G., Loboziak, S., Streel, M., 1998. Latest Devonian to early late Carboniferous biostratigraphy of northern Brazil: an update. Bull. du Cent. Rech. Elf Explor. Prod. 22.

Mesner, J.C., Wooldridge, L.C., 1964. Estratigrafia Das Bacias Paleozóica E Cretácea Do Maranhão. Bol. Téc. PETROBRÁS 7, 137–164.

Miall, A.D., 1977. A review of the braided-river depositional environment. Earth Sci. Rev. 13, 1–62. https://doi.org/10.1016/0012-8252(77)90055-1

Miall, A.D., 1978. Fluvial sedimentology.

Miall, A.D., 1996. The Geology of Fluvial Deposits. Sedimentary Facies, Basin Analysis, and Petroleum Geology, Geological Magazine. Springer-Verlag. https://doi.org/10.1017/S0016756897276983

Mountney, N.P., 2006. Eolian Facies Models, in: Facies Models Revisited. SEPM (Society for Sedimentary Geology), pp. 19–83. https://doi.org/10.2110/pec.06.84.0019

Mountney, N.P., 2012. A stratigraphic model to account for complexity in aeolian dune and interdune successions. Sedimentology 59, 964–989. https://doi.org/10.1111/j.1365-3091.2011.01287.x

Mountney, N.P., Howell, J., 2000. Aeolian architecture, bedform climbing and preservation space in the Cretaceous Etjo Formation, NW Namibia. Sedimentology 47, 825–849. https://doi.org/10.1046/j.1365-3091.2000.00318.x

Mountney, N.P., Thompson, D.B., 2002. Stratigraphic evolution and preservation of aeolian dune and damp/wet interdune strata: An example from the Triassic Helsby Sandstone Formation, Cheshire Basin, UK. Sedimentology 49, 805–833. https://doi.org/10.1046/j.1365-3091.2002.00472.x

Nemec, W., Postma, G., 1993. Quaternary alluvial fans in southwestern Crete: sedimentation processes and geomorphic evolution, in: Alluvial Sedimentation. International Association of Sedimentologists Oxford, pp. 235–276.

Olsen, H., Due, P.H., Clemmensen, L.B., 1989. Morphology and genesis of asymmetric adhesion warts—a new adhesion surface structure. Sediment. Geol. 61, 277–285. https://doi.org/10.1016/0037-0738(89)90062-6

Owen, G., 2003. Load structures: gravity-driven sediment mobilization in the shallow subsurface. Geol. Soc. London, Spec. Publ. 216, 21–34. https://doi.org/10.1144/GSL.SP.2003.216.01.03

Paola, C., Borgman, L., 1991. Reconstructing random topography from preserved stratification. Sedimentology 38, 553–565. https://doi.org/10.1111/j.1365-3091.1991.tb01008.x

Pérez Loinaze, V.S., Limarino, C.O., Césari, S.N., 2010. Glacial events in Carboniferous sequences from Paganzo and Río Blanco basins (northwest Argentina): palynology and depositional setting. Geol. Acta 8, 399–418.

Perlmutter, M.A., Matthews, M.D., 1989. Global cyclostratigraphy – A model., in: Cross, T.A. (Ed.), Quantitative Dynamic Stratigraphy. Prentice Hall, Englewood, pp. 233–260.

Plee, K., 2008. Geomicrobiological investigation of ooid cortex formation in a freshwater environment–Lake Geneva, Switzerland.

Retallack, G.J., 2001. Soils of the Past: An Introduction to Paleopedology: Second Edition, 2nd edition. ed, Soils of the Past: An Introduction to Paleopedology: Second Edition. https://doi.org/10.1002/9780470698716

Rubin, D.M., 1987. Formation of scalloped cross-bedding without unsteady flows. J. Sediment. Petrol. 57, 39–45.

Rubin, D.M., Hunter, R.E., 1982. Bedform climbing in theory and nature. Sedimentology 29, 121–138. https://doi.org/10.1111/j.1365-3091.1982.tb01714.x

Rubin, D.M., Hunter, R.E., 1983. Reconstructing bedform assemblages from compound crossbedding. Dev. Sedimentol. 38, 407–427. https://doi.org/10.1016/S0070-4571(08)70807-0

Rust, B.R., 1977. A classification of alluvial channel systems.

Sahney, S., Benton, M.J., Falcon-Lang, H.J., 2010. Rainforest collapse triggered Carboniferous tetrapod diversification in Euramerica. Geology 38, 1079–1082.

Scherer, C.M.S., 2000. Eolian dunes of the Botucatu Formation (Cretaceous) in southernmost Brazil: Morphology and origin. Sediment. Geol. 137, 63–84. https://doi.org/10.1016/S0037-0738(00)00135-4

Scherer, C.M.S., Goldberg, K., 2010. Cyclic cross-bedding in the eolian dunes of the Sergi Formation (Upper Jurassic), Recôncavo Basin: Inferences about the wind regime. Palaeogeogr. Palaeoclimatol. Palaeoecol. 296, 103–110.

Scherer, C.M.S., Lavina, E.L.C., 2005. Sedimentary cycles and facies architecture of aeolian-fluvial strata of the Upper Jurassic Guará Formation,

southern Brazil. Sedimentology 52, 1323–1341. https://doi.org/10.1111/J.1365-3091.2005.00746.X

Scotese, C.R. (2014) Atlas of Permo-Carboniferous Paleogeographic Maps (Mollweide Projection), Maps 53 – 64, Volumes 4, The Late Paleozoic, PALEOMAP Atlas for ArcGIS, PALEOMAP Project, Evanston, IL.

Souza, P.A., Matzembacher, L.T., Abelha, M., Borghi, L., 2010. Palinologia da formação piauí, pensilvaniano da bacia do parnaíba: Biocronoestratigrafia de intervalo selecionado do poço 1-UN-09-PI (Caxias, MA, Brasil). Rev. Bras. Paleontol. 13, 57–66. https://doi.org/10.4072/rbp.2010.1.07

Spalletti, L.A., Piñol, F.C., 2005. From alluvial fan to playa: an Upper Jurassic ephemeral fluvial system, Neuquén Basin, Argentina. Gondwana Res. 8, 363–383.

Stollhofen, H., Werner, M., Stanistreet, I. G., Armstrong, R. A., Fielding, C. R., Frank, T. D., & Isbell, J. L. (2008). Single-zircon U-Pb dating of Carboniferous-Permian tuffs, Namibia, and the intercontinental deglaciation cycle framework. Resolving the late Paleozoic ice age in time and space. Geological Society of America Special Paper, 441, 83-96.

Tabor, N.J., Montanez, I.P., 2002. Shifts in late Paleozoic atmospheric circulation over western equatorial Pangea: Insights from pedogenic mineral δ18O compositions. Geology 30, 1127–1130.

Taggart, S., Hampson, G.J., Jackson, M.D., 2010. High-resolution stratigraphic architecture and lithological heterogeneity within marginal aeolian reservoir analogues. Sedimentology 57, 1246–1279. https://doi.org/10.1111/j.1365-3091.2010.01145.x

Tettenhorst, R., Moore, G.E., 1978. Stevensite oolites from the Green River Formation of central Utah. J. Sediment. Res. 48, 587–594. https://doi.org/10.1306/212F74DC-2B24-11D7-8648000102C1865D

Todd, S.P., 1989. Stream-driven, high-density gravelly traction carpets: possible deposits in the Trabeg Conglomerate Formation, SW Ireland and some

theoretical considerations of their origin. Sedimentology 36, 513–530. https://doi.org/10.1111/J.1365-3091.1989.TB02083.X

Todd, S.P., 1996. Process deduction from fluvial sedimentary structures. Adv. Fluv. Dyn. Stratigr. 299–350.

Tribaldos, V.R., White, N., 2018. Implications of preliminary subsidence analyses for the Parnaíba cratonic basin, in: Geological Society Special Publication. Geological Society of London, pp. 147–156. https://doi.org/10.1144/SP472.3

Tunbridge, I.P., 1984. Facies model for a sandy ephemeral stream and clay playa complex; the Middle Devonian Trentishoe Formation of North Devon, U.K. Sedimentology 31, 697–715. https://doi.org/10.1111/J.1365-3091.1984.TB01231.X

Vaz, P.T., Rezende, N.G.A.M., Wanderley Filho, J.R., Travassos, W.A.S., 2007. Bacia do Parnaíba. Bol. Geociencias da Petrobras 15, 253–263.

VEEVERS, J. T., & Powell, C. M. (1987). Late Paleozoic glacial episodes in Gondwanaland reflected in transgressive-regressive depositional sequences in Euramerica. Geological Society of America Bulletin, 98(4), 475-487. https://doi.org/10.1130/0016-7606(1987)98<475:LPGEIG>2.0.CO;2

Vesely, F. F., Trzaskos, B., Kipper, F., Assine, M. L., & Souza, P. A. (2015). Sedimentary record of a fluctuating ice margin from the Pennsylvanian of western Gondwana: Paraná Basin, southern Brazil. Sedimentary Geology, 326, 45-63. https://doi.org/10.1016/j.sedgeo.2015.06.012

Vieira, L.V., Scherer, C.M. dos S., 2017. Facies architecture and high resolution sequence stratigraphy of an aeolian, fluvial and shallow marine system in the Pennsylvanian Piauí Formation, Parnaíba Basin, Brazil. J. South Am. Earth Sci. 76, 238–256. https://doi.org/10.1016/j.jsames.2017.03.009

Wanderley Filho, J., Eiras, J., Vaz, P., 2007. Bacia do Solimões. Bol. Geociencias da PETROBRAS.

Wanless, H.R., Shepard, F.P., 1936. Sea level and climatic changes related to late Paleozoic cycles. Bull. Geol. Soc. Am. 47, 1177–1206. https://doi.org/10.1130/GSAB-47-1177

Watts, A.B., Tozer, B., Daly, M.C., Smith, J., 2018. A comparative study of the Parnaíba, Michigan and Congo cratonic basins. Geol. Soc. Spec. Publ. 472, 45–66. https://doi.org/10.1144/SP472.6

Wilson, I.G., 1971. Desert Sandflow Basins and a Model for the Development of Ergs. Geogr. J. 137, 180–199.

Wizevich, M.C., 1992. Sedimentology of pennsylvanian quartzose sandstones of the lee formation, central appalachian basin: fluvial interpretation based on lateral profile analysis. Sediment. Geol. 78, 1–47. https://doi.org/10.1016/0037-0738(92)90111-4

Wright, V.P., 1992. Paleosol recognition: a guide to early diagenesis in terrestrial settings, in: Developments in Sedimentology. Elsevier, pp. 591–619.

Ziegler, A.M., Scotese, C.R., McKerrow, W.S., Johnson, M.E., Bambach, R.K., 1979. Paleozoic Paleogeography. Annu. Rev. Earth Planet. Sci. 7, 473–502. https://doi.org/10.1146/annurev.ea.07.050179.002353

ANEXO I
Título da Dissertação/Tese:
ESTRATIGRAFIA DE ALTA RESOLUÇÃO DE SISTEMAS EÓLICOS DURANTE PERÍODOS DE ICEHOUSE, FORMAÇÃO PIAUÍ, BACIA DO PARNAÍBA
Área de Concentração: Estratigrafia
Autor: **Carrel Kifumbi**
Orientador: Prof. Dr. Claiton Marlon dos Santos Scherer
Examinadora: **Profa. Dra. Ana Maria Góes**
Data: 27/09/2021
Conceito: A Excelente
PARECER: Carrel alcançou com excelência todos os requisitos exigidos para ter aprovada a sua tese de doutorado. Apresentou o volume da tese com excelente fundamentação teórica sobre sistemas eólicos e os resultados organizados em três artigos já submetidos a periódicos internacionais, dois em fase de revisão. Fez uma apresentação no tempo adequado com clareza e de forma didática. Respondeu com tranquilidade e erudição as perguntas formuladas, com espírito aberto a novas ideias, evidenciando maturidade científica. Pelo exposto acima, o considero aprovado com conceito A
Ciente do Orientador: Ciente do Aluno:

ANEXO I
Título da Dissertação/Tese:
ESTRATIGRAFIA DE ALTA RESOLUÇÃO DE SISTEMAS EÓLICOS DURANTE PERÍODOS DE ICEHOUSE, FORMAÇÃO PIAUÍ, BACIA DO PARNAÍBA
Área de Concentração: Estratigrafia
Autor: **Carrel Kifumbi**
Orientador: Prof. Dr. Claiton Marlon dos Santos Scherer
Examinador: **Prof. Dr. Roberto Iannuzzi**
Data: 27/09/2021
Conceito: A
PARECER: O conteúdo do documento apresentado configura-se em uma tese de doutorado, dada a extensão e profundidade com que é tratado o tema, bem como a qualidade dos artigos apresentados. O texto está bem escrito e de fácil compreensão, contendo uma excelente introdução aos princípios teóricos relacionados à temática abordada. Os artigos estão bem concatenados, de forma que constituem em um corpo coerente da tese. O candidato demonstrou didática na apresentação e segurança e conhecimento na argüição. O único ponto levantado por este examinador que deveria ser mais bem trabalhado futuramente relaciona-se a idade dos depósitos a partir do conhecimento bioestratigráfico existente para a Bacia do Parnaíba e bacias circunvizinhas. De qualquer forma, o documento, artigos associados e a defesa alcançaram o nível desejado em uma tese de doutorado e, portanto, considero o candidato APTO a obter a titulação de doutor.
Assinatura:  Data: 27/09/2021
Ciente do Orientador: Ciente do Aluno:

ANEXO I
Título da Dissertação/Tese:
ESTRATIGRAFIA DE ALTA RESOLUÇÃO DE SISTEMAS EÓLICOS DURANTE PERÍODOS DE ICEHOUSE, FORMAÇÃO PIAUÍ, BACIA DO PARNAÍBA
Área de Concentração: Estratigrafia
Autor: **Carrel Kifumbi**
Orientador: Prof. Dr. Claiton Marlon dos Santos Scherer
Examinador: Prof. Dr. Juliano Kuchle
Data: 27/09/21
Conceito: A - Excelente
PARECER: Tese apresentada com volume textual e apresentação oral bem estruturados, organizados, com informação clara e bem escrita e bem exposta.Tema complexo, o qual foi trabalhado com um volume de dados substancial e de forma científica bem organizada, acarretando em resultados com impacto científico, principalmente na reconstrução do Gondwana. O doutorando apresenta grande domínio do tema, o que demonstra sua capacitação plena. A arguição desenvolveu discussão em alto nível e idéias relevantes tanto no tema específico da tese, quanto em derivações futuras. Parabenizo o doutorando Carrel e seu Orientador Claiton pelo trabalho realizado.
Assinatura:  Juliano Kuchle 2021.09.28 10:46:25 -03'00' Data: 27/09/21
Ciente do Orientador: Ciente do Aluno: